CONCEPT DEVELOPMENT, FLOATING BRIDGE E39 BJØRNAFJORDEN

# Preferred solution, K12 – main report

CLIENT

Statens vegvesen

DATE: / REVISION: 15.08.2019 / 0

DOCUMENT CODE: SBJ-33-C5-AMC-90-RE-100

AAS-JAKOBSEN COWI Multiconsult

JOHS HOLT AkerSolutions entail NGI DISSING+WEITLING architecture a|s mossmaritime

**REPORT**

| | | | |
|---|---|---|---|
| PROJECT | Concept development, floating bridge E39 Bjørnafjorden | DOCUMENT CODE | SBJ-33-C5-AMC-90-RE-100 |
| SUBJECT | Preferred solution, K12 - main report | ACCESSIBILITY | Restricted |
| CLIENT | Statens vegvesen | PROJECT MANAGER | Svein Erik Jakobsen |
| CONTACT | Øyvind Kongsvik Nedrebø | PREPARED BY | Per Norum Larsen |
| | | RESPONSIBLE UNIT | AMC |


**SUMMARY**

This report outlines the preferred solution for crossing of Bjørnafjorden for phase 5 of the E39 Bjørnafjorden project, performed by the AMC project group.

Current version of this report is the final report issued for milestone 9 of this contract. Focus for this final report is to document the analyses and design work done as basis for choosing the preferred alternative, and the evaluation done hereto.

The preferred alternative is outlined to be K12, which is an end-anchored floating bridge with 3 clusters of supplementary moorings to avoid the possibility for unacceptable resonance from parametric excitation as well as to reduce the effective buckling and span length and thereby reduce cost.


| | | | | | |
|---|---|---|---|---|---|
| | | | | | |
| | | | | | |
| | | | | | |
| | | | | | |
| 0 | 15.08.2019 | Final issue | P. N. Larsen | A. Nesteby/ R.M.Larssen | S. E. Jakobsen |
| REV. | DATE | DESCRIPTION | PREPARED BY | CHECKED BY | APPROVED BY |

# TABLE OF CONTENTS

## List of appendices

| Appendix document ID | Appendix title |
|---|---|
| SBJ-33-C5-AMC-90-RE-101 | Appendix A: Drawings binder |
| SBJ-33-C5-AMC-90-RE-103 | Appendix C: Architectural evaluation |
| SBJ-33-C5-AMC-20-RE-105 | Appendix E: Aerodynamics |
| SBJ-33-C5-AMC-90-RE-106 | Appendix F: Global analyses - Modelling and assumptions |
| SBJ-33-C5-AMC-90-RE-107 | Appendix G: Global analyses - Response |
| SBJ-33-C5-AMC-21-RE-108 | Appendix H: Global analyses - Special studies |
| SBJ-33-C5-AMC-22-RE-109 | Appendix I: Fatigue analyses |
| SBJ-33-C5-AMC-27-RE-110 | Appendix J: Ship collision |
| SBJ-33-C5-AMC-22-RE-111 | Appendix K: Design of floating bridge part |
| SBJ-33-C5-AMC-22-RE-112 | Appendix L: Design of cable stayed bridge and abutments |
| SBJ-33-C5-AMC-26-RE-113 | Appendix M: Mooring system |
| SBJ-33-C5-AMC-28-RE-114 | Appendix N: Fabrication and marine operations |
| SBJ-33-C5-AMC-04-RE-115 | Appendix O: Material technology and steel in marine environment |
| SBJ-33-C5-AMC-90-RE-116 | Appendix P: Cost estimate |
| SBJ-33-C5-AMC-23-RE-118 | Appendix R: Risk assessment |
| SBJ-33-C5-AMC-90-RE-119 | Appendix S: Parametric excitation |

## List of enclosures in appendices

| Enclosure no. and title | Rev. date |
|---|---|
| **Appendix A: Drawings** | |
| See separate drawing list | - |
| **Appendix C: Architectural evaluation** | |
| Enclosure 1 - Architectural visualizations | 15.08.2019 |
| **Appendix E: Aerodynamics** | |
| Enclosure 1 - Tower Load Coefficients during construction | 15.08.2019 |
| Enclosure 2 - 10205546-08-NOT-016 Aerodynamic assessment | 28.01.2019 |
| Enclosure 3 - 10205546-08-NOT-060 Aerodynamic load coefficients sensitivity | 29.03.2019 |
| Enclosure 4 - 10205546-08-NOT-061 Wind load coefficients – Storebælt | 29.03.2019 |
| Enclosure 5 - 10205546-08-NOT-062 CFD analysis of cross sections | 24.05.2019 |
| Enclosure 6 - 10205546-08-NOT-068 Buffeting effects of inhomogeneity | 29.03.2019 |
| Enclosure 7 - 10205546-08-NOT-098 Bridge Closure Due To Wind | 24.05.2019 |
| Enclosure 8 - 10205546-08-NOT-176 Aerodynamic stability of K11 | 24.05.2019 |
| Enclosure 9 - 10205546-08-NOT-183 Inhomogeinity in wind – Effects on K12 | 15.08.2019 |
| Enclosure 10 - 10205546-08-NOT-184 Aerodynamic stability of K12 | 15.08.2019 |
| Enclosure 11 - 10205546-08-NOT-191 Cable vibrations of cable stayed bridge – K12 | 15.08.2019 |
| Enclosure 12 - 10205546-08-NOT-192 CFD Analysis of K12 | 15.08.2019 |
| **Appendix F: Global Analyses - Modelling and assumptions** | |
| Enclosure 1 - Full model description in spread sheet | 15.08.2019 |
| Enclosure 2 - 10205546-11-NOT-095 Analytic mooring line damping | 24.05.2019 |
| Enclosure 3 - 10205546-01-NOT-055-Programvare | 14.02.2019 |
| **Appendix G: Global Analyses - Response** | |
| Enclosure 1 - K12_07 Eigenmodes | 13.06.2019 |
| Enclosure 2 - K12_07 Load combinations direct method | 25.06.2019 |
| Enclosure 3 - K12_07 Load combinations factorized method | 02.08.2019 |
| Enclosure 4 - K12_07 Load combinations AUR method 100 year | 02.08.2019 |
| Enclosure 5 - K12_06 Load combinations AUR method 10 000 year | 21.06.2019 |
| Enclosure 6 - K12_07 Screening windsea 1year | 03.07.2019 |
| Enclosure 7 - K12_07 Screening windsea 100 year | 03.07.2019 |
| Enclosure 8 - K12_07 Screening windsea 10 000 year | 03.07.2019 |
| Enclosure 9 - K12_07 Screening swell 1 year | 06.07.2019 |
| Enclosure 10 - K12_07 Screening swell 100 year | 05.07.2019 |
| Enclosure 11 - K12_07 Screening swell 10 000 year | 04.07.2019 |
| Enclosure 12 - K12_07 Load combination motions | 26.06.2019 |
| Enclosure 13 - 10205546-11-NOT-059 Estimation of extreme response using the AUR method | 29.03.2019 |
| Enclosure 14 - 10205546-11-NOT-088 Variable static loads | 29.03.2019 |
| Enclosure 15 - 10205546-11-NOT-193 Long-term wave response | 15.08.2019 |
| Enclosure 16 - 10205546-11-NOT-196 Uncertainty assessment | 15.08.2019 |
| Enclosure 17 - Static results K12_07 | 15.08.2019 |
| **Appendix H: Global Analyses - Special studies** | |
| Enclosure 1 - 10205546-09-NOT-067 A simplified model to implement freeboard exceedance scenarios in OrcaFlex | 29.03.2019 |
| Enclosure 2 - 18-008-MCO-RT-001 Pontoon CFD (rev. B4) | 28.05.2019 |

| Enclosure no. and title | Rev. date |
|---|---|
| **Appendix I: Fatigue analyses** | |
| Enclosure 1 K12_05 Fatigue – Bridge girder screening | 21.05.2019 |
| Enclosure 2 K12_07 Fatigue – Bridge girder selected points | 15.08.2019 |
| Enclosure 3 Environmental load cases | 23.05.2019 |
| Enclosure 4 Environmental load cases – Subset for coupled analyses | 01.08.2019 |
| Enclosure 5 Local stress series from traffic | 07.06.2019 |
| **Appendix J: Ship collision** | |
| Enclosure 1 - Ship collision simulations for the Bjørnafjorden floating bridge Concept K12_06 | 27.06.2019 |
| Enclosure 2 - 10205546-11-NOT-076 Plastic capacity of column | 29.03.2019 |
| Enclosure 3 - Verification of fracture criterion | 27.06.2019 |
| **Appendix K: Design of Floating Bridge Part** | |
| Enclosure 1 - 10205546-13-NOT-020 Weight comparison of rectangular and A-shaped columns | 29.03.2019 |
| Enclosure 2 - 10205546-13-NOT-082 Railings on bridge girder | 29.03.2019 |
| Enclosure 3 - 10205546-13-NOT-083 Transverse trusses in bridge girder | 24.05.2019 |
| Enclosure 4 - 10205546-13-NOT-085 End of bridge girder at abutment north | 15.08.2019 |
| Enclosure 5 - 10205546-13-NOT-086 Column design | 24.05.2019 |
| Enclosure 6 - 10205546-13-NOT-087 Design of pontoons | 24.05.2019 |
| Enclosure 7 - 10205546-13-NOT-099 FEM analysis of bridge girder and column | 24.05.2019 |
| Enclosure 8 - 10205546-13-NOT-194 Shear lag and buckling effects of bridge girder concept 12 | 15.08.2019 |
| **Appendix L: Design of Cable Stayed Bridge and Abutments** | |
| Enclosure 1 - Capacity diagrams | 24.05.2019 |
| Enclosure 2 - Foundation stresses | 24.05.2019 |
| Enclosure 3 - Analysis of construction stages | 15.08.2019 |
| **Appendix M: Mooring systems** | |
| Enclosure 1 - 10205546-12-NOT-182 Geotechnics anchors K12 | 15.08.2019 |
| Enclosure 2 - 10205546-12-NOT-090 Geotechnical evaluation of anchor concepts | 24.05.2019 |
| **Appendix N: Fabrication and Marine Operations** | |
| Enclosure 1 - 10205546-13-NOT-185 Finite element analysis of locking joint | 15.08.2019 |
| Enclosure 2 - CAL-AB016101-001 Feasibility Study for Jacking of Bridge Sections | 15.08.2019 |
| Enclosure 3 - DRW-AB016101-001 Jacking of bridge sections (2 sheets) | 15.08.2019 |
| **Appendix O: Material technology and steel in marine environment** | |
| None | - |
| **Appendix P: Cost estimates** | |
| Enclosure 1 - Cost estimate K12 | 15.08.2019 |
| **Appendix R: Risk assessment** | |
| Enclosure 1 - Risk register - Operational phase | 15.08.2019 |
| Enclosure 2 - Risk register – Construction phase | 15.08.2019 |
| **Appendix S: Parametric excitation** | |
| Enclosure 1 - 10205546-11-NOT-092 Analysis of parametric resonance of single-degree-of-freedom systems using Newmark's method and Monte Carlo simulation | 24.05.2019 |
| Enclosure 2 - Parametric excitation results | 15.08.2019 |
| Enclosure 3 - 10205546-11-NOT-186 - Verification of modal interpretation of drag damping | 15.08.2019 |
| Enclosure 4 - 10205546-11-NOT-187 - Effect of KC-dependent drag coefficient on parametric excitation | 15.08.2019 |
| Enclosure 5 - 10205546-11-NOT-188 - Assessment of risk of parametric excitation of mooring cables | 15.08.2019 |
| Enclosure 6 - 10205546-11-NOT-189 - Effect of static forces on K12 | 15.08.2019 |

## List of drawings

| Drawing ID | Drawing title |
|---|---|
| SBJ-33-C5-AMC-22-DR-012 | General view, K12 |
| SBJ-33-C5-AMC-22-DR-101 | Cable stayed bridge, K12 - Base case layout, plan and elevation |
| SBJ-33-C5-AMC-22-DR-102 | Cable stayed bridge, K12 - Tower, elevation and sections |
| SBJ-33-C5-AMC-22-DR-103 | Cable stayed bridge, K12 - Steel box girder, section and details |
| SBJ-33-C5-AMC-22-DR-104 | Cable stayed bridge, K12 - Concrete box girder, section and details |
| SBJ-33-C5-AMC-22-DR-105 | Cable stayed bridge, K12 - Stay cable system |
| SBJ-33-C5-AMC-22-DR-106 | Cable stayed bridge, K12 - Piers in side span |
| SBJ-33-C5-AMC-22-DR-111 | Cable stayed bridge, K12 - Alternative layout, plan and elevation |
| SBJ-33-C5-AMC-22-DR-201 | Abutments, K12 - South, layout and sections |
| SBJ-33-C5-AMC-22-DR-202 | Abutments, K12 - North, layout and sections |
| SBJ-33-C5-AMC-22-DR-203 | Abutments, K12 - South and north, details |
| SBJ-33-C5-AMC-22-DR-300 | Floating Bridge Pontoon, K12 - General Arrangement, Dimensions |
| SBJ-33-C5-AMC-22-DR-301 | Floating Bridge Pontoon, K12 - Arrangement, Tank Plan |
| SBJ-33-C5-AMC-22-DR-302 | Floating Bridge Pontoon, K12 - Pontoon Bottom Plate, Dimension Plate and stiffeners |
| SBJ-33-C5-AMC-22-DR-303 | Floating Bridge Pontoon, K12 - Top-Plate, Dimension Plate and stiffeners |
| SBJ-33-C5-AMC-22-DR-304 | Floating Bridge Pontoon, K12 - Internal Plate, Longitudinal Structure 4000 mm from CL |
| SBJ-33-C5-AMC-22-DR-305 | Floating Bridge Pontoon, K12 - Internal Plate, Longitudinal Structure in CL |
| SBJ-33-C5-AMC-22-DR-306 | Floating Bridge Pontoon, K12 - Pontoon Side, Longitudinal Structure 7450 mm from CL |
| SBJ-33-C5-AMC-22-DR-307 | Floating Bridge Pontoon, K12 - Internal Structure, Transvers Frame No. 02 (No. 19) |
| SBJ-33-C5-AMC-22-DR-308 | Floating Bridge Pontoon, K12 - Internal Structure, Transvers Frame No. 07 (No. 14) |
| SBJ-33-C5-AMC-22-DR-309 | Floating Bridge Pontoon, K12 - Internal Structure, Transvers Frame No. 08 (No. 13) |
| SBJ-33-C5-AMC-22-DR-310 | Floating Bridge Pontoon, K12 - Internal Structure, Transvers Frame No. 09 |
| SBJ-33-C5-AMC-22-DR-351 | Floating Bridge Pontoon, K12 - Plan Bottom Deck, Fairlead reinforcement |
| SBJ-33-C5-AMC-22-DR-352 | Floating Bridge Pontoon, K12 - Plan Pontoon deck 11000 ab. Base line, Fairlead reinforcement |
| SBJ-33-C5-AMC-22-DR-353 | Floating Bridge Pontoon, K12 - Longitudinal Structure in CL, Fairlead reinforcement |
| SBJ-33-C5-AMC-22-DR-354 | Floating Bridge Pontoon, K12 - Longitudinal Structure 4000 mm from CL, Fairlead reinforcement |
| SBJ-33-C5-AMC-22-DR-355 | Floating Bridge Pontoon, K12 - Longitudinal Structure 7450 from CL, Fairlead reinforcement |
| SBJ-33-C5-AMC-22-DR-356 | Floating Bridge Pontoon, K12 - Curved Structure Bow and Stern, Fairlead reinforcement |
| SBJ-33-C5-AMC-22-DR-401 | Floating Bridge Girder, K12 - High Part Axis 3-8, Typical Plan |
| SBJ-33-C5-AMC-22-DR-402 | Floating Bridge Girder, K12 - High Part Axis 3-8, Typical Cross-section at Midspan |
| SBJ-33-C5-AMC-22-DR-403 | Floating Bridge Girder, K12 - High Part Axis 3-8, Typical Cross-section at Transition |
| SBJ-33-C5-AMC-22-DR-404 | Floating Bridge Girder, K12 - High Part Axis 3-8, Typical Cross-section above Column |
| SBJ-33-C5-AMC-22-DR-405 | Floating Bridge Girder, K12 - High Part Axis 3-8, Typical Transverse Bulkhead above Column |
| SBJ-33-C5-AMC-22-DR-406 | Floating Bridge Girder, K12 - High Part Axis 3-8, Typical Longitudinal Truss and Bulkhead |
| SBJ-33-C5-AMC-22-DR-407 | Floating Bridge Girder, K12 - High Part Axis 3-8, Typical Longitudinal Detail above Column |

| Drawing no. | Drawing title |
|---|---|
| SBJ-33-C5-AMC-22-DR-431 | Floating Bridge Girder, K12 - Low Part Axis 9-40, Typical Plan |
| SBJ-33-C5-AMC-22-DR-432 | Floating Bridge Girder, K12 - Low Part Axis 9-40, Typical Cross-section at Midspan |
| SBJ-33-C5-AMC-22-DR-433 | Floating Bridge Girder, K12 - Low Part Axis 9-40, Typical Cross-section at Transition |
| SBJ-33-C5-AMC-22-DR-434 | Floating Bridge Girder, K12 - Low Part Axis 9-40, Typical Cross-section above Column |
| SBJ-33-C5-AMC-22-DR-435 | Floating Bridge Girder, K12 - Low Part Axis 9-40, Typical Transverse Bulkhead above Column |
| SBJ-33-C5-AMC-22-DR-436 | Floating Bridge Girder, K12 - Low Part Axis 9-40, Typical Longitudinal Trusses and Bulkheads |
| SBJ-33-C5-AMC-22-DR-437 | Floating Bridge Girder, K12 - Low Part Axis 9-40, Typical Longitudinal Detail above Column |
| SBJ-33-C5-AMC-22-DR-451 | Floating Bridge Girder, K12 - Stiffener Details |
| SBJ-33-C5-AMC-22-DR-461 | Floating Bridge Girder, K12 - End of girder at North Abutment, Plan and Elevation |
| SBJ-33-C5-AMC-22-DR-462 | Floating Bridge Girder, K12 - End of girder at North Abutment, Sections |
| SBJ-33-C5-AMC-22-DR-471 | Floating Bridge Column, K12 - High Part Axis 3 - 8, Structural Arrangement and Dimensions |
| SBJ-33-C5-AMC-22-DR-481 | Floating Bridge Column, K12 - Low Part Axis 9 and above, Structural Arrangement and Dimensions |
| SBJ-33-C5-AMC-22-DR-491 | Floating Bridge High Part, K12 - Axis 3-8, Typical Structural Arrangement |
| SBJ-33-C5-AMC-22-DR-492 | Floating Bridge Low Part, K12 - Axis 9-40, Typical Structural Arrangement |
| SBJ-33-C5-AMC-22-DR-601 | Anchor, K12 - Suction anchor, typical |
| SBJ-33-C5-AMC-22-DR-701 | Mooring, K12 - Mooring line segmentation arrangement |
| SBJ-33-C5-AMC-22-DR-800 | Assembly and installation, K12 - Sections overview |
| SBJ-33-C5-AMC-22-DR-810 | Assembly and installation, K12 - Abutment north |
| SBJ-33-C5-AMC-22-DR-811 | Assembly and installation, K12 - North section installation |
| SBJ-33-C5-AMC-22-DR-812 | Assembly and installation, K12 - Floating bridge installation |
| SBJ-33-C5-AMC-22-DR-813 | Assembly and installation, K12 - Cable stayed bridge, Construction stages |
| SBJ-33-C5-AMC-22-DR-820 | Assembly and installation, K12 - Construction joint, Joint overview |
| SBJ-33-C5-AMC-22-DR-821 | Assembly and installation, K12 - Construction joint, Guide and positioning joint |
| SBJ-33-C5-AMC-22-DR-822 | Assembly and installation, K12 - Construction joint, Positioning joint |
| SBJ-33-C5-AMC-22-DR-823 | Assembly and installation, K12 - Construction joint, Locking joint construction 1 & 2 |
| SBJ-33-C5-AMC-22-DR-824 | Assembly and installation, K12 - Construction joint, Locking joint construction 3 |
| SBJ-33-C5-AMC-22-DR-850 | Assembly and installation, K12 - Floating bridge assembly site setup in Søreidsvika |
| SBJ-33-C5-AMC-22-DR-851 | Assembly and installation, K12 - Low floating bridge assembly method |
| SBJ-33-C5-AMC-22-DR-852 | Assembly and installation, K12 - High floating bridge assembly method |
| SBJ-33-C5-AMC-05-DR-900 | Road alignment overview |
| SBJ-33-C5-AMC-05-DR-910 | Road alignment K12, Part 1 |
| SBJ-33-C5-AMC-05-DR-911 | Road alignment K12, Part 2 |
| SBJ-33-C5-AMC-05-DR-920 | Road alignment K12, Detail geometry northern end |

# 1 Executive summary

The Norwegian Road Administration has requested planning and engineering services for further development of the Bjørnafjord crossing, consisting of evaluation and ranking of four nominated floating bridge solutions, in a concept development project phase denoted “Phase 5”.

The companies Aas-Jakobsen, COWI and Multiconsult with Johs. Holt have formed a Joint Venture to perform this task, involving the companies Aker Solutions, NGI, Entail, Dissing + Weitling and Moss Maritime as subconsultants. The project group is composed of companies with long history in the Bjørnafjorden project, and with key personnel with unique experience from the marine and bridge field, many with a combination of both.

A concept evaluation report outlines the process of ranking four alternative solutions for crossing E39 Bjørnafjorden:

Alternative K11: End-anchored floating bridge in accordance with Phase 4 of the project, optimized with respect to architecture, road alignment and layout.

Alternative K12: End-anchored floating bridge in accordance with Phase 4 of the project, optimized with respect to architecture, road alignment and layout, and with a supplementary mooring system. The mooring system would make the concept more robust and eliminate uncertainties from the potential phenomenon called “parametric instability”.

Alternative K13: Straight side-anchored floating bridge in accordance with Phase 4 of the project, optimized with respect to architecture, road alignment and layout.

Alternative K14: S-shaped side-anchored floating bridge, optimized with respect to architecture, road alignment and layout, and also with adjusted plan geometry to avoid uncertainties with respect to the articulation system in north end.

The ranking process has outlined K12 as the preferred solution. The chosen layout is shown in General View drawings included in Appendix A of this report.

Throughout this phase of the project, advanced static and dynamic analyses in both frequency domain and time domain have been performed in order to make a thorough design. A risk-based approach has ensured that major risks are identified and sorted out. Risk analyses on operational and construction phases have been used actively in the design process by means of frequent workshops to mitigate risk elements.

During the work, considerable attention has been paid to the phenomenon “parametric instability” or parametric resonance. In contrast to traditional resonance, where an external force applied at or near a natural frequency of the structure results in resonance, parametric resonance is caused by an oscillating variation of one or more of the system properties. The focus for the Bjørnafjorden Bridge has been parametric excitation caused by an axial force variation that induces variation in the geometric stiffness of the system. There is no generally accepted design approach available for this phenomenon today. Hence, concrete conclusions should be drawn with care. Other main focus areas for the work include:

- Ship collision
- Combined wind and wave action
- Fatigue
- Comfort criteria
- Temporary phases

- Anchor locations
- Visual impact
- Robustness

The study has produced a relevant basis for a detailed cost estimate and evaluation of the concept.

A ranking of the four concepts K11 to K14 is conducted by assessing the concepts against a chosen set of impacts. A comparative risk assessment is executed, and the accumulated risk is an important part of the final appraisal. The results of the assessment is collected in an appraisal summary table that form the basis of the recommendation of the best concept, see table below.

*Table 1-1 Appraisal summary*

| **Concept** | **K11** | **K12** | **K13** | **K14** |
|---|---|---|---|---|
| Cost, rank | 2 | 1 | 4 | 3 |
| Cost, significance | (--) | 0 | (---) | (--) |
| Visual Impact, rank | 1 | 1 | 4 | 3 |
| Visual Impact, significance | 0 | 0 | (--) | - |
| Risk, rank | 4 | 1 | 3 | 2 |
| Risk, significance | (---) | 0 | (--) | - |
| **Overall rank** | **4** | **1** | **3** | **2** |

All three steps of the development have concluded that alternative K12, end anchored floating bridge with supplementary moorings, is superior to the other alternatives. It appears as a cost effective and robust solution without major risk elements and with the best aesthetic score. It combines the major advantages from the other alternatives without having major drawbacks.

Alternative K11 generally represents a less robust concept than alternative K12. Further, even though a considerable effort has been carried out, uncertainties remains with regards to “parametric instability”, representing risks for irreversible and unstable behaviour. These risks are regarded unacceptable.

Alternatives K13 and K14 have challenges regarding anchor locations in steep areas and in rock areas. They are also considered to be less attractive with regards to aesthetic appearance.

With regards to costs alone, K12 is beneficial compared to the other alternatives, however, the cost difference between the alternatives is regarded as small.

Conclusively, K12 is a robust concept that combines state of the art technology and solutions in a way that will create a world breaking record in bridge construction.

*Figure 1-1 K12 from view point south*

*Figure 1-2 K12 from north*

# 2 General

## 2.1 Introduction

To construct a floating bridge to cross Bjørnafjorden is perhaps the largest technical challenge in the field of transportation in Norway in modern times. The project will put Norway on the map as a leading developer of future strait crossing concepts, bringing the whole industry a long step forward technologically. As with all technical solutions that cover new technology, it is important to identify and assess the particular challenges of the proposed solutions, which can also have a major impact on the implementation of the project.

A number of challenges have been identified in earlier phases of the project and taken into account in cost-vice uncertainty assessments. In this phase of the project, phase 5, it is a focus on reducing these uncertainties to both reduce the overall costs as well as to recommend a selection of alternative based on the most reliable analyses and assessments.

## 2.2 Project challenges and risks

The project group's work on the floating concepts in the previous phases of the Bjørnafjorden project, was largely characterized by analysis-driven design development, and through this work the design group gained a good basic understanding of the behaviour of the structures. Some items remained open towards the end of the previous phase and are therefore explored more closely in phase 5 of the project. In parallel, considerable academic work has been done regarding the response and sensitivity of the different concepts. Some of the challenges may require further work to be solved, and the role of the project group is primarily to evaluate the consequences of the various challenges and how they may be considered during the remaining design phases.

The design team has focused on the following elements in the design development and verification course for the current project phase:

- Dynamic stability of the end-anchored bridge (e.g. parametric resonance).
- Fatigue evaluations globally and locally.
- Effect of hydrodynamic interaction between pontoons.
- Effect of inhomogeneous sea and wind.
- Evaluation of possible coupling effects between different environmental contributions.
- Evaluation of ship impact.
- Evaluation of movement and updated comfort requirements.
- Evaluation of the effect of various damping contributions.
- Reduce uncertainties in construction, interconnection and installation methods.
- Robustness check of damaged conditions.
- Anchor locations.
- Risk assessment and mitigation measures

## 2.3 Project goals

The project will recommend activities and plans for the next phase of the project, phase 6, which is planned to be the last phase before the detail design phase.

The overall target for phase 5 of the project has been to recommend a solution for the crossing that is minimized with respect to risk and cost as well as optimized with respect to aesthetics, construction methods, operation and maintenance.

In addition, the goal is to conduct such a comprehensive evaluation and documentation, that it ease the way forward for the Client towards a final realization of the project.

# 3 Description, evaluations and risk assessment of K12 base case solution

## 3.1 General

After establishing the initial base cases for K11 to K14, the project team has further developed and evaluated these base cases throughout the process. The purpose of this is as follows:

- Improve ranking methods
- Cost estimations
- Risk assessment
- Perform updated ranking
- Determination of structural details
- Optimization

The following items are however unchanged from the initial stage:

- Road alignment
- Pontoon distance of 125 m
- Pontoon shape
- Girder height

For the stay cable bridge, only minor changes have been made, the back span column and the tower are modified. The main span of 380 m is kept for all concepts.

The main changes from initial base cases, are changes in cross-sectional properties of main girder and column, abutment in north and that the layout of mooring lines is updated.

In the process, the design team has been focusing on tasks which will influence the concepts and especially tasks which result in differences between the concepts.

The process has led to a ranking of base cases K11 to K14, where alternative K12 if found to be superior to the others.

## 3.2 The K12 curved end anchored bridge with supplementary side anchors

### *3.2.1 Key figures*

*Table 3-1 K12, curved end anchored bridge with supplementary side anchors*

| Description | Unit | Quantity | Comment |
|---|---|---|---|
| Total bridge length | m | 5530 | |
| Floating part length | m | 4750 | |
| Fixed part length | m | 780 | |
| Span width floating part | m | 125 | |
| Span width main span | m | 380 | |
| Min. horizontal radius | m | 5000 | |
| Top elevation floating part | m | 18 | |
| Max. road alignment inclination | % | 3 | |
| Ship channel (width x height) | m | 250 x 45 | |
| No. of pontoons | - | 38 | |
| Pontoon dimension (length x width) | m | 53 x 14.9 | “Circtangular” shape |
| Draft pontoons | m | 5.0 | 7.5m for anchored pontoons |
| Freeboard pontoons | m | 3.5 | |
| Number of pontoons with anchors | - | 3 | |
| Total number of anchors | - | 12 | |
| Column shape | - | Rectangular | With chamfered corners |
| Tower shape | - | A | |
| Bridge deck height floating part | m | 4 | |
| Bridge deck width floating part | m | 27 | |
| Bridge deck height fixed bridge part | m | 3.5 | |
| Bridge deck width fixed bridge part | m | 28 | Distance between cables 1m below top face elevation |

### *3.2.2 Overall description*

The K12 bridge concept is an end-anchored floating bridge similar to alternative K7 from phase 4 of the project. It is adjusted to fit performed optimizations with respect to architecture, road alignment and layout as well as introducing supplementary side anchors in three locations along the bridge. The adjustments from earlier phases involve for instance:

- A straight cable stayed part in the horizontal plane.
- A reduced main span length of 380m.
- Optimized vertical curvature for landscape adoption in north and south as well as improving the driving impression.
- Back span adjustment in cable stayed bridge introducing asymmetric stay configuration and concrete viaduct.
- Increase typical floating bridge span to 125m.

- Introduce revised boundary conditions between bridge girder and tower as vertical aligned sliding bearings on each side of the bride deck.
- Introduce optimized bridge girder shape externally and internally with regards to heavy bending moment and shear lag reaction as well as shaped to avoid major wind drag.
- Introducing sets of side anchors in three locations along the floating bridge to avoid unwanted parametric response.

In principal, the solution is an end anchored floating bridge with supplementary sideways supports from moorings anchored to the sea bottom. The shape is C-formed in the horizontal plane, and the road inclines smoothly from an overall elevation of 18m across the fjord up a main span with a one tower cable stayed fixed bridge at the south end of the bridge, where major ships can pass. The floating pontoons, pontoon columns and the bridge girder are in steel except for a concrete viaduct part in the back span of the cable stayed bridge. The columns in the fixed part as well as the main tower and abutments are in concrete.

General plots of the bridge are shown below.

*Figure 3-1 Overview K12*

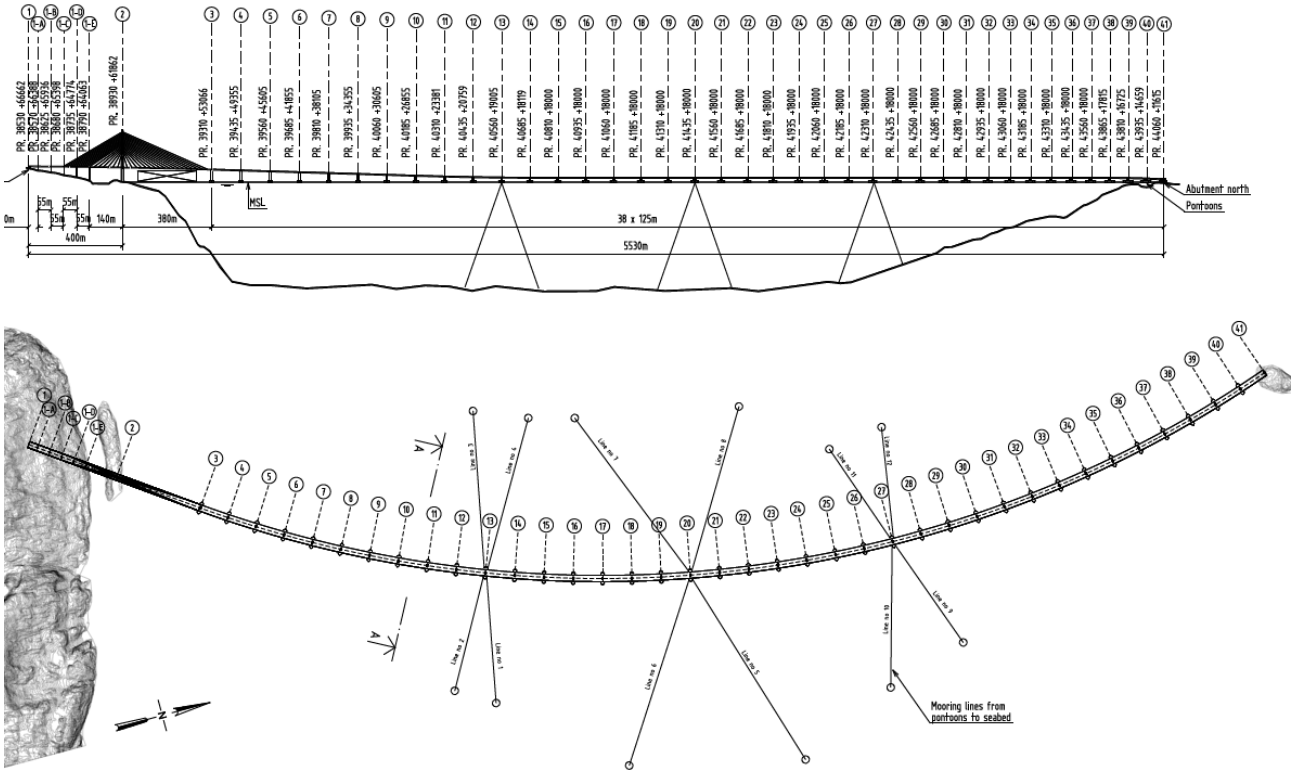


*Figure 3-2 General view K12*

### *3.2.3 Governing conditions and special challenges*

The K12 bridge concept is an arch type bridge which is curved in the horizontal plane with a radius of 5000 m for the floating part and straight for the stay cable bridge in south. The girder is fixed at abutment in south and in north and supported sideways and vertical at the tower using sliding bearings. In the back span of the stay cable bridge the girder is monolithically fixed to the columns. The bridge girder is supported with three mooring clusters, each with 4 mooring lines. The clusters are placed at 1/3 and 2/3 positions of the bridge as well as in the middle. All the mooring lines are anchored with suction anchors located on a relative flat seabed with sufficient seabed soil for installation and stability. The mooring lines consist of a top chain, a 124 mm steel wire and a bottom chain.

The bridge girder in the floating part is an orthotropic steel box girder 4 m in height and 27 m wide without the wind nose. The girder has span lengths of 125 m and is supported on steel columns placed on steel pontoons. The columns have a quadratic shape towards bridge deck and pontoons in order to make the connection simple and favourable for fatigue loading. The columns have chamfered corners in the middle part to reduce wind load and for improved aesthetic. The pontoons have a circtangular shape, and are 53 m long and 14.9 m wide. The ordinary pontoons have a draught of 5 m while the anchored pontoons have a larger draft of 7.5 m. The freeboard is chosen to be 3.5 m.

The stay cable bridge in south, which is described in chapter 7, has a main span of 380 m giving ample space for a required navigation width of 250 m. The stay cable bridge is self-anchored in the in the back span girder using a heavier concrete section supported on piers. In this way the length of the back span can be shortened and is independent of the position of the abutment which can be placed where the girder meets the terrain. Reasons for shorter back span can be aesthetic aspects,

economy and increased vertical stiffness of main span. Increased vertical stiffness will, however, give increased response from tidal water so the designer must balance the effect of reduced deformation due to traffic loading and wind loading against the increased response from tidal water variations. For aesthetic reasons it was decided to support the girder sideways at tower giving a narrow A-shaped tower.

Design of the bridge girder is described in chapter 6.7. The steel box has transverse trusses and bulkheads with centre distance approximately 4.0 m. The top plate thickness is 16 mm while the bottom plate thickness varies from 12 mm in span to 22 mm at the supports. The sections are checked according to Eurocode NS-EN 1993-1-5 in ultimate limit state for Von Mises stresses and for direct stresses accounted for plate buckling effects. Since the code is not conclusive for section which are not double symmetric, two methods have been used for the latter check. The methods differ most if the moment about the two axis gives stresses of equal magnitude. It is believed that the second method where sectional modulus is calculated for the individual positions in section gives the most realistic value, although this method may in some cases underestimate the capacity of section. The correct answer is if sectional properties is calculated for the combined effect of forces, but this is a tedious task which can be done only for a few selected sections and load cases.

Longitudinal walls in girder are introduced to reduce the shear lag effects in ULS and fatigue calculations. At present, the shear lag effects are calculated according to chapter 3 in EN 1993-1-5:2006. The shear lag is also verified with a finite element analysis giving similar values. For the present layout, the effective bending stiffness due to shear lag in ULS is approximately 95% of the gross bending stiffness for span sections. For SLS and FLS the stiffness is approximately 75%. For support section the stiffness is 100 % in ULS and 80 % in SLS and FLS. It is chosen to use the SLS stiffness in the global analysis while the respective stiffness in ULS and FLS is used for stress calculations. The shear lag will depend on the type of loading and calculations according to Eurocode is based on distributed loads. Other possible loadings are dynamic loading mobilizing the mode with pontoons going up and down (stamping mode) and point loads from traffic. The first loading will give an effective length of 1.0 L as compared with the distributed load of 0.7 L at span section and 0.5 L at support. The Eurocode will for this load case give a conservative shear lag. For point loads in centre of all span the effective length is 0.5 L which for span section will give more shear lag. However, for FLS calculation, traffic load will only load one span at a time and the corresponding effective length is 0.68 L for span section which is close to the 0.7 L used in Eurocode. It is therefore concluded that shear lag effects based on distributed loads will be acceptable for both span section and support section.

Fatigue calculation of bridge girder includes stress cycles from global response from environmental loads and traffic loads and from response from local traffic loads. Reference is made to chapter 13 for details. It is seen that when including stress cycles from local traffic loads minimum plate thickness of 16 mm will be required. Traffic load model 4 given in EN 1991-2:2003 is defined by the Client. This model is believed to give too high axle loading for Norwegian roads. It is therefore decided to define the maximum axle load for traffic type “medium distance” that satisfy the fatigue capacity of a 16 mm top plate. Thus, on drawings and for material amounts, a minimum thickness of 16 mm for the top plate is chosen.

The development of K12 concept is shown in Figure 3-3, Figure 3-4 and Figure 3-5. In the initial stage of the project, status 1, two mooring clusters where placed in 1/3 position of the girder with the aim of supressing the first asymmetric dynamic mode for the curved bridge. This reduced the dynamic wind response and increased the lowest buckling capacity. The stiffness of each cluster was approximately 1000 kN/m which makes the arch effective to withstand asymmetric loading and still

maintain the arch action for uniformly transverse loading. The mooring layout was not so effective to supress higher horizontal modes with eigen periods from 10 to 30 seconds which can be triggered by swell waves and by parametric excitation. In order to influence these modes, the stiffness of mooring must be increased considerable which is not practical with the chosen steel lines. Also increased mooring stiffness will mobilize unwanted mooring forces from first order waves and temperature changes.

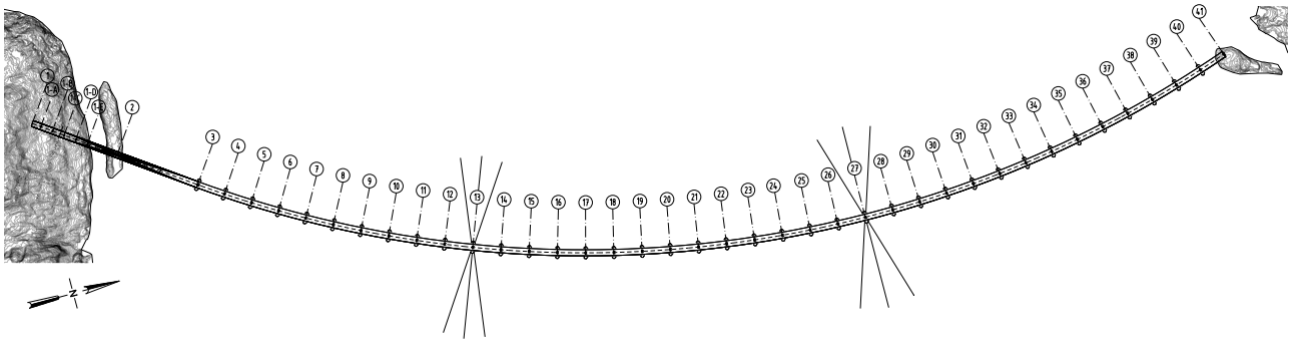

*Figure 3-3 Status 1, 2019-01-28, 2 x 6 = 12 anchor lines*

In the development phase of the project, Status 2, a mooring layout equal to the straight bridge was tried. This layout will control more modes and thus reduce the dynamic from higher modes. However, it was a challenge to find adequate anchorage position at seabed for suction anchor which are safe for submarine landslide during an earthquake. Especially were the anchorage of the mooring cluster in north and south challenging.

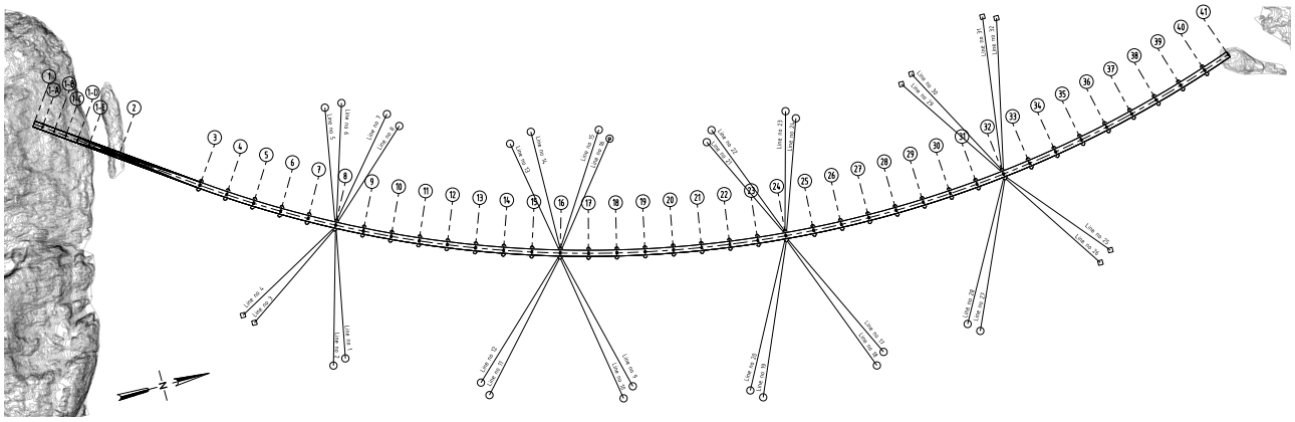

*Figure 3-4 Status 2, 2019-03-29, 4 x 8 = 32 anchor lines*

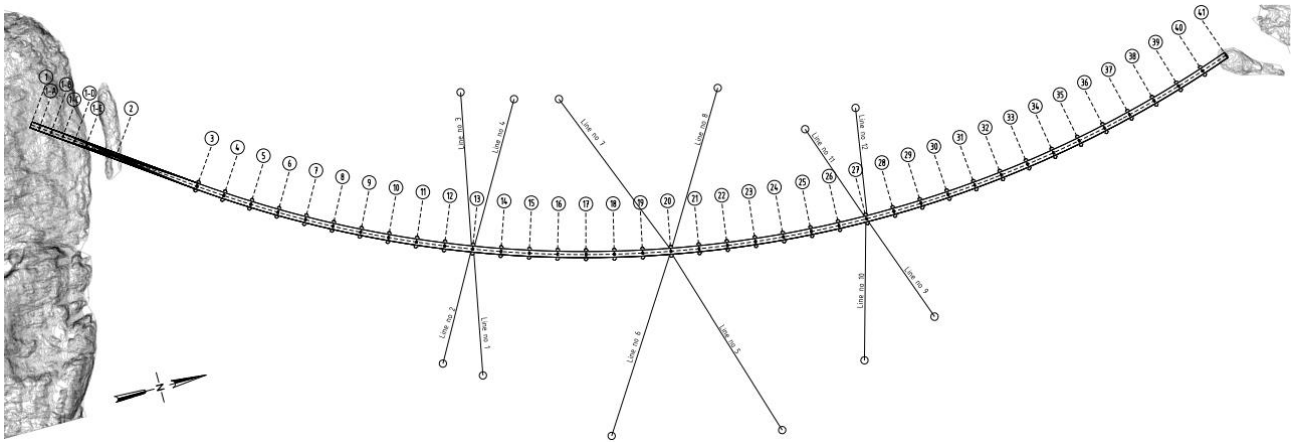

*Figure 3-5 Begrunnet innstilling, 2019-05-24, 3 x 4 = 12 anchor lines*

In the final stage, the design group wanted to restrict mooring cluster within 1/3 of the bridge length of the middle part of the fjord for geotechnical reasons. Status 1 had shown that cluster in 1/3 point was effective. In the final layout an extra cluster was placed in the centre of the bridge giving a total of 3 clusters each with 4 mooring lines.

The design group developed a method to optimize the mooring line damping as a part of the analysis. The response of the mooring lines in the critical frequency range is governed by the quasi-static response, meaning that the most important factors for the quadratic mooring line damping are drag coefficient, diameter, weight, length and pretension of the mooring lines. The damping will increase with pretension up to a given level. For the chosen mooring lines, this level is approximately 3000 kN. The chosen pretension is approximately 2000 kN giving a horizontal stiffness of clusters varying from 350 kN/m to 800 kN/m. The sensitivity of quadratic damping due to change in pretension has been investigated. Reducing the tension by 30% will reduce the damping ratio by 50-60 %. For swell sea this result in an increased moment of 10% corresponding to a nominal stress of approximately 20 MPa. It is seen that the damping level for the present K12 is in an area where the response is little sensitive to change in damping ratio of 50%.

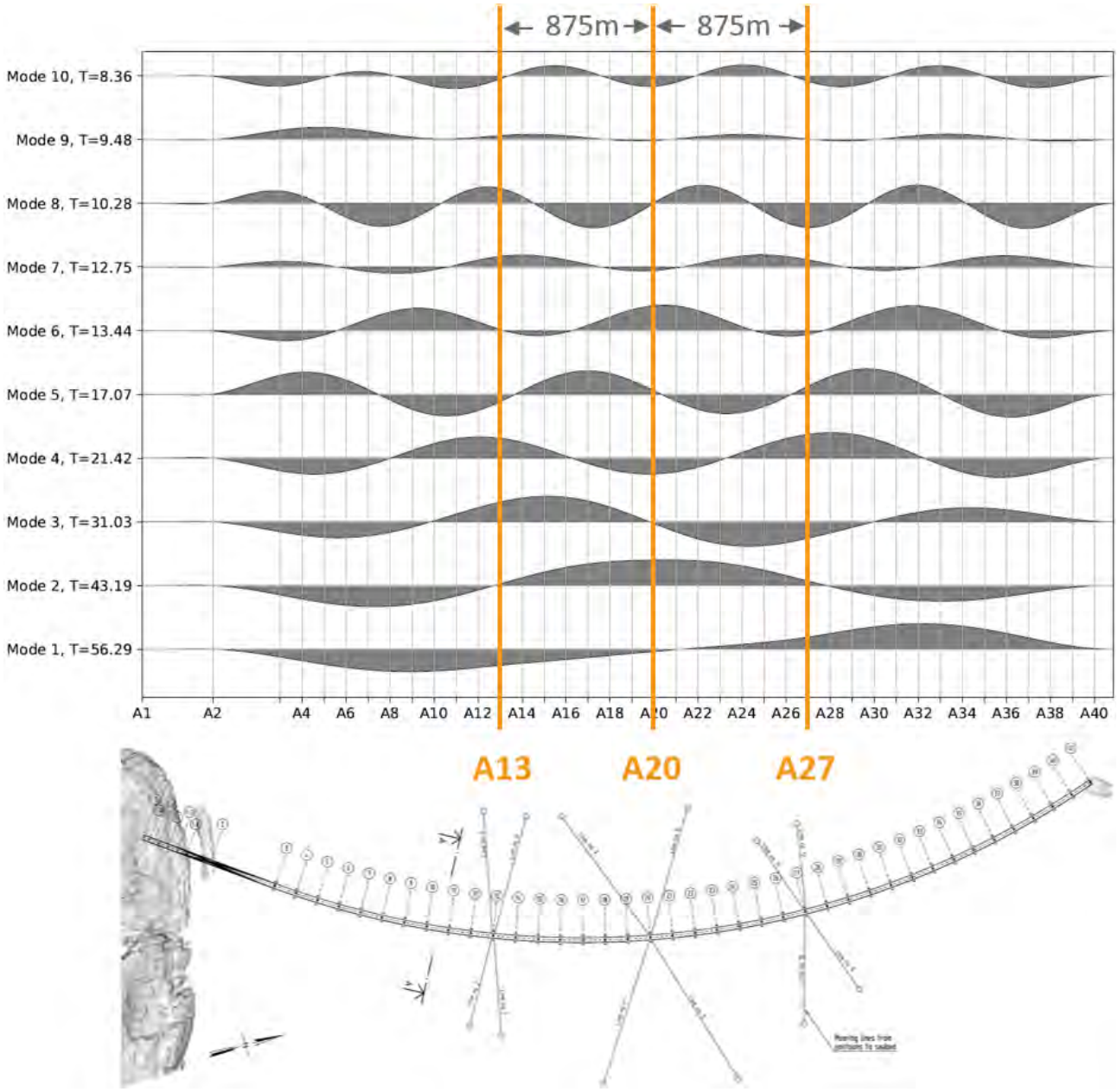


*Figure 3-6 Horizontal eigen modes for K12*

In Figure 3-6 the 10 first transverse eigen modes are shown together with the position of the 3 mooring clusters. Compared with a bridge with no mooring lines, the stiffness of the 3 cluster will influence mode 1 and 2 while mode 3 to 6 is not significantly influenced by the mooring stiffness. However, the damping of the mooring cluster will be significant for all the 6 modes except for mode 5, reference is made to Figure 3-7 which show the damping with and without mooring lines.

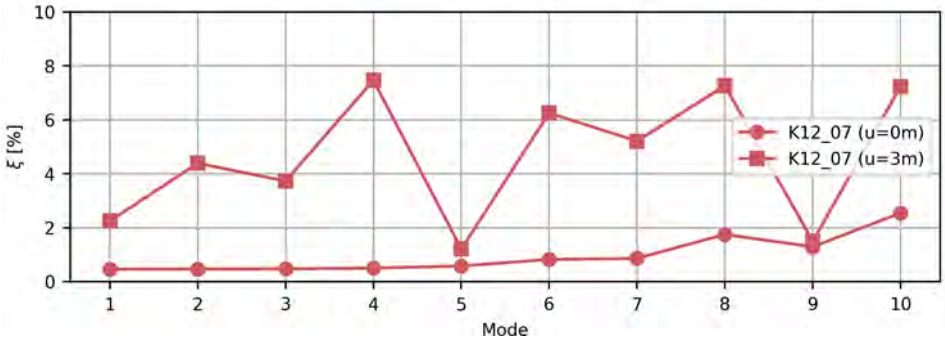


*Figure 3-7 Damping ratio of the first 10 horizontal modes*

Mode 6 in Figure 3-6 is the dominating axial mode which can be mobilized by swell waves. This in turn can trigger mode 4 by parametric excitation. The damping in mode 6 will help to reduce the axial force induces by swell waves. Further, will damping from mooring lines effectively reduce the response in mode 4 which potentially can be parametric excited by mode 6. For further details about parametric excitation, reference is made to chapter 12.

### *3.2.4 Pros and cons compared to the other alternatives*

The K12 alternative is a-hybrid solution between the classic end anchored floating bridge and the side anchored. It embraces the benefits of each solution to become the most optimum solution for the crossing with respect to:

- Keep the aesthetical benefits from the end anchor solution K11.
- Provide side anchor safety to the bridge against dynamic parametric response, ship collision and global buckling.
- Enable cost optimization of steel girder due to low risk level and supplementary supports from side anchors
- Believed to be most robust alternative due to increased level of redundancy

To summarize towards the other alternatives, the advantages with K12 are:

- The most aesthetical alternative (equal to K11)
- The lowest investment cost
- The lowest total cost (sum of investment cost and operational cost).
- The lowest operational risk (equal to K13 and K14)
- The lowest overall risk (Sum of operational and installation risks)
- The highest redundancy for accidental situations.

A challenge of K12 is believed to be that the element of mooring/anchor is introduced to the solution. This is however judged to be mainly a cost issue, since a large deal of knowhow of production, installation and operation of moorings is available within the Norwegian offshore industry. The potential disadvantage of moorings is just valid when compared to K11. K12 has less moorings than K13 and K14, and thus less operational costs and risk.

Similar to above, to summarize possible disadvantages with K12 compared to the other alternatives:

- Higher operational costs than K11, due to the introduction of moorings. The differences in cost compared to K11 is less than 1,5% of the investment cost.
- Higher installation risk than K11 due to the moorings. As stated above, the risk related to the moorings is however judged to be low, due to extensive experience and knowhow related to moorings.
- Anchorage at seabed (however placed in the middle part of the fjord which is beneficial compared with K13 and K14).
- Increased force in moorings due to temperature loading of superstructure.
- Some uncertainty related to availability due to wind climate (The uncertainty is less for K13 and K14, but equal for K11).

Final remarks regarding some detail observations that the K12 concept has:

- No expansion joints
- Moderate response in ULS condition.
- Moderate dynamic response in transverse direction which is beneficial for fatigue life.
- Possibility to control parametric resonance by damping from mooring lines.
- High buckling capacity of girder in transverse direction compared with K11.
- High robustness against non-uniform transverse loading as well as ship collision.

## 3.3 Cost estimates

The cost of the bridge is estimated comprising abutments, road north, floating bridge, cable stayed bridge, equipment and technical installations.

Total length calculated is 5771m including 110m road north. The estimate starts at stage profile 38.499m and ends at 44.270m.

The investment cost comprises all the costs regarding deliverables, assembly and transport, including temporary works and other works done on site.

The quantities are derived based on the performed design and the produced drawings, and can be summarized as given in the table below.

*Table 3-2 Quantities as basis for cost estimation*

| Main elements and sub elements | Material | Unit | Quantity |
|---|---|---|---|
| | | | |
| B Structure | | | |
| B1 Cable stayed bridge | | | |
| B1.1 Concrete girder | concrete | m3 | 8 300 |
| B1.2 Steel girder | steel | tons | 8 500 |
| B1.3 Columns (on shore) | concrete | m3 | 5 650 |
| B1.4 Tower above foundation | concrete | $m^3$ | 7 900 |
| B1.4 Tower above foundation | steel | tons | 300 |
| B1.5 Tower foundation | concrete | $m^3$ | 2 400 |
| B1.6 Stay cables | steel | tons | 1 000 |
| B1.7 Abutment south | concrete | m3 | 4 100 |
| B2 Abutment north | | | |
| B2.1 Abutment north, Gulholmane | concrete | m3 | 8 800 |
| B3 Road north | | | |
| B3.1 Excavating, blasting and landfill | road length | m | 110 |
| B3.2 Superstructure, road | road length | m | 110 |
| B3.3 Concrete bridge, north | concrete | $m^2$ | 1 350 |
| B3.4 Additional work/deliverables | | LS | |
| B4 Pontoons | | | |
| B4.1 Pontoon without moorings | steel | tons | 28 599 |
| B4.2 Pontoon with moorings | steel | tons | 3 224 |
| B5 Superstructure floating bridge | | | |
| B5.1 Girder | steel | tons | 69 037 |
| B5.2 Pylons on pontoons | steel | tons | 6 681 |
| B6 Assembly, superstructure floating bridge | | | |
| B6.1 Storage and logistics, girder elements | | LS | |
| B6.2 Assembly of large elements (pontoon + column + girder) | | LS | |
| B7 Moorings | | | |
| B7.1 Anchors, steel | steel | tons | 1 641 |
| B7.2 Chain stopper | steel | tons | 108 |
| B7.3 Chain | steel | tons | 1 175 |
| B7.4 Wire | steel | tons | 617 |
| B7.5 Coupling elements | | no. | 60 |

| | | | |
|---|---|---|---|
| B8 Assembly on site | | | |
| B8.1 Transport and installation of anchors | | LS | |
| B8.2 Pre installation of moorings | | LS | |
| B8.3 Hook-up and tensioning of mooring lines | | LS | |
| B8.4 Transport and installation of bridge on site | | LS | |
| B9 Equipment | | | |
| B9.1 Paving | asphalt | m² | 152 847 |
| B9.2 Road signs | | LS | |
| B9.3 Road lights | | LS | |
| B9.4 Railing | length rail | m | 45 288 |
| B9.5 Bearings | | no. | 4 |
| B9.6 Dehumidification equipment | | LS | |
| B9.7 Escalator and stairs | | LS | |
| B9.8 Additional installations | | LS | |

The calculated costs are as follows:

*Table 3-3 Total cost*

| **Investment cost** | **Cost (NOK)** | **Length (m)** | **NOK / m** |
|---|---|---|---|
| Cable stayed bridge | 1 083 868 600 | 791 | 1 370 251 |
| Floating bridge | 6 993 253 144 | 4 820 | 1 450 882 |
| Road north | 124 000 000 | 160 | 775 000 |
| Paving and equipment | 303 204 595 | 5 661 | 53 560 |
| **Sum** | **8 504 326 339** | **5 771** | **1 473 631** |

** 2019 level of costs*

For details, see Appendix P.

## 3.4 Risk assessment

### *3.4.1 Introduction*

Risks are an inherent part of both the design, construction and operational phase of a major infrastructure project such as the floating bridge E39 Bjørnafjorden. If identified and mitigated already in the early phases it will contribute to an optimized design and construction.

During this phase, four concepts have been evaluated and finally one concept has been selected. The concept selection is based on cost, visual impact and risk as depicted in appendix R, which also outlines the overall process behind the concept selection.

Risks for each of the four concepts have therefore been identified, assessed and potentially mitigated. Based on these risk assessments, the comparative assessment has formed the basis for ranking of the concepts according to their respective risk profile. This assessment has been carried out for both risks related to the construction and installation phase as well as risk related to the operational phase.

The risk ranking is a part of the overall concept evaluation conditional on concept compliance with rules and regulations.

The objectives of the risk management process can be considered two-fold.

1. An *optimization of design choices and construction methods* for each of the four concepts to achieve a balanced risk profile and identify mitigations that can secure budget/schedule and minimize risk of violating rules and regulations.
2. A *comparative risk assessment* to identify and highlight inherent differences between concepts to be used for concept evaluation.

### *3.4.2 Risk assessment framework*

General principles for risk management are applied in the project to the processes related to construction and operation. Thus, hazards are systematically identified and assessed, and mitigation measures are identified and used as means of reducing or clarifying risks. The process is supported by workshop sessions and is part of the project management process.

The risk management process is captured in a risk register. The risk register lists the identified risks, the risk evaluation and mitigation measures. The headers used are shown in the table below. The format used for this register makes it easier to compare concepts while at the same time being able to extract the risk register for each individual concept after concept selection. Furthermore, it ensures that the four risk assessments are conducted in a comparable manner such that the risks of one concept is not considered in more detail than another.

| ID | | Hazard description | | | | | | Risk level | | | | Mitigation | Responsible |
|---|---|---|---|---|---|---|---|---|---|---|---|---|---|
| Index no | Phase | Hazard | Design criteria | Consequence | Cause | In-place mitigation measures | Comment | K11 | K12 | K13 | K14 | Further mitigation measures/ actions | Responsible |

The risk is generally considered the product of probability of occurrence and consequence (or severity). It is, however, for this phase not considered preferable to evaluate the risks quantitatively and instead, risks are categorized and evaluated qualitatively in categories High, Medium and Low. Medium and High risks require that further mitigation measures must be identified and if possible be implemented in the design or the construction and installation methodology. High risks will generally be associated with very severe consequence which require major design changes or even significant concept changes. Effect of mitigation measures are either unidentified or very expensive or extensive.

### *3.4.3 Risk assessment process*

The risk assessment process leading to the recommendation of K12 as the preferred solution – also from an isolated risk point of view – is documented in Appendix R. Based on these comparative assessments, the risks relevant the preferred solution K12 have been subject to further detailing and are used as a tool for optimizing the design and the construction and installation methodology for K12. Thus, the remaining risks of importance for K12 are those that are not yet detailed to a level allowing for an evaluation as low risk hazards or those which are inherently of significance for the concept chosen and will require special focus throughout the design, construction and installation.

### *3.4.4 Risk assessment - operation*

From appendix R, it is seen that the topics of the remaining significant operational risks for K12 are:

- Operational availability (design criteria)
- Comfort criteria (design criteria)
- Ship collision (design criteria)
- Fire and explosion
- Vandalism/terrorism to floating or cable stayed bridge

A number of the medium risks remaining relate directly to fulfilment of design criteria and others are more general of nature. The medium risks for K12 are unchanged from the comparative risk assessment.

With respect to the operational availability and the comfort criteria further work shall be put into these criteria in the coming phases. Operational availability must be at least 99.5% meaning that the bridge can only be allowed unavailable 44 hours per year. The metocean design basis provided in this phase indicate that there could be an issue with closure due to wind effects on vehicles for certain wind direction. The alignment for K12 is particular sensitive to the highly turbulent wind from the southern sector and therefore these are assessed to Medium risk of exceeding criteria. Further analysis based on long term distribution of the wind should be undertaken but in agreement with NPRA this risk is flagged here but should not at current state impact the recommendation of concept.

The medium risk registered for ship collision is reflecting that a smaller change to the column design can be necessary in order to fulfil the requirements to ship collision loading as is. It is expected that further analyses will bring utilization down and show that the cross-sectional area of the columns is sufficient, and it is therefore not implemented in the design.

For risks related to fire, explosion, vandalism and terrorism the risk level is defined as medium to indicate the uncertainty related to these topics based on the limited work that has been put into these topics at current point in time.

More significant risks, which through the project phases are brought to low risk level for K12 by extensive analyses are:

- Parametric excitation
- Global instability
- Local and global ship collision
- Anchors and mooring lines (including geohazard)

The distribution on risk levels for the remaining 25 relevant operation risks are shown in Figure 3-8.

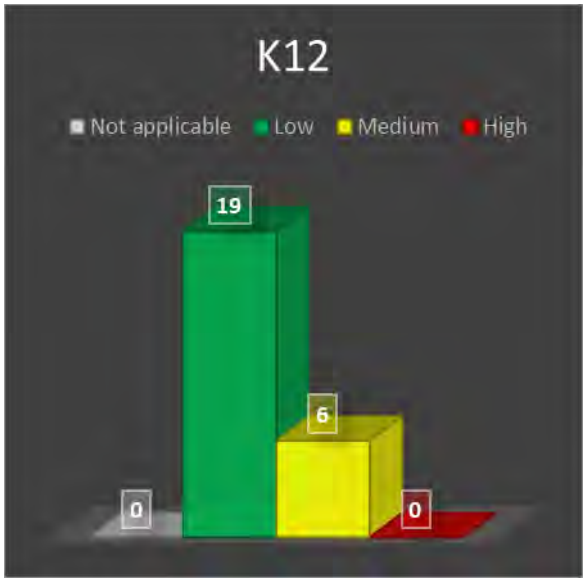


*Figure 3-8 Chart showing distribution of operation risk levels for concept K12*

### *3.4.5 Risk assessment - construction and installation*

From appendix R, it is seen that the topics of the remaining significant construction and installation risks for K12 are:

- Skidding and moving of the floating low-bridge at the inshore assembly line
- Connection of the low and high floating bridge sections
- Tow of the 4.5 km floating bridge from assembly location to site
- Lining up floating bridge and connecting winch wires to north section
- Engagement of guiding system in north, rotating bridge to final orientation, connecting winch wires in south and engaging positioning system joints in north and south
- Ship collision risk in all construction phases

A number of mitigations are identified for the remaining significant risks and many already implemented in the proposed construction and marine operations. Some of the medium risk operations such as the tow to site have an inherent risk, which will remain irrespective of the mitigations implemented. The entire operation of construction a floating bridge of these dimensions is of course not standard, and focus shall be on risk mitigation continuously throughout design and construction as the methodologies develop. However, the identified risks are all judged to be of manageable character given appropriate evaluation and detailing.

The distribution on risk levels for the remaining 23 relevant construction risks are shown in Figure 3-9.


*Figure 3-9 Chart showing distribution of construction risk levels for concept K12*

### *3.4.6 Overall risk assessment*

Evaluation of risks taking into account construction as well as the permanent situation for the floating bridge over Bjørnafjorden shows that even though a number of significant risks are and generally will be part of such a project, there is identified no showstoppers for concept K12. Thus, the concept seems robust from a construction and an operational point of view.

## 3.5 Further optimization

The aspects described below are measures for optimization that should be evaluated in later phases of the project. These possible optimizations described usually influence both visual impact, costs and construction and should therefore be carefully evaluated.

### *3.5.1 Span length evaluation*

Span length of 125 m is chosen for K12. For comparison between concepts, it has been considered beneficial to have the same span length. The design group recognizes that a 100 m span will give less steel in the girder itself, however more pontoons. Earlier investigation has shown that response from wind driven waves and swell gives similar response for 100 and 125 m span.

For the wind load the exposed area of girder will be reduced by 1-3.5/4 = 12.5% by going from a girder height of 4 m to 3.5 m. The drag factor will be approximately 10 % higher for the 3.5 m height, according to the wind tunnel tests resulting in a reduced wind load on girder of only 3%. Furthermore, the dimension of the column will be kept, since ship impact governs the design of these. Thus, the drag force of column per meter bridge length is increased by 125/100- 1 = 25%. In total the middle wind response will be nearly unchanged. Investigation show that the dynamic wind response will not increase proportional with the increased drag force, since increased drag also will give increased damping.

The difference will therefore mainly come from static vertical loading from permanent loads and traffic.

From permanent loads, the steel reduction in girder is approximately 1 t/m by going for 100 m instead of 125 m. Present fatigue calculation has shown that the top plate in girder should be

minimum 16 mm. This will also apply for 100 m span. Thus, no savings can be made for the top plate by going from 125 m to 100 m span.

Investigation show that wave loads will increase somewhat due to higher interaction effect between pontoons for 100 m. This may not be significant for ULS design, but may affect fatigue life which must be investigated.

Furthermore, a span length of 125m between the columns are preferred over 100m span length for aesthetic reasons. This is to achieve the most open structure as possible.

*Figure 3-10 125m span length*

*Figure 3-11 100m span length*

### *3.5.2 Roll stiffness of pontoons*

The length of pontoons is chosen to be 53 m long for all axes at this stage. The following aspect influence the roll.

- Roll due to traffic
- Roll stability during construction
- Roll stability during operating condition

Roll due to traffic shall be limited to 1 degree for 70 % of characteristic traffic loading. If traffic is placed on the shoulder of the roadway a roll of 1.9 x 0.7 = 1.33 degree is obtained around axis 6 which is above the given criterion, Ref. memo 10205546-11-NOT-088 chapter 3.2.5. If traffic is placed in the middle of the actual traffic lanes the resulting roll will be 1.05 degree which is close to the criterion. It must be considered if it is proper to place the traffic within the actual traffic lanes.

The overall roll stability of the high part of floating bridge is investigated for the effect of weight of traffic combined with wind on vehicles during 1-year storm condition which will determine if the chosen pontoons are adequate. This check is performed with wind on vehicles over half the bridge length and over the whole bridge length. The corresponding vehicle load considering traffic in one direction is only 20 kN/m compared with the ordinary 60 kN/m for load length shorter than 200 m. This load conditions will therefore not be governing compared with the ordinary ULS 2 where traffic dominates with load length less than 200 m and therefore wind on traffic can be neglected for global response.

### *3.5.3 Cable stayed bridge solution*

The cable stay bridge solution is determined from one way of construction this part using a steel box as a cantilever system in main span and partly in the back span, while the rest of the back span viaduct is done by means of a concrete bridge girder. An alternative to this is meant to be further utilization of the concrete girder in the whole back span. This may ease the construction and may also be more cost effective, but is kept as an option to the base case solution at this stage of the project. The cost effectiveness will depend on the unit price relation between steel and concrete erected at site.

In this alternative solution it has also been considered to verify if longer side- and viaduct spans will be feasible utilising the natural strength of the 3.5m deep concrete deck box structure, thereby save one pier and improve architecture with a shorter side span in combination with equal stay spacing. The concrete deck might also be extended further, say 40m, into the main span with possible cost saving as a result. This option might be possible as the ULS and ALS ship collision forces during this phase of the project, have stabilised at a limited bending moment of approximately 3000-3500 MNm, which the concrete box structure can easily resist. The development of the cable stayed bridge is presented as "alternative" concept in the figure below and also in a separate drawing in the drawings binder, see Appendix A. See also architectural evaluation in chapter 5.6.

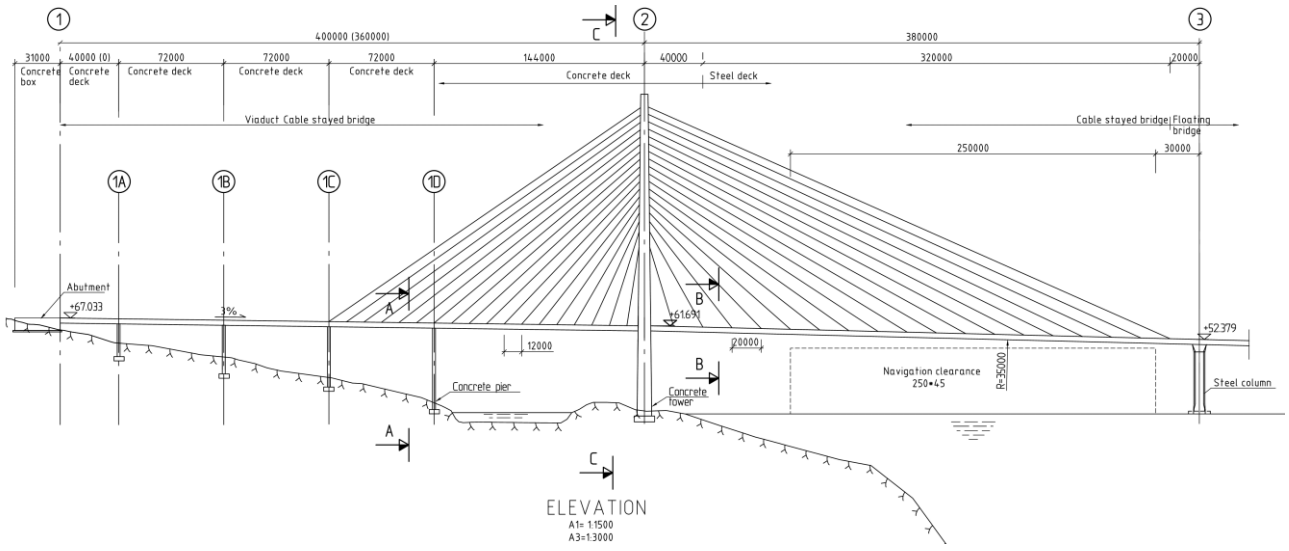


*Figure 3-12 Cable stayed bridge – "alternative" concept*

### *3.5.4 Possible visual improvements*

#### *3.5.4.1 A-shaped columns*

*Figure 3-13 "Base case" single columns and “optional” A-shaped columns*

Overall, the A-column is found to be the most aesthetical pleasing version. It describes in a logical way that the bridge is standing on its pontoons. The single vertical column version may appear irrational as it looks like a more conventional type standing on solid ground, not a column standing on a floating element. From an architectural point of view, it is therefore recommended to perform a further investigation of the feasibility and costs for the A-column in later stages.

The A columns is proposed with a dimension of 5.0 m x 8.0 m for each leg. Compared with the base case this will increase the column weight by approximately 50 %. The A column is expected to be more vulnerable for ship impact hitting the pontoons at a skew angle than the base case column.

### *3.5.4.2 Visual improvement, road alignment*

In the base cases shown, the road alignment is not optimized with respect to visual impact. In a later phase, this should be studied more carefully to find the optimum solution. This should at least involve the following aspects:

- Optimization with respect to landscape in south end
- Optimization/increase of vertical radius between horizontal floating bridge part and the inclined part
- Landscape/Waterscape adaption in north end

*Figure 3-14 Landing area south, K12*

#### *3.5.4.3 Visual improvement, tower*

The A-tower stands out as natural focus point in the landscape and has a strong "signal effect". Efforts should therefore be done to optimize this element aesthetically. Some ideas are outlined in chapter 5.7 and in appendix C to this report. Also, the importance of an elegant light scheme is emphasized, see figure below.

*Figure 3-15 Light scheme A tower*

# 4 Road alignment

The road alignments are designed for a fixed link consisting of a floating bridge combined with a cable stayed bridge across Bjørnafjorden from Reksteren in Tysnes Community to Gullholmane in Os Community.

Different alignments have been evaluated. The alignments are based on the previous bridge concepts alternative K7 but optimized to alternative K12.

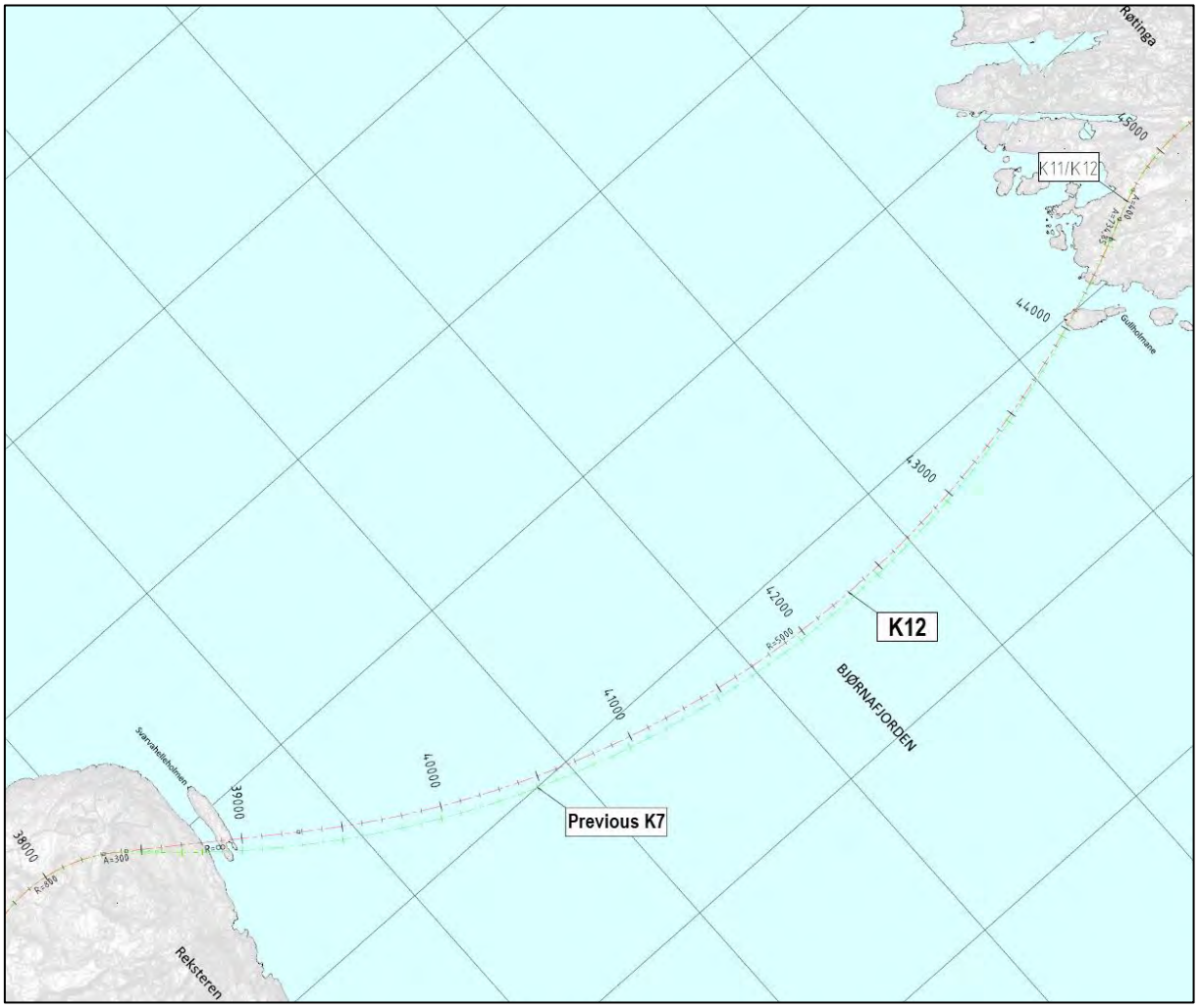


*Figure 4-1 Road alignment*

The road outside the bridge is placed on rock ground or fillings of blasted rock. From south, the road has a 3 km long road on land between a long tunnel and the bridge crossing Bjørnafjorden. From Gullholmane there is a filling and the road goes directly into a tunnel under Røtinga and Søre Øyane. The tunnels on each side give plenty of blasted rock on each side of the bridge available for fillings.

The road design class is to be H8 according to the N100 (Vegdirektoratet, 2013). This road class was originally suitable for traffic volume 12000-20000 AADT (Annual Average Daily Traffic) up to design speed 100 km/h. A new road class suitable for 110 km/h is described in NA-rundskriv 2015-02 (Vegdirektoratet 2015), and this is the road class this road has to be designed for the time being.

The stop sight as it is defined in “NA-rundskriv 2015/2” determines the minimum vertical radius to R=14100 m. In the south we have constructed a large vertical radius on the cable stayed bridge of

R=35000 m (alt. K11/K12 and K14) and R=50000 m (K13). This solves the sight problems that could be the result from tide and traffic load on a vertical curve at the start of the floating bridge.

The slope from the level of the cable stayed bridge down to the constant level over Bjørnafjorden at elevation +18 is 3 %. 5 % is maximum slope for this road class, but it is not advisable to use this maximum slope if you could avoid it. In this case we have large curves and 3D-studies show that 3 % is more in harmony with the other dimensions.

The concave vertical curve when the slope of 3 % meet the horizontal level is much larger than in earlier stage (R=5000 m). The current drawings are showing R=18000 in order to improve aesthetics. This curve could be even larger (R=40000 m) as desired from the architect. The economic consequences of lower slopes and larger curves should however be evaluated.

In the north, the road will go down into a tunnel under the sea, and this situation means that the vertical curve will start on the bridge and that the height at the abutment is about 5-6 m lower than the constant level of +18. This happens in the same area as the tide and the traffic load on the floating bridge will reduce the stop sight length. The minimum vertical curve should not be used where tide on a daily basis reduces the stop sight length. The vertical curve in the north is therefore increased to R=16000 m and the tunnel is about 2 m higher on the drawings than in earlier stages of the project.

# 5 Architecture

## 5.1 Introduction

An architectural evaluation is performed for the four bridge concepts. The evaluation focus on the aesthetical expression of the different floating bridge parts and cable stay bridge parts, including the overall alignment of the bridge concepts. The C-shaped bridge solution as in K12, is found to be superior to the other alternatives, aesthetically.

## 5.2 Alignment

It is important to make the road and bridge alignment blend in with the surrounding landscape. As the landscape surrounding Bjørnafjorden is a very scenic environment, it is especially important to make the bridge alignment an extension of the approaching road network with its movement through the landscape. When viewed from shore, the bridge should follow the curvatures of the landscape as much as possible and thereby feel more coherent with the existing landscape.

From a driver's point of view, a curved alignment provide an opportunity to experience the bridge and its elements in a shifting perspective. The shifting perspective of the tower makes it visually interesting and enables the drivers to see the tower as more than just as a portal.

The C-curve is a simple alignment which gently expresses the structural static system in the open waterscape. It seems very logical for a floating element, like a tensioned "Bow".

The curvature presents the main span and tower beautifully when approached from north. When continuing across the bridge, the drivers are guided smoothly towards it. From the south, the drivers will experience a dramatic "revealment" of the main span, tower, fjord and floating bridge when driving through the terrain cuts and onto the bridge.

*Figure 5-1 K12 - C-shaped bridge*

## 5.3 Columns

Overall, the A-column is found to be the most aesthetical pleasing version. It describes in a logical way that the bridge is standing on its pontoons. The single column version may seem irrational as it looks like a more conventional type standing on solid ground. From an architectural point of view, it is recommended to perform a further investigation of the feasibility and costs for the A-column in later phases.

## 5.4 Bridge girder

The tapered bridge girder is preferred in order to keep the visual impression of the bridge girder as slender as possible. The bottom flange should preferably correspond with the width of the column shaft. It is also recommendable to have the same bridge girder section on the floating bridge and cable stayed bridge in order to avoid unsightly transitions.

## 5.5 Pontoons

In the following phase, we recommend a further investigation of the feasibility and costs for various shapes of the pontoons. If possible, the visual expression of the pontoons should be enhanced without compromising safety or economy.

## 5.6 Cable stayed bridge

The inclining vertical profile and one-sided navigational span at the southern landing leads to an asymmetrical bridge. The “basecase” of our cable stayed side span has asymmetry to some degree and quite short spans. The side span stay arrangement is combined by two systems which can look unorganized from some angles.

The proposed “optional” side span underlines the asymmetry even more and extends the back span with 50%, which is more pleasing from an aesthetical point of view.

*Figure 5-2 "Basecase" stay cable and back span arrangement and “optional” arrangement*

## 5.7 Tower

The A-tower stands out as the most logical structure for the main span, both structurally and aesthetically. The simple pointiness of the A-shaped tower creates a natural focus point in the landscape and has a strong “signal” effect. The flared legs below the deck feels like the right answer to the horizontal forces that needs to be taken in the deck.

The tower is located on Svarvhelleholmen adjacent to the navigational clearance area. This provides an opportunity to have tapered tower legs standing on a small area on the island and the foundation to be below the ground covered by rocks.

The preferred “optional” tower is more refined and has a lighthouse beacon on top. With an elegant light scheme, the tower will be visible from a great distance at night. It will visually give the tower a certain lightness and elegance – an Icon for the fjord crossing.

It is recommended that this is further investigated in the next phase.

*Figure 5-3 "Base case" tower design and “optional” tower design*

# 6 Design of floating bridge part

## 6.1 General

Appendix K outlines the design of the floating bridge part. The fabrication of the bridge girder is described in Appendix N.

The results and evaluation of the fatigue analyses are given in appendix I and the results and evaluation of the analyses due to ship impacts are given in appendix J.

In this design chapter the design forces in ULS is also shown with envelope plot. For more information refer to appendix G.

The floating bridge part consists of the bridge girder, columns and pontoons. The typical floating bridge span is 125 meters. The floating bridge is divided in high part, valid for axis 3 – 8, and low part, valid for axis 9 - 40.

The focus has been to optimize the design of the floating bridge with respect to reduce the fabrication costs and increase the amount of automatic welding, and this in combination with a robust design.

*Figure 6-1 Typical floating bridge at lower part showing bridge girder, column and pontoon*

## 6.2 Materials

The floating bridge part is made of steel plates and profiles with material quality S420 M/N except for the pontoon plates in the splash zone which is of material quality superduplex 25CR. For the S420 M/N, the yield strength is 420 MPa and the ultimate strength is 500 MPa, according to NS-EN 1993-1-1:2005/A1+NA:2015. For the super duplex 25CR, the yield strength is 550 MPa and the ultimate strength is 800 MPa.

The material factor for steel design in ULS is 1.1, according to NS-EN 1993-2:2006+NA:2009.

## 6.3 Design load combinations in ULS

Ultimate limit state combinations were performed based on separate simulations of each load component (uncoupled approach) and combined with individual load factors. These results were used in design development, and several design iterations have been performed. Two methods were used for load combinations; a direct method based on combination of time series of the individual loads or a factorized method in which design forces are established individually and then combined. The former method can maximize the stress in each selected design point and is used for all design evaluations, but the latter gives an easier overview of the contributions of the individual load components. See Appendix G [1] for more info.

For the presented plot in this chapter the direct method is used. The ULS results comprises ULS2 which is dominating traffic load combined with 1-year environmental loads and ULS 3 which is 100 years environmental an no traffic on bridge.

*Table 6-1 Combination into – ULS2*

| Load group | Load_factor | Return_period [years] | Software system | Result type |
|---|---|---|---|---|
| **Permanent** | 1.20 | N/A | RM Bridge | Static |
| **Temperature** | 0.84 | N/A | RM Bridge | Static |
| **Traffic** | 1.35 | N/A | RM Bridge | Static |
| **Tide** | 1.12 | 100 | Orcaflex | Static |
| **Dynamic wind 1 y** | 1.12 | 1 | Orcaflex | Time series |
| **Static wind 1y** | 1.12 | 1 | Orcaflex | Static |
| **Wave 1 y** | 1.12 | 1 | Orcaflex | Time series |
| **Swell 1 y** | 1.12 | 1 | Orcaflex | Time series |
| **Current** | 1.12 | 100 | Orcaflex | Static |

*Table 6-2 Combination into – ULS3*

| Load group | Load_factor | Return_period [years] | Software system | Result type |
|---|---|---|---|---|
| **Permanent** | 1.20 | N/A | RM Bridge | Static |
| **Temperature** | 0.84 | N/A | RM Bridge | Static |
| **Tide** | 1.60 | 100 | Orcaflex | Static |
| **Dynamic wind 100 y** | 1.60 | 100 | Orcaflex | Time series |
| **Static wind 100 y** | 1.60 | 100 | Orcaflex | Static |
| **Wave 100 y** | 1.60 | 100 | Orcaflex | Time series |
| **Swell 100 y** | 1.60 | 100 | Orcaflex | Time series |
| **Current** | 1.60 | 100 | Orcaflex | Static |

## 6.4 ULS design forces for bridge girder

Envelope plots of the design forces in ULS 2 and ULS 3 are shown in this chapter. Responses for all concepts are shown in the same plots to better illustrate the differences.

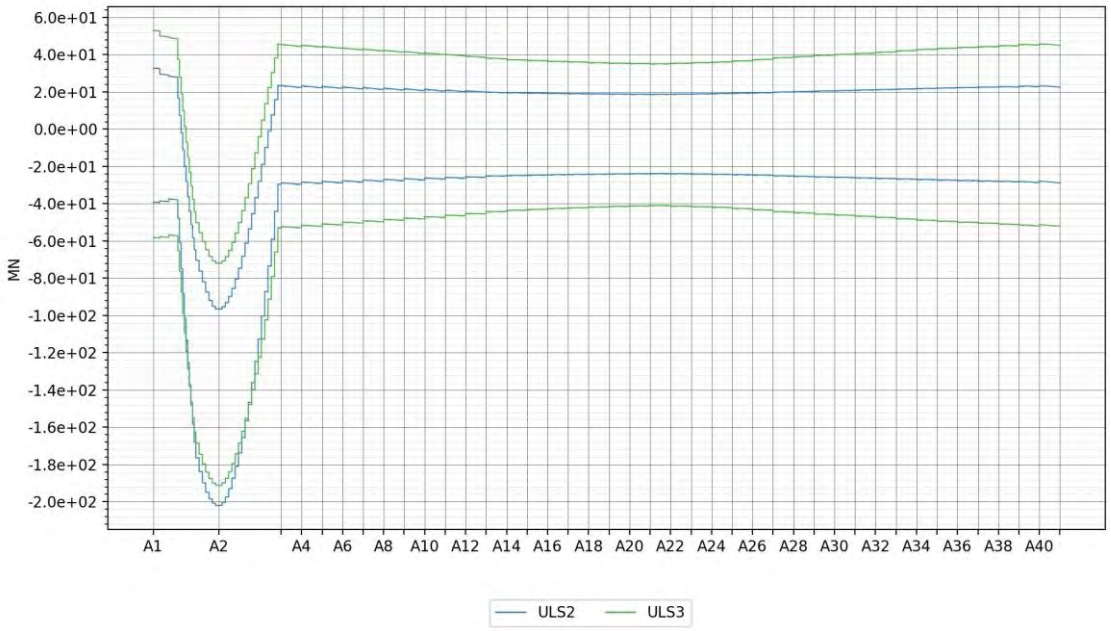


*Figure 6-2 Bridge girder axial force – ULS for K12_07.*

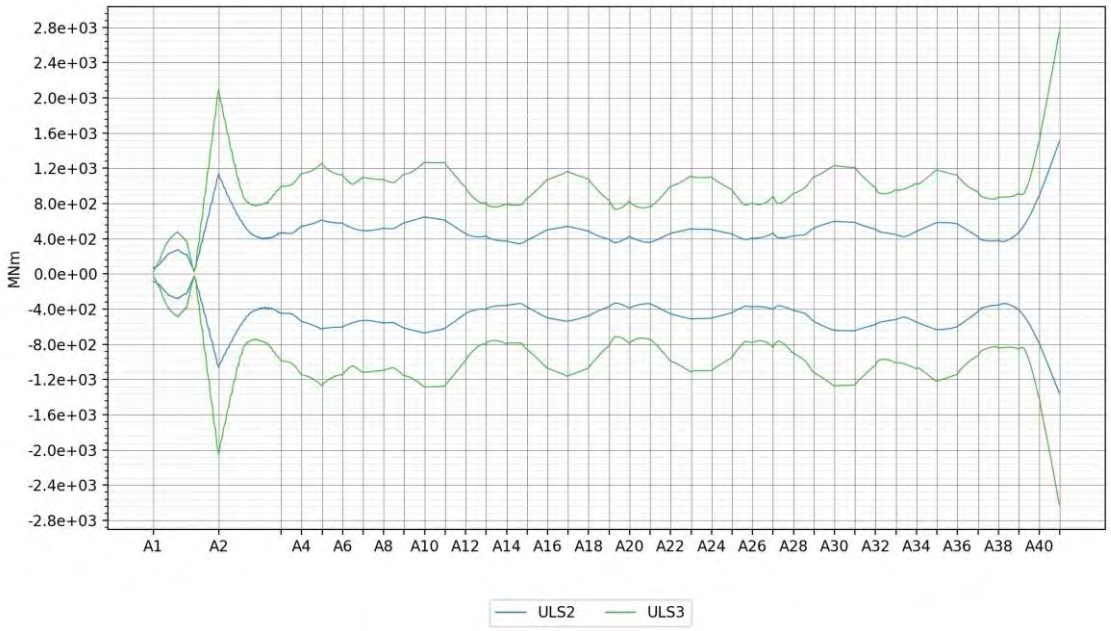


*Figure 6-3 Bridge girder bending moment about strong axis – ULS for K12_07.*

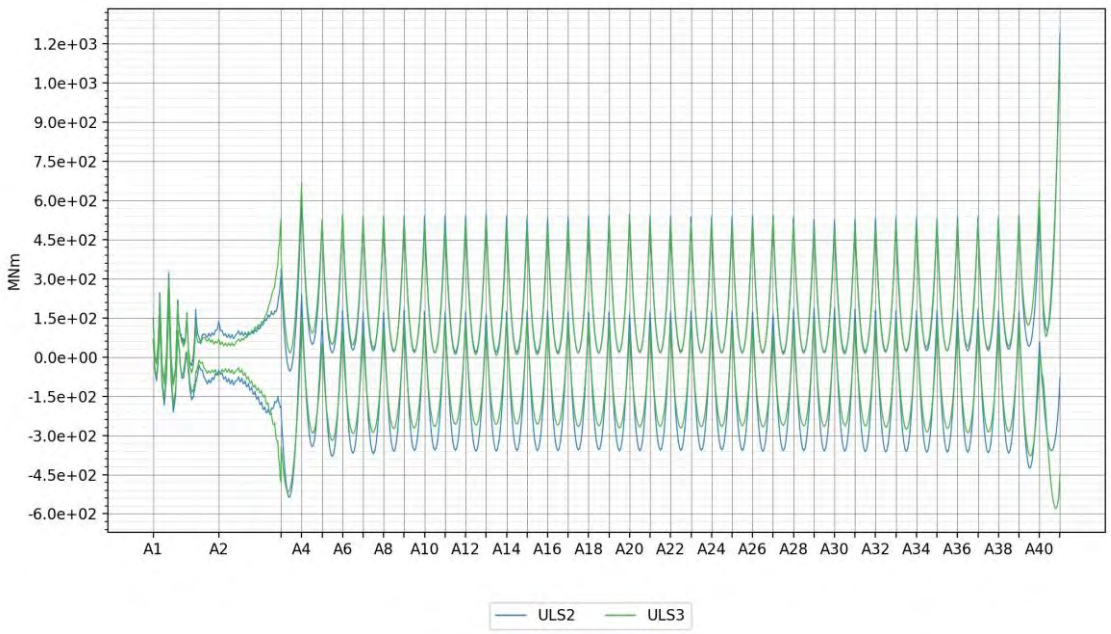


*Figure 6-4 Bridge girder bending moment about weak axis – ULS for K12_07.*

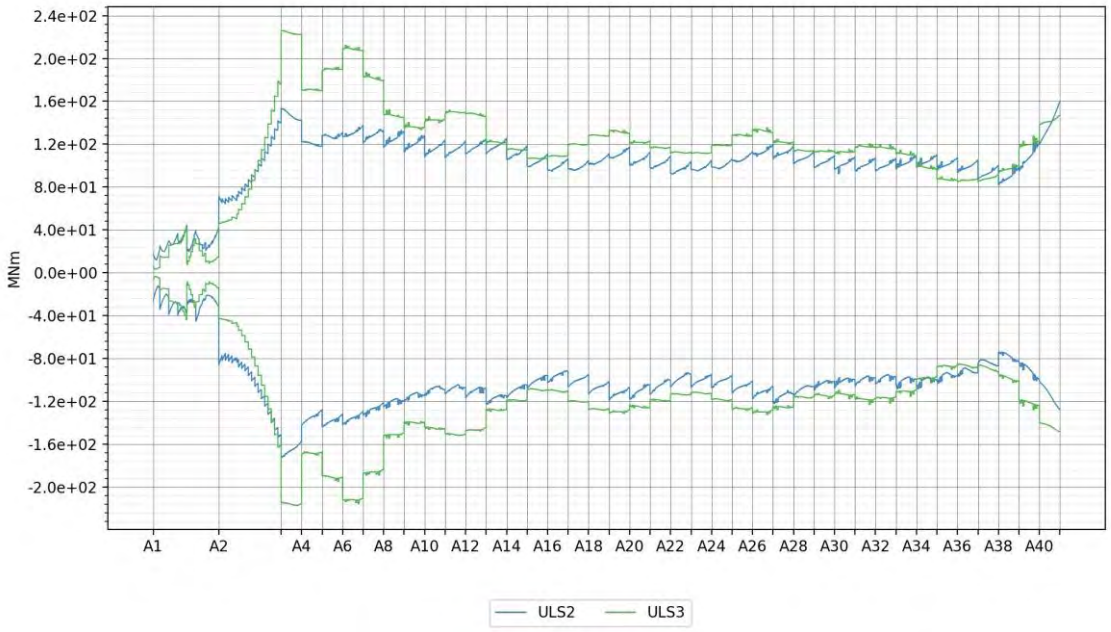


*Figure 6-5 Bridge girder torsional moment – ULS for K12_07.*

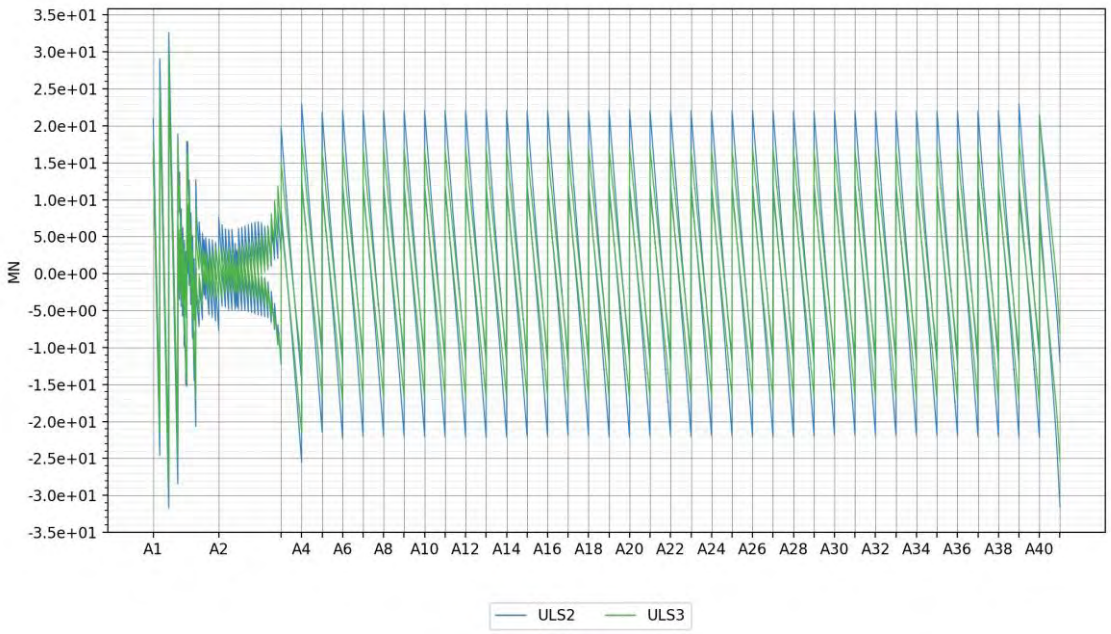


*Figure 6-6 Bridge girder vertical shear force – ULS for K12_07.*

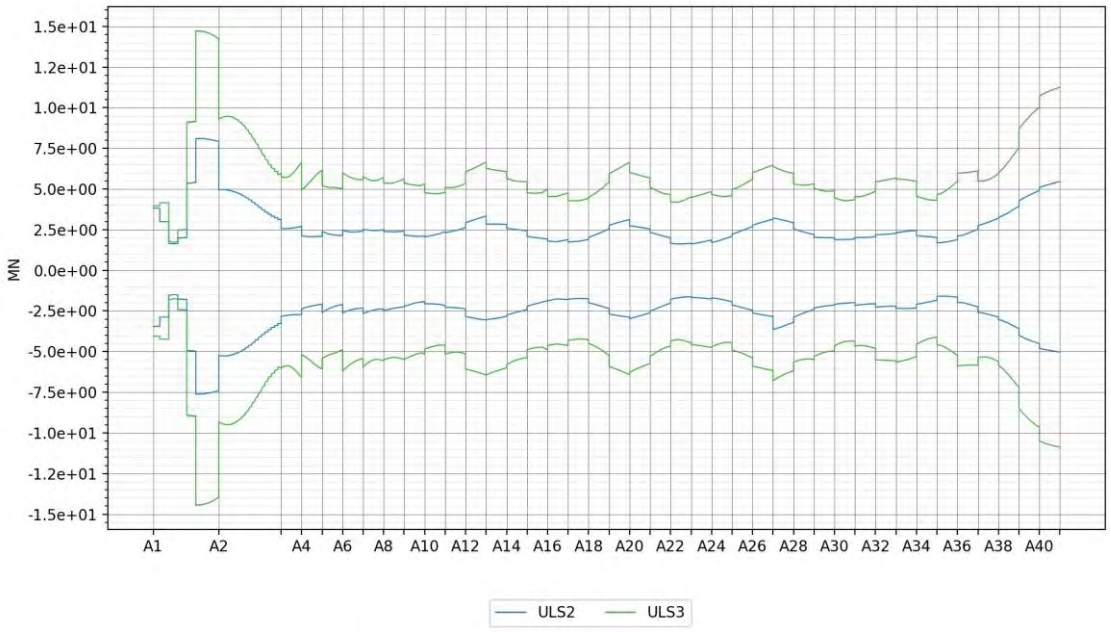


*Figure 6-7 Bridge girder transverse shear force – ULS for K12_07.*

## 6.5 Response in girder from individual load cases

In this chapter the contribution of response from selected individual load groups are shown. The bridge girder response for various load components are shown in Figure 6-8 to Figure 6-13.


*Figure 6-8 Overview of axial force contribution from slowly varying loads (top) and wave and wind loading (bottom) for the K12_07 concept.*

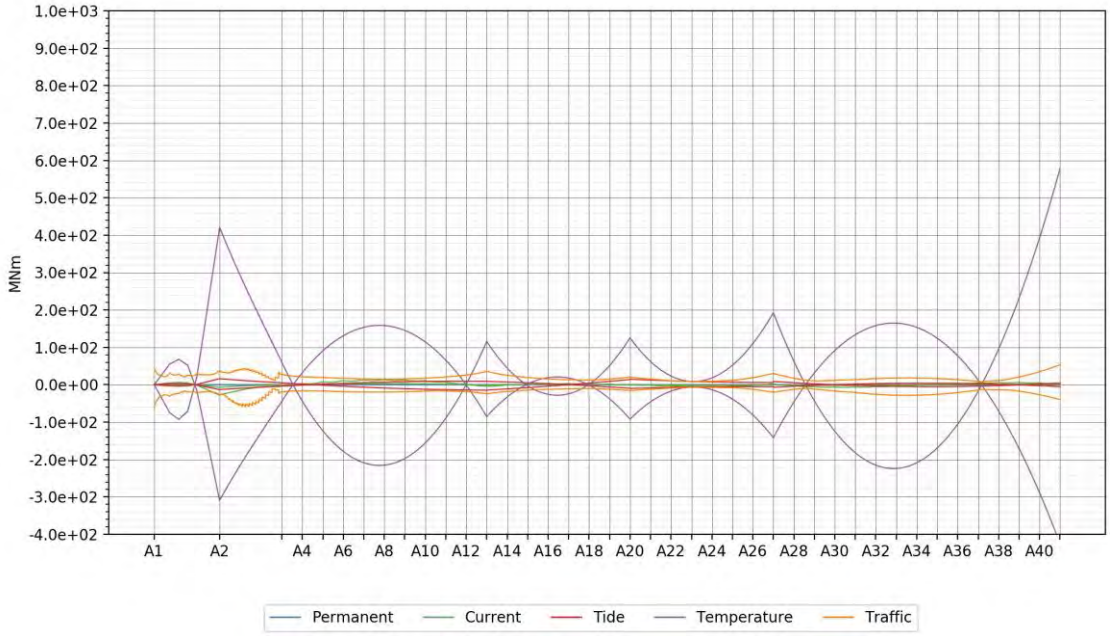


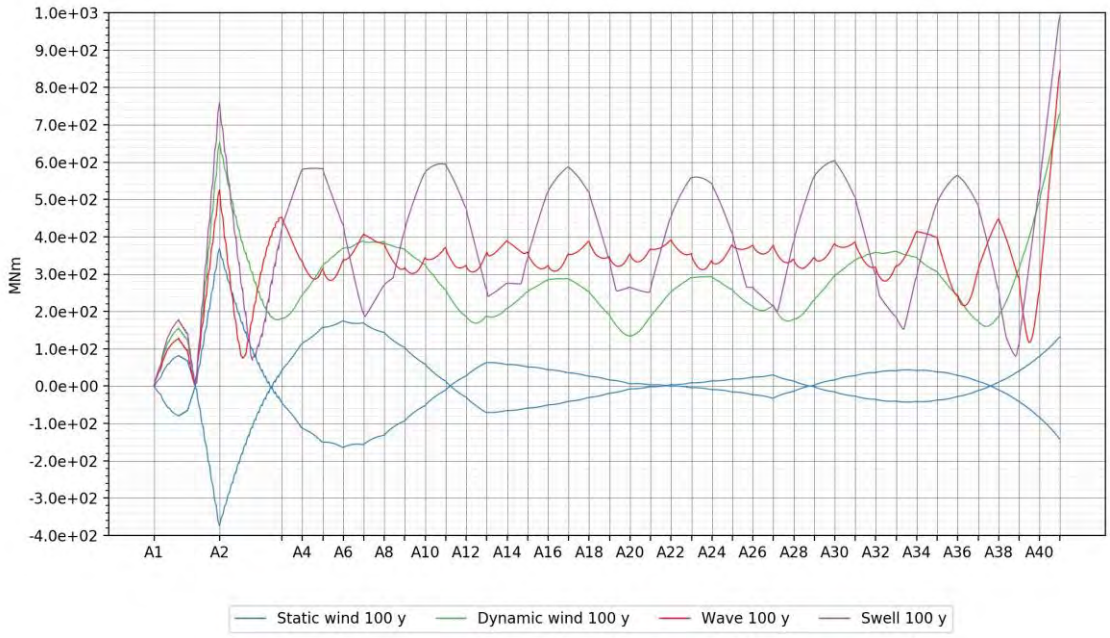


*Figure 6-9 Overview of strong-axis bending moment contribution from slowly varying loads (top) and wave and wind loading (bottom) for the K12_07 concept.*


*Figure 6-10 Overview of weak-axis bending moment contribution from slowly varying loads (top) and wave and wind loading (bottom) for the K12_07 concept.*

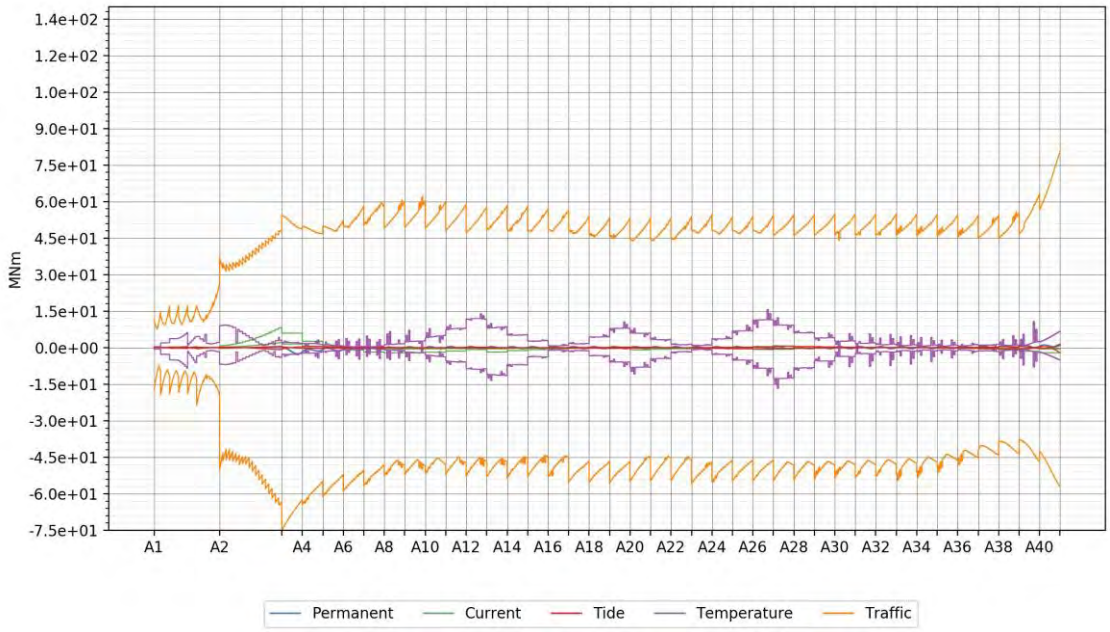


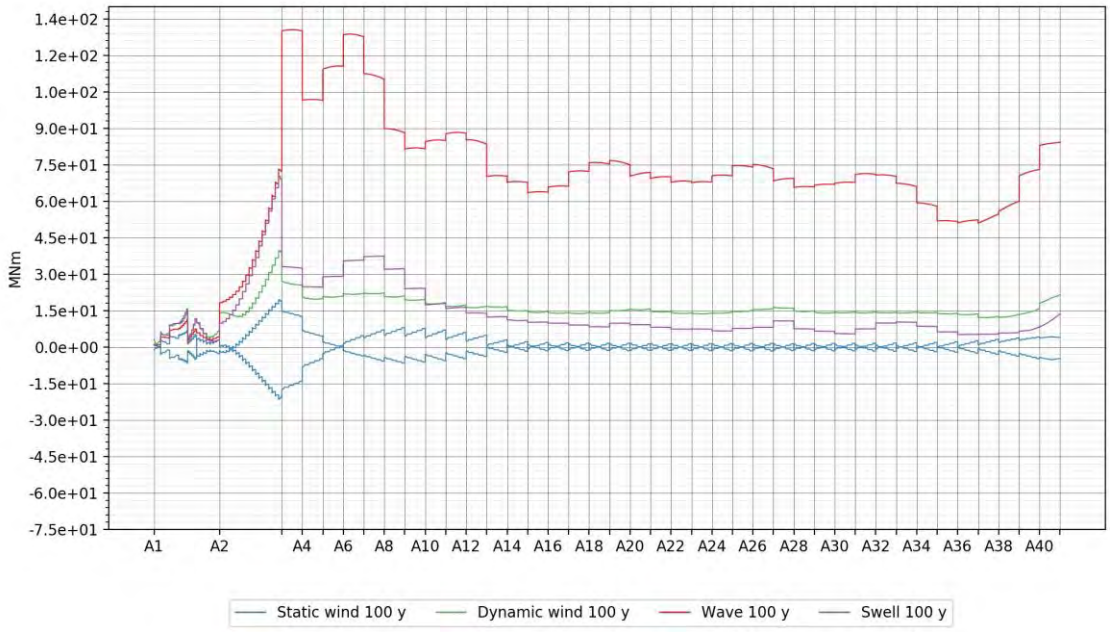


*Figure 6-11 Overview of torsional moment contribution from slowly varying loads (top) and wave and wind loading (bottom) for the K12_07 concept.*

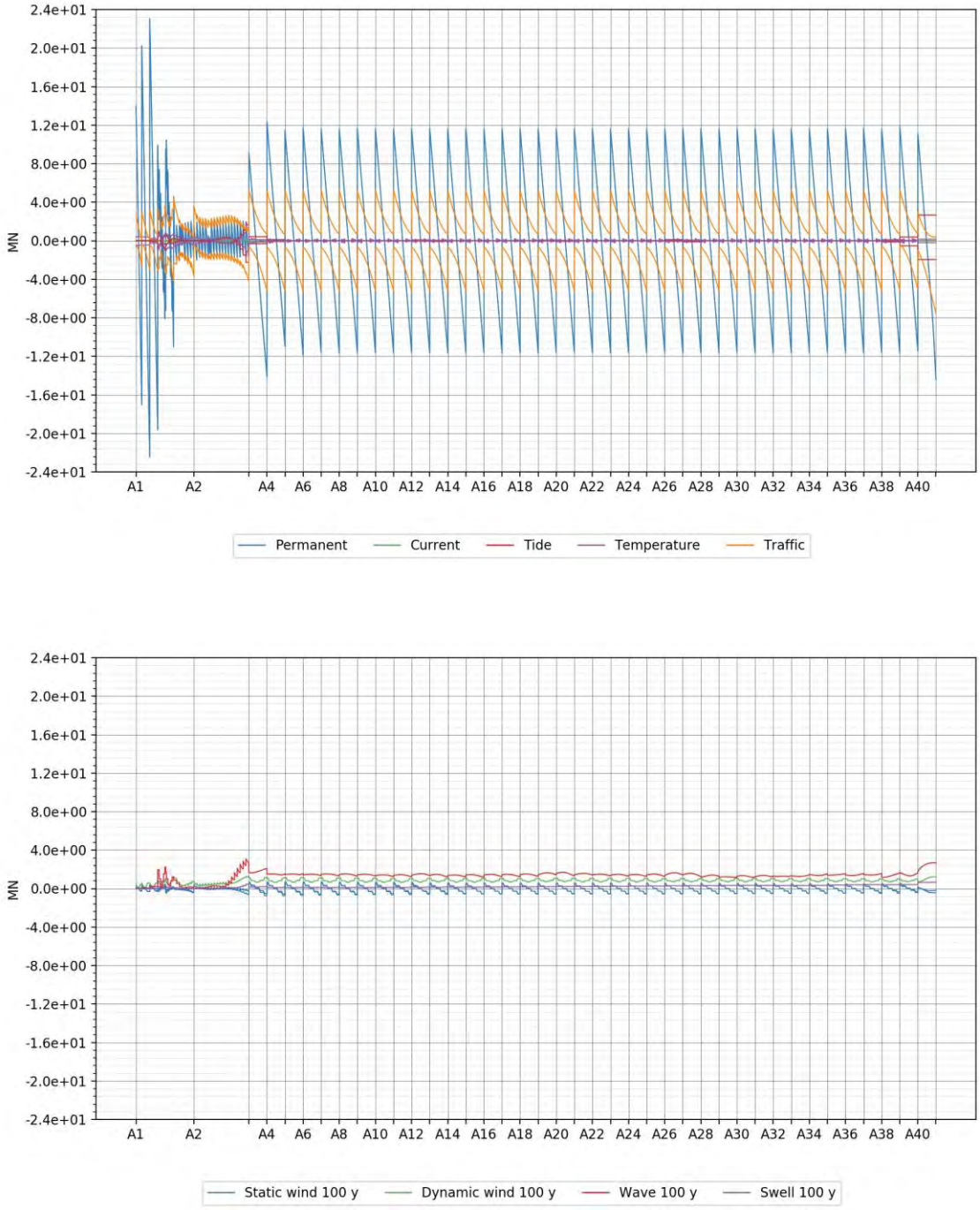


*Figure 6-12 Overview of vertical shear force contribution from slowly varying loads (top) and wave and wind loading (bottom) for the K12_07 concept.*


*Figure 6-13 Overview of transverse shear force contribution from slowly varying loads (top) and wave and wind loading (bottom) for the K12_07 concept.*

## 6.6 Global deformation and acceleration from individual load cases

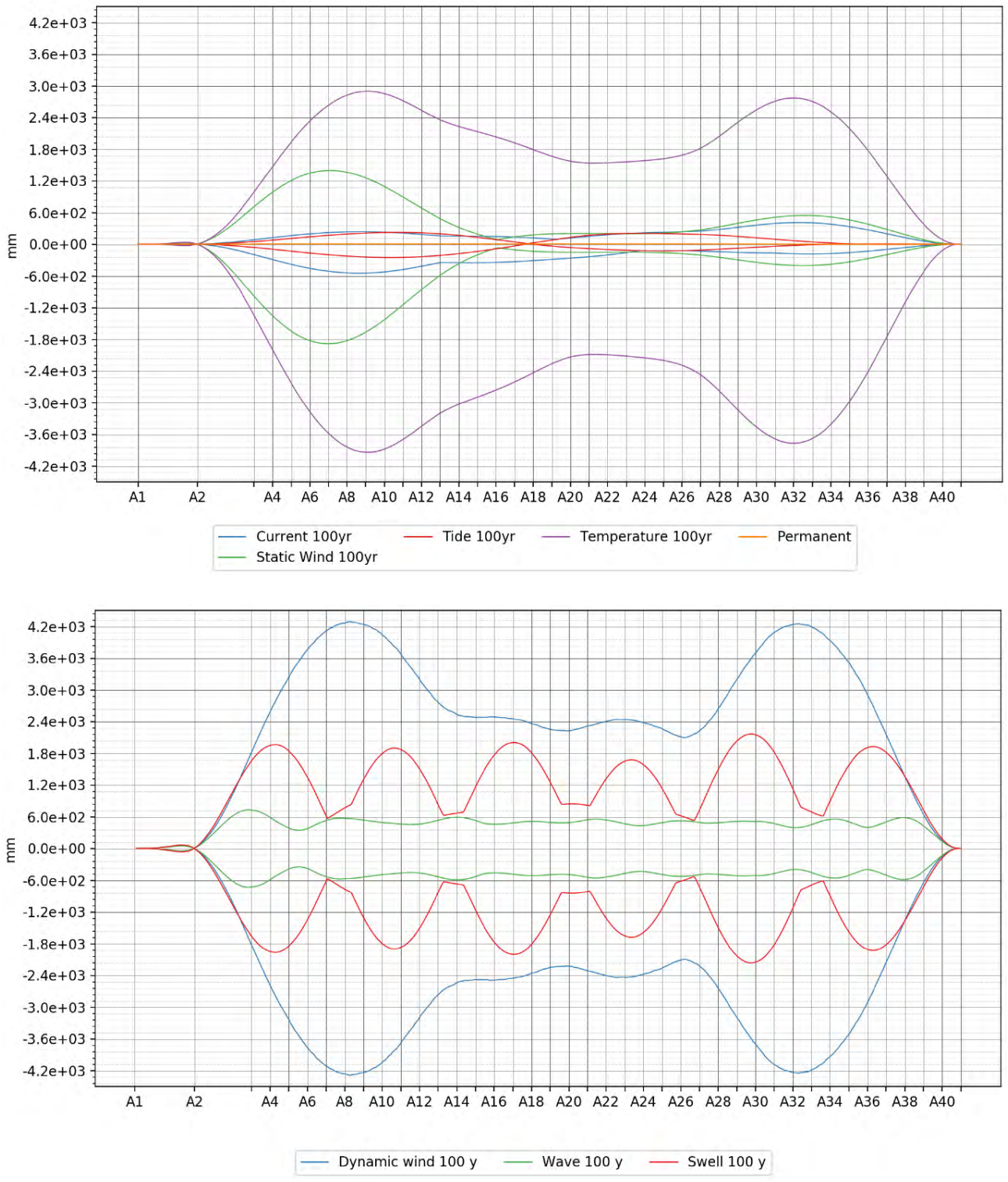


*Figure 6-14 Overview of contributions to transverse displacements from slowly varying (top) and wave and wind (bottom) load components for the K12_07 concept, 100 year return period.*

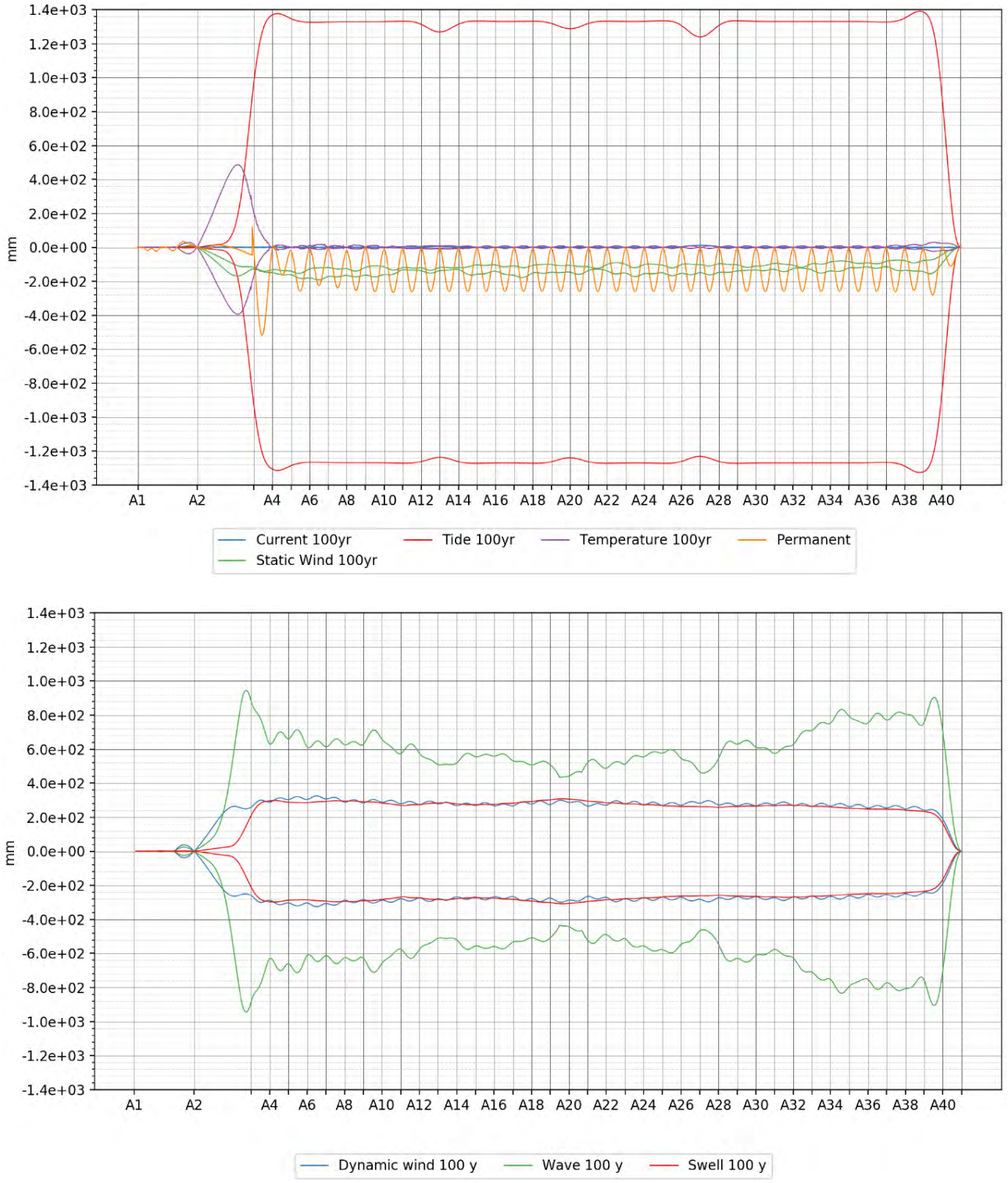


*Figure 6-15 Overview of contributions to vertical displacements from slowly varying (top) and wave and wind (bottom) load components for the K12_07 concept, 100 year return period.*

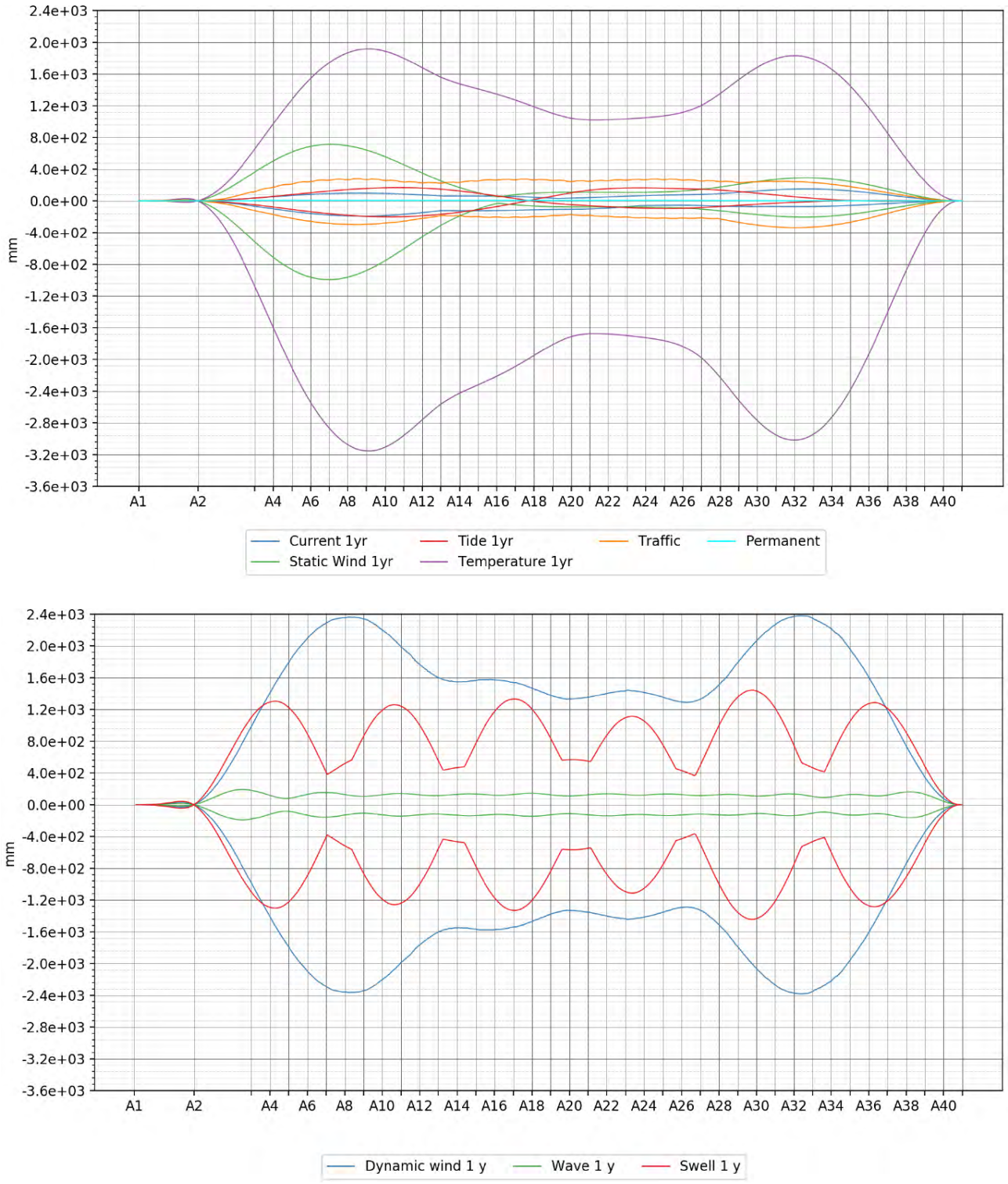


*Figure 6-16 Overview of contributions to transverse displacements from slowly varying (top) and wave and wind (bottom) load components for the K12_07 concept, 1 year return period.*

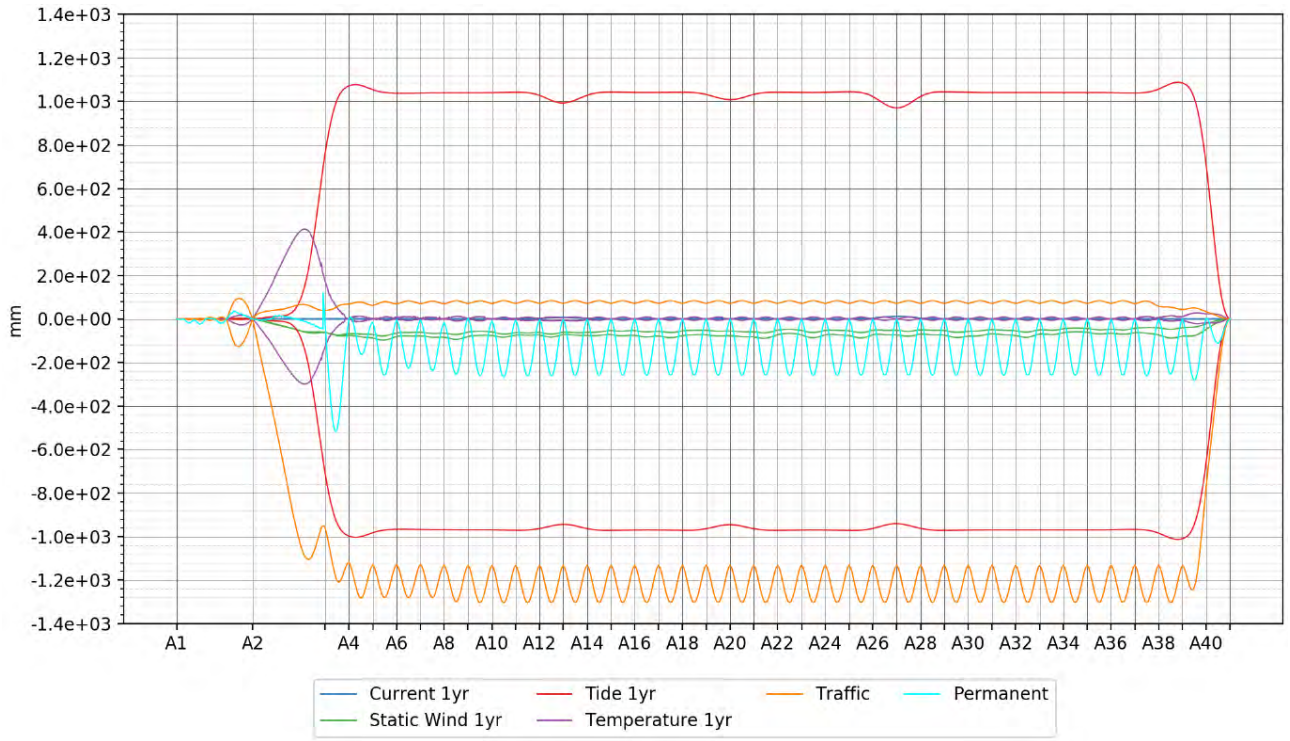


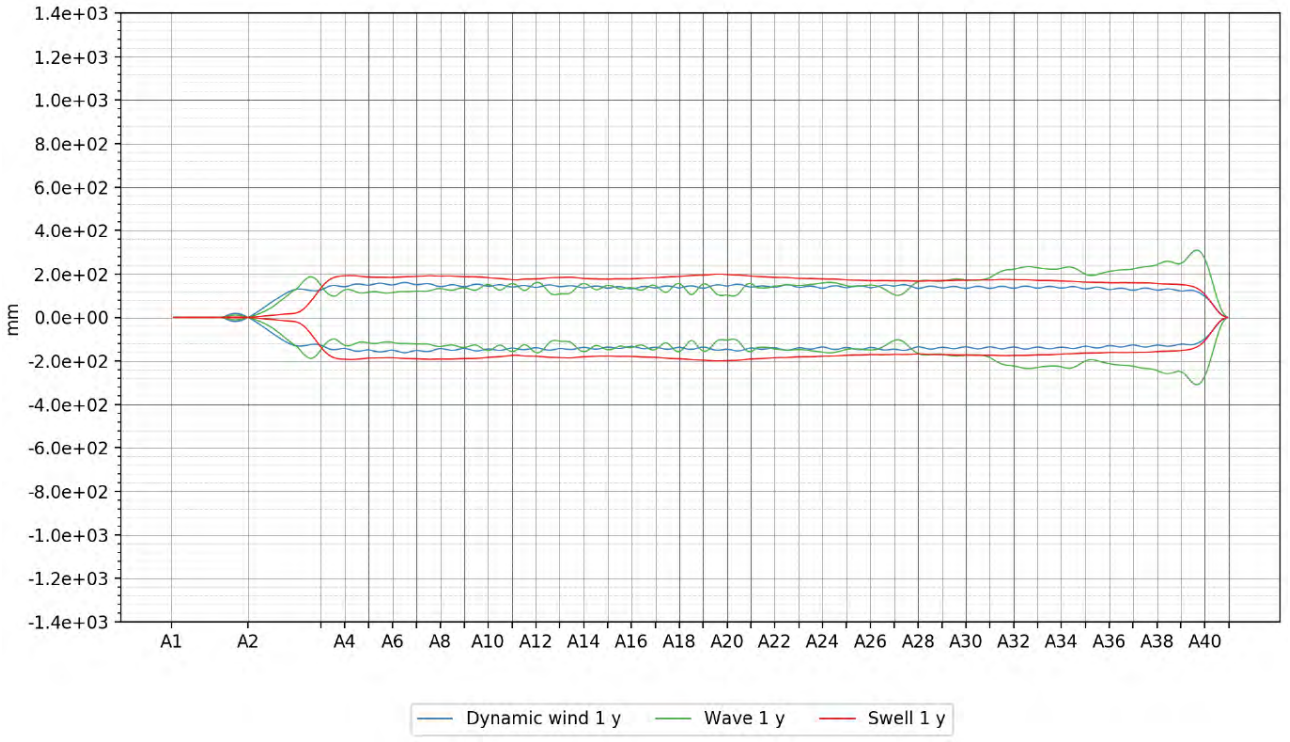


*Figure 6-17 Overview of contributions to vertical displacements from slowly varying (top) and wave and wind (bottom) load components for the K12_07 concept, 1 year return period.*

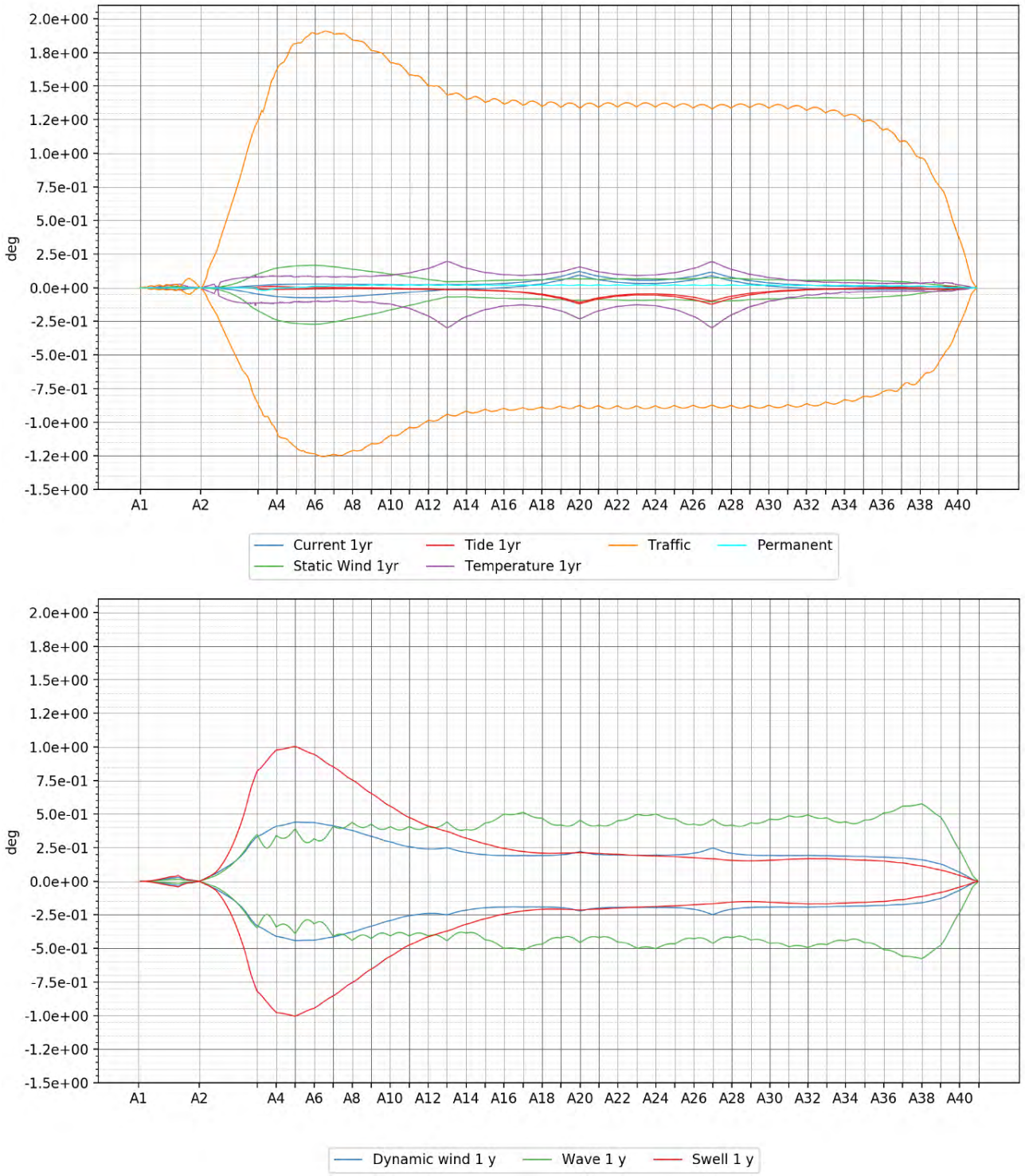


*Figure 6-18 Overview of contributions to rotation about the longitudinal bridge axis from slowly varying (top) and wave and wind (bottom) load components for the K12_07 concept, 1 year return period.*

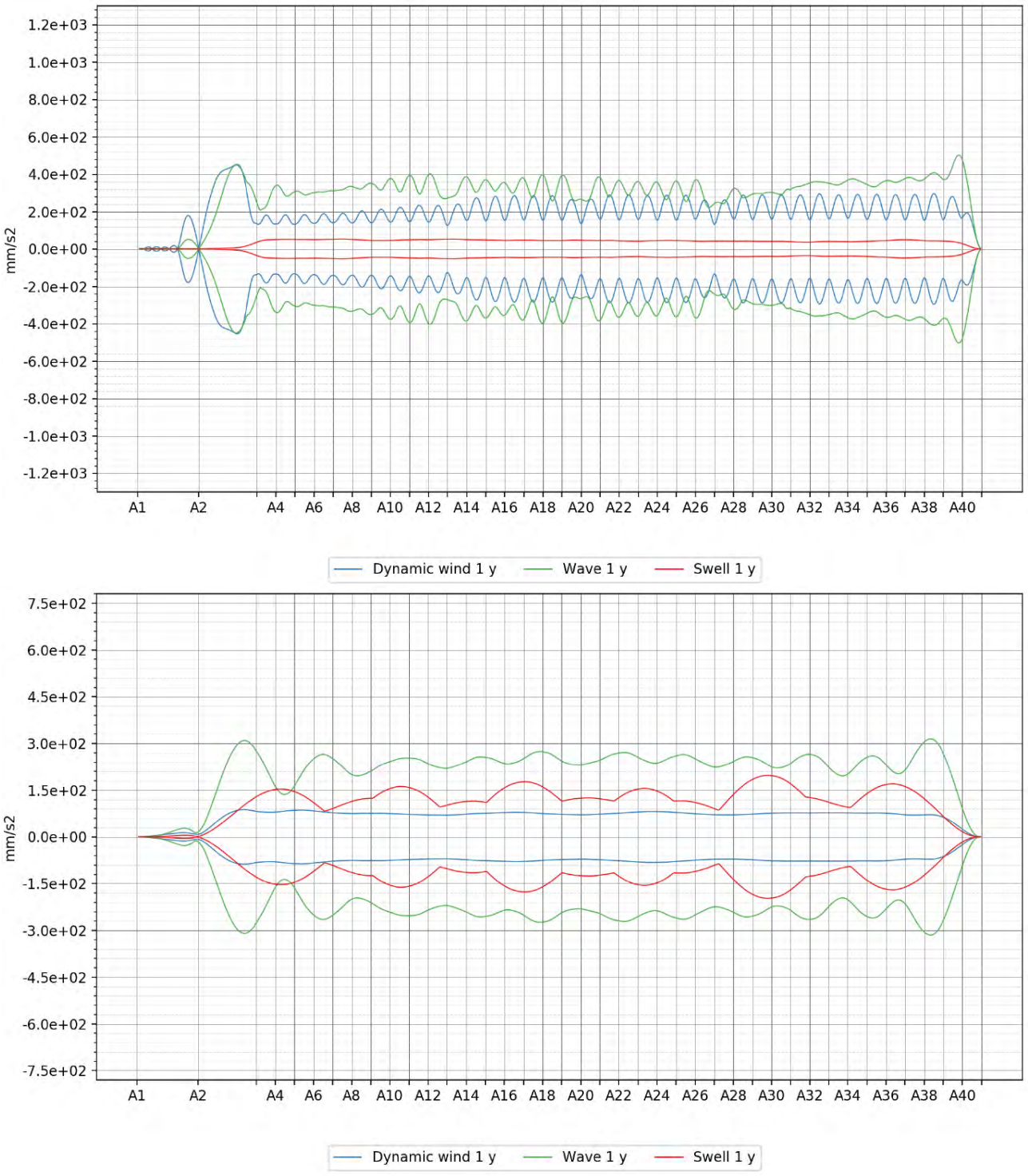


*Figure 6-19 Overview of contributions to vertical (top) and transverse (bottom) acceleration from wave and wind load components for the K12_07 concept, 1 year return period.*

## 6.7 Design of bridge girder

To simplify the design of the box girder and thereby reduce the fabrication costs and increase the amount of automatic welding, the recommended design is a rectangular shape where the lower flange is partly shaped towards the outer webs that are approximately half the height of the box.

The bridge girder has separate wind fairings, to be designed for optimized aerodynamic shape. These fairings are not included in the overall structural strength of the box girder and can therefore be of light weight.

The total width of the box girder without wind fairings is 27 m, and the total height is 4 m.

The design of the stiffeners is based on panel buckling, fabrication costs and interface between bridge girder and column. Below the top deck plate, trapes stiffeners must be applied. In the interface between the bridge girder and column, bulb stiffeners are preferable. To simplify the design, the longitudinal bulb stiffeners active in the interface between bridge girder and column was kept continuous. Elsewhere, the longitudinal trapes stiffeners were used.

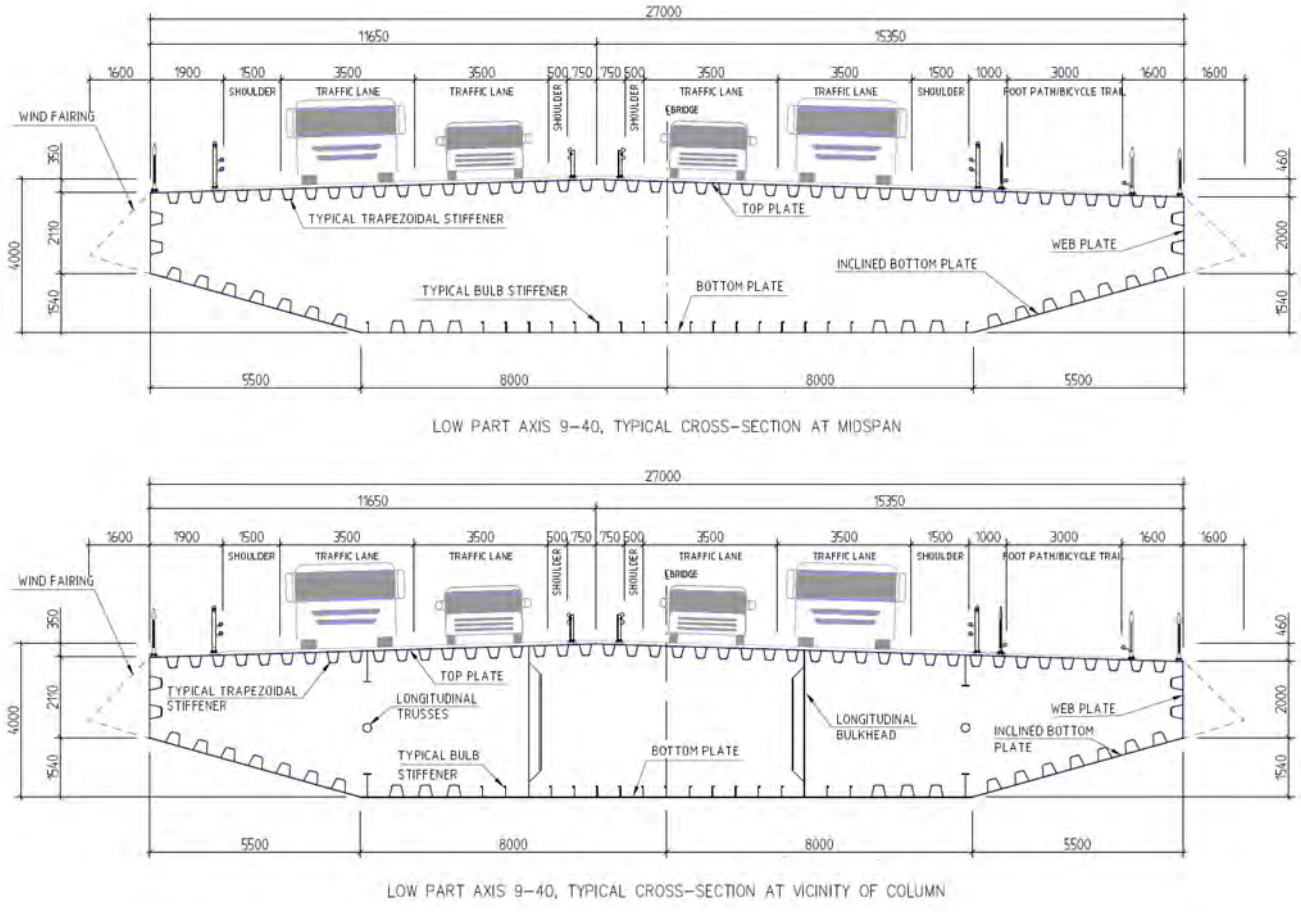


*Figure 6-20 Geometric shape of bridge girder at midspan and in vicinity of column*

The bridge girders are designed with transverse trusses and bulkheads with cc 4.0 m. Longitudinal walls as trusses and bulkheads are introduced to reduce the shear lag effect in ultimate limit state and fatigue limit state. The walls are placed as shown in the figure below. Note that no longitudinal walls are placed in the midspan. The effective bending stiffness is reduced by approximately 75 % in midspan and 80 % at support for fatigue calculations.

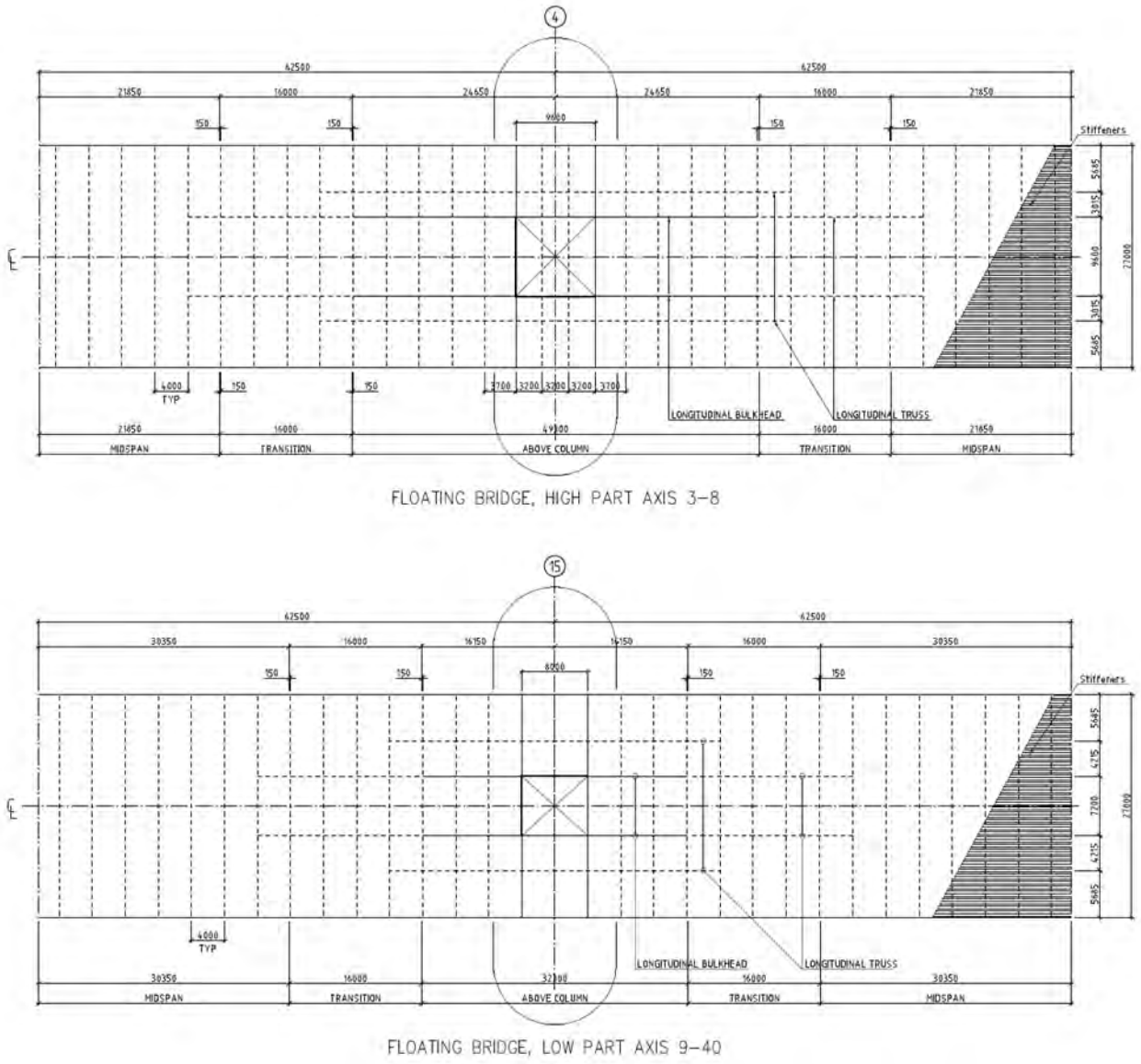


*Figure 6-21 Plan view of bridge girder*

Based on the results from the global analyses, the plate thicknesses and stiffeners for the different concepts were optimized.

The concept K12 is developed with three different types of sections along the bridge girder; one slimmer at midspan, another strengthened above the column and a transition section in between. In addition, the sections at midspan and above the columns for axis 3 – 8 are additional strengthened.

The plate thicknesses for the bridge girder skin plates for all concepts are given in table below.

The bridge girders are designed with transverse trusses and bulkheads with cc approximately 4.0 m. The transverse trusses and bulkheads help to carry dead loads and traffic loads from the orthotropic deck plate out to the outer vertical web-plates in the box girder. The trusses and bulkheads also give a rigid support to the longitudinal stiffened plates and helps to maintain the shape of the steel box. The design with calculations for the transverse trusses in the bridge girder is given in Appendix K, attached memo 10205546-13-NOT-083.

*Table 6-3 The plate thicknesses for the bridge girder skin for K12*

| **Concept K12** | **Axis 3 - 8** | | | **Axis 9 - 40** | | |
|---|---|---|---|---|---|---|
| | Midspan | Transition | Above column | Midspan | Transition | Above column |
| Top plate [mm] | 16 | 16 | 16 | 16 | 16 | 16 |
| Web plate [mm] | 14 | 14 | 20 | 12 | 14 | 14 |
| Inclined bottom plate [mm] | 14 | 16 | 22 | 12 | 16 | 20 |
| Bottom plate [mm] | 14 | 16 | 22 | 12 | 16 | 20 |
| Length within span of 125 m [m] | 43.7 | 32.0 | 49.3 | 60.7 | 32.0 | 32.3 |
| Length applied in global analysis | 3/8 L | 2/8 L | 3/8 L | 4/8 L | 2/8 L | 2/8 L |

When designing the bridge girder, effects of shear lag and plate buckling must be taken into account at the ultimate, serviceability and fatigue limit state. Appendix K, enclosed memo 10205546-13-NOT-194 “Shear lag and buckling effects of Bridge Girder”, present the design requirements and the applied design approach accounting for these effects. Longitudinal bulkheads are chosen so that the shear lag in ultimate limit state is negligible. In SLS and FLS the shear lag effect with respect to bending stiffness is 75 to 80 % of the stiffness of gross area of section. In chapter 3.2.1.3 it is argued that shear lag calculation based on distributed load as specified in Eurocode, will give acceptable results for the governing load condition for this floating bridge (point load in one span and stamping mode of pontoons).

Sufficient capacity of the bridge girder subject to compression and biaxial bending is verified based on equation (4.15) in NS-EN 1993-1-5:2006 + NA 2009. Equation (4.15) is a linear summation of the utilization that each force component utilizes the capacity corresponding to the respective type of force (Method 1). Due to the bridge girders shape with an inclined bottom plate, the capacity check will give conservative utilization results for biaxial bending when the utilization about each axis is large at the same time.

Since the Eurocode does not account for conservative utilizations due to geometric shapes, a second way of performing the capacity check has been introduced (Method 2). In the second method, the geometric shape is considered in the capacity check by calculating the utilization at all the 7 extremity points of the girder on the effective elastic section modulus for the specific point.

All sectional properties of the girder are given in Appendix K, enclosed memo 10205546-13-NOT-194 “Shear lag and buckling effects of Bridge Girder”.

Analysis show that the static motions due to traffic will satisfy the limitation given in Design Basis, ref Appendix K.

In the next chapter envelope plots of the maximum von Mises stresses are shown for all the concepts. For control of plate buckling capacity refer to appendix K.

## 6.8 Von Mises stresses in girder in ultimate limit state

The results of maximum von Mises stresses, include the effect from all sectional forces, along the bridge based upon the result of the global analyses are shown in the figure below, extracted from enclosure 2, K12_07 Load combination direct method. ULS2 is traffic loads with reduced environmental loads and ULS3 is 100-years environmental loads without traffic.

ULS2 is governing except for the strengthened bridge girder towards the North abutment. The utilization for the floating bridge girder between axis 3 and 40 is 1.00, occurring at midspan between axis 3 and 4.

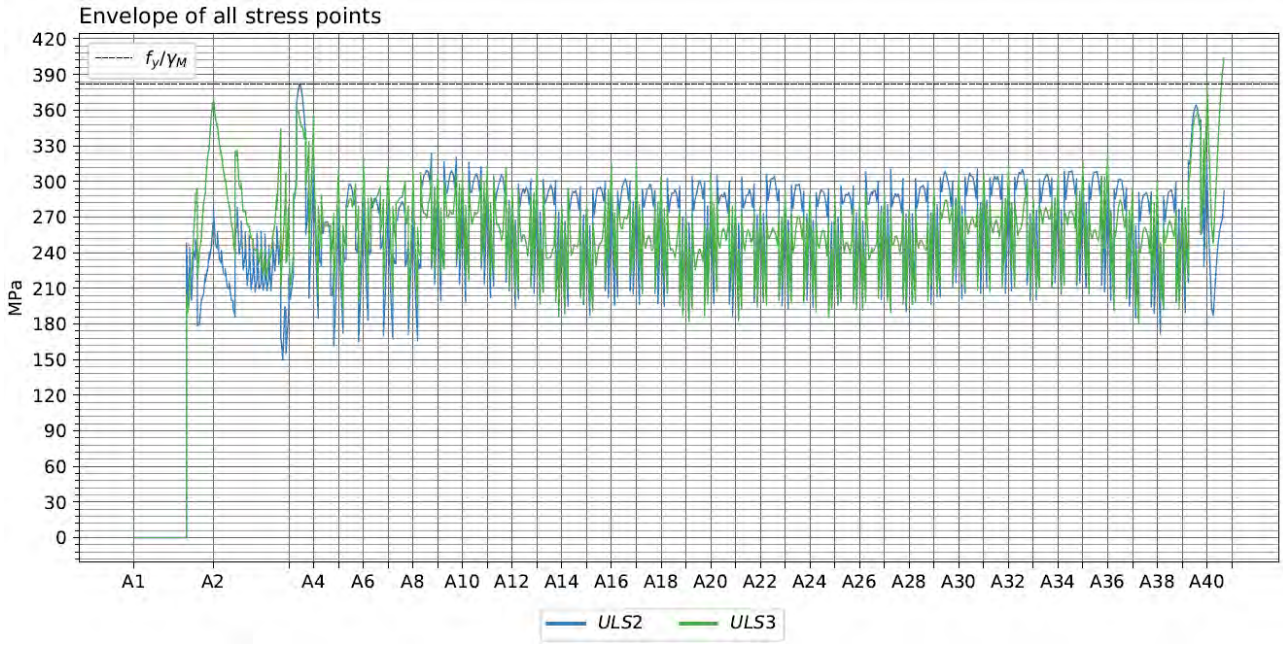


*Figure 6-22 Maximum von Mises stresses along the bridge for K12_07.*

## 6.9 Plate buckling capacity of girder in ultimate limit state

The utilizations of capacity check along the bridge are shown in the figures below, extracted from Appendix G, enclosure 2, K12_07 Load combination direct method.

The capacity check is performed with the two methods described in Appendix K, attached memo 10205546-13-NOT-194.

Except for the ends of the floating bridge girder, the utilizations for plate buckling capacity are at acceptable values. The maximum utilization ratio between axes 3 and 4 is 1.09 with method 1 and 1.03 with method 2. The maximum utilization ratio at axis 40 is 1.21 indicating need of local reinforcement.

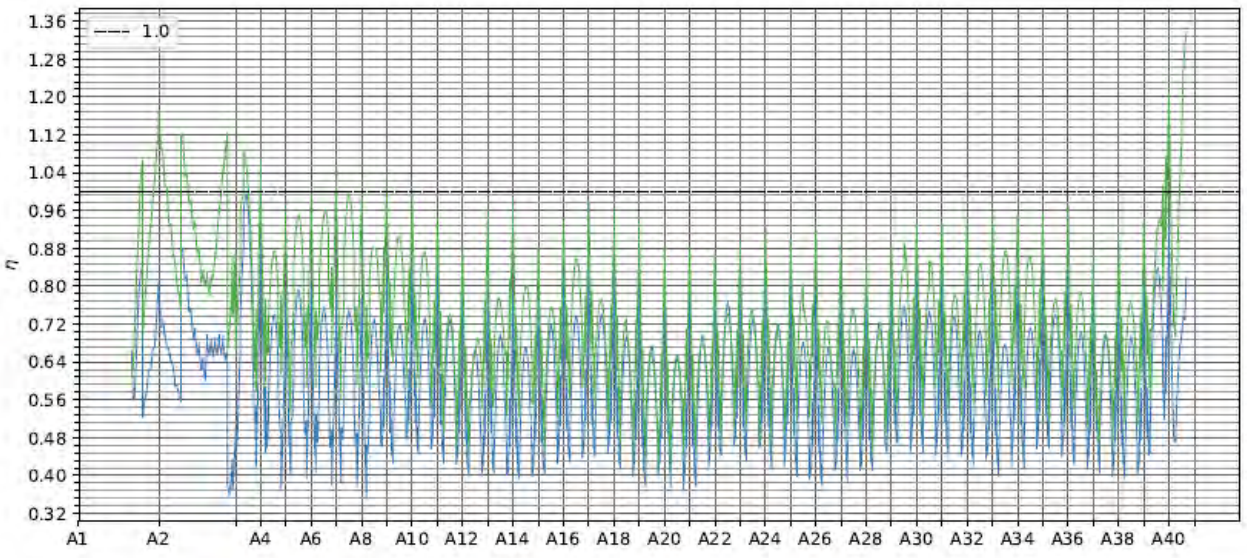


*Figure 6-23 The utilization of capacity check along the bridge for K12_07 with method 1*

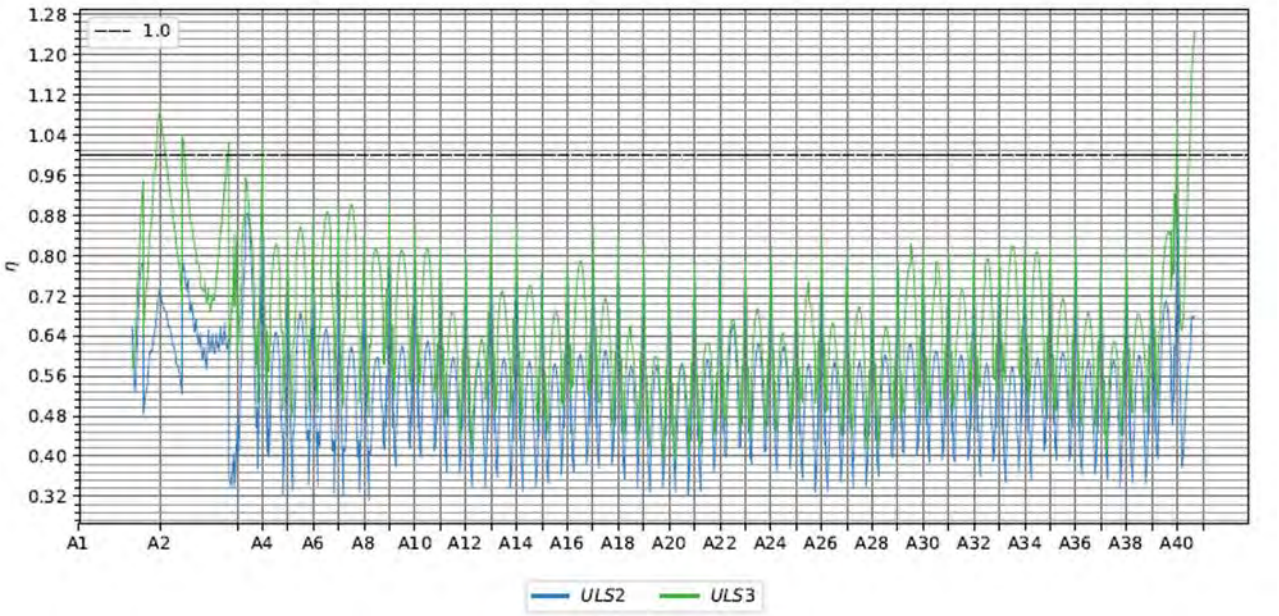


*Figure 6-24 The utilization of capacity check along the bridge for K12_07 with method 2*

## 6.10 Design of pontoons

There are two different pontoon designs; a pontoon without mooring lines and with supports for mooring lines. Freeboard of all pontoons are 3.5 m.

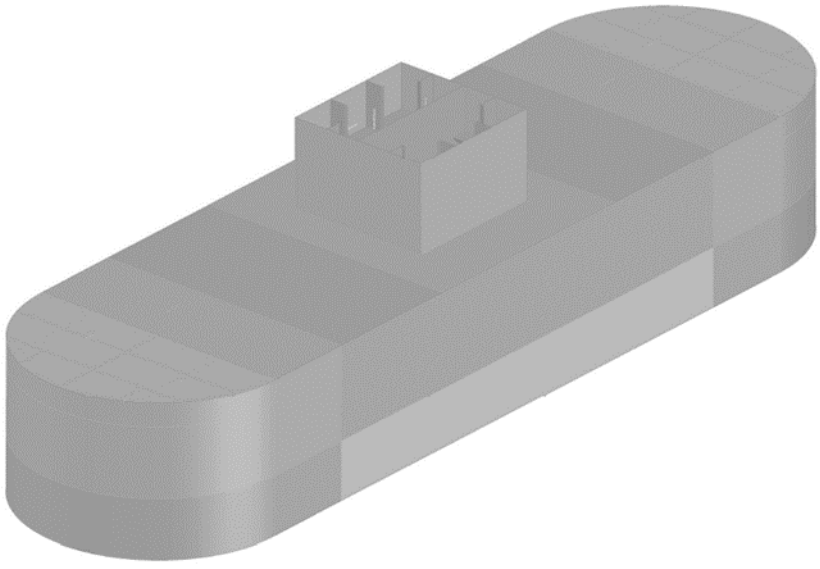

*Figure 6-25 The geometric shape of pontoon without mooring lines*

The proposed structural dimensions show acceptable utilization both with regards to maximum allowable stress level and minimum scantling requirements and buckling utilization, for both ULS and ALS conditions. The structural net scantling weight for the “base case” pontoon without mooring lines is 705 ton for a displacement of 3710 m3. These pontoons are 53 m long, 14.9 m wide and 8.5 m deep. The structural weight for the “base case” pontoon with mooring lines is 934 ton for a

displacement of 5565 m3. These pontoons are similar to the pontoons without mooring, but with a height of 11.0 m. For cost estimate the steel weight estimates are increased by 15 % to cater for local strengthening around column base and for a possible increase in length of some of the pontoons in high bridge area.

To avoid corrosion, the outer surfaces in the splash zone are made of steel material grade 25CR super duplex. The splash zone of a vertical extent of 6.5 m, is based on vertical movement from environmental loads with a return period of 100 years. This is conservative considering that according to DNVGL-OS-C101, the 100-year wave height shall be divided by three.

## 6.11 Design of column

There are two different column designs; one for axis 3-8 the higher bridge part, and another for axis 9-40 the lower bridge part.

The proposed design with calculations is given in Appendix K, attached memos 10205546-13-NOT-086 and 10205546-13-NOT-099.

The columns are designed as rectangular sections towards the bridge girder and pontoons. The middle part of the columns has chamfered corners and is narrower than the top and bottom. This is done to improve wind drag, and to give the columns a more aesthetic appearance.

The main dimensions for the columns at axis 3-8 are 7.6m x 7.6m at the middle part. The height of the columns differs between 45.6m and 26.9m. The main dimensions for the columns at axis 9-40 are 5.2m x 6m at the middle part. The height of the columns differs between 23.1m and 10.5m.

At the four corners between the column and the bridge girder/pontoon, there is casted details to simplify the welding and improve the fatigue life.

The columns with a skin plate thickness of 25 mm have capacity to withstand ULS combinations based on elastic capacity. However, the columns have insufficient capacity to withstand ALS combinations with ship impact. With an increase in plate thickness from 25 mm to 40 mm, the columns can absorb approximately 50 % of the currently defined energy during an impact. Another alternative is to increase the size of the narrow middle part of the columns.

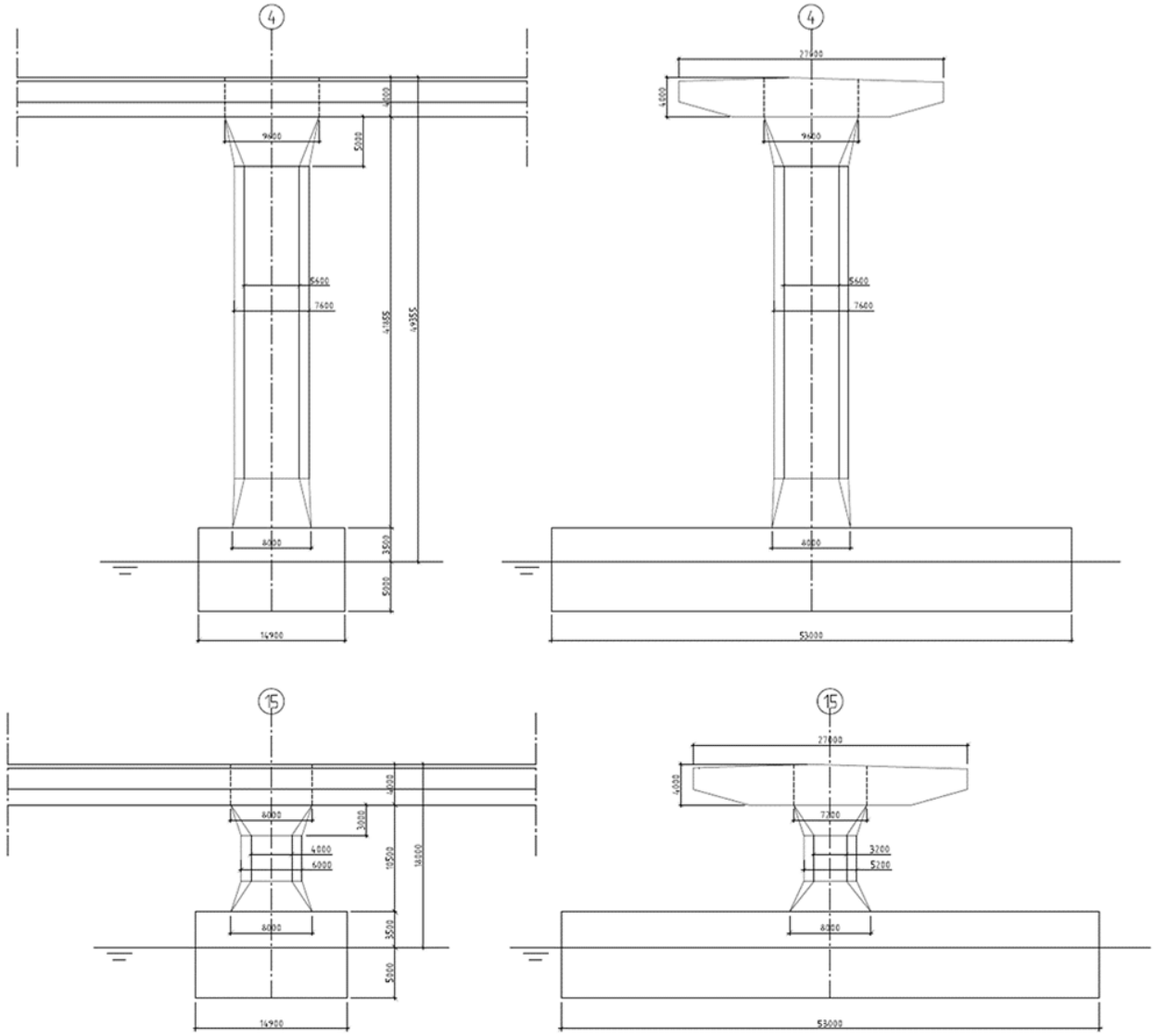


*Figure 6-26 The geometric shape of column for higher and lower bridge part*

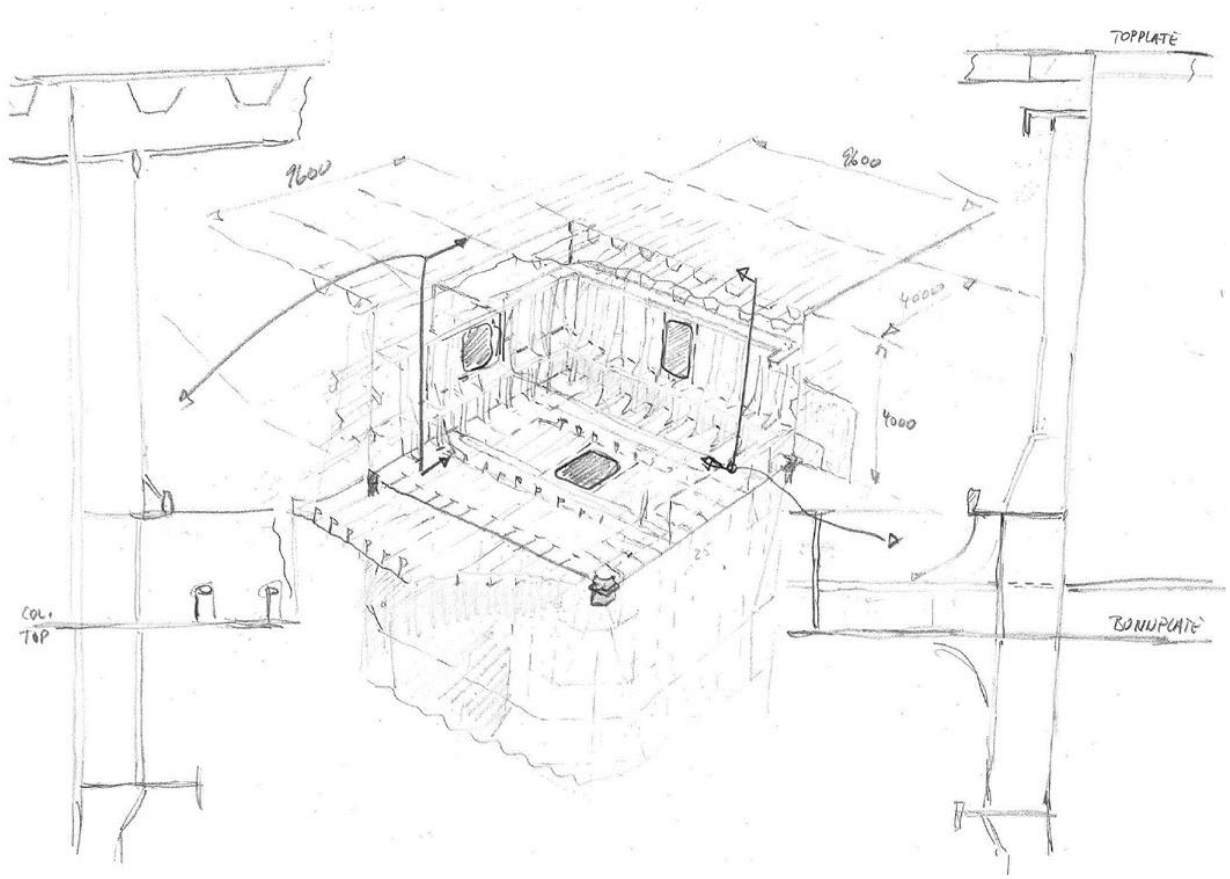


*Figure 6-27 Connection between column and bridge girder*

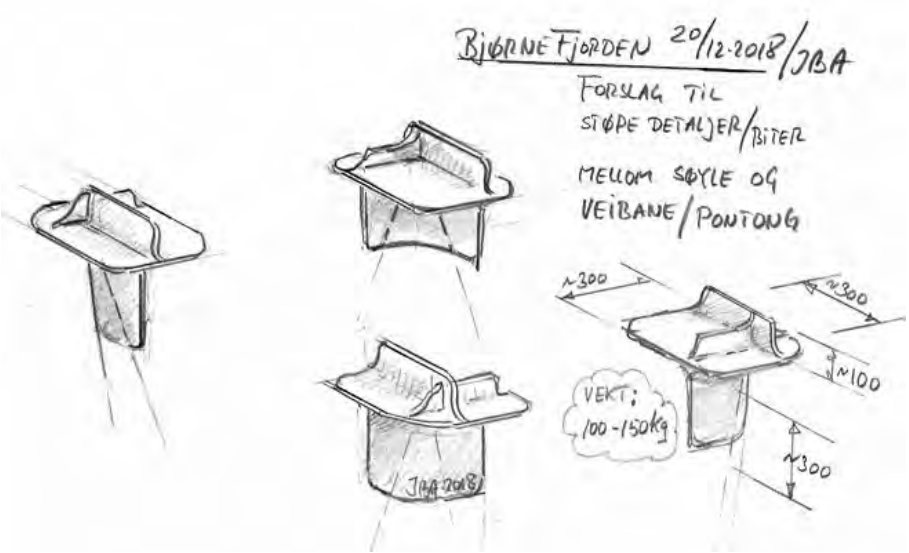


*Figure 6-28 Cast steel details at the four corners of the column*

Even though the current design is a single vertical column, there was performed a comparison with an A-shaped column as proposed by the architects. Appendix K, enclosed memo 10205546-13-NOT-020 compares the required steel weight required to carry the loads from an eccentric ship impact between a rectangular and an A-shaped column design.

## 6.12 Weight estimate of floating bridge part

An estimate of the total steel weight for the floating bridge is given in the table below.

*Table 6-4 Estimates of total steel weight for the floating bridge part for K12*

| | **Steel Weight Estimate (Ton)** |
|---|---|
| Pontoon without moorings | 24 899 |
| Pontoon with moorings | 2 803 |
| Columns (incl 40mm plate) | 6 681 |
| Bridge girder | 69 037 |
| **Total sum steel for floating bridge part** | **103 420** |

The weight of the columns is based on 40 mm skin plate thickness. The increased weight of 15 % for pontoons is not included in the table above. However, these increases are included in the final material quantities.

The length of floating bridge part is 4770 m for K12.

# 7 Design of cable stayed bridge and abutments

## 7.1 Introduction

The cable stayed bridge is constituting the south portion of the Bjørnafjorden Bridge, "cantilevering" from Reksteren across the Svarvahelleholmen Island and connecting to the floating bridge at axis 3. The tower is positioned on the island, while the 380 m main span allows the navigation to pass under at a height of 45 m and a width of 250 m or more. The bridge spans from the south abutment to the tower are 40 + 4 x 55 + 140 m = 400 m. This span arrangement and the corresponding cable stay configuration (380 m main span/250 m side span/18 stays/4 fans) is the result of an evaluation of feasible cable stayed bridge options that fit with the general scheme of the floating bridge. The concept layout is presented in Figure 7-1.

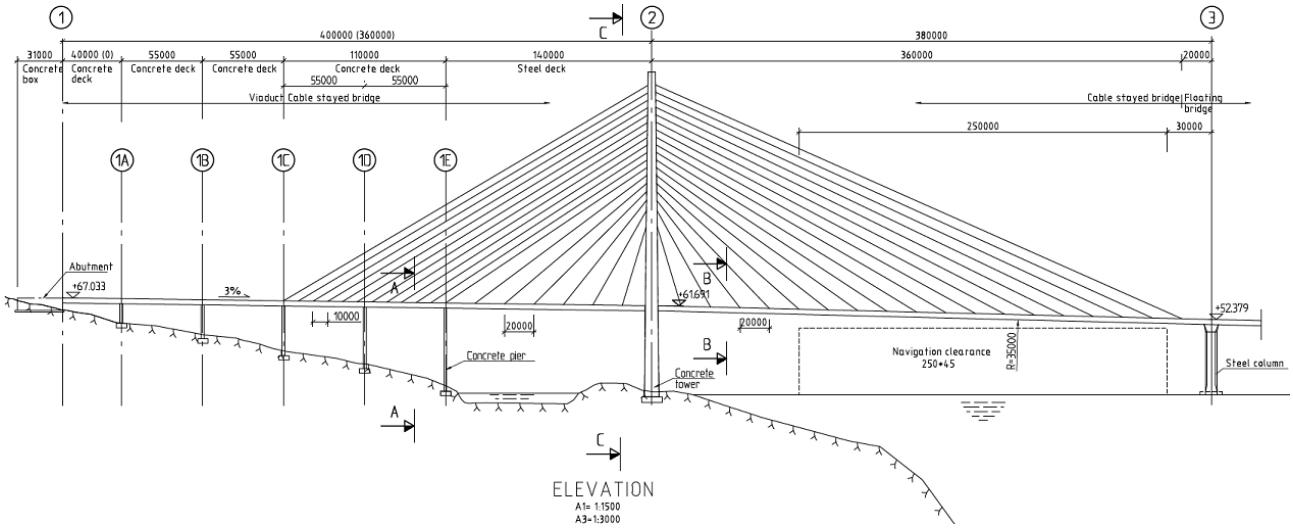


*Figure 7-1 Cable stayed bridge – concept layout*

The stayed span lengths lead to an asymmetrical bridge which becomes natural as piers can be erected on shore in the side span supporting the deck girder and moreover giving stiffness to the entire cable stayed bridge. The bridge deck is in principle divided into a steel portion above water, and concrete above land continuing with the concrete viaduct spans. The cable stayed bridge is of a fully conventional type, and the most significant influence from the floating bridge is in general tidal variation and to some extent wave motion of pontoon at axis 3.

*Figure 7-2 Cable stayed bridge – visualisation*

The entire cable stayed bridge has a straight horizontal alignment and a visualisation of the bridge can be seen Figure 7-2.

## 7.2 Concept for cable stayed bridge and south abutment

Of the 380 m long main span, 360 m belongs to the cable stayed bridge, whereas the remaining 20 m is part of the floating bridge. The 20 m distance from the last stay cable to the first pontoon of the floating bridge can be further fine-tuned later. With the 140 m side span there is totally 500 m closed steel box girder within the cable stayed bridge. The remainder of bridge deck, 2x55 m = 110 m cable stayed side span and three viaducts spans, all together 260 m, is a closed concrete box structure. The tower, piers and abutment are concrete constructions.

The bridge deck and tower have a tight fit in transverse direction where the deck is supported on normal sliding bearings to the tower legs allowing only longitudinal movements of the deck. The tower therefore becomes a strong point being able to accommodate the high transverse loading from ship collision and normal ULS load situations. The bridge superstructure is furthermore integrated with the abutment and the piers and the ship collision impact and ULS load combinations therefore also lead to high lateral loads to the side span piers.

The thermal contraction/expansion of the viaduct spans results in flexure of the piers. In general, the aim has been to minimise number of bridge bearings and to avoid expansion joints in the bridge deck, neither at the abutment, at the tower nor at the intersection to the floating bridge. Axial compression forces in the bridge deck caused by stay inclinations are in balance about the tower, whereas other axial loads are transmitted through the cable stayed bridge to the abutment.

At the tower section of the bridge deck, the ULS strong axis bending moment becomes 2100 MNm, while the ALS ship collisions to the pontoons or deck house impacts to the floating bridge deck structure lead to a 50% higher moment of 3300 MNm.

From above is seen that the most severe impact from the floating bridge is the ship collision to the bridge deck and the first pontoon of the floating bridge. These load situations are however fully common design situations for a cable stayed bridge which therefore is built using well-known standard solutions not adding significant risks to the project.

**Alternative bridge deck layout:**

The selected concept doesn't necessarily show the fully optimal solution for the cable stayed bridge. An alternative concept has therefore been considered if longer side- and viaduct spans will be feasible utilising the natural strength of the 3.5 m deep concrete deck box structure, thereby save one pier and improve architecture with a shorter side span in combination with an equal stay spacing. The concrete deck might also be extended to the tower and further say 40 m into the main span reducing the cost and improve the bridge appearance of having an equally stay spacing throughout the entire side span as a result. This option has become possible as the ALS ship collision forces have stabilised at a moment of 3300 MNm, which the concrete box structure can easily resist. The development of the cable stayed bridge "alternative layout" is shown in Figure 7-3.

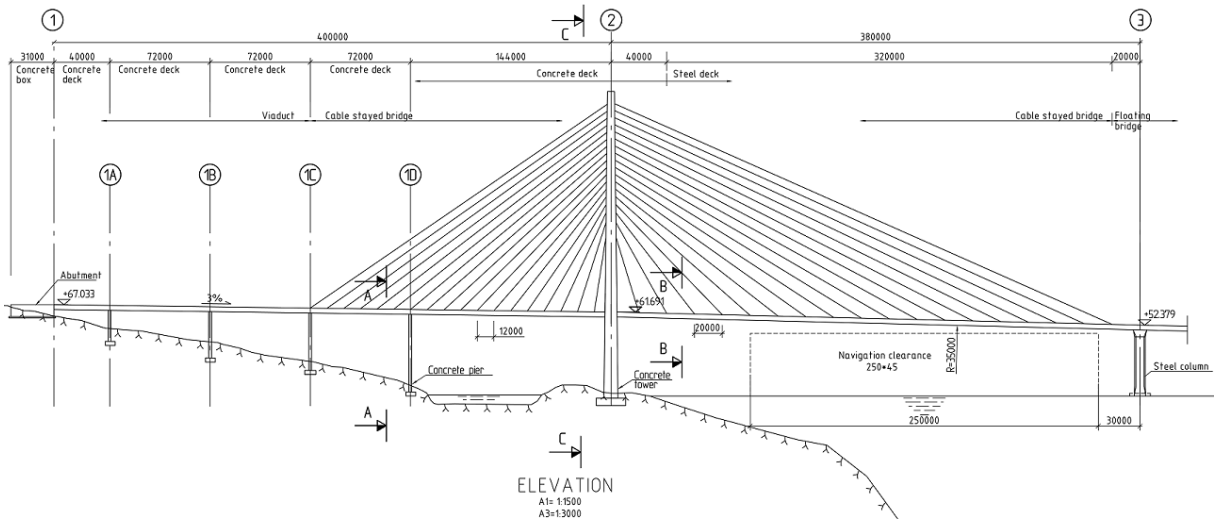


*Figure 7-3 Cable stayed bridge – alternative concept layout*

## 7.3 Concept for north abutment

At the north end of the floating bridge, a large concrete abutment ties the bridge to the Gulholmane Island. There is no expansion joint at this end either, and the structure is subjected to high axial loads in combination with very high bending moments due to transverse wind and wave loads to the floating bridge. The governing maximum ULS bending moment becomes 2400 MNm, while the governing moment in the ALS ship collision situations becomes 5900 MNm. Both ship collisions to the pontoons or deck house impacts to the floating bridge deck structure are critical and the above results are based on refined ship collision analyses. To reflect the high ship collision forces transferred into the abutment the fill inside the abutment is iron ore.

## 7.4 Steel deck

For the selected concept, the steel bridge deck starts 140 m from the tower into the side span and continues throughout the entire main span of 380 m until 20 m from the first pontoon pier A3. The length of the steel deck then becomes 500 m with an average total girder weight of 17.0 t/m. The steel deck is much lighter than the concrete deck and therefore a natural choice for the main span. In the side span the steel deck has been chosen going 140 m into the span due to expected high bending moments round strong axis from ship impact in the tower region and furthermore to span over the water to the first pier A1E.

A cross section of the bridge girder can be seen in Figure 7-4 where the steel girder is optimised for the cable stayed bridge having a reduced girder depth of 3.5 m instead of 4.0 m as for the floating bridge. The cross section is more aerodynamically shaped with wind noses and wider to accommodate the cable anchorages. A wider deck is also beneficial withstanding the large moments round strong axis from ALS ship collision as well as normal ULS. The outer vertical web plate from the floating bridge spaced 27.0 m can be found unchanged in the cross section layout for the cable stay bridge, now supporting the stay anchorages.

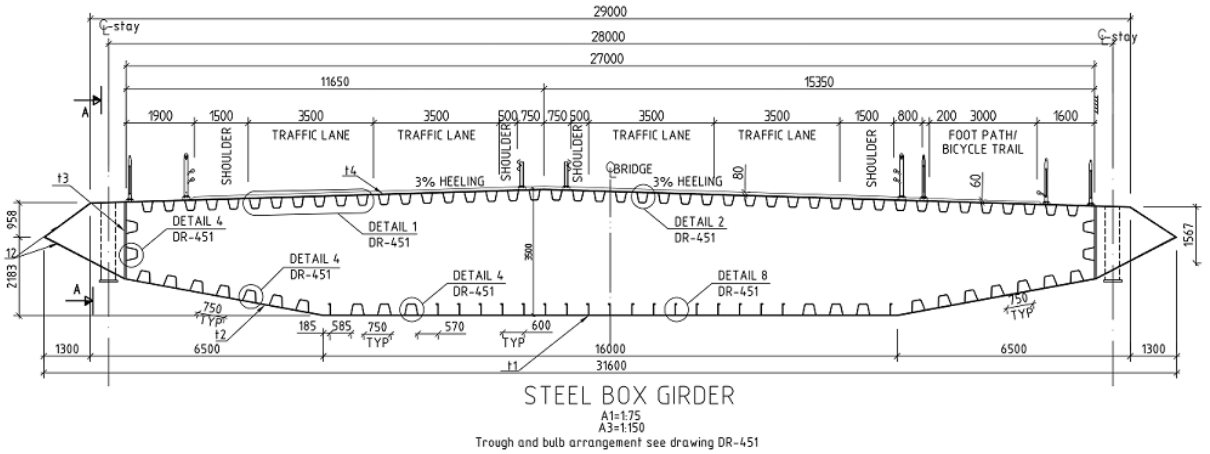


*Figure 7-4 Steel bridge girder – cross section, longitudinal steel*

The deck plate varies from a minimum thickness of 16 mm up to 20 mm when approaching the tower from both side- and main span and again when approaching the first floating bridge pier 3. Fatigue calculations carried out documents that a deck plate of min 16 mm will be necessary instead of the more conventional 14 mm primary due to truck loading. The trapezoidal stiffeners underneath the deck plate vary from minimum 8 to 10 mm, again to accommodate the fatigue requirements.

The bottom plate and the inclined web plates varies from a minimum thickness of 12 mm up to 20 mm near the tower and again when approaching the first floating bridge pier 3. For the bottom plate the principles using bulb stiffeners are chosen due to preference of the floating bridge.

The standard cross section (type H1) with minimum properties will provide enough strength within the side span and major part of the main span, however some reinforcement of the cross section (type H2) is needed in the tower region due to ship impact and when approaching the floating bridge.

The layout of the transverse truss diaphragm is also like the floating bridge and can be seen in Figure 7-5. The transverse truss solution is spaced 4.0 m in the bridge line and has been selected as it is lighter than a full plated diaphragm solution even for the 3.5 m girder height. The cable stays are anchored into tubes slotted through the edges of the deck girder. The tubes are extended above deck level also housing the dampers.

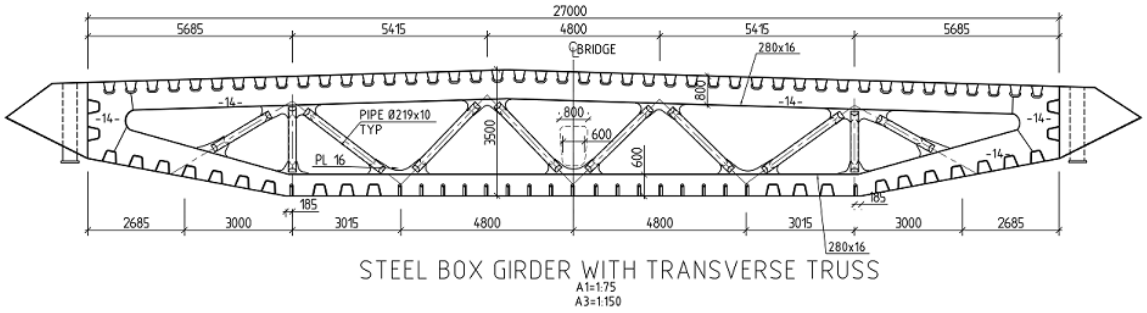


*Figure 7-5 Steel bridge girder – layout of transverse truss diaphragm spaced 4.0 m*

The deck constitutes an important part of the cable stayed bridge which is a well-documented standard product not adding a significant risk to the project. The steel girder is selected to grade S420 with a quantity of 8600 t.

## 7.5 Concrete deck

The closed 4-cell concrete deck that constitutes the 3 viaduct spans and the two stayed spans has ample reserves to cater for the various load effects, thus a moderate amount of posttensioning will be sufficient. The concrete bridge deck is fully fixed in the abutment and to the steel deck. The total length for the concrete deck is 260 m. In the 110 m closest to the tower, stay cables are anchored in the cross section through tubes cast with the concrete housing the passive end of the cables sticking through the bottom. A cross section of the concrete box girder can be seen in Figure 7-6.

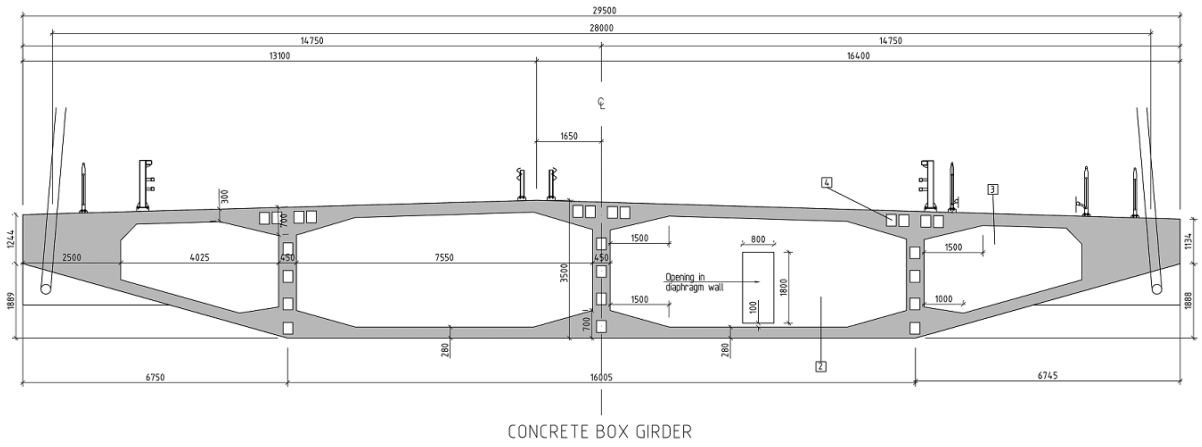


*Figure 7-6 Concrete box girder - cross section*

The cross section height is 3.5 m fitting the steel deck and somewhat optimal for a span length of 55 m and upwards to 70 m. The thickness of the bottom slab is 280 mm while the top slab is 300 mm and web thicknesses are 450 mm. Diaphragms are used at each pier and at each stay cable anchor. The diaphragm thickness is 3000 mm at piers and 500 mm at stay cable anchorages. Prestressing tendons are used in longitudinal direction and normal reinforcement amount of 160 kg/m$^3$ is used.

Construction of the bridge girder for the selected concept can be done by movable scaffolding system (MSS) spanning from pier to pier, incremental launching (ILM) or cast in place using traditional scaffolding supported on ground.

The concrete girder of the cable stayed bridge can be seen to consist of well documented standard products not adding significant risks to the project.

## 7.6 Bridge girder joint

The joint between the steel bridge girder and the concrete girder is located 135 m from the tower near the first side span pier. Here the strong axis bending moment due to ship collision is reduced to 50% of the maximum moment at the tower or less and the connection by means of post-tensioning cables and high-strength bars will then be less demanding.

The joint will be based on the same principles as used for the Pont de Normandie in France. The posttensioning cables will be anchored a certain distance from the joint inside the steel box and be cast in the concrete deck. Along the circumference of the steel box a number of high strength bars will be installed at tight spacings.

The connection could be established in two steps. First the steel box and the concrete deck is brought near to each other and partially stressed. In this locked situation a stich joint concrete (grout) is cast ensuring the complete connection of the two bridge deck types. After curing of the stich joint, the cables and bars are fully tensioned. The bridge girder joint of the cable stayed bridge

is not a standard solution but is however well-known technology from other large cable stayed bridges as the Pont de Normandie in France and the Russky Bridge in Russia.

## 7.7 Tower

The tower has a distinct A-shape that is architecturally preferred, and which is optimal seen in relation to the demanding ship collision loads being able to accommodate large forces in the transverse direction.

The tower is a concrete structure 220 m tall and A-shaped, meaning it has a high transverse stiffness and strength. The tower will also act strong for uneven loading of the cable planes in traffic and ship collision situations due to the interconnection of the legs at the top. The lower legs and cross beams are strong and forms a frame able to transfer large horizontal loads from ship impact to the ground. The form is technically sound and aligns well with the architect's preference, see Figure 7-7 and Figure 7-9.

The lower legs taper towards the foundation, where the bending moments therefore become small, hence the leg sections need to be large where they meet the cross beams. The frame connection requires transverse posttension from outside leg to outside leg through the cross beam, and likely also vertical posttensioning some depth down the inner flange of the lower leg.

Due to esthetical reason the tower foundations are selected fully buried into the ground.

Above the bridge deck, the tower legs are slender due to aesthetic reasons meaning that the compartment becomes compact. Moreover, the anchorages have been placed asymmetric in the legs making it possible to position all the stay anchorages along a straight line meeting each other at the tower top. At the location of steel boxes for the cable stay anchorages, there is only limited space for a stair to pass on one side of the asymmetrical placed stay anchorages. The space will however be large enough to allow for stay stressing equipment during construction, see Figure 7-8.

The analyses show that ship collisions and ULS tower demands are almost equally important. The concrete tower structure of the cable stayed bridge can be seen to be well documented standard products built before and therefore not adding significant risks to the project.

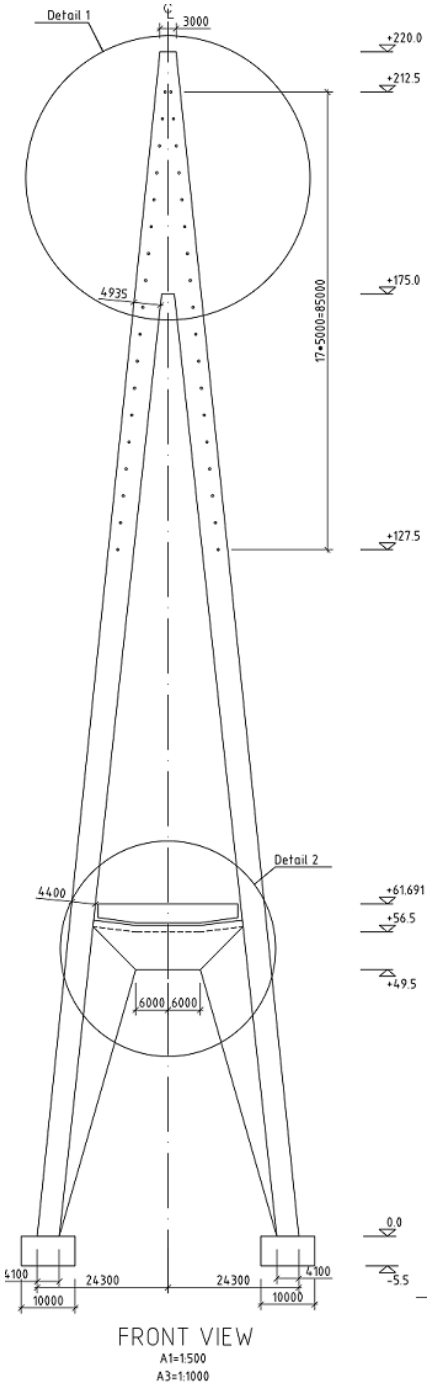


*Figure 7-7 Tower – front view*

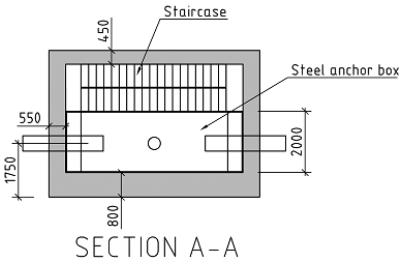


*Figure 7-8 Tower – plan section through leg at stay anchorages*

A visualisation of the cable stayed bridge can be seen in Figure 7-9 where the tower forms almost a lighthouse landmark.

*Figure 7-9 Cable stayed bridge with the tower forming a light house landmark*

## 7.8 Cable stays

The cable stays are parallel multi-strand cables having 31 strands nearest the tower, each 15.7 mm in diameter increasing in 6 steps up to 67 strands for the longest stays. The wire strength is 1860 MPa and hot dip galvanised and PE-sheathed individually and enclosed in HDPE-pipes. The cables have anchorages that fit with the steel tubes integrated with the main structure at either end. The stays are constructed by strand-by-strand tensioned from the tower.

The stays are arranged in 4 fans, each having 18 cables, the shortest nearest to the tower are subjected to the lowest loads, whereas the flattest outermost cables have the highest loads. The cables outbalance each other horizontally at the tower anchorage, however minor deviations are acceptable, and forces may be slightly redistributed.

The cable stay stressing ends are anchored in steel boxes in the tower legs making the tensioning process easy, whereas their passive ends are anchored at the bottom end of steel tubes sticking trough the verges of the bridge deck. Dampers are furthermore provided at the upper part of the tubes above deck level.

All load effects are comparable with those of other cable stayed bridges, except wave load effects to the longest stays nearest to the first pontoon of the floating bridge. In the present design the distance to the first stay is set to 20 m distance, but it is evaluated that the distance can be increased by further 20 m without any notable impact to the design.

The cable capacity for fatigue is checked and found to be very high. Traffic contributes most to fatigue near the tower while tide contributes most to fatigue in the northern bridge end in vicinity of the first floating bridge pontoon.

Additional damping might be necessary for the longest stays if snow is expected to accumulate on the stays. Other bridges have additional damping installed to safeguarding against stay oscillations due to possible snow accumulation, also well known by the Joint Venture.

The stays constitute an important part of the cable stayed bridge, however, they are well-documented standard products that are not supposed to add a significant risk to the project. The total quantity is 1000 tonnes approximately.

## 7.9 Side span piers

The concrete piers are rectangular, 10–11 m wide and 2.0–2.5 m thick. The height varies in accordance with the terrain, and the tallest pier is about 56 m. The piers will be governed by the ship collision effects (ALS) and forces from the load combination ULS3 (environmental load dominant). For the longest pier 1-E the load situation with wind on free standing pier is slightly governing for the foundation size and the reinforcement in the bottom of the pier.

The pier foundations are also rectangular and will be cast directly on rock or blasted rock with a concrete scaling. All the foundations are placed above water but buried into the ground due to esthetical reason. The piers can be cast by jump- or slip forming.

## 7.10 South abutment

The bridge deck is without expansion joints and instead fixed to the abutments in both south and north. Even with the piers integrated with the bridge deck, the south abutment is not subjected to high forces from ship collision, as was the case for the previous phase concepts. The tower will instead shelter the side span deck structure and the abutment against large bending moments round strong axis coming from ship collision and the ULS environmental load combinations will be dominant. The abutment can therefore be designed for the longitudinal tension force in the bridge deck. The force requires a gravity construction that can resist the longitudinal force by means of friction. The abutment is a cell concrete structure 30 m long and 28 m wide and 9.5m high filled with gravel.

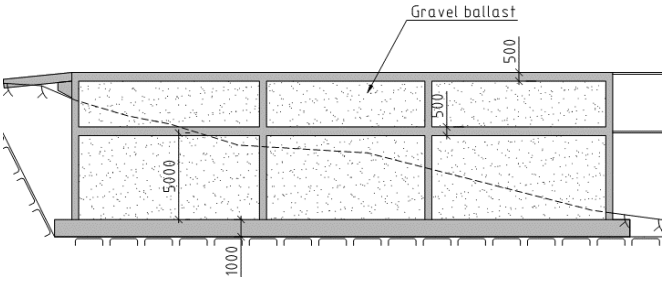


*Figure 7-10 South abutment – longitudinal section*

## 7.11 North abutment

The north abutment is fully exposed to the full ALS ship collision impact to the floating bridge pontoons or deck house collision to the bridge deck plus the normal ULS environmental load dominant combinations. The road is located at level 11.6 m and the foundation is positioned above water level. It has been necessary to design a concrete cell structure large enough to contain enough ballast in order to prevent rotation of the structure by means of friction between the base and ground.

The governing maximum ULS bending moment round strong axis becomes 2400 MNm, but the totally governing moment comes from the ALS ship collision situations of 5900 MNm. Both ship

collisions to the pontoons and deck house impacts to the floating bridge deck structure govern the design.

The abutment size becomes 50 m long and 36 m wide with a footprint of 52 m x 38 m. The fill inside the abutment is done with heavy ballast of iron ore. The abutment is presented in Figure 7-11 and can be seen to be a large box structure with longitudinal walls lining up with the longitudinal bulkheads in the steel floating bridge.

The bridge deck adjacent to the north abutment is widened and has increased strength compared with normal sections of the floating bridge. The joint between the abutment concrete structure and the steel deck of the floating bridge is secured with 150 nos. longitudinal posttensioning tendons.

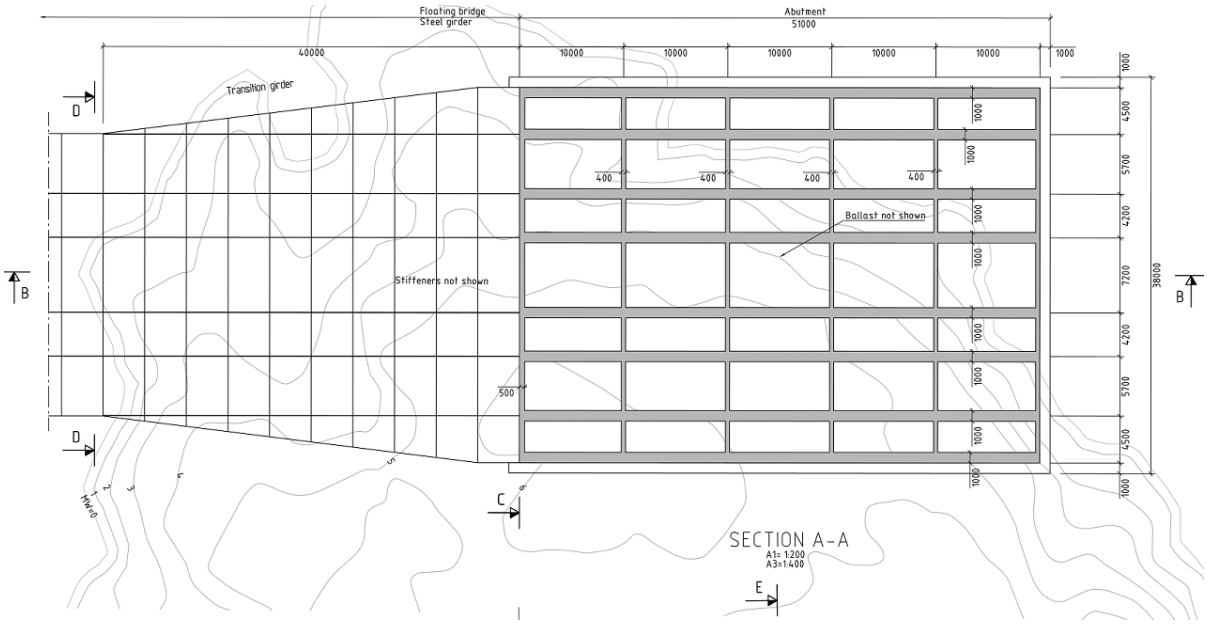


*Figure 7-11 North abutment - horizontal section*

Below is shown an illustration of the northern abutment and the tunnel entrance

*Figure 7-12 Illustration of the northern abutment and the tunnel entrance*

## 7.12 Design verification

This section presents briefly the philosophy behind the design and the verification method of the different bridge and abutment components. The overall design principles and the global FE-modelling will not be presented here as they are documented elsewhere. For a more detailed design verification of the cable stayed bridge and abutments, please refer to Appendix L.

**Steel deck:**

As explained earlier the design verification is carried using two different section types, cross section type H1 with minimum skin plate thicknesses and a reinforced section type H2, which compared to H1 is reinforced by 35-40% in area and strength. Below in Figure 7-13 is presented a graph taken from the global model. The graph presents the different cross section types utilised in the global FE-modelling. It can be seen that H2 is used strengthening the deck in the vicinity of the tower at position A2 and when approaching the first pontoon of the floating bridge in position A3. The remaining steel deck has cross section type H1 and for the concrete deck only cross section type C1.

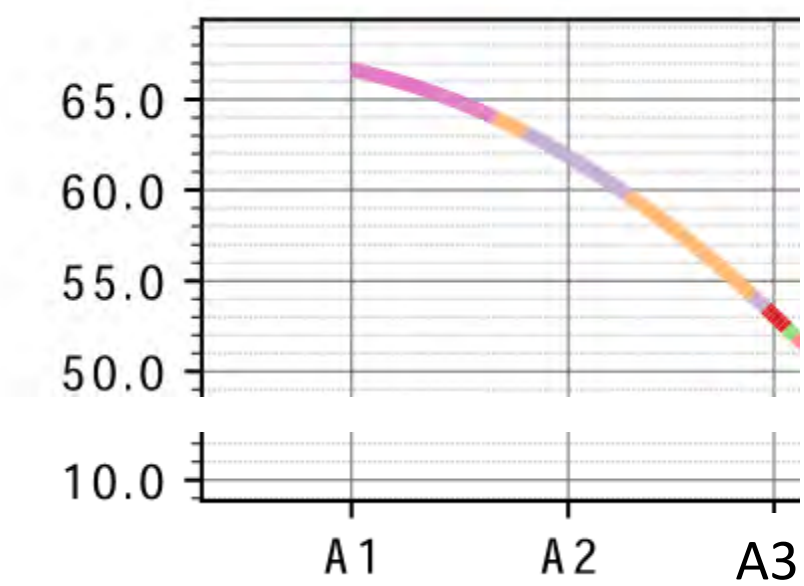


*Figure 7-13 Global FE-model, cross section types along the cable stayed bridge, y-axis is elevation of deck x-axis - A1 is start of side span, A2 is Tower position, A3 is position of first pontoon*

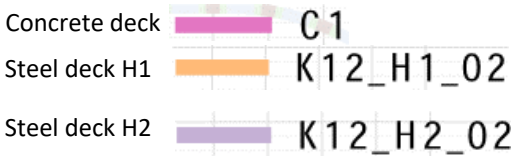


A summary of ULS analyse results represented by the important bending moment round strong axis is shown in Figure 6-3.

The maximum moment occurs at the tower for the ULS3 load combination with a maximum value of 2100 MNm. It can further be seen that ULS3 (environmental load dominant) in general is worse than ULS2 (traffic load dominant).

For the ULS load situations, the material factor is $\gamma_m$ =1.1, which for steel S420 with mostly thin plates gives $f_{yd}$ = 420/1.1 = 382 MPa. This value has been used as the limit in the von Mises plots shown for the ULS2 (traffic load dominant) and ULS3 load situations (environmental load dominant), see Figure 6-22.

The design verification is done within the global FE-model by postprocessing routines using the same principles as for the floating bridge. In Figure 6-24 is presented the ULS design verification using the reduced width method in accordance with Eurocode, referred to as "method 2".

In general, it is seen that ULS3 load situations govern the design and the utilisation ratio is below 1.0 unless for 3 small peaks – one at the tower locations, another at the intersection between cross

section type H1/H2 and the third when approaching the first pontoon of the floating bridge. All peaks of over utilisation are small and found acceptable at this stage of design. Steel from other locations can be moved to these areas bringing the utilisation below 1.0 without increasing the total steel deck quantity.

A summary of ALS analyses results represented by the important bending moment round strong axis are shown in Figure 14-1. For the ALS load situations, yielding becomes $f_{yd}$ = 420/1.0 = 420 MPa.

From the figure can be seen that deck house collision in general is worse that the pontoon collision, which is also applicable for the cable stayed bridge. The maximum bending moment round strong axis becomes 3300 MNm for deck house collision and 2800 MNm for pontoon collision.

The envelope of von Mises stresses in the bridge girder are shown in Figure 14-3. The response is almost within the elastic range for the cable stayed bridge, see A1-E to A3 which is judged to be fully acceptable for the design verification of the ALS load situations at this stage of the project. Please furthermore note that a full design verification using the reduced width method has not been performed for the ALS design situations. However, based on results from the ULS analyses, it can be expected that the utilisation will increase by approximately 10% when considering the full design verification using reduced width method (method 2). For the ALS ship collision this over utilisation is however found acceptable at this stage of the design.

**Concrete deck:**

Capacity diagrams for bending-axial interaction are plotted for design forces at the side span support axes below. The reinforcement and prestressing amounts are chosen so that capacities are fulfilled for the different sections and load situations. It is possible, without getting any high reinforcement amounts or congestion problems, to increase the capacity considerably.

The capacity diagram for the section shows that moment about strong axis is most critical compared to the moment about weak axis. The most critical load is the ALS ship impact.

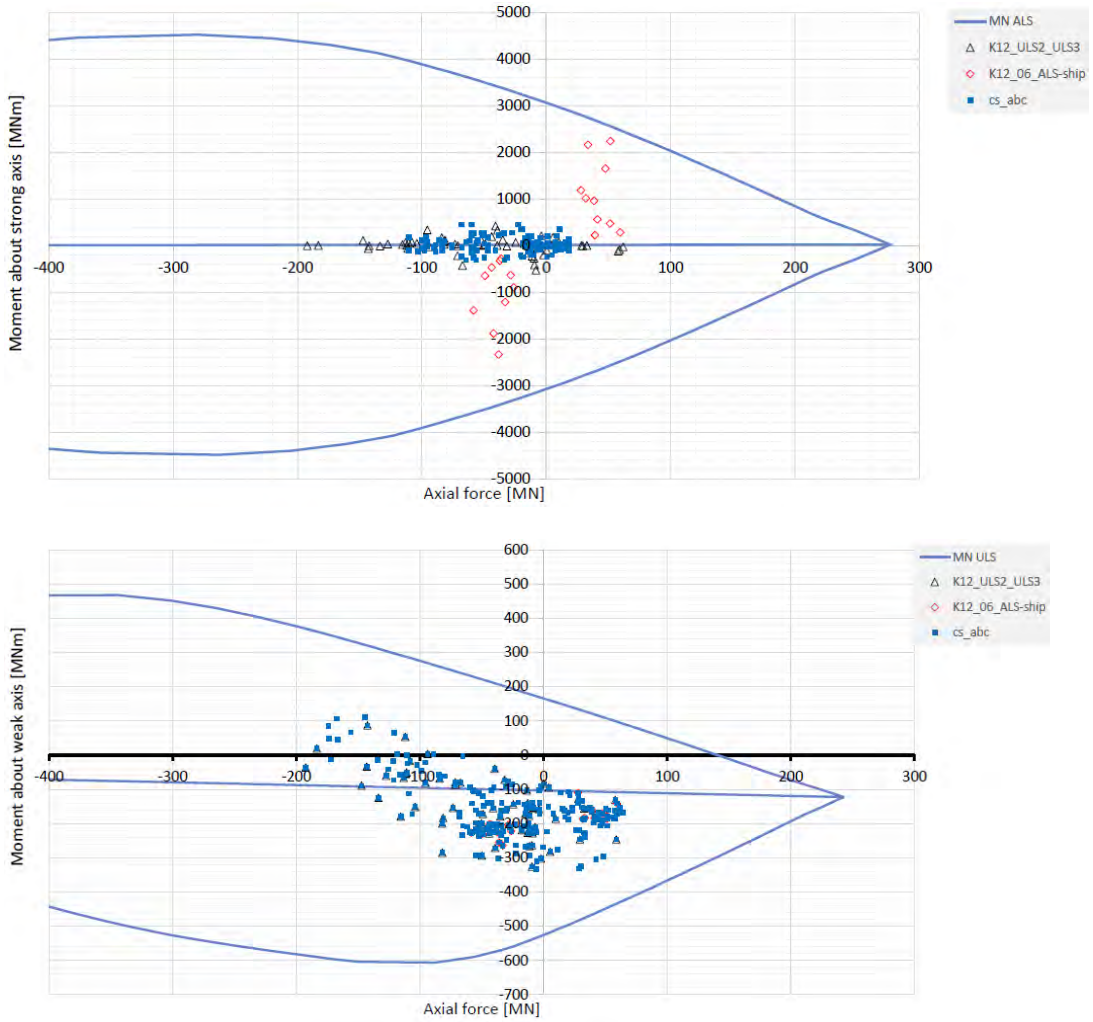


*Figure 7-14 Capacity diagrams. Concrete bridge deck at side span support axes. Triangle – ULS2 & ULS3, red diamond – ALS ship collision, blue square – erection situations*

**Tower:**

Here the important tower section of the leg at cross beam interface will be verified using capacity diagrams for bending-axial interaction, see Figure 7-15.

The capacity diagram for the leg sections shows that moment about transverse axis is most critical compared to the moment around longitudinal axis. The most critical load is wind on the free-standing tower during the construction stage situations.

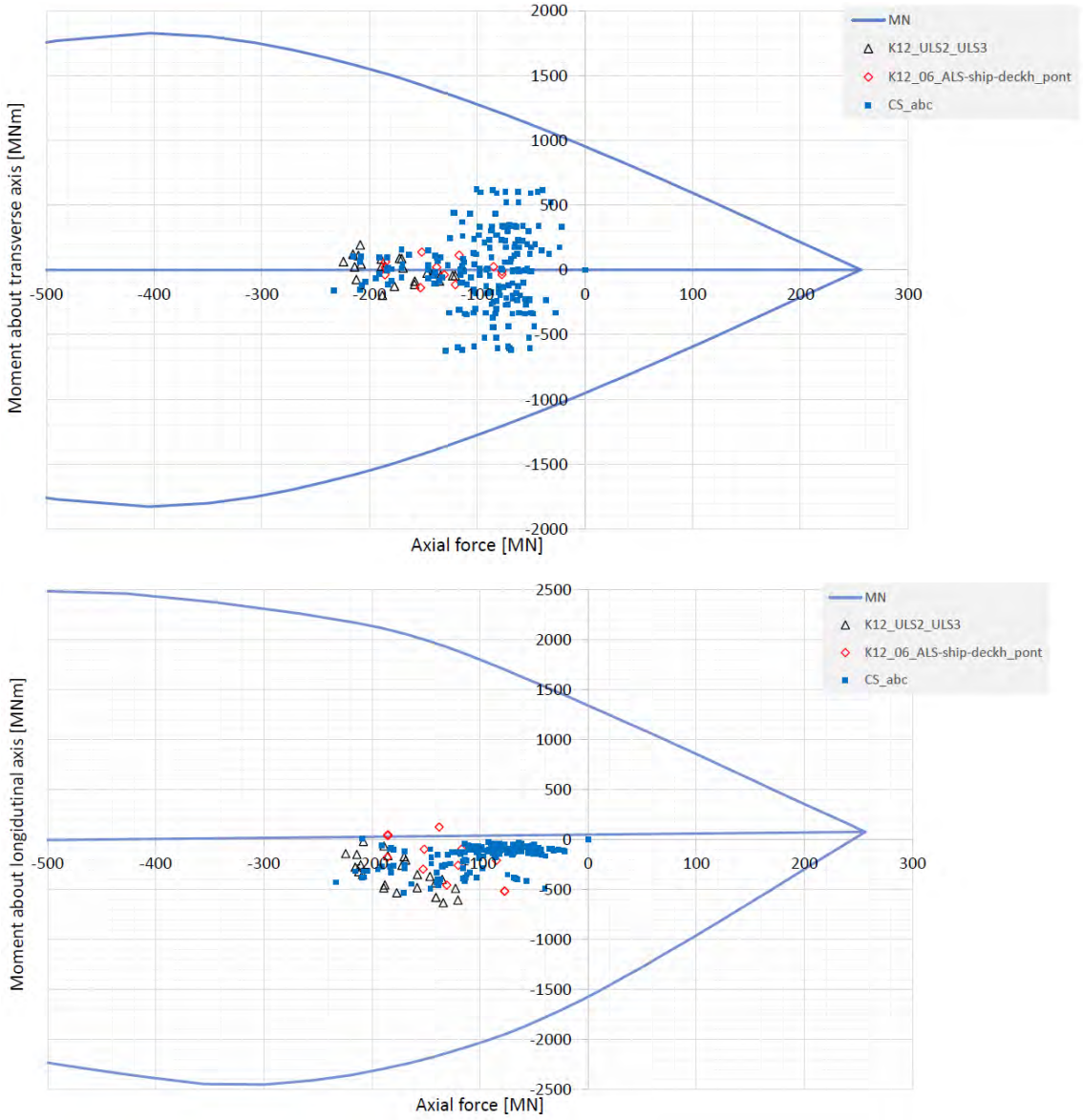


*Figure 7-15 Tower legs at cross beam interface, capacity diagrams. Triangle – ULS2 & ULS3, red diamond – ALS ship collision, blue square – erection situations*

The capacity diagrams for the cross beam itself are not presented here, but both wind in construction stage, ULS and loads from ALS ship impact are governing load situations. Moment about the horizontal axis is the governing action.

The foundation sizes are governed by wind forces on free standing tower during construction.

**Cable stays:**

The max/min ULS stay cable forces are presented in Figure 7-16, where also the stay capacities are plotted. Stay forces are below capacities and no slack is observed even in the min ULS load situations. In general, the permanent load is dominant, followed by traffic load, whereas wind and wave loads are of relatively little influence.

The characteristic maximum and minimum stay forces are furthermore presented in Figure 7-17 and Figure 7-18 for each load group – dead load, traffic, temperature, dynamic 100 year wind+wave+swell, dynamic 1 year wind+wave+swell and finally 100 year wave loading.

The most noticeable effect for wind and wave is the wave load effects to the stays nearest to axis 3, and their side span stays.

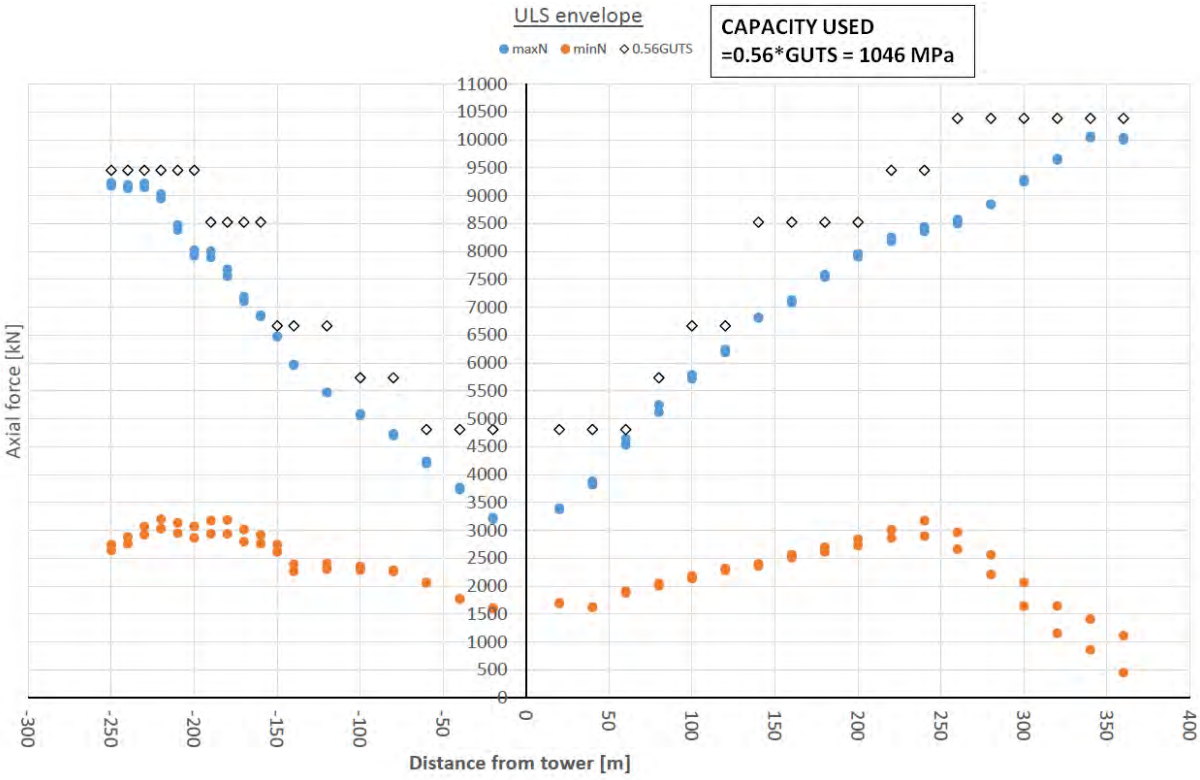


*Figure 7-16 Stay cables. Max and min ULS forces and capacity*

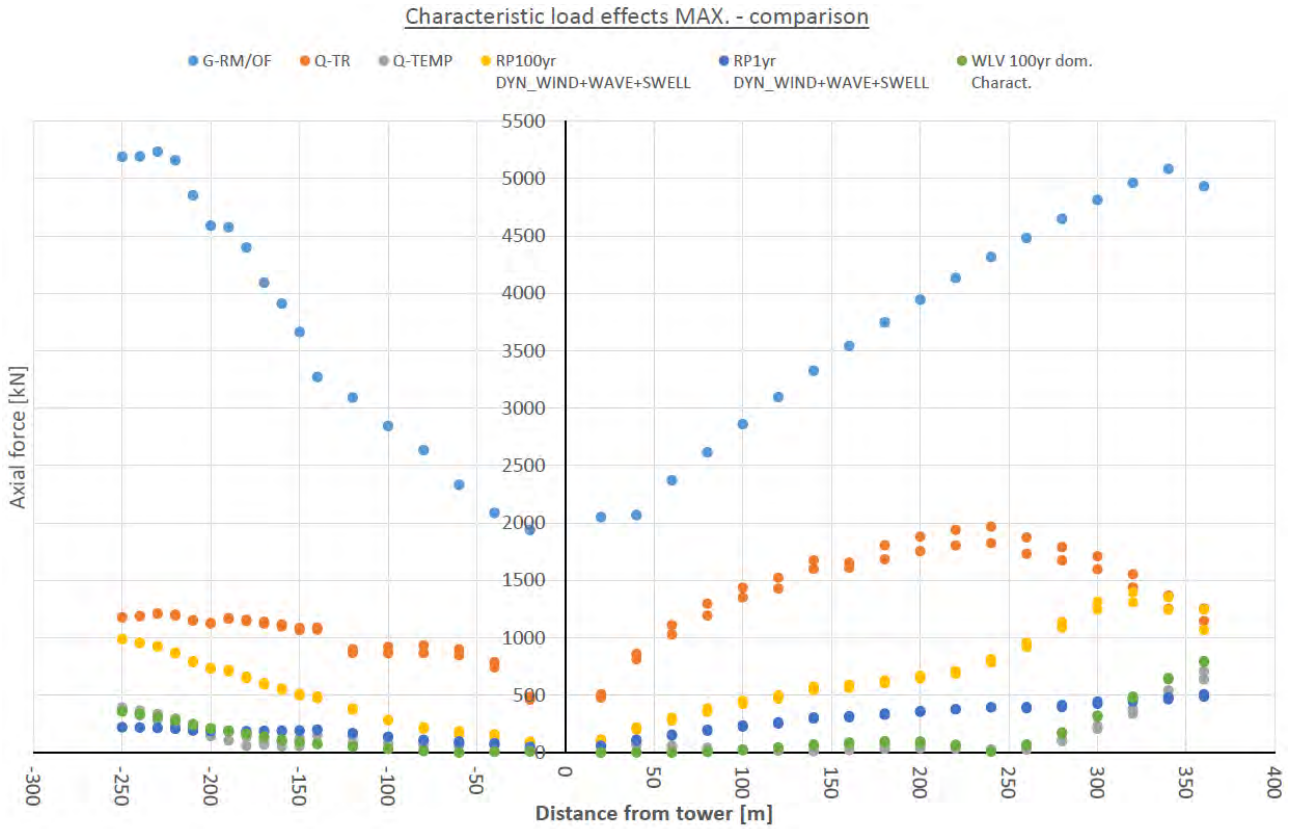


*Figure 7-17 Stay cables. Max characteristic load group forces*

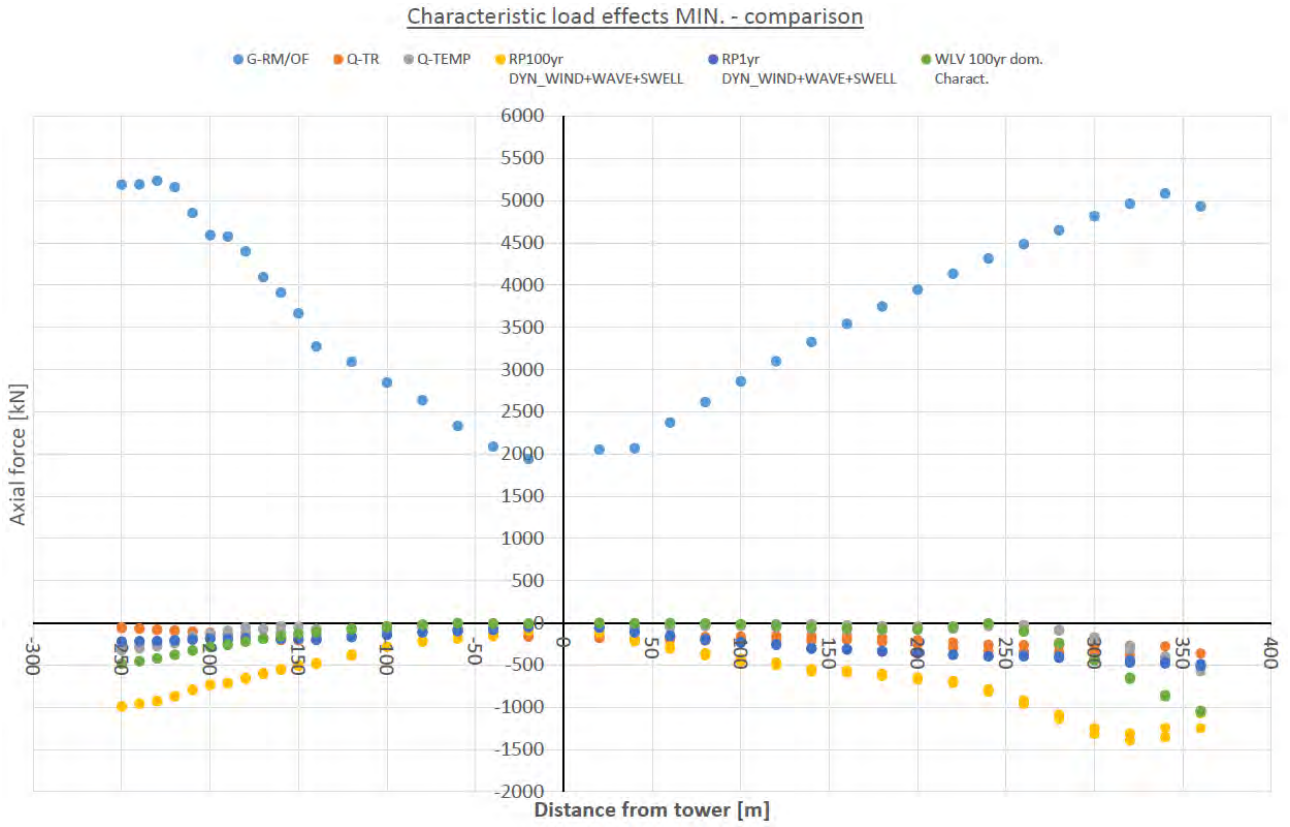


*Figure 7-18 Stay cables. Min characteristic load group forces*

**Side span piers:**

Capacity diagrams for bending-axial interaction are plotted for the piers at the foundation interface for both ULS and ALS load situations, see Figure 7-19.

Generally, the bending moment about the transverse axis in phase A1 will be more critical than the bending moment about the longitudinal axis.

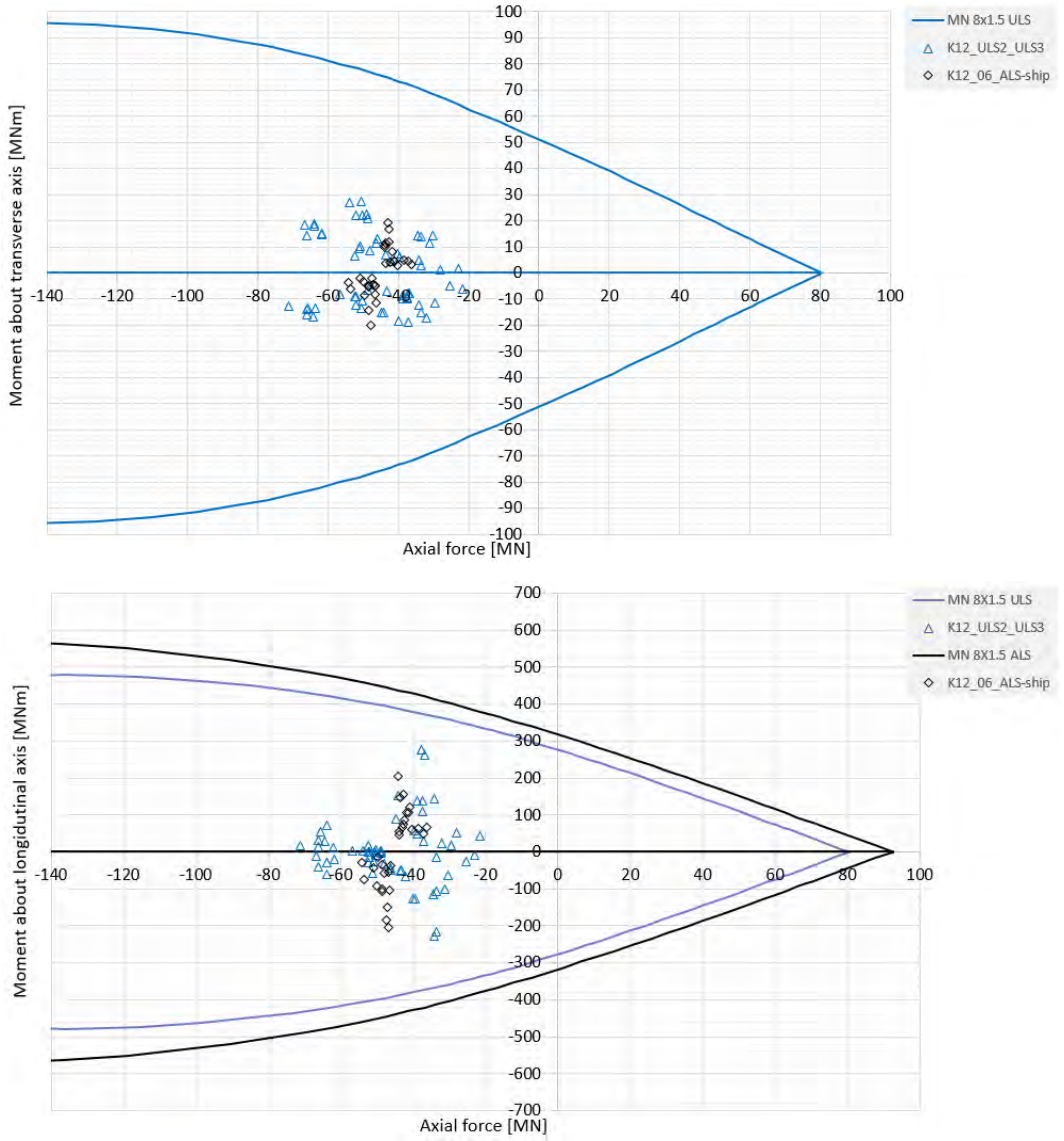


*Figure 7-19 Side span pier, ULS & ALS, capacity diagrams Triangle – ULS2 & ULS3, diamond – ALS ship collision*

**South- and north abutment:**

At this stage it is chosen to design the abutments by considering their self-weight only. The necessary weight is estimated by using a friction coefficient of 1.0 for the resulting shear from horizontal loads and moment about the vertical axis, (twisting moment), on an effective area, (length/width reduced with twice the eccentricity in each direction). The stability is checked for both ULS and ALS ship impact. The ULS combination that gives the highest demand is ULS 3 (wind and wave dominant). The joint between the floating bridge steel girder and the abutment concrete walls are prestressed ensuring no tension occurs in the SLS condition.

## 7.13 Quantities - summary

For easy reference, a summary of the overall quantities for the cable stayed bridge and the south- and north abutment is presented in Table 7-1.

*Table 7-1 Overall quantities for cable stayed bridge and abutments*

| Item | | Construction unit | Quantity |
|---|---|---|---|
| Cable stayed bridge | Concrete | Tower foundation, concrete B45 | 2400 $m^3$ |
| | | Tower, concrete B45 | 7900 $m^3$ |
| | | Bridge deck, concrete B45 | 8300 $m^3$ |
| | | Piers & foundations, concrete B45 | 5600 $m^3$ |
| | Steel | Bridge deck, steel S420 | 8500 t |
| | | Tower anchor boxes, steel S355 | 300 t |
| | | Stays, cable steel 1860 MPa | 1000 t |
| Abutments | South | Abutment south, concrete B45 | 4100 $m^3$ |
| | | Abutment south, ballast gravel | 4500 $m^3$ |
| | North | Abutment north, concrete B45 | 8800 $m^3$ |
| | | Abutment north, ballast iron ore | 12000 $m^3$ |

# 8 Mooring systems

## 8.1 General on mooring system

A mooring system has been developed to support the floating bridge concepts for crossing Bjørnafjorden. The curved bridge concept has three moored pontoons relatively close to the centre with four mooring lines each, giving a total of 12 mooring lines anchored to the seabed. All anchors are suction anchors located on a relatively flat seabed with sufficient seabed soil for installation and stability. The figure below shows typical mooring system on seabed map and corresponding Orcaflex analysis model:

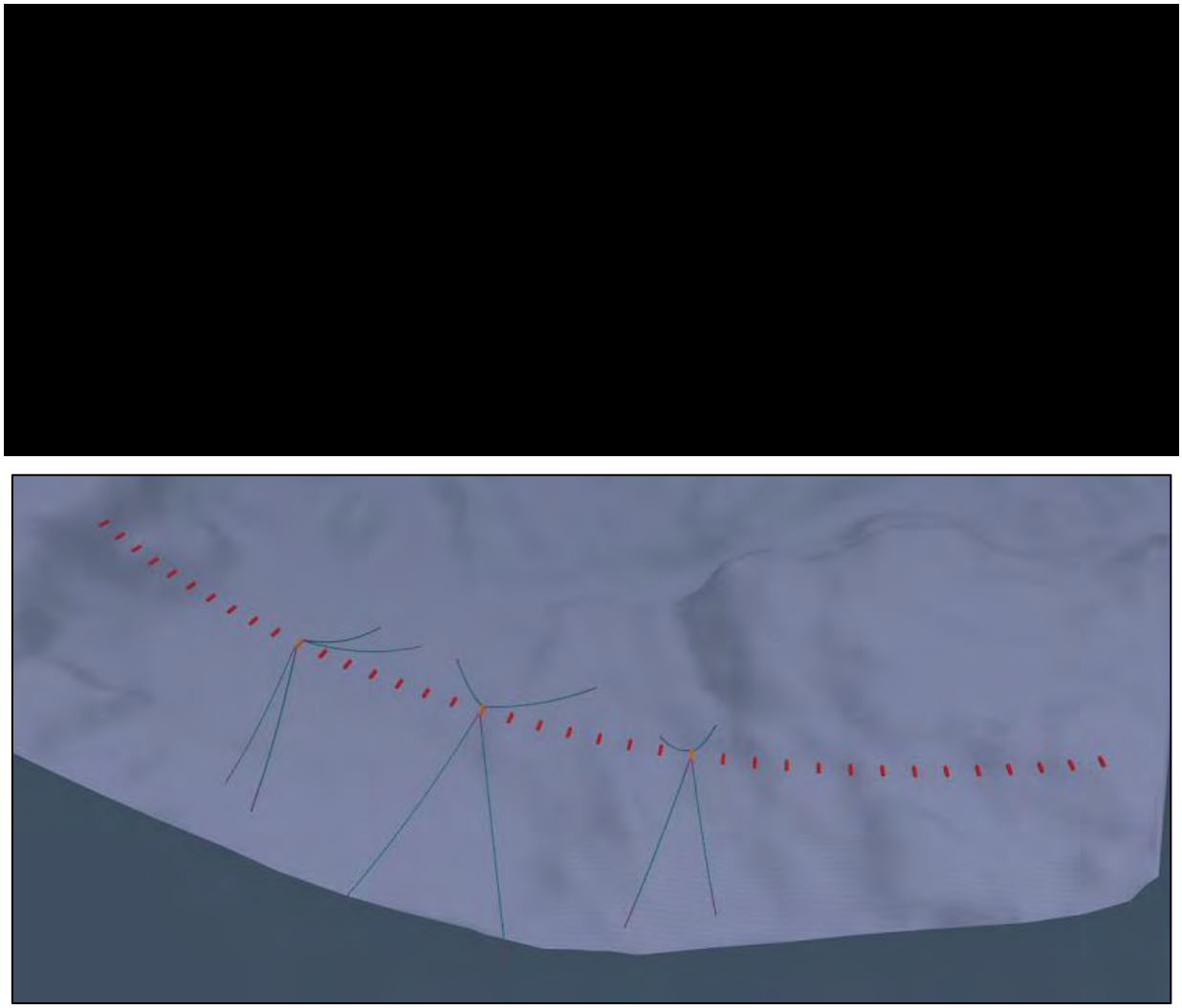

*Figure 8-1 Typical mooring system on seabed map (top) and in Orcaflex model (bottom), K12.*

All components of the mooring system are well known from floating offshore installations all around the world. Four dual axis fairleads are installed on the three moored pontoons. The fairleads will reduce any chain bending moments on the top end of the mooring chain. The fairleads are installed close to the bottom of the moored pontoons. This is done to reduce corrosion on the top end mooring chain and to avoid damage from ship collision.

The mooring lines have R4 chain and 124 mm coated steel wire ropes. All lines have 50 m top chain between fairlead connection on the pontoon and the wire rope segment. All lines have 100 m bottom chain between the wire rope segment and the anchor. Mooring line pretension has been

optimized to give the desired line pretension or transverse restoring stiffness for each pontoon. The mooring line tension will also provide minimal total enforced loads from the mooring lines on each pontoon during equilibrium bridge position in calm weather. The mooring lines are pretensioned to 1.9-2.6 MN, providing a relatively taut system where the bottom chain most of the time will be suspended and not lay on the seabed. Mooring line segmentation principles are presented below for suction and gravity anchors:

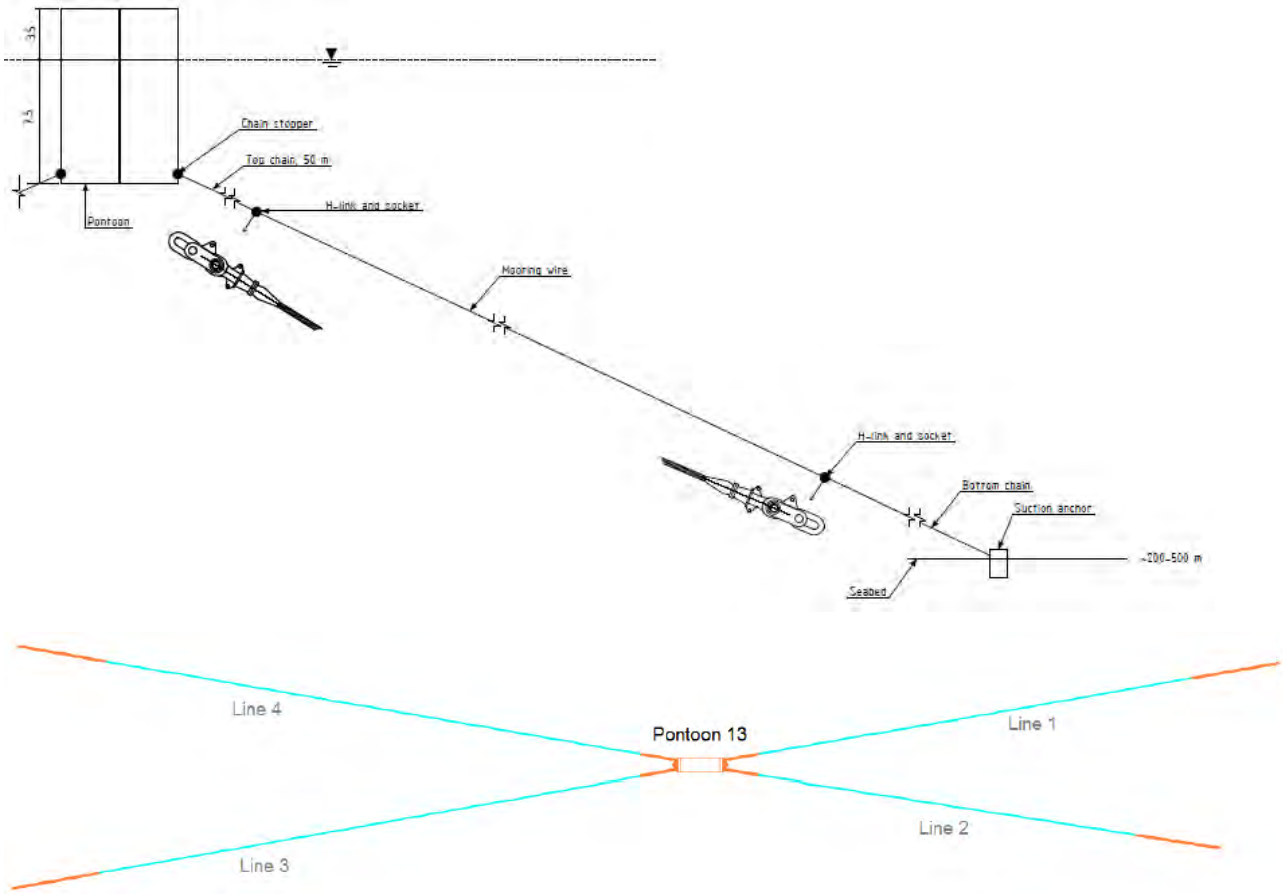


*Figure 8-2 Typical mooring line segmentation with suction anchor (side view and top view)*

Anchors locations are found to suit both a symmetrical mooring spread and locations on seabed with acceptable condition such as seabed slope and soil thickness. Anchor positions are based on anchor suitability maps showing colour coded areas for each anchor type and recommendations from NGI based on the same geotechnical data. All anchors are located around 350-500 m water depth on relatively flat parts of the seabed. All anchors also have an alternative identified location close to the original location as a backup.

## 8.2 Results from mooring analysis

Mooring calculations has been performed for worst intact condition, after multiple line breaks, during ship collision and fatigue life of mooring lines. Maximum intact mooring loads for each line are presented below:

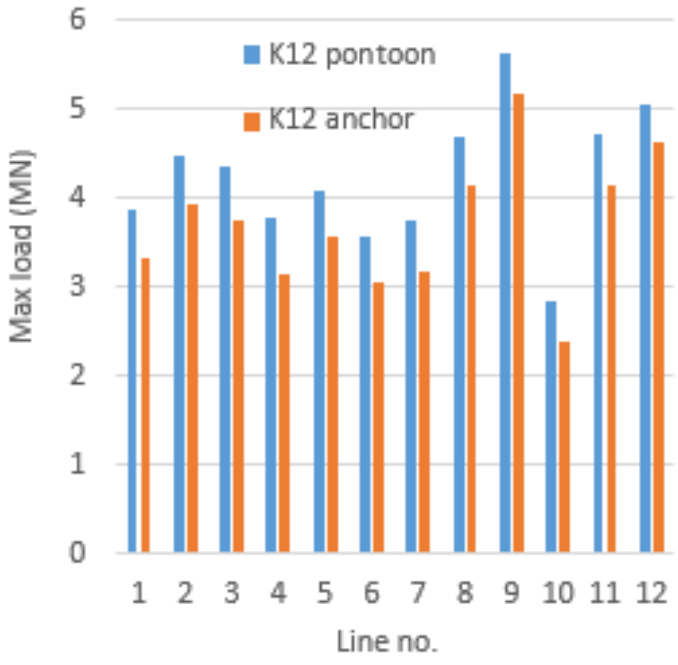


*Figure 8-3 Maximum intact mooring line loads*

Damage condition has been analyzed for line break (removing several lines) and transient loads during ship collision. Maximum damage mooring loads for each line are presented below:

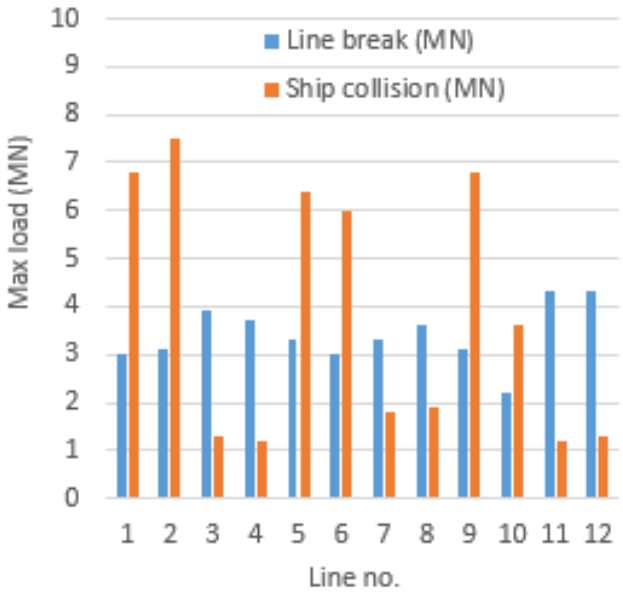


*Figure 8-4 Maximum damage mooring line loads*

Maximum mooring line loads establish the minimum safety factors. The minimum safety factors and requirements are presented below:

*Table 8-1 Line safety factors*

| Safety Factor (-) | Pontoon | Anchor | Required |
|---|---|---|---|
| ULS | 3.02 | 2.90 | > 2.20 |
| ALS line break | 3.95 | | > 1.50 |
| ALS ship collision | 2.27 | | > 1.10 |

The mooring system design life will be 100 years. All components will either be replaced or have 100-year fatigue life. Top chain and steel wires should be replaced once, thus having 50 years fatigue life. All other mooring system components will have at least 100-year fatigue life. Minimum fatigue life of all mooring lines is presented below:

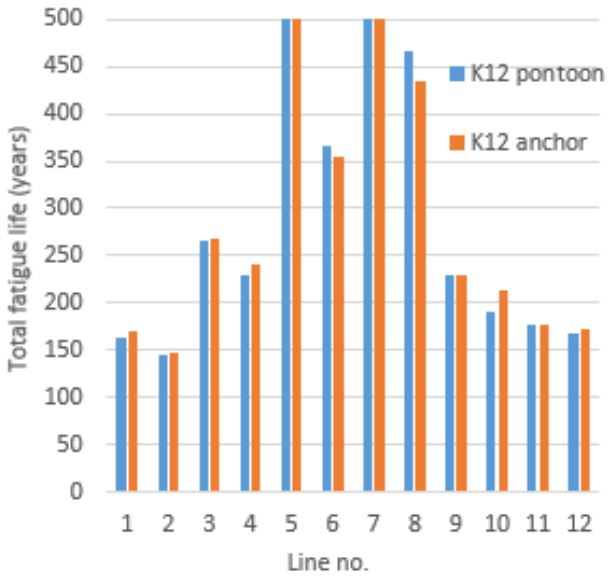


*Figure 8-5 Fatigue life of mooring lines*

The results show that utilization and fatigue life vary significantly between the lines for all bridge concepts. The line fatigue calculations have also been checked with simplified estimations due to OPB/IPB. The results suggest that OPB/IPB on top end of the chain is relatively small and will have a minor impact on the fatigue life.

All mooring lines satisfy the given requirements to loads and fatigue life.

## 8.3 Geotechnical evaluation

Bjørnafjorden is characterized by steep flanks with slope angles exceeding 30°, surrounding the essentially flat central fjord basin. In the shallower areas, the terrain is hummocky due to bedrock outcrops. However, several tens of meters of sediment has accumulated in the basin and significant sediment thicknesses are encountered even in slopes with more than 20° inclination. The soil conditions at the site are primarily the result of the glacial processes and the sediments consist of soft clays.

Several anchor types have been evaluated for mooring of the floating bridge concepts. The suction anchor is considered the most suitable due to its proven technology, its ability to sustain high design loads and its flexibility to be designed to accommodate the varying sediment thicknesses in the fjord.

Suitable anchor locations are found for the investigated bridge concepts. The seabed at the anchor locations is relatively flat with acceptable and favourable thickness of top soft sediments at most locations for suction anchors.

The bridge will be moored by 12 suction anchors. The suggested anchor diameter is for all but two anchors D=6 m and the skirt penetration depth vary between 10 m and 18 m. At two locations the anchors have D=8 m and skirt penetration depth 14 m. This is suggested due to the more limited sediment thickness. Near each of the suggested anchor locations it has been checked that it is possible to relocate an anchor if required. Industry practice has often been to require a distance >3 diameters from the target location if the first installation fails and the anchor must be relocated.

Significant earthquakes may trigger submarine slope instabilities with run outs that may hit one or more anchors. The anchor locations were selected by trying to reduce the risk of being hit by a submarine slide, but it is still possible, and at certain locations it is likely that one anchor or one anchor cluster may be severely damaged by the impact in the event of a major slide. At locations where the sediment thickness is large, say >25 m, there could be a potential for oversizing the anchor to be able to resist a major slide impact. However, there are many uncertainties to such calculations and in particular the ploughing depth of the sliding masses.

For further details, see appendix M with enclosed memos 12-NOT-182 and 12-NOT-090.

*Table 8-2 Anchor type, dry weights and dimensions*

| Anchor no | Anchor type | Anchor dry weights | Anchor dimensions | |
|---|---|---|---|---|
| | | | Diameter (m) | Depth (m) |
| 1 | Suction | 144 t | 6 | 18 |
| 2 | Suction | 144 t | 6 | 18 |
| 3 | Suction | 144 t | 6 | 18 |
| 4 | Suction | 126 t | 6 | 15 |
| 5 | Suction | 126 t | 6 | 15 |
| 6 | Suction | 126 t | 6 | 15 |
| 7 | Suction | 126 t | 6 | 15 |
| 8 | Suction | 144 t | 6 | 18 |
| 9 | Suction | 169 t | 8 | 14 |
| 10 | Suction | 97 t | 6 | 10 |
| 11 | Suction | 126 t | 6 | 15 |
| 12 | Suction | 169 t | 8 | 14 |

# 9 Aerodynamics

## 9.1 General

This section contains a summary of aerodynamic assessment of the K12 alternative for the Bjørnafjorden crossing. Further details are given in Appendix E: Aerodynamics. The work has been focused on the following tasks:

1. Derive aerodynamic load coefficients for the relevant cross sections. For the most important cross section, the stiffening girder, a CFD analysis was performed. The coefficients are calibrated towards the wind tunnel tests and used as input to the analysis.
2. Perform aerodynamic stability analysis of K12 to assure that the behaviour of the bridge is predictable.
3. Assess the effect on dynamic response of the bridge due to variation of wind parameters along the alignment (i.e. inhomogeneity of wind).
4. Identification of other aerodynamic phenomena which can impact the design or operability of the structure.

It is recommended to perform detailed wind tunnel test before concluding on the girder cross sectional design and cable design.

## 9.2 Aerodynamic coefficients and aerodynamic derivatives

Aerodynamic coefficients, both static and aerodynamic derivatives, was calculated by use of CFD (discrete vortex method). The CFD results were calibrated versus wind tunnel tests and take into account near ground effects for the low part of the bridge. For the high bridge part at zero degree angle of attack, Cd was found to be 0.68. Near ground effects increase these numbers by 20%. Traffic typically increased the drag factor with 70%. Aerodynamic coefficients is also given for cables (typically Cd=0.8), towers and columns (both typically Cd=1.5). An example of output from the CFD analysis is shown in Figure 9-1, the static aerodynamic coefficients of the bridge girder in Table 3 and the aerodynamic derivatives in *Figure 9-2 Aerodynamic derivatives for the K12 cross section from discrete vortex simulations*

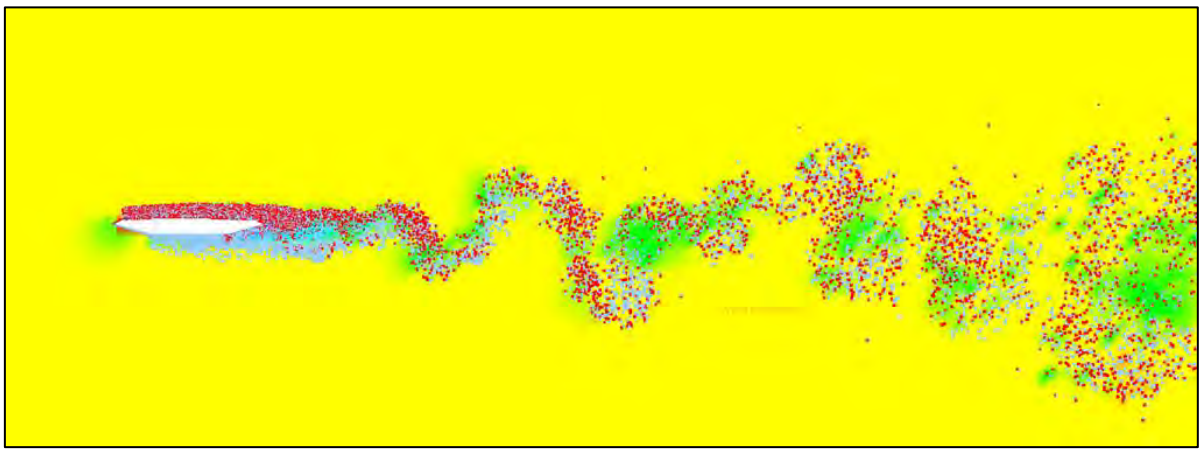

*Figure 9-1 Example of output from CFD analysis*

*Table 3 Aerodynamic load coefficients used in integrated analysis*

| AOA | AOA | Cd [] | Cd [] | Cd [] | Cd [] | Cl[] | dCl[] | Cm[] |
|---|---|---|---|---|---|---|---|---|
| [deg] | [rad] | HB | HB/wT | LB | LB/wT | | [1/rad] | |
| -8,00 | -0,140 | 1,261 | 2,144 | 1,513 | 2,572 | -0,941 | | 0,110 |
| -5,00 | -0,087 | 0,883 | 1,501 | 1,060 | 1,801 | -0,731 | 4,148 | 0,069 |
| -3,00 | -0,052 | 0,752 | 1,278 | 0,902 | 1,534 | -0,579 | 4,502 | 0,033 |
| -1,50 | -0,026 | 0,699 | 1,188 | 0,839 | 1,426 | -0,456 | 3,839 | 0,007 |
| 0,00 | 0,000 | 0,681 | 1,158 | 0,817 | 1,389 | -0,378 | 3,247 | -0,019 |
| 1,50 | 0,026 | 0,672 | 1,142 | 0,806 | 1,371 | -0,286 | 3,667 | -0,045 |
| 3,00 | 0,052 | 0,687 | 1,168 | 0,824 | 1,401 | -0,186 | 3,487 | -0,067 |
| 5,00 | 0,087 | 0,766 | 1,302 | 0,919 | 1,563 | -0,073 | 2,727 | -0,096 |
| 8,00 | 0,140 | 0,909 | 1,545 | 1,091 | 1,854 | 0,052 | | -0,125 |

HB=High Bridge, LB=Low Bridge, wT=with Traffic, ALL=valid for whole bridge

Coefficients derived for turbulent flow.

For the traffic cases the reference height is the height of the bridge deck without the traffic box

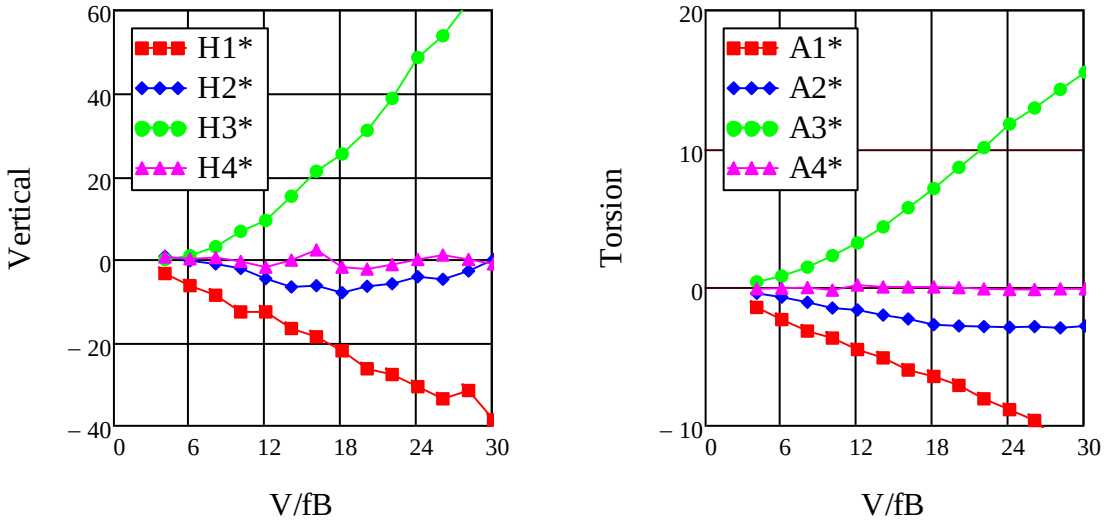


*Figure 9-2 Aerodynamic derivatives for the K12 cross section from discrete vortex simulations*

## 9.3 Wind input

Chapter 2 in the Metocean Design basis give details about how the wind shall be defined for the structure and is based on a wind measurement campaign at the bridge site. Among other things it specifies a variation of the magnitude of the mean wind speed along the alignment and gives range of possible variations of wind parameters.

For the actual design wind input is taken from N400 standard values. Where N400 does not give any indications, ESDU is used. Table 4 shows the values used in design.

Variation of mean wind along the alignment was addressed in a separate study summarized below and reported in detail in Appendix E: Aerodynamics.

*Table 4 Recommended wind input for analysis*
*According to clarification 304624-1-A-0041 N400 values are used in design*

| Parameter | Z=10m | Z=50m | P-level |
|---|---|---|---|
| xLu [m] | 100,0 | 162,1 | N400 |
| xLv [m] | 25,0 | 40,5 | N400 |
| xLw [m] | 8,3 | 13,5 | N400 |
| Au | 6,8 | 6,8 | N400 |
| Av | 9,4 | 9,4 | N400 |
| Aw | 9,4 | 9,4 | N400 |
| Cux (*) | 3,0 | 3,0 | N400 |
| Cuy | 10,0 | 10,0 | N400 |
| Cuz | 10,0 | 10,0 | N400 |
| Cvx (*) | 6,0 | 6,0 | N400 |
| Cvy | 6,5 | 6,5 | N400 |
| Cvz | 6,5 | 6,5 | N400 |
| Cwx (*) | 3,0 | 3,0 | N400 |
| Cwy | 6,5 | 6,5 | N400 |
| Cwz | 3,0 | 3,0 | N400 |
| (*) Not given in design basis – N400 or ESDU values used. | | | |

## 9.4 Dynamic effects of inhomogeneity

### *9.4.1 General*

The effect on the dynamic response of inhomogeneity in the wind due to aerodynamic forces has been studied in the frequency domain. The analysis is performed with a simplified frequency domain method implemented. The main simplification is on the load model, it is linearized, and that only the resonant part of the response is included. A separate check was performed to estimate the effect of including the background part of the response, and it increased the standard deviation with about 6% compared to what is reported herein. Only response from wind is included in these results.

All results were measured towards results from standard N400 formulas with the following values, which corresponds to parameters with 100y return period:

Basic wind speed at z=10m : vb=25.2m/s
Surface roughness: z0=0.01
Length scale at z=10m: xLu=100m
Spectral shape parameter: Au=6.8
Decay parameters: Cux=3, Cuy=10, Cuz=10

As a first step a comparison between the simplified method (blue line), time domain response calculations by Orcaflex and hand calculations was performed. The results are shown in Figure 9-3. As can be seen the agreement is fairly good.

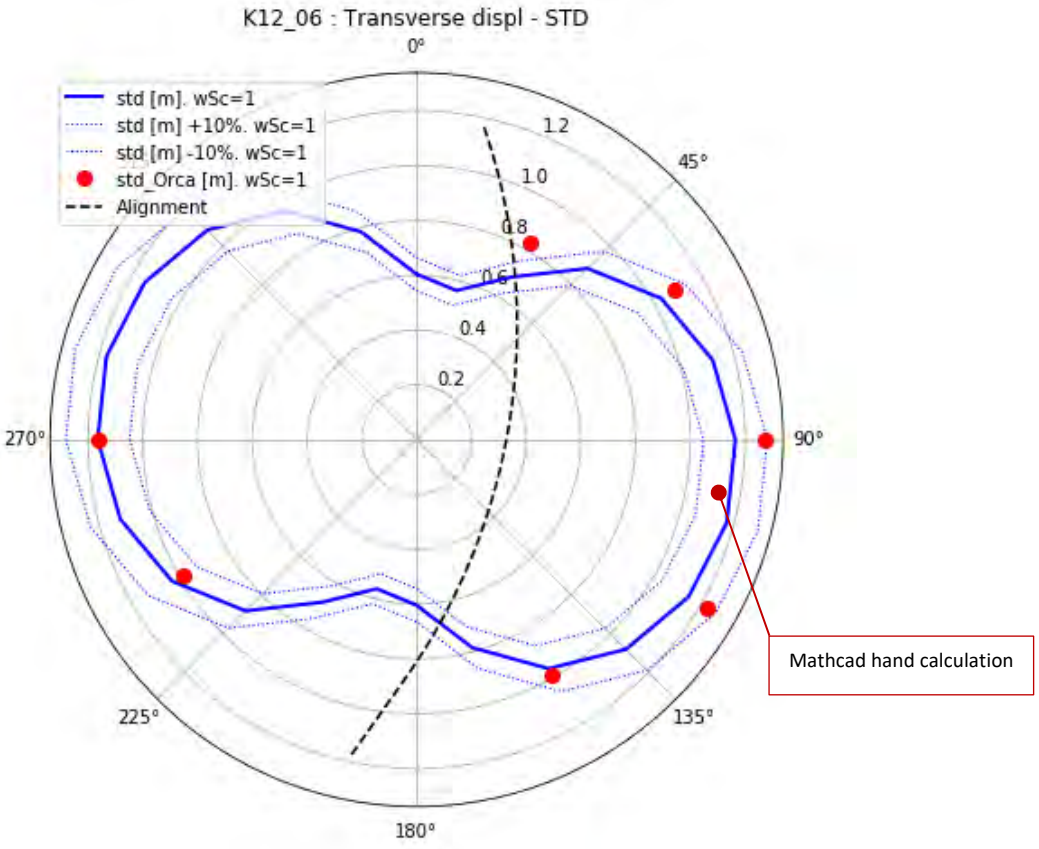


*Figure 9-3 Comparison of standard deviation between simplified method and Orcaflex*
*Blue solid line: Simplified method. Blue dotted lines: Simplified method +/- 10%*
*Red dots: Orcaflex (average of 10 runs). Black broken line: Alignment of K12*

### *9.4.2 Dynamic response effects of variation of mean wind speed along the alignment*

The Metocean Design Basis specifies possible variation of the mean wind speed along the alignment. The dynamic response effect is studied for constant wind along the alignment (1.0V, where V is a reference mean wind speed), linearly varying from 0.6V at one end to 1.0V on the other, linearly varying from 1.0V at one end to 0.6V on the other and linearly varying from 0.8V at one end, 1.0V in the middle and 0.8V at the other end.

Figure 9-4 summarizes the result of this analysis performed for wind from all directions. Generally, maximum dynamic response is found for wind perpendicular to the main axis when the mean wind is uniformly distributed along the alignment. For cases with non-uniform distribution of mean wind, the dynamic response is smaller than for the case with uniform distribution.

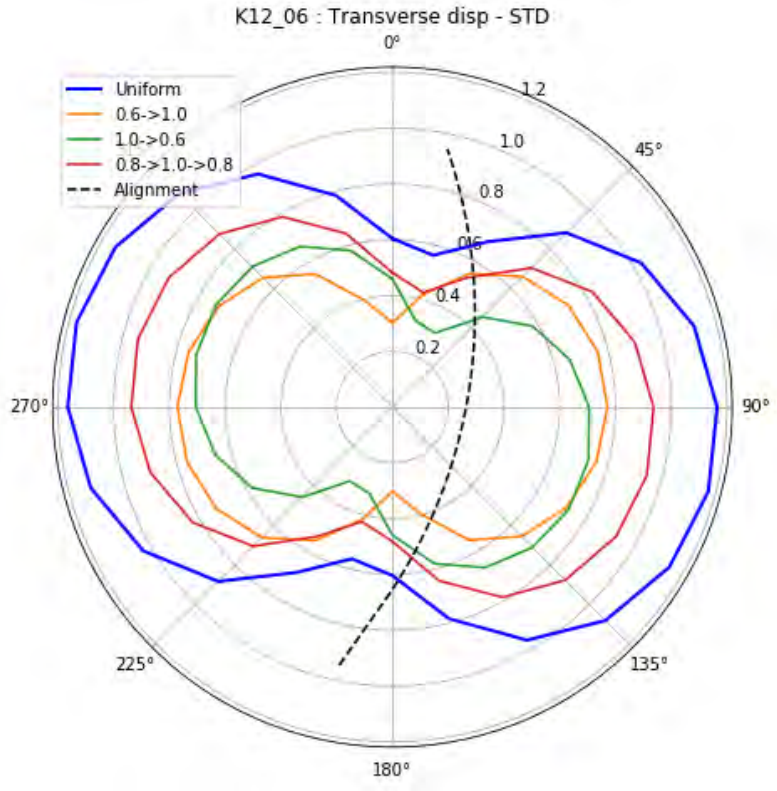


*Figure 9-4 Dynamic response from varying mean wind profile along the deck. The variation is from south towards north. I.e. for the yellow line the mean wind varies from 0.6 in the south to 1.0 in the north.*

### *9.4.3 Sensitivity to change in wind input*

In Metocean Design basis the key parameters are presented as P-values, representing probability of occurrence lower than the specified value. In order to understand the sensitivity of the variation several relevant parameters were calculated and compared to the reference value; uniform wind as documented above.

Results are calculated for all angles of attack and presented as standard deviation of transverse displacement in a polar diagram.

The following values were used in the study (P10 – P50 – P90 values)

xLu = 66,6m – 143,2m – 361,6m
Au = 3.8 – 7.3 – 16.3
Cux = 5,0 – 7,0 – 10,0
Cuy = 6,4 – 9,0 – 10,8

These values were compared to the N400 reference values and given as the thick blue line in Figure 9-5. In addition to the thick blue reference line, +/- 10% deviation from this line is marked for reference. Additional results are shown in Appendix E: Aerodynamics.

Based on these results the general conclusion is:
For xLu values in medium range gave the highest response.
For Au increased values gave increased response.
For Cux and Cuy low values gave highest response.

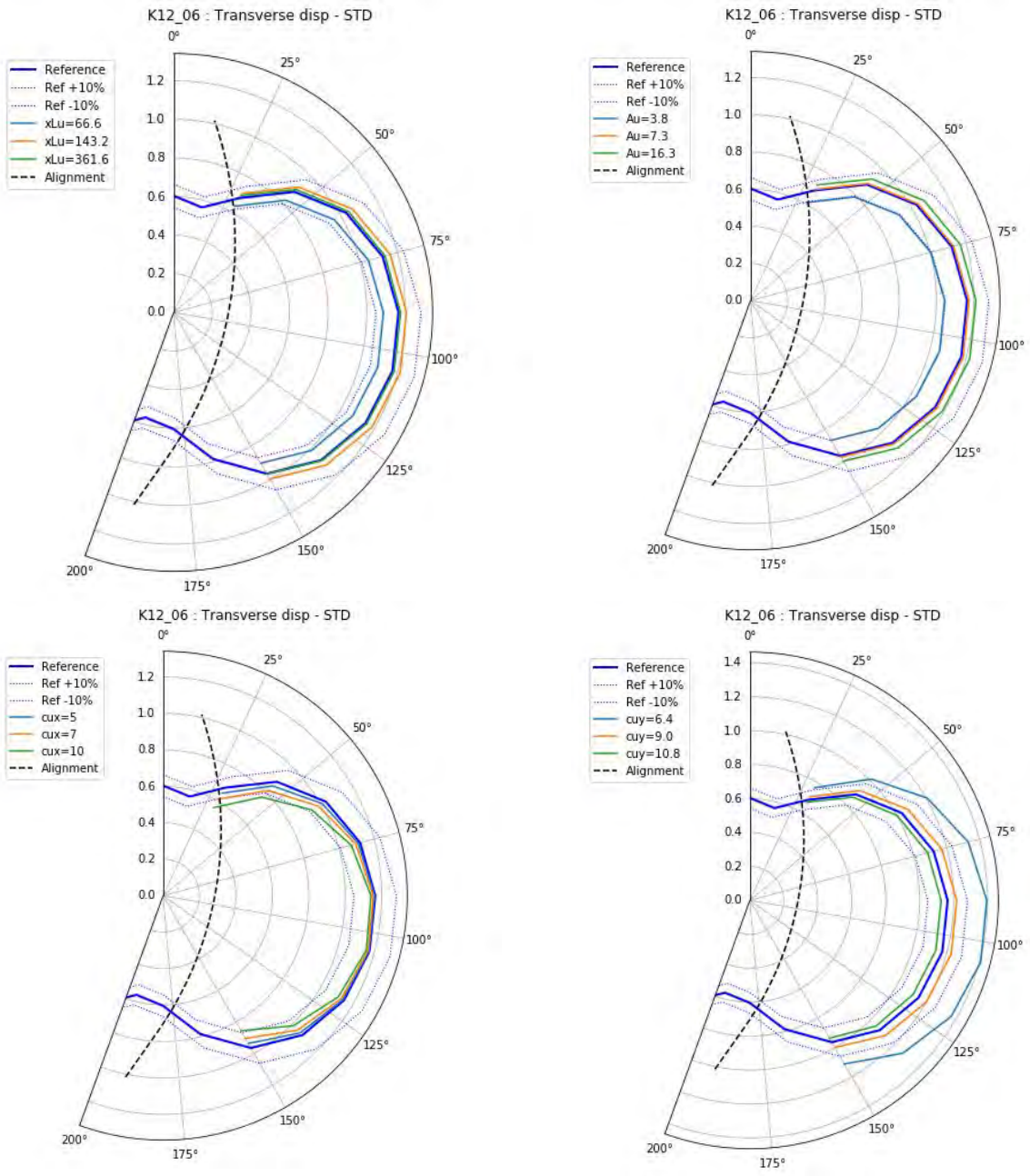


*Figure 9-5 Top Left: Variation of xLu. Top Right: Variation of Au. Bottom left: Variation of cux. Bottom right. Variation of cuy*

## 9.5 Aerodynamic stability

### *9.5.1 Galloping, static divergence, classical flutter and torsion instability*

The stability limit for high wind speed phenomena is calculated based on N400 to 81.7 m/s. The bridge system was checked for galloping, static divergence, and torsion instability and it is found aerodynamically stable.

Classical flutter is studied in more detail below. It involves as a minimum two modes of motion. A torsion mode and a vertical bending mode of similar mode shape but with a lower eigenfrequency. The critical wind speed for onset of classical flutter is reached when the wind loading on the bridge girder makes the bending and torsion frequencies equal thereby establishing a resonant exchange of energy between to two modes. This in turn leads to divergent coupled torsion bending oscillations of the bridge girder. In cases where more vertical modes exist below the torsion mode these vertical

modes may couple to form a compound vertical mode shape which couples with the torsion mode at the onset of flutter.

The input to the flutter calculation constitutes the modes assumed to couple into flutter, the corresponding modal masses and eigenfrequencies and aerodynamic derivatives particular to the bridge deck.

The present multi-mode flutter analysis of Bjørnafjorden K12 alternative assumes that the first torsion mode and 9 vertical bending modes with frequencies lower than the torsional frequency may couple into flutter;
Torsional mode: 30.
Vertical modes: 15, 16, 17, 18, 19, 20, 21, 23, 25

The mechanical damping of the bridge structure is an important parameter in flutter calculations as the requirement for onset of flutter is that the apparent aerodynamic damping exhausts the available mechanical damping. In the present context the mechanical damping available is obtained as the sum of the structural damping, the viscous damping, the hydrodynamic damping and the damping of the anchor lines. Aerodynamic damping is excluded as this component is included in the aerodynamic derivatives and varies as a function of wind speed.

The compound mechanical damping available in the bridge structure for the selected 10 modes are summarized in Table 5 from which it is noted that the lowest modal damping level is $\zeta = 0.0524$ obtained for mode 18 which is assumed as a conservative lower bound for the flutter calculations.

*Table 5 Compound mechanical damping computed for the selected flutter modes*

| | **Mode 15** | **Mode 16** | **Mode 17** | **Mode 18** | **Mode 19** |
|---|---|---|---|---|---|
| Damping [rel-to-crit] | 0.0955 | 0.0950 | 0.0937 | 0.0524 | 0.1184 |
| | Mode 20 | Mode 21 | Mode 23 | Mode 25 | Mode 30 |
| Damping [rel-to-crit] | 0.0966 | 0.1147 | 0.1160 | 0.1033 | 0.1545 |

Flutter diagrams showing the outcome of the 10 mode analysis are shown in Figure 9-6. The apparent damping level to be balanced by the aerodynamics is $g = 2\zeta = 0.105$, see section 6.

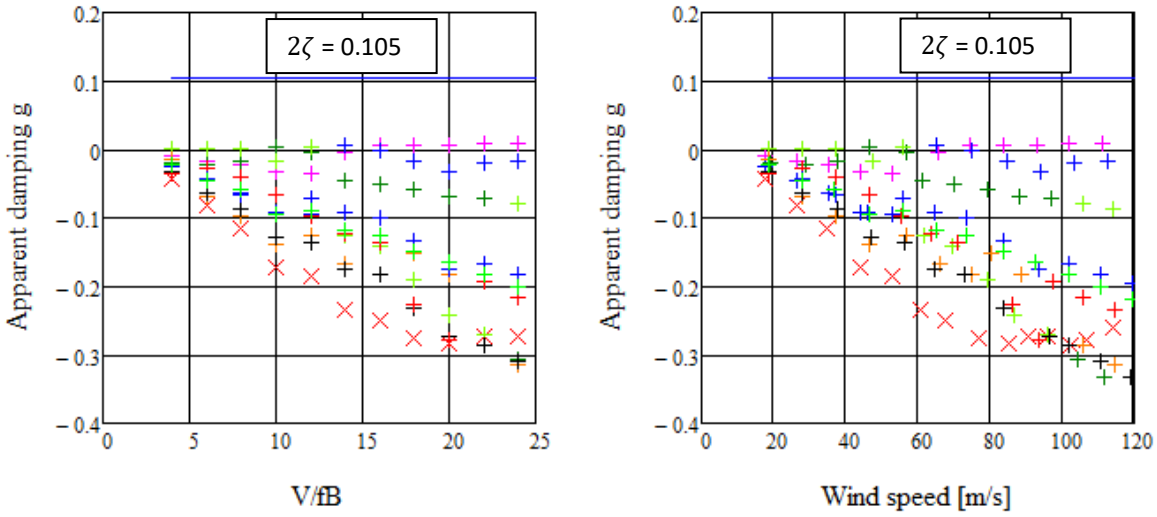


*Figure 9-6 Apparent aerodynamic damping as function of normalized and absolute wind speed for $2\zeta = 0.105$ Bjornafjorden K12*

From Figure 9-6 it is noted that all apparent damping levels remain below $2\zeta$ = 0.105 for all wind speeds below 120 m/s. Hence the bridge is stable against classical flutter up to and beyond the N400 requirement of 81.7 m/s. It is noted that slightly positive apparent damping is found for wind speeds above $V/fB$ > 10 or 45 m/s which indicates onset of flutter had the compound mechanical damping been below 0.003 ($g$ = 0.006) as may be the case for land based suspension bridges. Further details and references are given in Appendix E: Aerodynamics.

### *9.5.2 Vortex induced vibration of the bridge girder*

Vortex shedding in the wake of box girders may result in limited amplitude oscillations of the bridge girder at wind speeds where rhythmic vortex shedding locks on to a vertical bending or torsion eigen mode.

Practical experience from suspension bridges with shallow trapezoidal box girders have shown that vortex induced oscillations are usually confined to vertical modes only and occur at low wind speeds typically less than 12 m/s and for weather conditions with low atmospheric conditions.

Vortex induced vibrations of suspension bridges (Osterøy bridge, Norway and Storebælt East bridge, Denmark) has proven to be linked to severe flow separation and associated rhythmic vortex shedding at the knuckle line between the horizontal bottom plate and the lower inclined downwind side panel. Wind tunnel research has demonstrated that severe flow separation and vortex shedding can be avoided if the angle between the horizontal bottom plate and the lower side panels can be kept at approximately 15 deg. The 15 deg principle was recently introduced for the design of the girder of the Hålogaland Bridge, Norway and has proven to be free of vortex induced vibrations in full scale as well as in wind tunnel tests.

The design of the cross section shape of the girders of Bjørnafjorden bridge incorporates the 15 deg. principle. Thus, vortex induced vibrations are not expected to be an issue for the present design.

### *9.5.3 Vibration of stay cables*

The following aerodynamic cable instabilities has been evaluated below:

- Dry galloping – an instability associated with asymmetric flow separation on the cable cross sections. The asymmetry may be caused either by the cable being in the critical Reynolds number range or by cable surface irregularities (on the HDPE tube). The analysis conclude that additional damping is needed to suppress this phenomenon. See Appendix E: Aerodynamics for details.
- Rain / wind galloping – an instability associated with rain water draining along the cables causing the circular cable cross sections to be asymmetric to the wind. When including mechanical dampers all cables are predicted to be stable against rain / wind galloping, see Appendix E: Aerodynamics for details.
- Vortex induced vibrations – an instability associated with the alternating formation and shedding of vortices along the separation lines at the upper and lower sides of the stay cable. See below for a summary and Appendix E: Aerodynamics for further details.
- Ice / sleet galloping – an instability associated with the deposit of ice, snow or sleet along the cables causing the circular cable cross sections to be asymmetric to the wind. See below for a summary and Appendix E: Aerodynamics for further details.

Common to the above instabilities are that they may be mitigated or delayed to higher wind speeds by introduction of additional mechanical damping to the stay cables. Thus, for cable stayed bridges it

is expected that additional damping in some form is needed to damp out cable vibrations. Figure 9-7 shows an example of one such system. The typical damping obtained from a system like this is 275 kNs/m, which for the current cables equates to an additional damping of about 2% of critical.

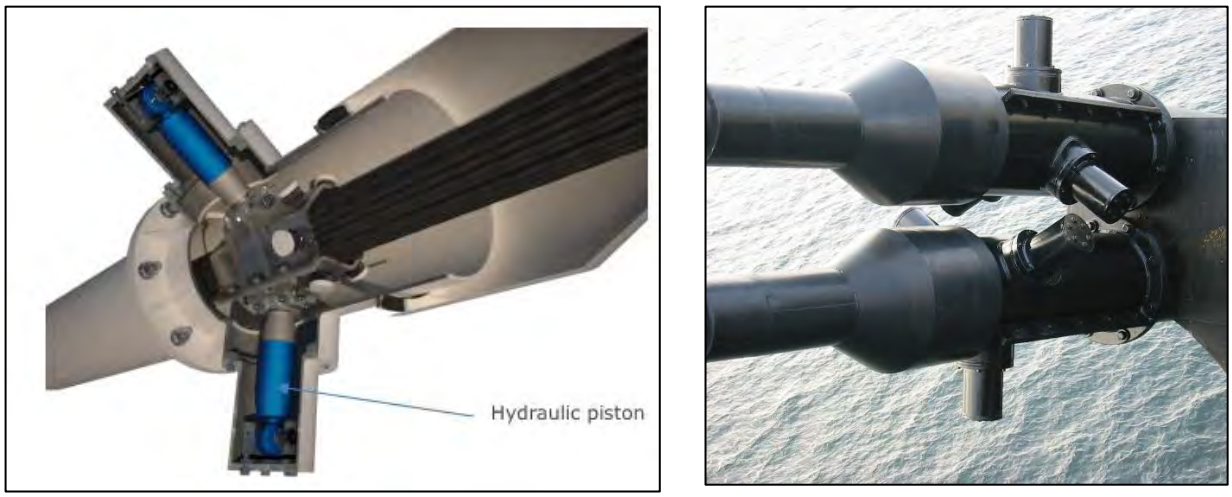


*Figure 9-7 Hydraulic stay cable damper (Freyssinet IRD type). Cross section view (left). External view twin stay cables, Øresundsbron [right)*

The cable stayed bridge supports a main span of about 360m. Based on the current geometry the vibration frequency can be calculated. The lowest frequency varies from about 0.3Hz for the longest stays to 1.7Hz for the shortest. The distribution is shown in Figure 9-8.

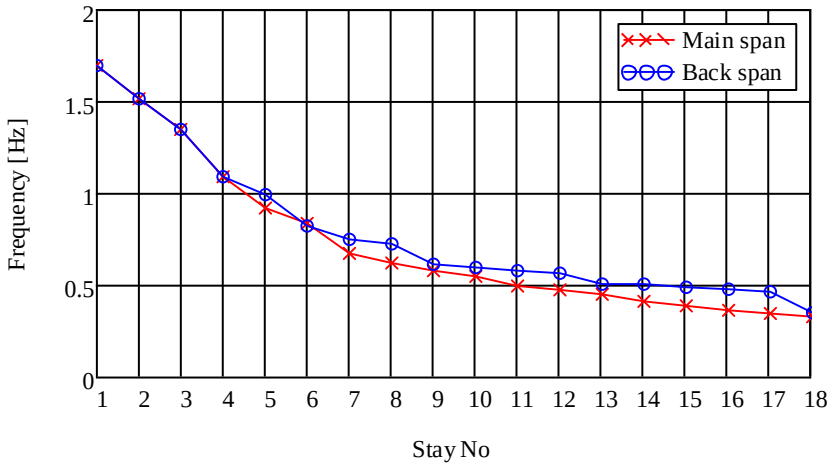


*Figure 9-8 Lowest vibration frequency of each stay*

**Vortex induced vibrations**

Vortex shedding excitation of a stay cable may occur when the frequency $f_{vtx}$ of vortices shed in the wake of the cable coincides with one of the eigenfrequencies $f_n$of the cable, $f_v = f_n$.

Following EN1991-1-4 the vortex shedding frequency is related to the wind speed and cable cross section diameter $b$ through the Strouhal Number (St=b*f/V=0.18). Thus, critical wind speed for the stays are calculated to 1.5m/s for the shortest stays to 0.5m/s for the longest.

Proceeding with calculations according to method 1 in EN1991-1-4 it is found that higher modes are more critical than lower, and that dampers are necessary if vortex induced vibrations occur. Figure 9-9 shows that vortex induced vibrations is suppress with dampers installed.

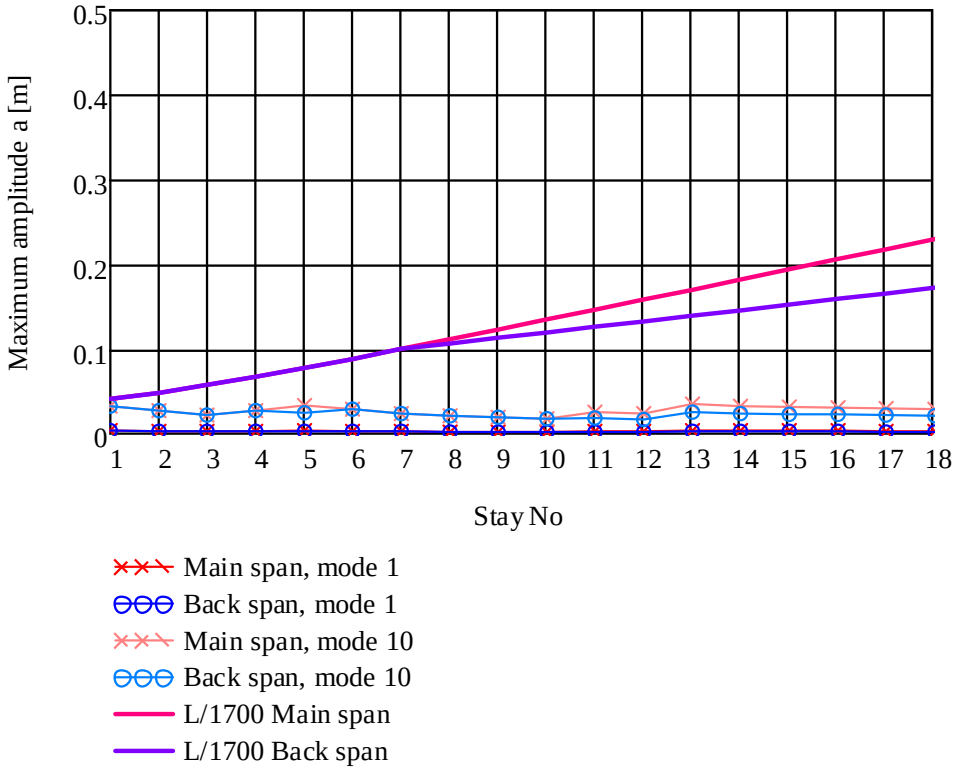


*Figure 9-9 Estimated response of vortex induced vibration with dampers installed*

**Ice/sleet galloping**

EN1991-1-4, Table E.7, proposes that galloping due to ice / sleet deposits is a similar process to classical den Hartog galloping and is caused by the change of the exterior cable surfaced due to ice accretion. For evaluation it may be represented by the stability parameter $a_G = 1$. However, contrary to dry galloping discussed Appendix E, the aerodynamic force coefficients and thus $a_G$ are assumed to independent of wind speed and thus also of the Reynolds' Number.

Based on the same calculation method as in Appendix E, where both aerodynamic and external dampers is included, it is found that the cables are stable for this phenomena for wind speeds up to 15 m/s, see Figure 9-10. The values presented in this figure is valid for cables with ice/sleet along the whole length. If ice accretion is restricted to a limited part of the cable the galloping excitation will be less and in part counterbalanced by positive aerodynamic damping along the parts of the cables free of ice / sleet.

Appendix E also reference a method for evaluating the stability with the cable partly covered by ice/sleet. Based on this analysis the cable will be stable for wind speeds above 54m/s when the cable is iced up less than 22% of its length.

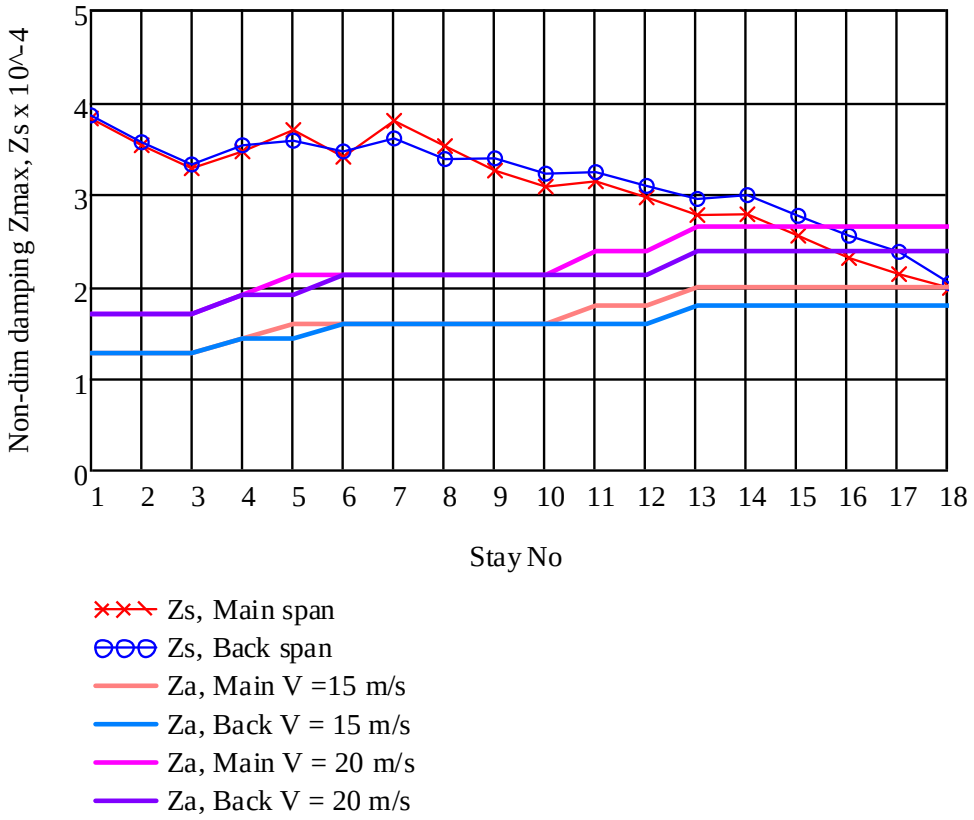


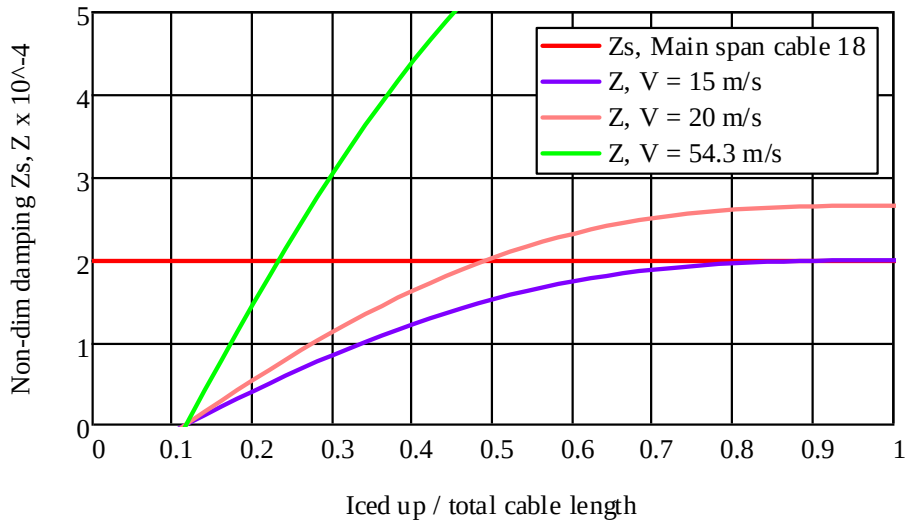


*Figure 9-10 Top: Calculated non-dimensional structural cable damping parameters $Z_s$ and aerodynamic damping parameters $Z$ corresponding to ice / sleet galloping at wind speeds 15 m/s and 20 m/s. Bottom: Evaluation stability based on relative length of ice/sleet coverage.*

## 9.6 Practical considerations regarding wind from the southern sector

In previous phases of the Bjørnafjorden project it has been concluded that the bridge availability is above 99.5%. The main contributor to bridge closure is closure due to wind on vehicles. In the updated Metocean Design Basis specified for this project the turbulence intensity from the southern sector is increased from about 12% to 30%. This implies a significant increase in wind gust compared to the mean wind speed, and thus, increased transverse forces acting on vehicles passing this sector of the bridge. In particular, vehicles will be negative affected by wind having its main direction from it side.

Figure 9-11 shows the wind rose, sector with increased turbulence and the different alignments. As can be seen, vehicles on K11 and K12 will experience side wind when passing the southern sector. In order to secure safe passage of these vehicles, mitigations may be needed. This could be e.g. closing the bridge for lower mean wind speed (this will have a considerable effect on the availability), establishing wind screens or other measures.

Before starting exploring the consequences of mitigation we recommend to:

- Look at the wind measurements to see if the turbulence intensity can be reduced or the width of the sector with increased turbulence intensity can be specified in more detail.
- Do more detailed analysis on bridge closure. For these analysis Weibull parameters for long term distribution is needed for all sectors.

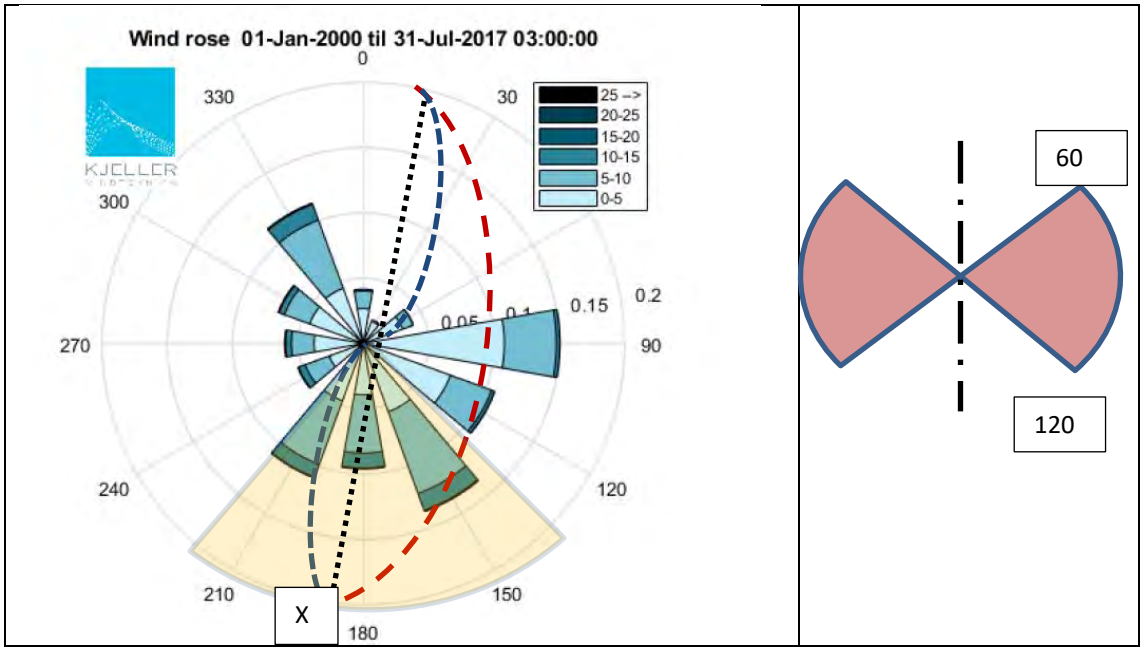


*Figure 9-11 Left: Wind rose and area of increased turbulence intensity (Yellow), compared to K12 (Red), K13 (Black) and K14 (Blue).*
*Right: Critical wind direction compared to alignment (red).*

# 10 Global analyses

## 10.1 Overall description of bridge concepts

In the following a description regarding modelling, analysis procedures, loading and response is given. A more detailed description of modelling and assumptions is given in Appendix F. Response evaluations are given in Appendix G.

The K12 bridge concept features an arch-type bridge with three mooring clusters, with an arch radius of 5000 m ending in a straight cable-stayed bridge in south. Mooring lines contributes to resistance against transverse loads, increase the buckling capacity and provides damping for various excitation modes. There are three mooring clusters in pontoons A13, A20 and A27. The latest iteration number for the concept was 7, and the iteration was termed K12_07.

The Southern end of the bridge starts with a straight cable-stayed bridge. A free span of about 380 m yields a navigational channel width of more than 250 m. The bridge girder is supported into the tower in vertical and sideways direction. Back span columns are rigidly connected to the bridge girder. Towards the Northern end the bridge girder strength is gradually increased in the last 40 m towards the abutment. The bridge girder is fixed to ground at both abutments. See Appendix L [2] for more details on the cable-stayed bridge and abutments.

A circtangular shape of the pontoon was selected, with a pontoon spacing of 125 m. A draught of 5 meters is defined for pontoons without mooring lines, and an additional draught of 2.5 m is required to support the vertical load component of moorings (line weight and pretension).

Full mooring lines were included in the simulations, in which the various segments of chain and wire were modelled explicitly. Soil stiffness was not accounted for in the global simulations. Mooring lines and anchor locations are shown in Appendix M [3].

Documentation of the simulation model is given in Appendix F [4]. Here variation of cross-sectional properties along bridge girder is documented in detail. Full documentation of the mooring system can be found in appendix M [3].

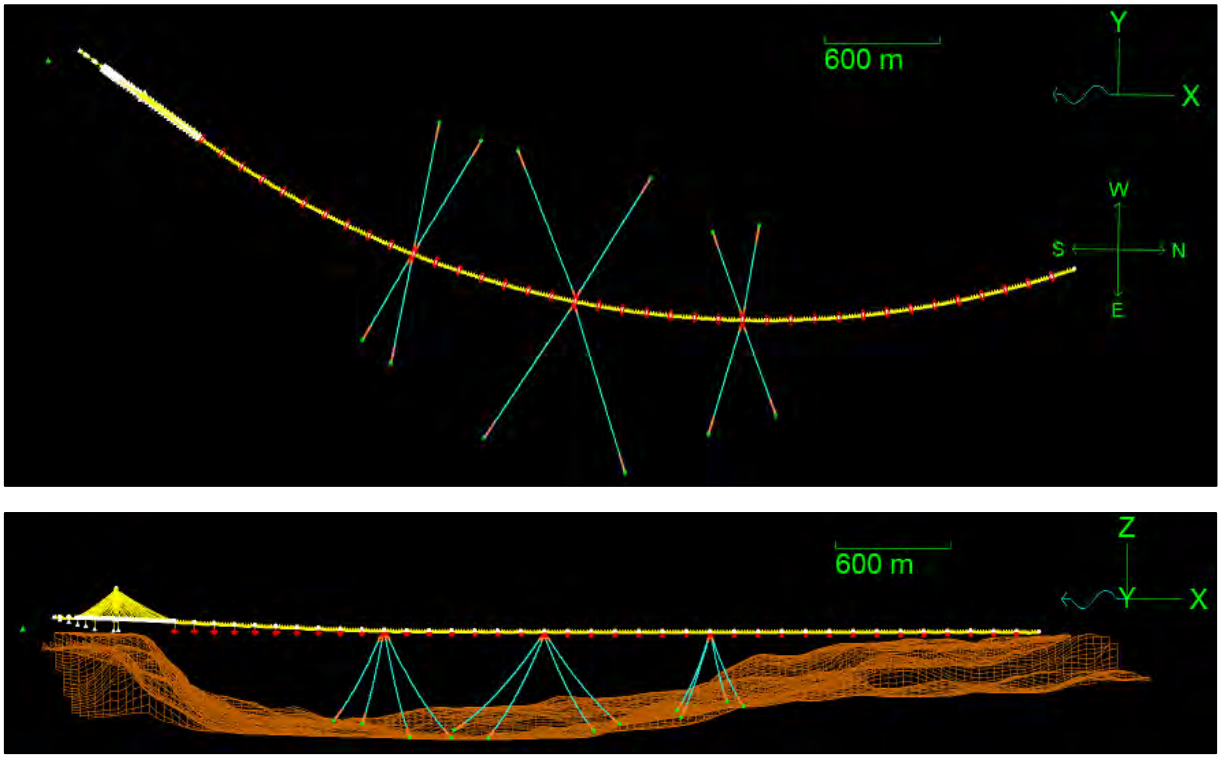


*Figure 10-1 Plan and side view of bridge concept K12_07*

Figure 10-2 shows the discretization of cross-sectional property types along the bridge girder and Table 10-1 lists the key properties for each property type, where

M – Unit mass pr. meter

Iy – Second area moment about weak axis

Iz – Second area moment about strong axis

J –Torsional constant

Ax – Cross-sectional area

Ly – Width of segment in transverse direction

Lz – Height of segment

VCGt – Distance from top of segment to centre of gravity.

The values for weak-axis moment in Table 10-1 are corrected for shear lag in a serviceability limit state, see Appendix K [5] for more info. The listed unit mass includes structural mass + five ton/m added mass that accounts for asphalt and railings. For the steel girder a constant structural mass of 14 ton/m is considered. The actual mass varies somewhat along the girder, see Appendix K [5] for details.

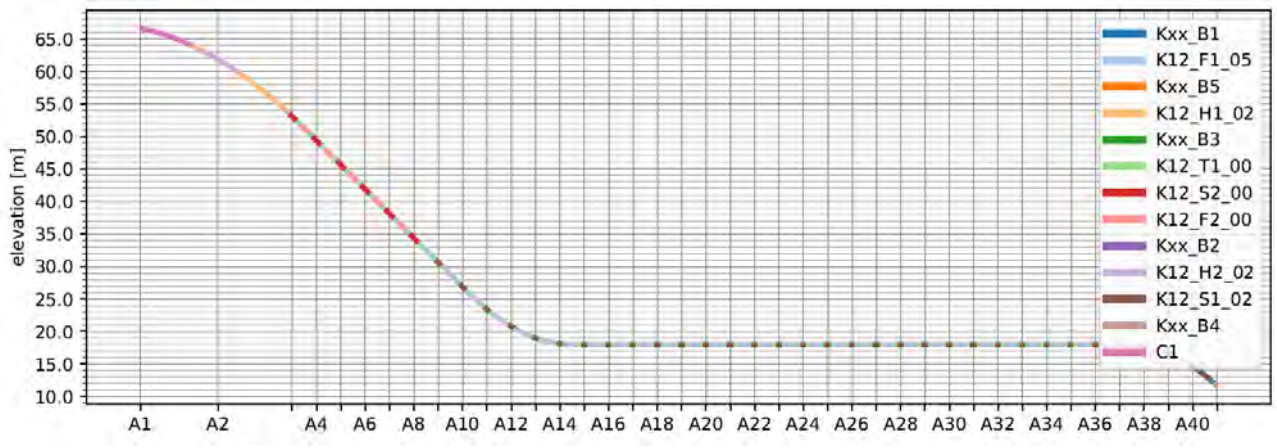


*Figure 10-2 Sectional property definition for K12_07*

*Table 10-1 Key sectional properties for K12_07*

| | M | Iy | Iz | J | Ax | Ly | Lz | VCGt |
|---|---|---|---|---|---|---|---|---|
| | [tonne/m] | [m^4] | [m^4] | [m^4] | [m^2] | [m] | [m] | [m] |
| K12_S1_02 | 19 | 3.668 | 110.4 | 11.349 | 1.779 | 27 | 4 | 1.989 |
| K12_S2_00 | 19 | 3.785 | 121.83 | 12.01 | 1.8829 | 27 | 4 | 2.041 |
| K12_T1_00 | 19 | 3.311 | 98.583 | 10.105 | 1.521 | 27 | 4 | 1.878 |
| K12_F2_00 | 19 | 2.781 | 89.597 | 9.4228 | 1.331 | 27 | 4 | 1.763 |
| K12_F1_05 | 19 | 2.569 | 84.698 | 8.6111 | 1.2699 | 27 | 4 | 1.682 |
| K12_H1_02 | 19 | 2.534 | 89.531 | 6.629 | 1.297 | 27 | 3.5 | 1.463 |
| K12_H2_02 | 19 | 3.64 | 123.34 | 9.663 | 1.797 | 27 | 3.5 | 1.633 |
| C1 | 79.1 | 40.5 | 2138 | 135.4 | 27.951 | 29 | 3.5 | 1.463 |
| Kxx_B1 | 19 | 5.32 | 170 | 18.2 | 2.09 | 27 | 4 | 1.989 |
| Kxx_B2 | 20.52 | 5.95 | 226 | 20 | 2.28 | 27 | 4 | 1.989 |
| Kxx_B3 | 25.16 | 7.7 | 314 | 24.3 | 2.86 | 27 | 4 | 1.989 |
| Kxx_B4 | 29 | 9.74 | 423 | 28.5 | 3.34 | 27 | 4 | 1.989 |
| Kxx_B5 | 30.12 | 10.06 | 461 | 29.7 | 3.48 | 27 | 4 | 1.989 |

## 10.2 Modelling methodology

Four different simulation software have been used for global response assessments during design development with various strengths and weaknesses:

- RM-Bridge for permanent and traffic loads
- Orcaflex for wave loading in frequency and time domain, and wind loading in time domain
- Novaframe for dynamic wind response in frequency domain
- LS-DYNA for local and global ship collision simulations

In addition, a range of software were utilized for input generation and special studies, such as Wamit, Wasim, Rhino and Windsim.

A common modelling approach was needed to coordinate the different global models during the rapid design development process. Hence, the model description was created independent of the different software and used as a common basis to establish models for each software. The detailed modeling approach varies somewhat due to varying methods and limitations in the individual software, but the common basis ensures consistent models and enables more rapid design iterations. Figure 10-3 illustrates the main methodology. For details on the modelling approach, see Appendix F [4].

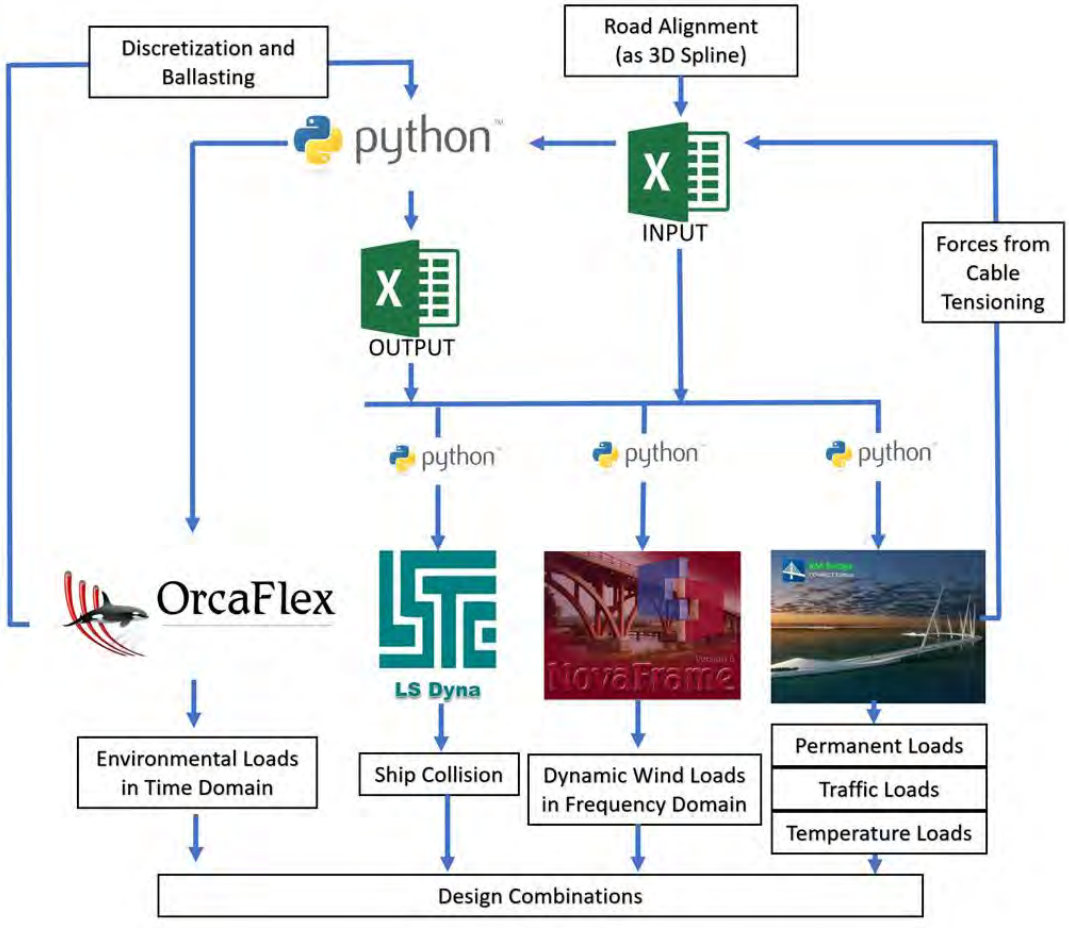


*Figure 10-3 Illustration of information flow in the modelling and simulation system*

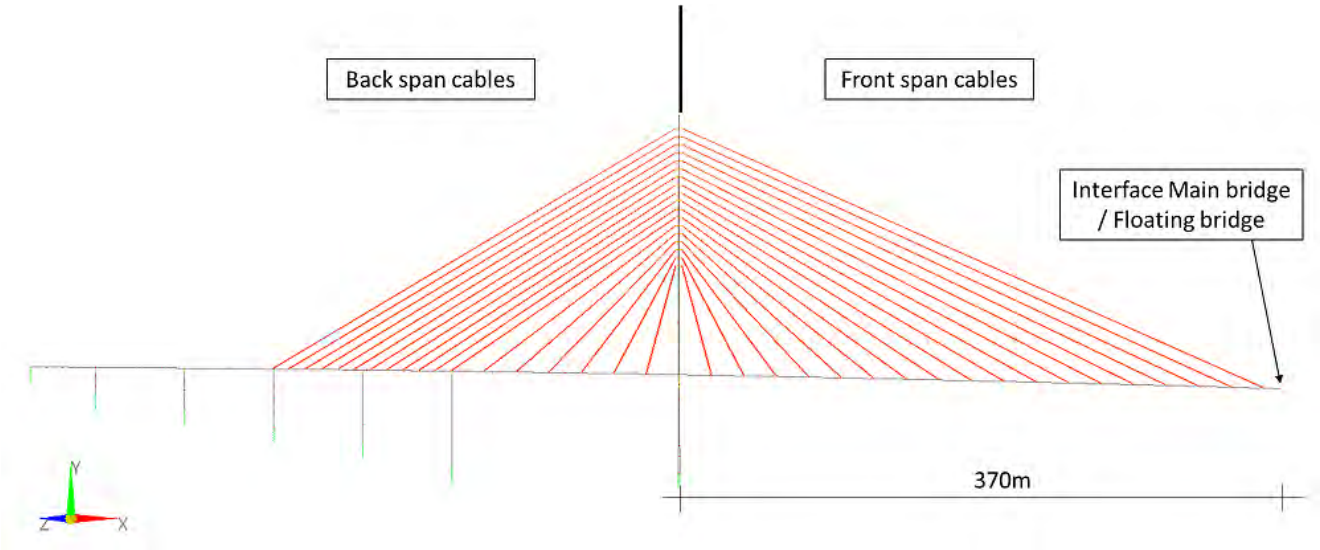


*Figure 10-4 The structural model of the cable stay bridge*

## 10.3 Tensioning of cable-stayed bridge

The cable tensioning optimization is performed in the RM Bridge Enterprise software. A separate analysis schedule for the optimization labelled as "FormFinding" is established within the model. Only the main bridge is activated where the interface to the floating bridge part is 370m from the centre of the Pylon in axis A2.

In order to use a linear cable formulation, the sagging effect is included by an effective E-modulus estimated based on the permanent load situation according to Ernst formula.

## 10.4 Pontoons

The geometry of the pontoon has been the topic of investigations in previous phases, where a kayak type pontoon was found to have better response characteristics in the 100-year extreme wind wave conditions. Since the Metocean conditions for Bjørnafjorden have been updated with less severe extreme wind waves, it is not certain if the wind waves are governing for the design. In addition, it is considered more cost-effective to construct a circtangle shape pontoon. Therefore, a circtangle shaped pontoon is chosen as base case for the present study. Two pontoon types were used, both developed for a 125 m span length. Properties are given in the table below and Figure 10-5.

The assumed structural weight of the pontoon is higher than the calculated mass of the pontoon (705 and 934 ton, see Appendix K), leaving a significant margin for weight increase without affecting the global dynamic response.

| **Pontoon type** | Moored | Conventional |
|---|---|---|
| Length [m] | 53 | 53 |
| Width [m] | 14.9 | 14.9 |
| Draft [m] | 7.5 | 5.0 |
| Mass [ton] | 1540 | 985 |
| Displaced volume [$m^3$] | 5566 | 3710 |
| C33 [kN/m] | 7460 | 7459 |
| C44 [kNm/rad] (only contribution from water plan area) | 1,56 E6 | 1,56 E6 |
| Ixx [ton $m^2$] | 415 E3 | 252 E3 |
| Iyy [ton $m^2$] | 63,8 E3 | 33,1 E3 |
| Izz [ton $m^2$] | 430 E3 | 252 E3 |

| | | |
|---|---|---|
| Center of gravity [m] | -2.0 | -0.75 |

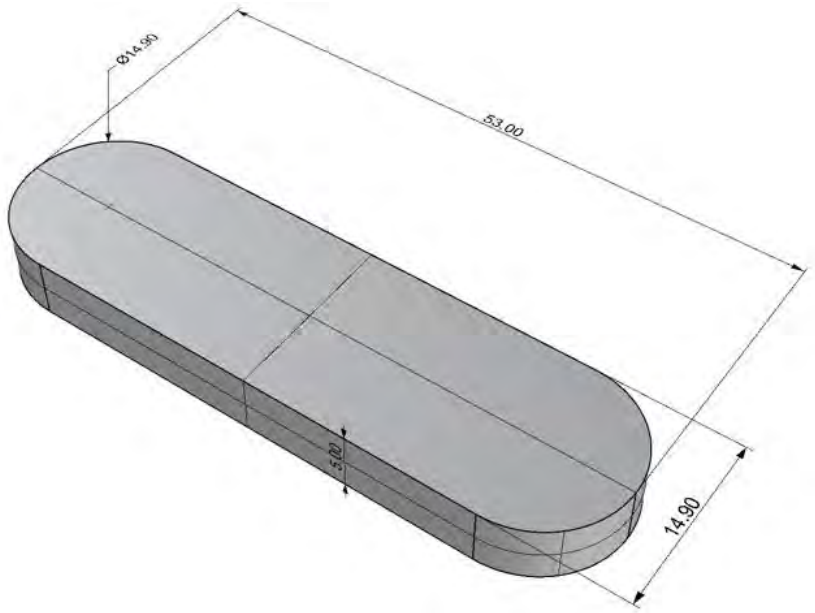


*Figure 10-5 Underwater part of the circtangle geometry selected for bridge with for 125m span width*

## 10.5 Aerodynamic loading

In order to find wind loading on the bridge aerodynamic parameters must be defined. These are differentiated between high-bridge and low-bridge coefficients. Aerodynamic parameters are defined in detail in Appendix E [6], and the applied values assume the presence of a wind nose to improve the drag coefficient. In Figure 10-6 the applied drag coefficients for the bridge girder is shown. The transition between high and low bridge is defined as axis A12. All columns are modelled with a drag coefficient of 1.5. Drag factors for cables are defined as 1.2 and 0.8 below and above 20 m/s wind. For simplicity a factor of 1.0 is used for all wind speeds; overestimating the extremes but underestimating the milder conditions. Aerodynamic loads on the pontoons is simplified to use the same drag and lift coefficients as for viscous drag and with the actual exposed area and air density, but with a mean wind load and direction only.

Aerodynamic damping is included by using buffeting theory with relative wind velocities for all elements except the pontoon.

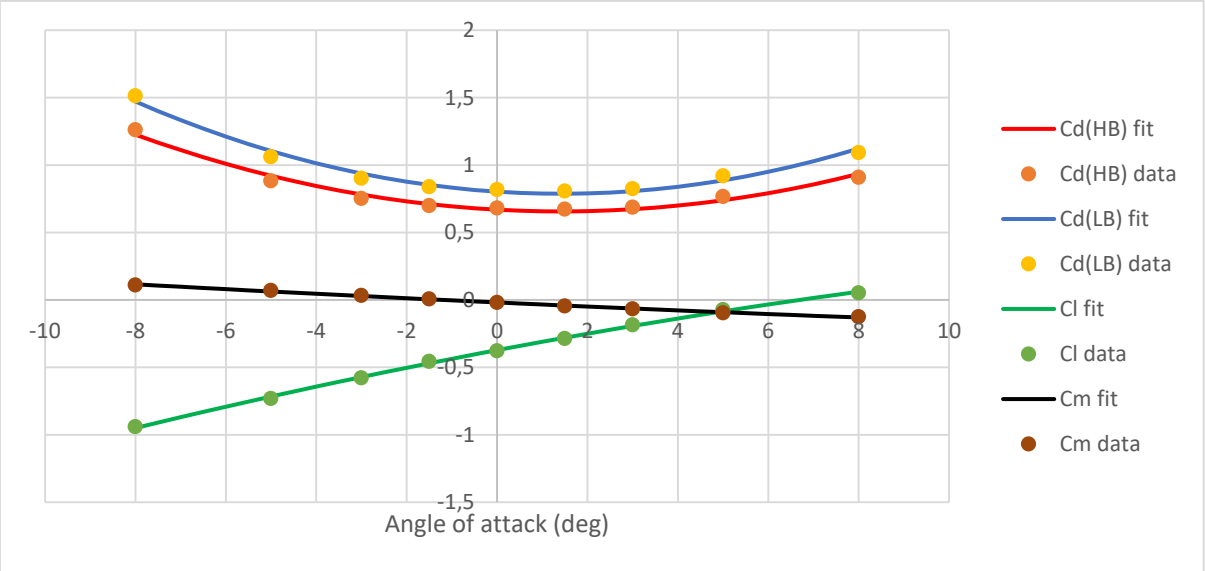


*Figure 10-6 Aerodynamic coefficients for bridge girder as applied in the simulations for high bridge (HB) and low-bridge (LB) respectively*

## 10.6 Basic load description

The following basic load cases are included in the performed analyses:

- Permanent loads
- Temperature loads
  - Thermal loading on the bridge as described in ref [7]
- Traffic loads
  - The traffic loading on the bridge as described in ref [7].
- Tidal loads
  - Tidal variation around the mean water lever (+0.77m) taken as +1.33 and -0.97 m for 100 year high and low tide respectively
- Current loads
  - Current load profiles as described in Appendix G
- Wave loads
  - Wave loads from wind generated waves and from swell generated waves as found from the screening activity described in Section 10.8.
- Wind loads
  - Wind loading as described in Section 10.8.

## 10.7 Eigenmodes

Eigenmodes are extracted from all used dynamic computer models and used as basis for evaluation of the models. Transverse eigenmodes from Orcaflex models are shown in the following to give the reader an understanding of the behavior of the four concepts. Reference is made Appendix F and G with enclosures for more complete results.

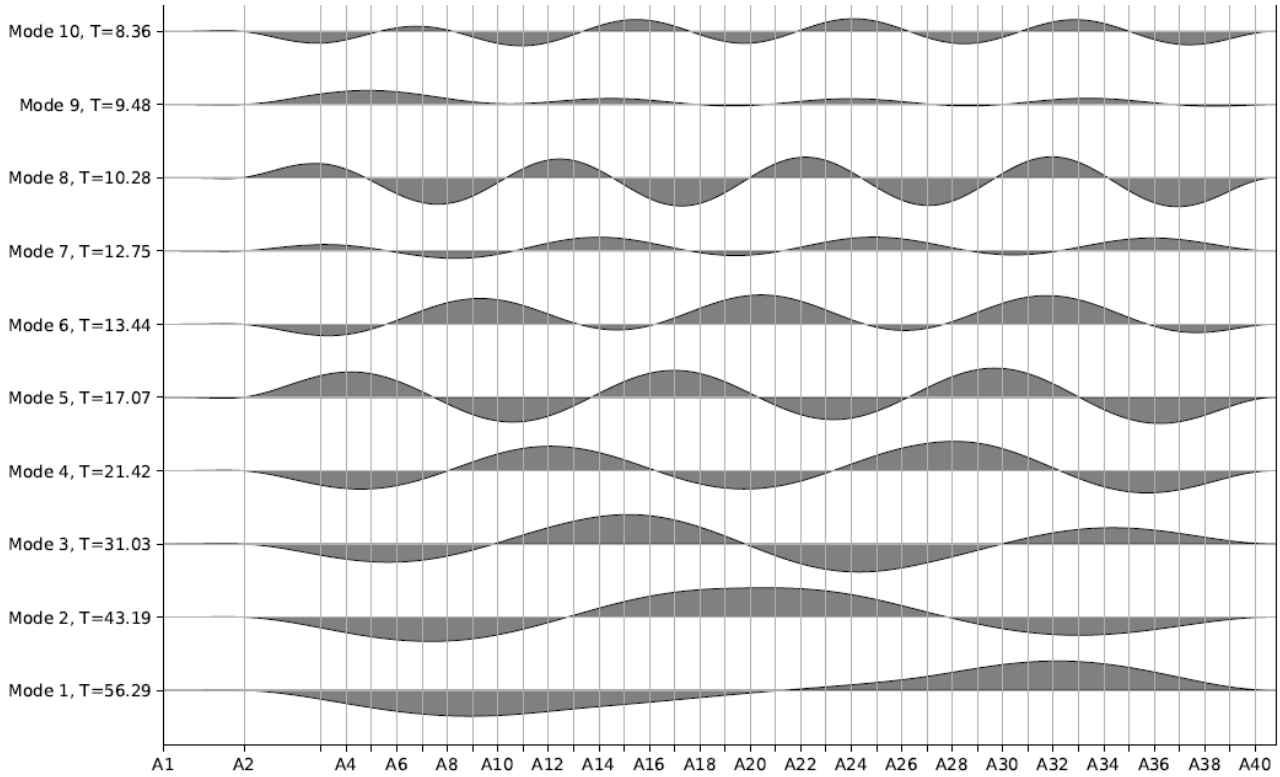


*Figure 10-7 Orcaflex transverse eigenmodes for K12_07*

## 10.8 Environmental loading conditions

### *10.8.1 Environmental screening*

A screening of wave conditions was performed (example shown in Figure 10-8 and Figure 10-9), and used to select key environmental conditions that give maximum response for selected response variables. The screening was performed for all concepts. Full wave screening results are given as Enclosures to Appendix G [1].

Wind response was simulated using 10 seeds from various directions and used to select the worst seed for further load combination.

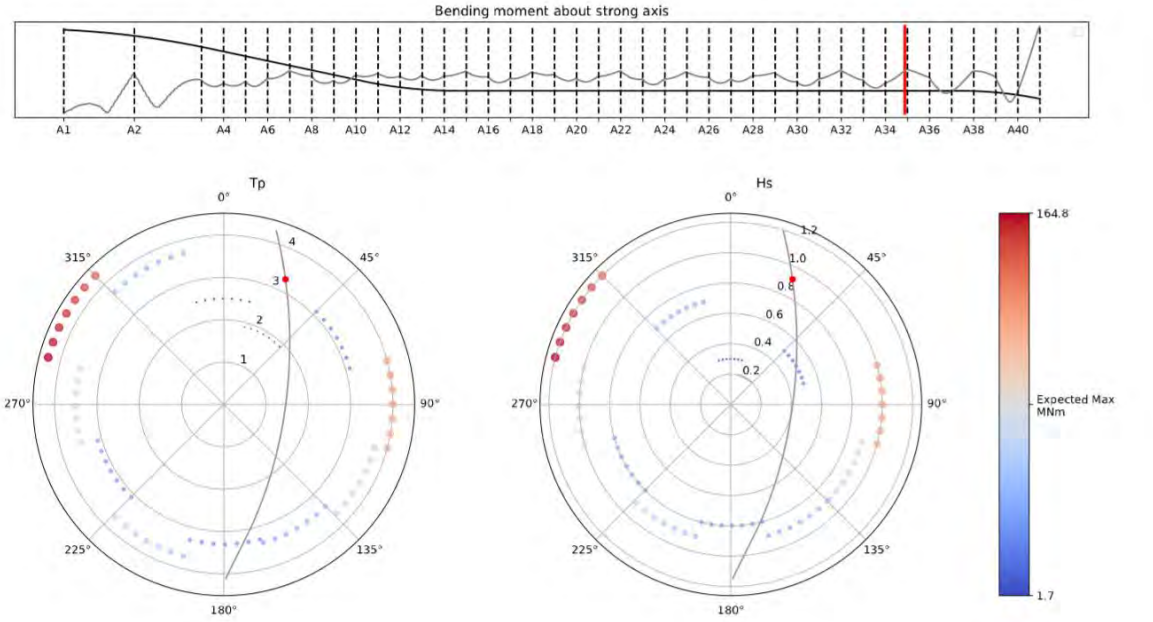


*Figure 10-8: Example of screening study for strong-axis bending moment for K12_07, wind sea 1-years.*

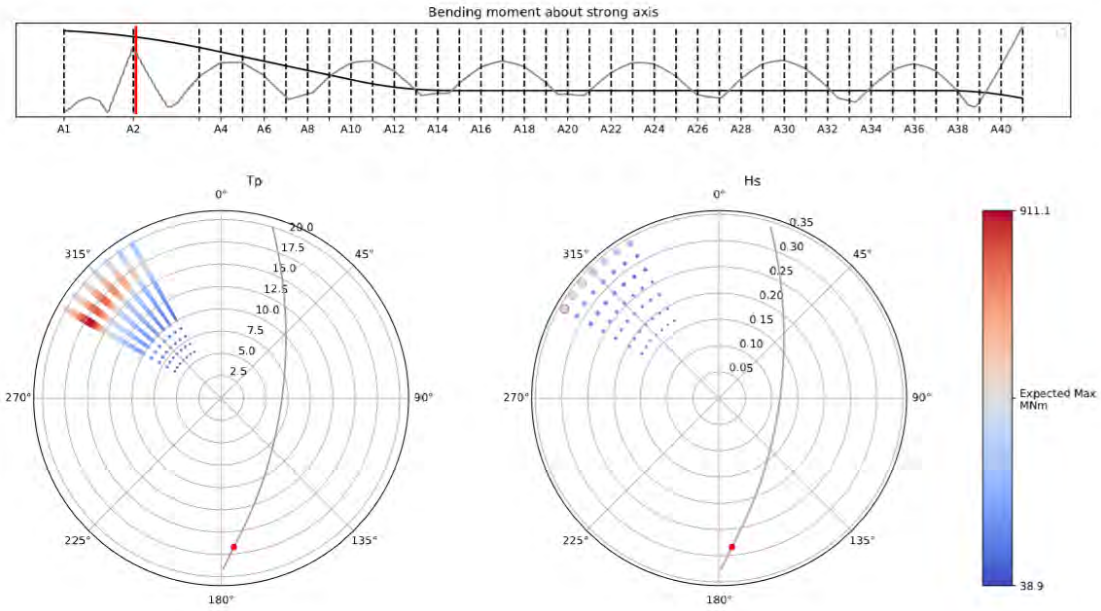


*Figure 10-9: Example of screening study for strong-axis bending moment for K12_07, swell, 100-years.*

### *10.8.2 Selected environmental conditions*

The following shows the selected environmental conditions for 100-year return period. For 1- and 10000-year return periods, see Appendix G [1].

#### *10.8.2.1 Wind-waves and swell*

The following wind-wave and swell waves were used for ULS assessment in the results reported herein, based on the screening study mentioned above. The sea states are selected based on a thorough screening in frequency domain of the various wave components with variation of period, direction and spectral components.

*Table 10-2 Selected design load cases for the 100-year wind waves*

| | Design case 1 | Design case 2 | Design case 3 | Design case 4 |
|---|---|---|---|---|
| **Hs [m]** | 2.1 | 2.1 | 1.4 | 2.0 |
| **Tp [s]** | 5.5 | 5.5 | 4.6 | 5.2 |
| **Wave Direction [deg]** | 75 | 105 | 195 | 315 |

*Table 10-3 Selected design load case for the 100-year swell*

| | Design case 1 | Design case 2 |
|---|---|---|
| **Hs [m]** | 0.34 | 0.34 |
| **Tp [s]** | 17.25 | 13.25 |
| **Wave Direction [deg]** | 300 | 300 |

#### *10.8.2.2 Wind loading alone*

Wind loading is found from the aerodynamic parameters given in Figure 10-6 and the wind speed. Definition of the wind conditions are for ULS assessments are based on the following:

$$V(z) = C_r(z) \cdot V_b$$

$$C_r(z) = k_T \cdot \ln\frac{z}{z_0}$$

$$V_b = C_{dir} \cdot C_{prob} \cdot V_{b0}$$

$$V_{b0} = 24.3\,m/s \quad k_T = 0.17 \quad z_0 = 0.01\,m$$

The results are based on 10 seeds of 1-hour simulation for each condition. For further description of the wind input parameters, reference is made to Appendix E. For description of the loading procedure reference is made to Appendix F.

| Return period | $C_{prob}$ |
|---|---|
| 1 year | 0.75 |
| 100 year | 1.04 |
| 10 000 year | 1.26 |

| Direction | $C_{dir}$ |
|---|---|
| 280 | 1.00 |
| 100 | 0.85 |

| Return period | Direction [deg] | Vb [m/s] | V @ 2m [m/s] |
|---|---|---|---|
| 1 year | 280.00 | 18.2 | 16.3 |
| 1 year | 100.00 | 15.5 | 13.8 |
| 100 year | 280.00 | 25.2 | 22.5 |
| 100 year | 100.00 | 21.4 | 19.2 |
| 10.000 year | 280.00 | 30.7 | 27.4 |
| 10.000 year | 100.00 | 26.1 | 23.3 |

### *10.8.3 100 year combined wave/wind/current*

The following environmental conditions were simulated in time-domain with coupled wind- and wave response, each with 10 seeds for an ULS verification. For ALS checks of post-damage capacity, the worst seed was selected and used for checking.

*Table 10-4: 100-year return period combined wave/wind/current design load cases*

| Concept | Combi-nation | Hs [m] ww/sw | Tp [sec] ww/sw | Direction [deg] ww/sw | Basis Wind Speed [m/s] | Wind Direction [deg] | Current Speed [m/s] | Current Direction [deg] |
|---|---|---|---|---|---|---|---|---|
| **K12_07** | 0 | 1.4/0.34 | 4.6/17.25 | 195/300 | 25.2 | 280 | 1.7 | 280 |
| **K12_07** | 1 | 1.4/0.34 | 4.6/13.25 | 195/300 | 25.2 | 280 | 1.7 | 280 |
| **K12_07** | 2 | 2.0/0.34 | 5.2/17.25 | 315/300 | 25.2 | 280 | 1.7 | 280 |
| **K12_07** | 3 | 2.0/0.34 | 5.2/13.25 | 315/300 | 25.2 | 280 | 1.7 | 280 |
| **K12_07** | 4 | 2.1 | 5.5 | 75 | 21.5 | 100 | 1.7 | 100 |
| **K12_07** | 5 | 2.1 | 5.5 | 105 | 21.5 | 100 | 1.7 | 100 |

## 10.9 Load combination and correlation

The following briefly describes the load combination and correlation considerations used for the results given in this report. Details can be found in the relevant enclosures to Appendix G [1].

### *10.9.1Direct method*

With the direct method, all dynamic load groups simulated and combined by direct summation of time series. There are two versions of this method: coupled or uncoupled. The primary method is the uncoupled where the time domain analysis of wind-waves, swell and wind loads are analysed separately and combined separately. When time series of the total dynamic forces (wind-waves, swell and wind) have been established these can be further processed in the following ways:

- Extreme value estimation of individual dynamic force components and subsequent combination with static loads to arrive at total design forces for ULS/ALS.
- Combination with static loads to establish total design force time series. These time series can be further used for the following purposes:
    - Find min/max and associated values for different response variables. This is typically used for structural capacity checks.
    - Generate Von Mises stress time series. This allows for an accurate prediction of the stress response in the bridge, and extreme value estimation can be performed directly on the stress processes.

- Similarly, cross section capacity checks can also be performed directly on the force time series.

In the second version of the direct method, the coupled version, all dynamic load groups, wind-waves, swell and wind loads, are applied simultaneously. The time series of the total dynamic forces are then established directly and further processing of this is performed as for the un-coupled version. The uncoupled approach is compared to the coupled approach, and the uncoupled is in general found to be conservative. See Appendix G [1] for a discussion.

### *10.9.2 Factor method*

With the factor method, design force values are established for all individual load groups separately (un-coupled) and combination factors are used to account for the correlation between dynamic load groups and individual force components. This method is only applied for the bridge girder and is used primarily as a tool in the design process to better understand the contribution from individual load groups.

### *10.9.3 Extreme value estimation*

Two different methods are used for extreme value estimation of the dynamic response processes.

1. Peak factor method. Based on zero up-crossing frequency under assumption of a Rayleigh distributed process. This is typically used for single seed realizations.
2. AUR method (average up-crossing rate). Used when multiple seeds are run per environmental condition and for non-Rayleigh distributed processes. This method can e.g. be used directly on the von mises stress processes that is non-gaussian in nature. See ref. [8] for a discussion of the methodology.

## 10.10 ULS response summary

The bridge is designed in ULS by the use of partial factor method according to Eurocode. Load combination factors are taken from Table 8 in the Design basis [9].

Three load combinations are considered for the design in ULS:

- **ULS1: Dominating permanent load (G-EQ$_K$).** Traffic is included with 1-year environmental load.
- **ULS2: Dominating traffic (Q-Trf$_K$)**. Traffic is included with 1-year environmental load.
- **ULS3: Dominating environmental load (Q-E$_{env(100y)}$).** 100 years environmental load is included. Bridge is closed for traffic.

Ultimate limit state combinations were performed based on separate simulations of each load component (uncoupled approach) and combined with individual load- , correlation- and combination factors. These results were used in design development, and several design iterations have been performed. Results for both the direct method and the factor method are established. The former is used for all design evaluations, but the latter gives an easier overview of the contributions of the individual load components. Both results are included as enclosures to Appendix G.

ULS1 are found not to be of great importance to the rating of the four concepts. This combination may be of some importance to checking of the cable dimensions of the cable-stayed bridge but is found to be of minor importance for other structural parts.

The ULS2 combination contains 1-year environmental conditions together with traffic. This combination is thus checked using aerodynamic coefficients representing traffic on the bridge girder.

Load reactions for this combination is described in detail in Appendix G (in appendix and in enclosures to appendix).

The main combined environmental response is given in ULS3. An overview of this response is given in Section 0. More detailed description of the load reactions for this combination is given in Appendix G (in appendix and in enclosures to appendix).

## 10.11 Direct method coupled vs. un-coupled response

Coupled environmental load simulations were also performed in time-domain in which all environmental loads were included simultaneously. Ten seeds were run for each environmental condition and the extreme values were estimated using the AUR method at the 90-percentile level (as opposed to expected max for the uncoupled responses).

The comparison has been performed for ULS3 and examples of the response are shown in Figure 10-10 (axial force), Figure 10-11 (strong-axis bending moment) and Figure 10-12 (von mises stresses). Note that the comparison is both expected max vs. 90-percentile and coupled vs. uncoupled response; the former was used in the design development, the latter is the more correct answer.

The uncoupled method is conservative for strong axis bending moment, while it is unconservative for axial force. The other force components have a similar level of magnitude. The uncoupled strong-axis moment is governed by a swell condition with around 17s Tp. For coupled simulations with the same swell period the other loads (wind sea and wind) cause enough disturbance to reduce the excitation of that mode considerably.

The uncoupled method is conservative for the calculated Von Mises stress. The basis for the design development thus far has been to use the maximum von mises stress from a single 1-hour realization with the uncoupled method. The comparison shows that this approach generally gives higher stresses than the 90 percentile values from the coupled analysis.

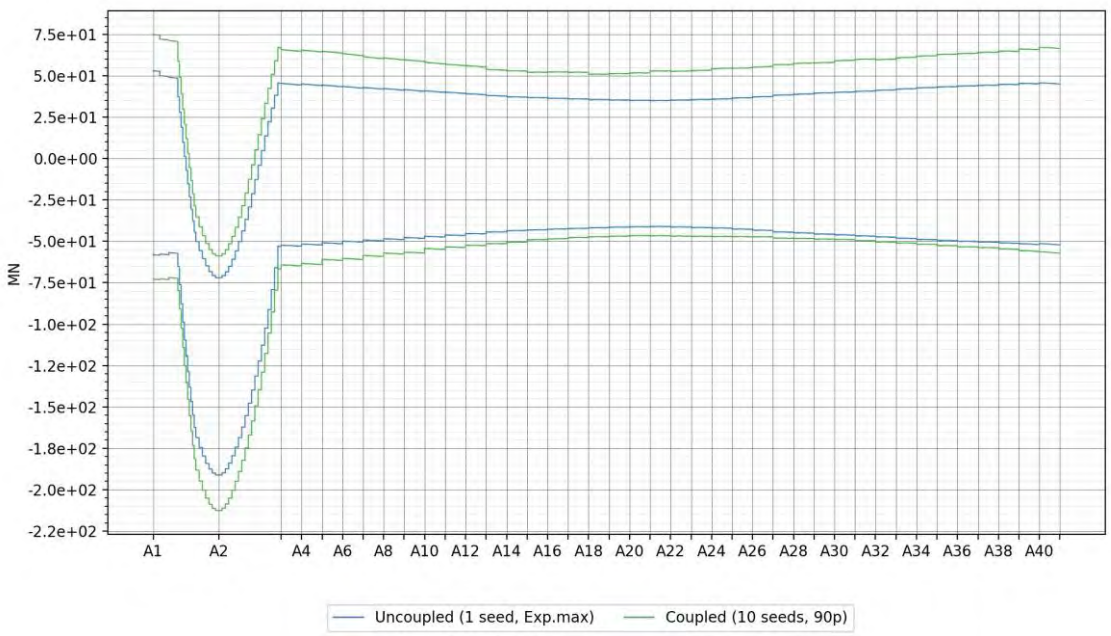


*Figure 10-10 Coupled vs. uncoupled environmental loads for K12_07: Axial force*

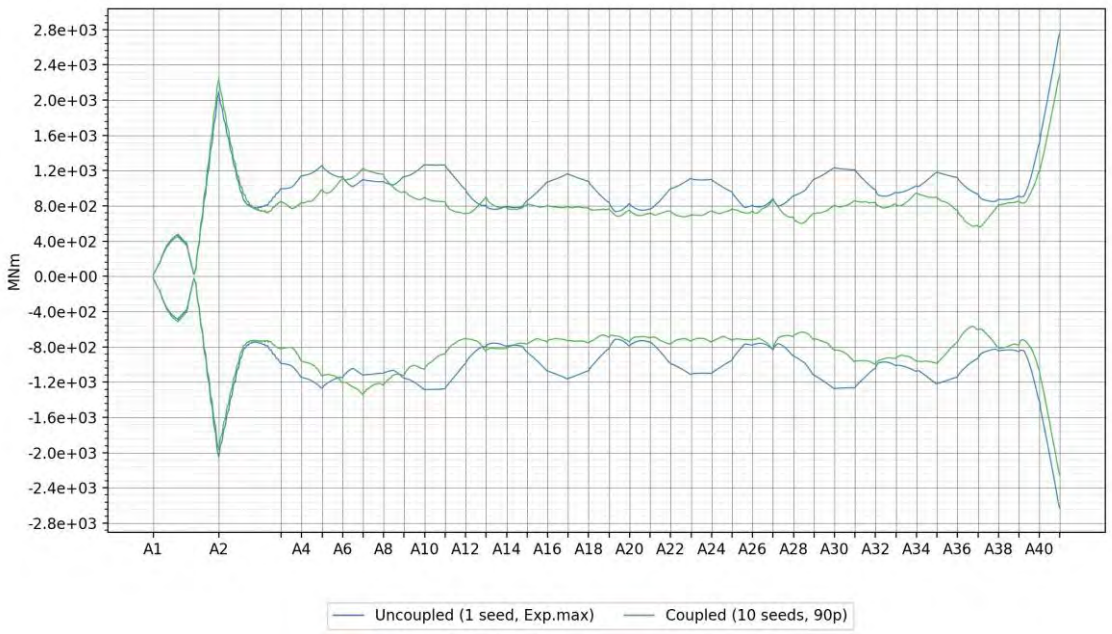


*Figure 10-11 Coupled vs. uncoupled environmental loads for K12_07: Bending moment about strong axis*

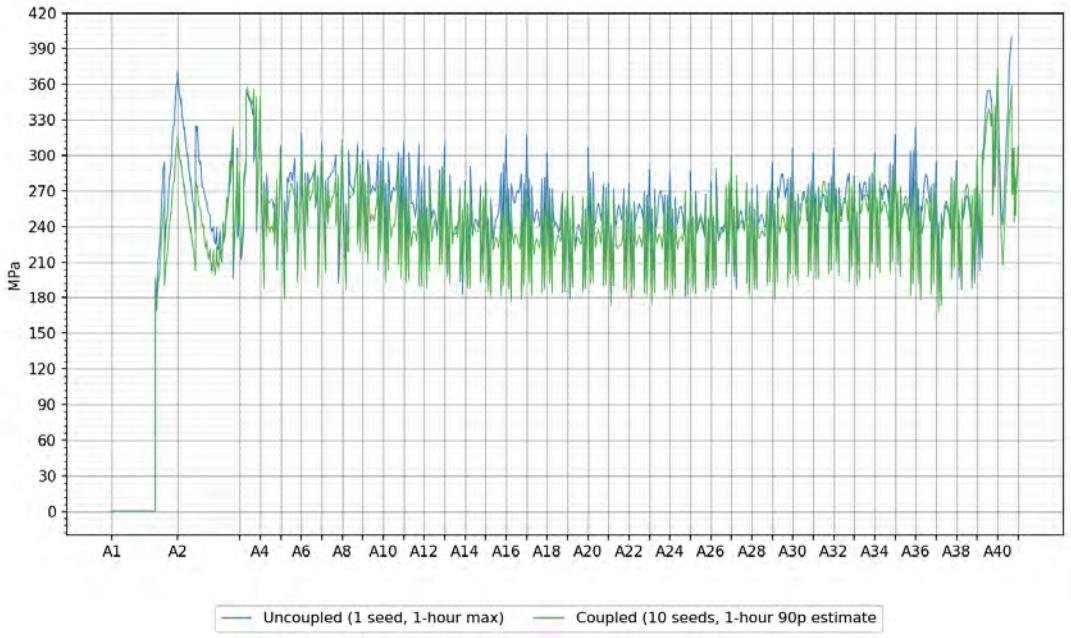


*Figure 10-12 Coupled vs. uncoupled environmental loads for K12_07: Max Von Mises*

## 10.12 Comfort evaluation

A comfort evaluation was performed using the overall vibration total value (OVTV), in which a weighted sum of RMS accelerations was evaluated. Local vehicle response was modelled based on input from SVV in [10]. More detailed description and results may be found in Appendix G, Section 5. The evaluation was performed for the K12_05 iteration of the concept in which the mooring system different from the K12_07 iteration. Spot checks indicate that the motions in a one-year condition was fairly similar between the two iterations, and the results are thus considered valid.

The evaluation was conducted along the 1-year contour with waves and wind run separately in frequency domain and local wind on the vehicle based on a time series. The forward speed of the vehicle was accounted for when evaluating the encountered acceleration response from dynamic bridge response and the local wind time series was generated based on the instantaneous vehicle heading as it drives over the bridge. The results in Figure 10-13 and Figure 10-14 show that wind and waves utilize about 15% each of the OVTV criterion, whereas local wind on the vehicle utilize 300% of the criterion. Hence, the OVTV criterion would not be satisfied even for a rigid bridge. The dynamic bridge motion is around 10% of the discomfort, and around 30% of the specified maximum OVTV value.

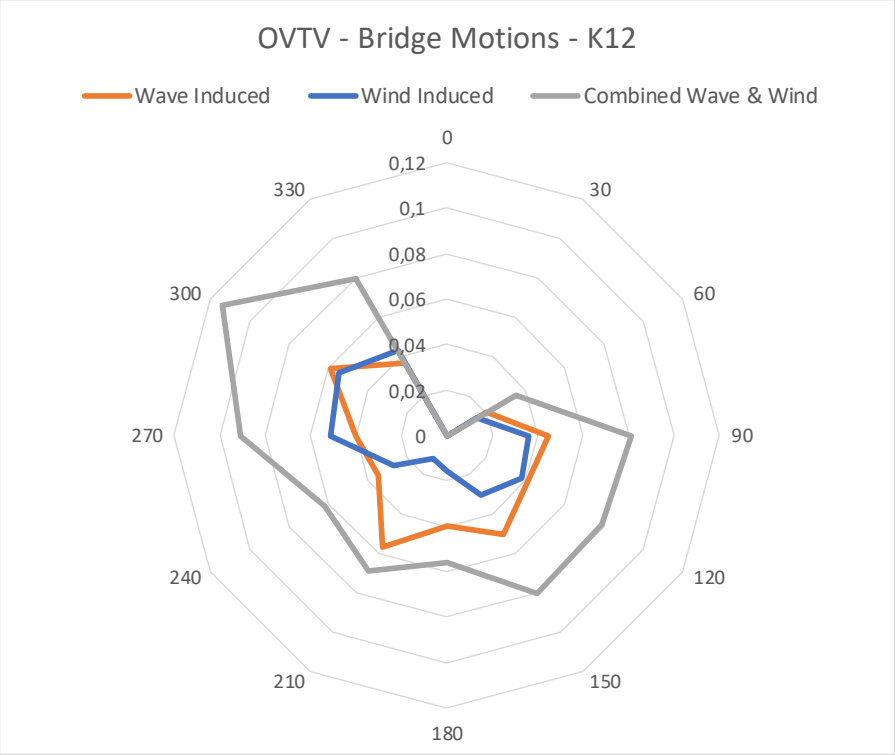


*Figure 10-13 Contribution from bridge dynamics based on wave and wind to the OVTV comfort criterion.*

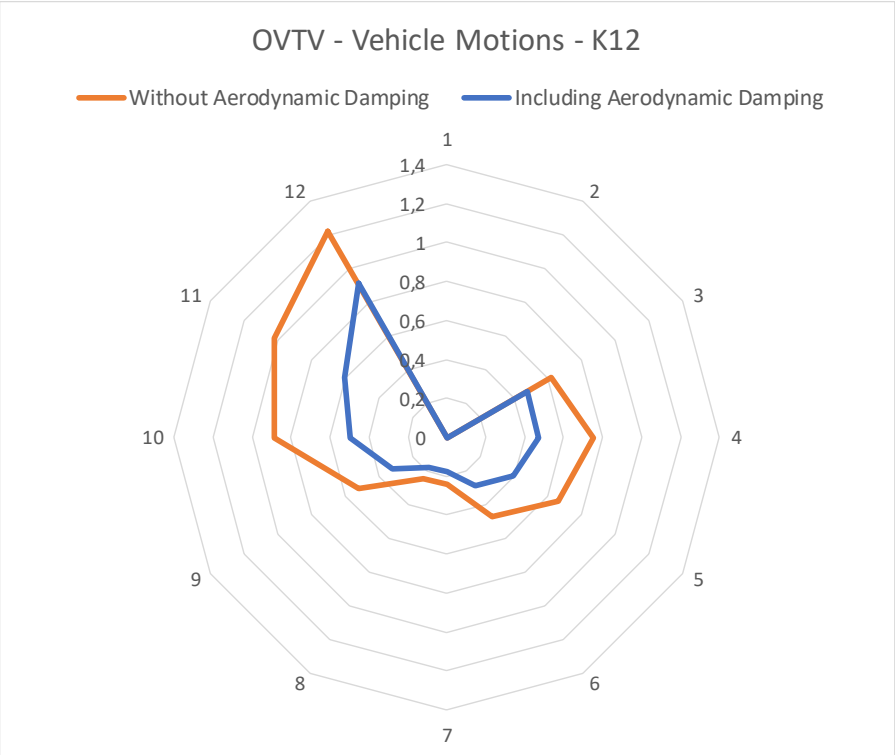


*Figure 10-14 OVTV – Wind on vehicle model*

Based on the OVTV evaluation for wind on a stationary vehicle it is observed that the vehicle damping level in sway is very important for the overall results. If the assumed sway damping is correct, the findings show that the OVTV criterion is dominated by the local wind loads on vehicle. A few effects could be considered in further work, possibly reducing the lateral accelerations:

- Time-dependent aerodynamic coefficients accounting for the time required to get stable drag and lift coefficients
- Effect of forward speed on vehicle response parameters

As a general comment, the reduction of wave condition from the metocean design basis in phase 3 to phase 5 of the project gives a significant reduction of bridge motions, and it is expected that the same would be observed if comparing OVTV results of the two phases.

## 10.13 Accidental limit state response

### *10.13.1 Intact conditions – 10 000-year environment*

The response to 10 000-year environmental conditions was in Phase 3 of the project found to not be dimensioning as the increase in bridge response was below the load factor of 1.6 applied to the ULS loads. Similar assessments have been performed in this phase:

- Wind waves and swell cases are screened in frequency domain to identify a few governing environmental scenarios
- Wind is assumed coming either from the west or east perpendicular to the main crossing direction
- Coupled dynamic simulations were performed in time-domain with 10 seeds for each environmental condition
- The response was evaluated at the required 95-percentile level using the AUR method and compared with the ULS response at the 90-percentile level
- The permanent and environmental load factor of 1.2 and 1.6 respectively was used for the ULS results, whereas a factor of 1.0 was used for both the for 10 000-year results.
- Note that the material factor also changes from 100 to 10 000 years, this should be considered when assessing the response.

Some sectional responses are compared in Figure 10-15 to Figure 10-17. The sectional forces from 10 000-year environmental response is in general somewhat larger than the ULS response. It is not evaluated if this is due to the environment alone or the increased percentile level from 90 to 95. For stresses (Figure 10-18) the difference is less, and the 10 000 year 95-percentile and 100-year 90-percentile with load factors yields similar utilization of the bridge girder.

The design development has been performed with 100-year ULS results as a basis. The yield response is governed by the 100-year condition. As some of the sectional loads were higher for the 10 000-year response it is recommended to do a more comprehensive evaluation of the 10 000-year response during the next phase of the project, especially to evaluate that the buckling capacity of the structural elements are within the required margins.

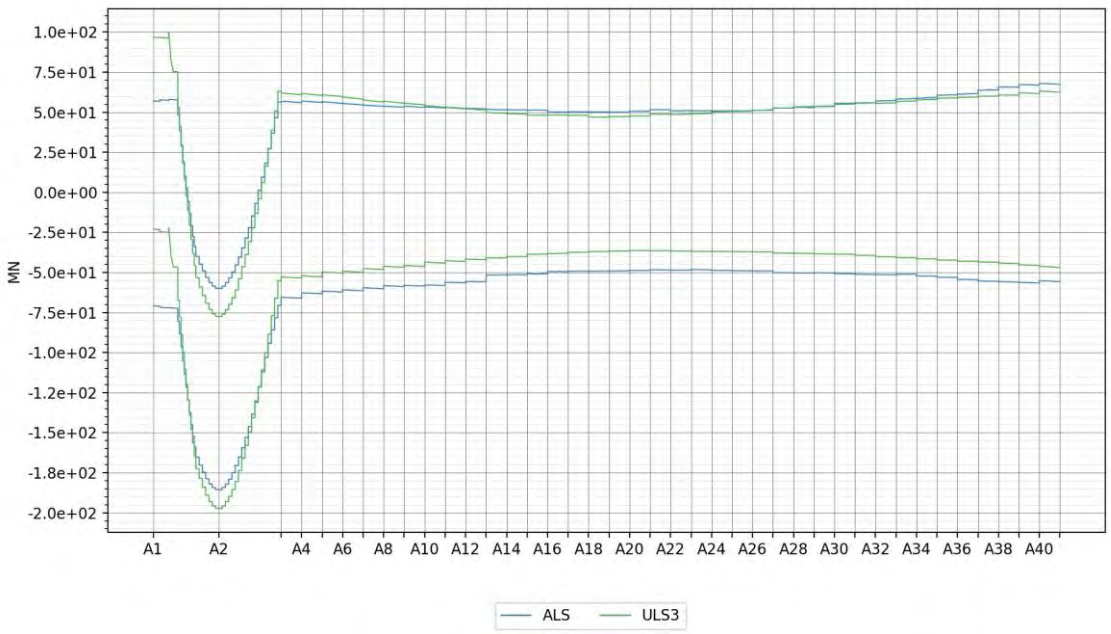


*Figure 10-15 ALS (K12_06) vs. ULS (K12_07): Axial force*

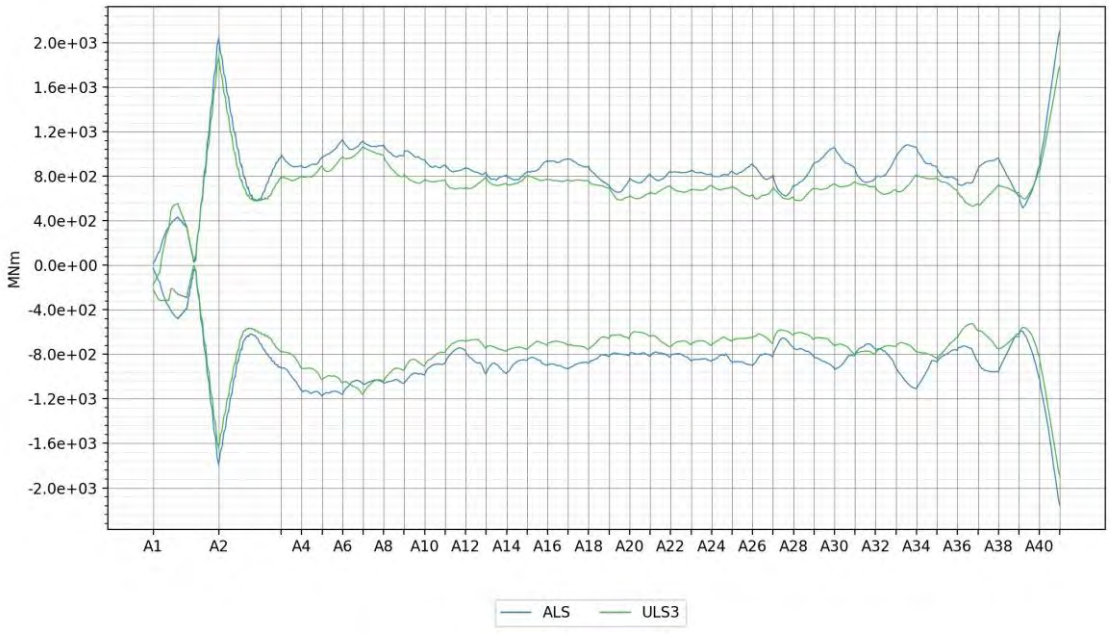


*Figure 10-16 ALS (K12_06) vs. ULS (K12_07): Bending moment about strong axis*

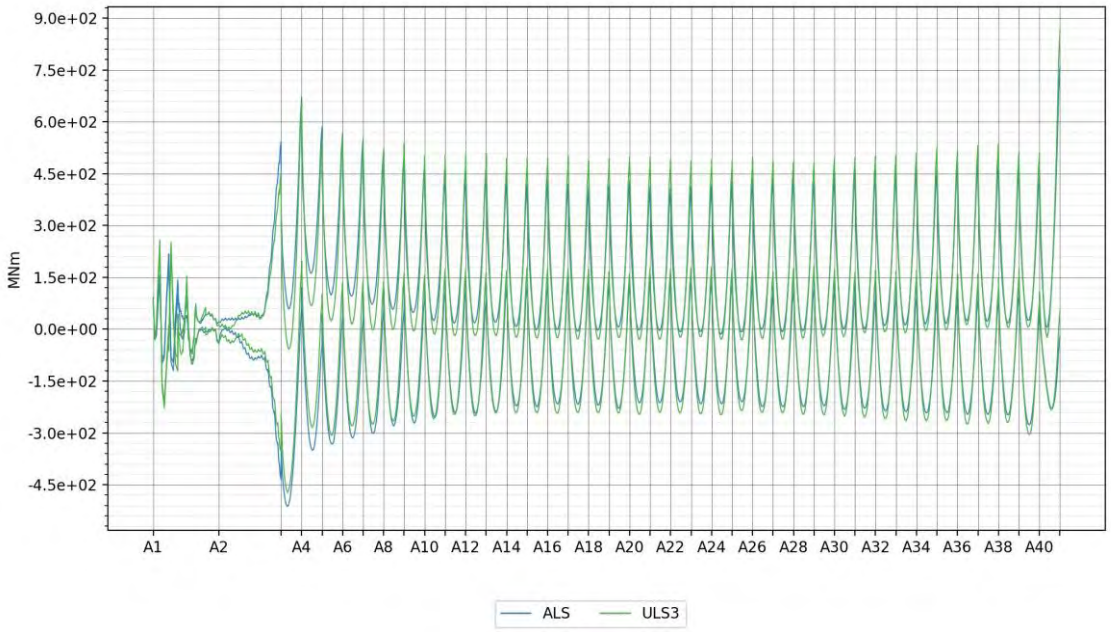


*Figure 10-17 ALS (K12_06) vs. ULS (K12_07): Bending moment about weak axis*

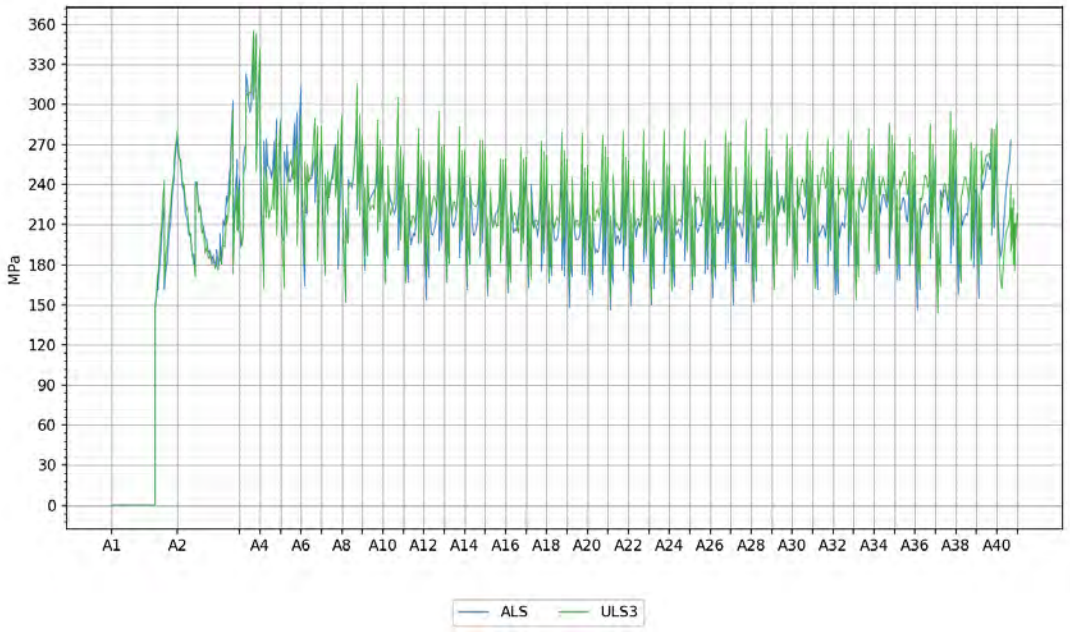


*Figure 10-18 ALS (K12_06) vs. ULS (K12_07): Max Von Mises*

### *10.13.2 Damaged condition – 100-year environment*

Accidental limit state capacity has been checked for damaged conditions of the bridge, with flooding, damaged bridge girder due to ship collision and loss of a mooring cluster. Only loss of a mooring cluster gave a significant increase in the dynamic response from a 100-year environmental condition, but the increase in responses were lower than the allowable utilization.

For loss of mooring lines, the loss of one side of a mooring cluster (2 lines) were checked for all moored pontoons. In addition, a sensitivity study was performed with loss of one side of two mooring clusters, either on A13 and A20 or A20 and A27. See Figure 10-19.

Flooding of a moored pontoon with a flooded volume of 2000 m3 and partial loss of waterplane stiffness in heave and roll was simulated for K12, and found to primarily affect weak-axis shear forces and moments with an increase of 35%, well within the margin from load factors.

Detailed results are given in Appendix G. The analyses show that capacity is still within the capacity of the ULS regime. Peak values of mooring line forces after line failure are all below the breaking strength of the mooring lines, and progressive collapse is thus not of concern.

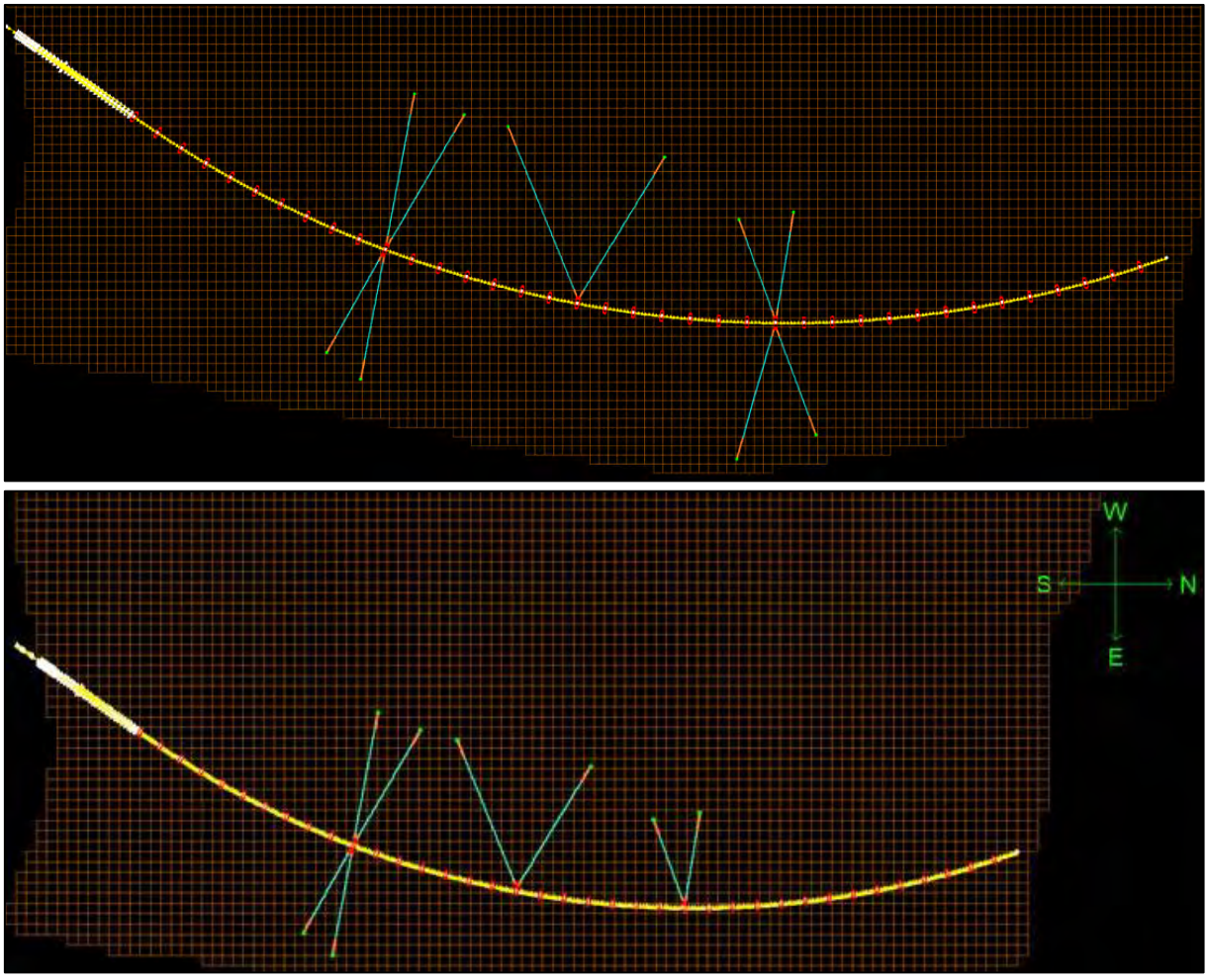


*Figure 10-19 Example of model for loss of mooring lines – loss of two lines in group A20 (top) and loss of two lines in two clusters A20 and A27 (bottom).*

## 10.14 Sensitivity studies

Sensitivity studies were performed for both modelling assumptions (simulation time, ramp-up, frequency components etc) in Appendix F and response sensitivity (wave spectrum parameters, mooring line damping, second order wave drift forces etc.) in Appendix G. Key findings are given below:

- Response from wind-waves is not sensitive to variation in wave spectrum parameters, whereas swell waves are moderately sensitive. Swell waves are extremely sensitive to period.
- Mooring line damping is dependent on the line pretension and thereby the static transverse offset of the bridge girder. For a selected condition with extreme offset due to temperature and tide (>10000-year return period) the mooring line damping was reduced with 70%, resulting in an increased strong-axis moment in swell of about 10%.
- Variations of abutment stiffness in a reasonable range does not affect global bridge behavior.
- If the effect of traffic is included for ULS2 (increased mass, aerodynamic drag and hydrodynamic excitation) the strong-axis bridge response increases somewhat (but is still lower than ULS3). Weak-axis moment are worse for the conventional ULS2 check.
- Second order wave drift forces affect the mean bending moment about strong axis but not the dynamic values. It is considered to not have a significant effect on the bridge response but should be included for completeness in future simulations.
- The wave spectrum discretization is analysed with respect to the total number and distribution of the wave components. A refined spectrum discretization method has been proposed and benchmarked against the equal energy discretization method. The analysis shows the importance of including enough wave components in the simulation in order to capture the physics correctly, otherwise key response modes artificially fall outside of the excited regime. The analysis also shows that applying a refined spectrum discretization method with less wave components can increase the precision and decrease the computation time.
- The IFORM-methodology was used to evaluate the 100-year response in the bridge girder, and uncertainties in the metocean contours and long-term response predictions were identified.

# 11 Global analyses – special studies

Studies related to hydrodynamic effects such as viscous damping, wave-current interaction, hydrodynamic interaction effects and freeboard exceedance are described in Appendix H [11].

## 11.1 Viscous drag on pontoons

Viscous drag loads were evaluated based on literature studies and CFD simulations. The drag coefficient suggested from the CFD analysis in steady-flow conditions is 0.41, which is somewhat higher than the value of 0.30 estimated based on literature review. A strong dependence on the Keulegan-Carpenter number was found, with increasing drag coefficient with decreasing KC number (decreasing relative motion amplitudes).

A conservative estimate of the drag coefficient's KC dependence, where linear interpolation can be assumed between the points, has been established in Figure 11-1. It is assumed that the drag coefficient for KC < 0.5 is equal to the value at KC = 0.5 since we do not have data below this KC number. Similarly, it is assumed that at KC = 60 the drag coefficient is equal to in steady-flow conditions.

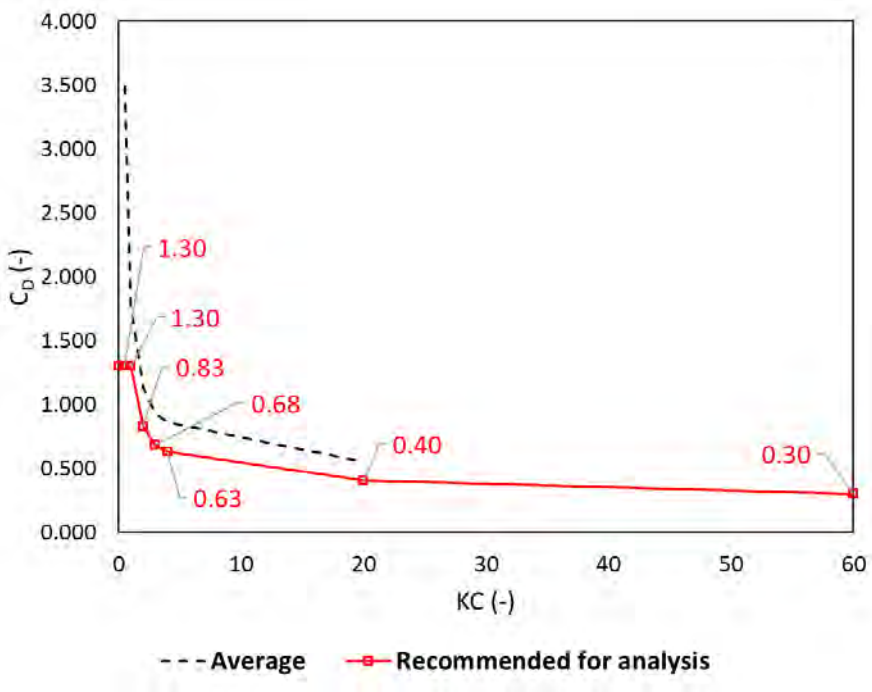


*Figure 11-1 KC-dependent Morison drag coefficients for pontoon proposed for global analysis model (red line with square markers). The numbers indicate the value of the drag coefficient in the different data points.*

## 11.2 Wave-current interaction

Wave-current interaction effects are examined by performing hydrodynamic analysis in Wasim and comparing hydrodynamic coefficients, i.e. radiation and wave excitation loads, with results obtained with Wadam (Wamit). The global effect was investigated for a few scenarios. Wave-current interactions may cause rather large changes to the excitation loads, especially if the waves and current come from opposing directions. The effect was more significant for sway and roll than for heave. An example is shown for wave excitation loads in roll in Figure 11-2.

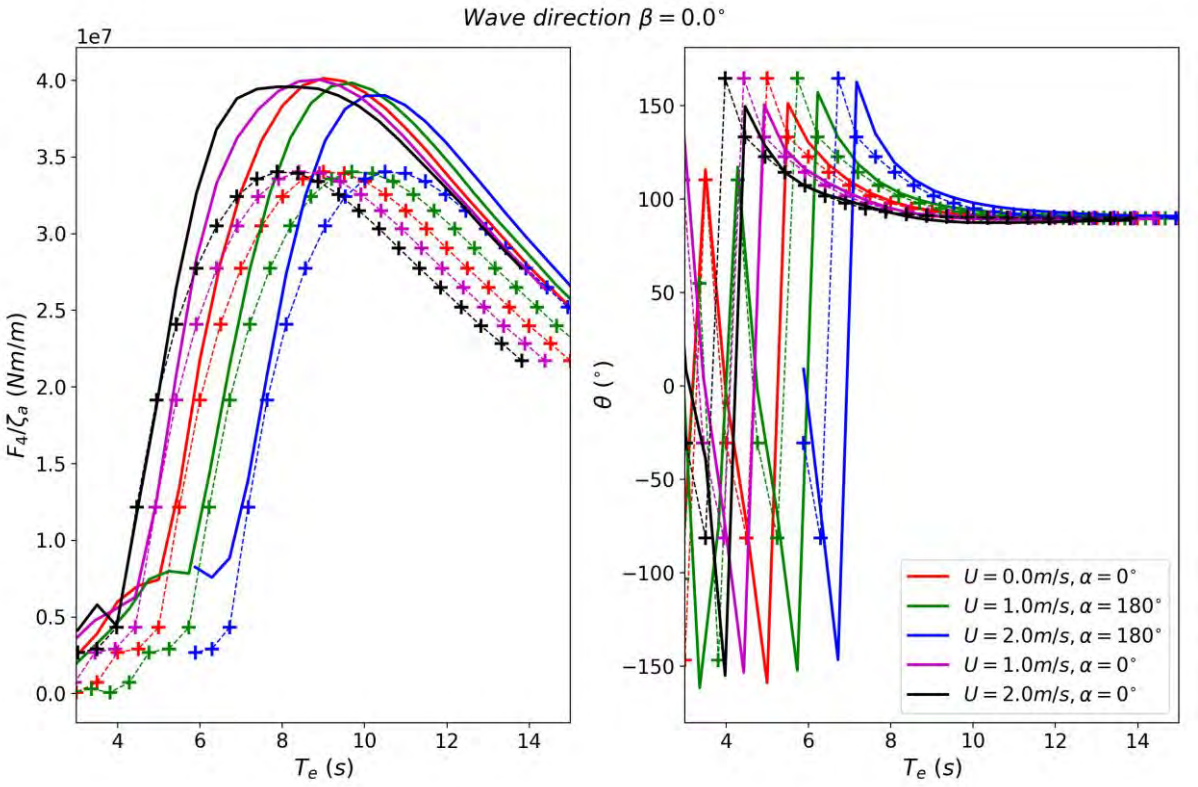


*Figure 11-2 Wave excitation loads in roll, wave direction 0°. Wadam results plotted as a function of encounter period $T_e$ are dashed with (+) markers.*

The global analysis of wave-current interaction shows large influence on almost all response variables. This is partly due to a doppler-shift of the wave excitation frequency, and partly due to an additional change in the radiation solution and wave excitation loads due to wave-current interaction. With ~~a~~ current in opposite direction of the waves, the encounter frequencies for the waves are decreased and different eigenmodes can be excited. With a current velocity of 1.5 m/s in opposite direction of the 100-year easterly wind wave, the resulting bridge response is significantly increased compared to the zero-current case, especially for strong axis moment.

The realism of the studied case with an extreme current opposing the extreme wind wave must be further studied. Updated metocean data is required to determine a realistic combination of opposing current and wind waves, before the load effects due to wave-current interaction effects can be reliably established for the selected concept. Here the global effect has been checked for K13 only and the results indicate an increase for this combination of current, waves and concept of 20% on the bridge girder utilization. Hence, the design of the floating bridge should contain a certain level of robustness to allow for such effects.

## 11.3 Hydrodynamic interaction between pontoons

The hydrodynamic interaction between pontoons has was evaluated by finding pontoon hydrodynamic coefficients from Wamit for a simulation in which the two neighbouring pontoons were included (an example is given in Figure 11-3). These characteristics were applied to all pontoons in the global analysis model and compared with simulations in which hydrodynamic interaction was neglected.

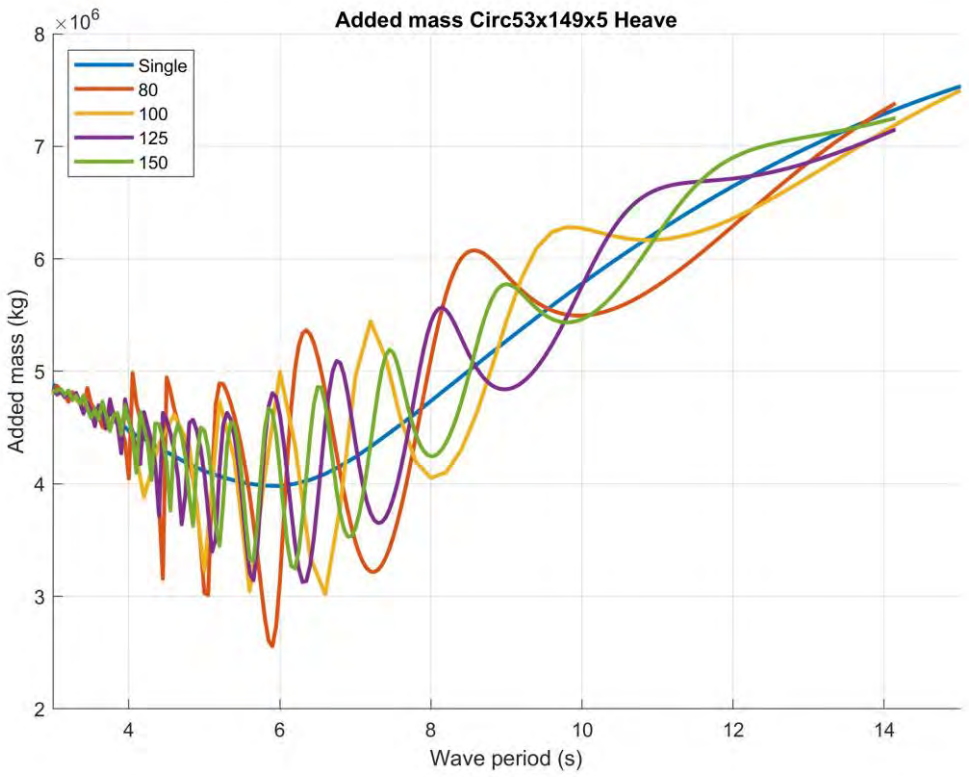


*Figure 11-3 Heave added mass (A33) for different span widths*

It was found that hydrodynamic interaction has an influence on the response; the effect is found to be largest for the vertical motion and the weak axis moment. Figure 11-4 shows an example of the global strong-axis response, for which the response is worse when not considering hydrodynamic interaction. Further, the hydrodynamic interaction effect is larger for shorter span widths. This is checked in the global analysis by comparing 100 m span width and 125 m span width, with and without hydrodynamic interaction. The effect may be important for typical fatigue sea states and is recommended for further studies during the next phase of the project.

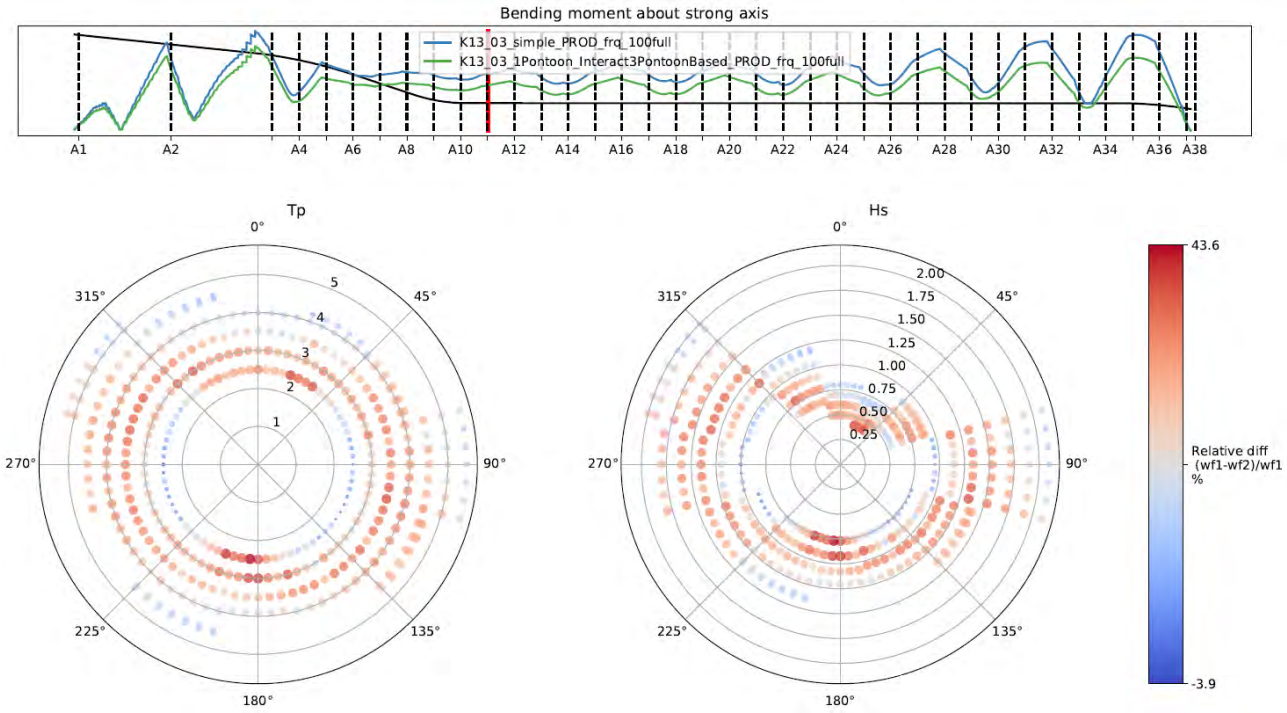


*Figure 11-4 Difference in strong axis bending moment without (blue/wf1) and with (green/wf2) hydrodynamic interaction with 125m span width (K13_03)*

## 11.4 Second order wave effects

The effect of computing full quadratic transfer functions (QTF) in WAMIT for the slowly varying drift loads on a pontoon has been compared with the Newman approximation. The comparison shows that the Newman approximation is conservative for the most relevant wave periods and is recommended for further design work. Figure 11-5 illustrates the difference between the Newman approximation and the full QTF, in which a positive number gives a more conservative response with the Newman approximation.

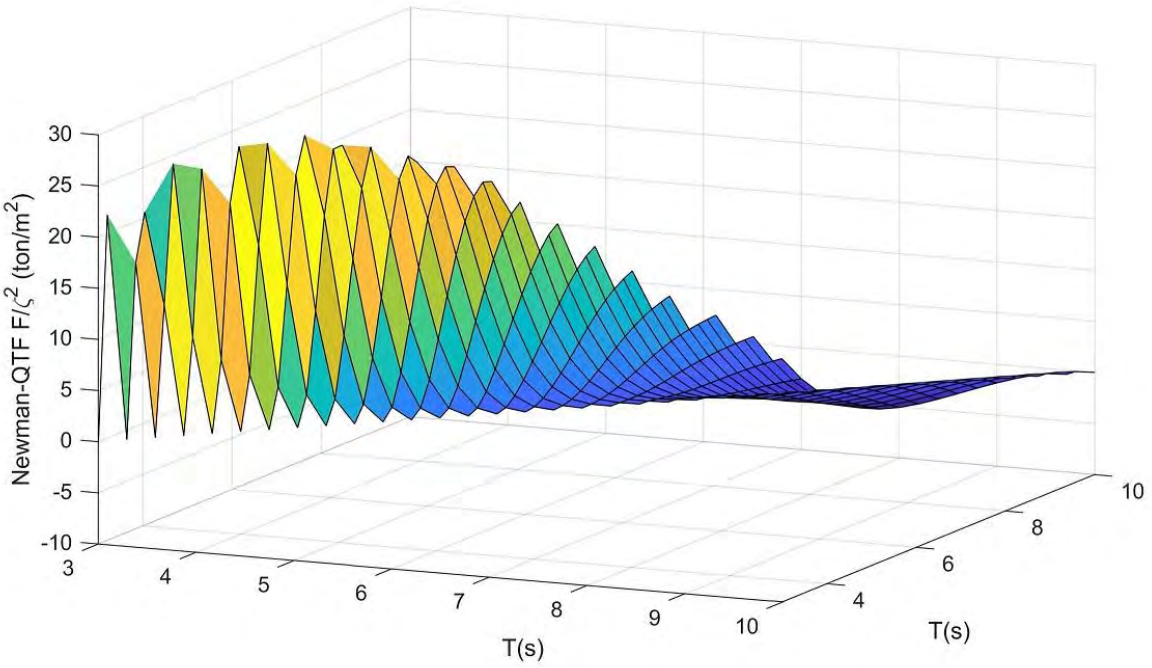


*Figure 11-5 Difference between the geometric mean Newman approximation and the full QTF, (only one side of the diagonal is plotted)*

## 11.5 Inhomogeneous wave field

Simplified analyses have been performed with an inhomogeneous wave field, considering phase difference and wave height variation separately.

A fully uncorrelated wave field between the pontoons have been simulated by changing the phase angle of the wave excitation load coefficients for every pontoon with a few seed variations. A considerable influence on the response was found with around 30% variation of strong-axis moment (an example is given in Figure 11-6), but the maximum loads were reduced for the considered cases.

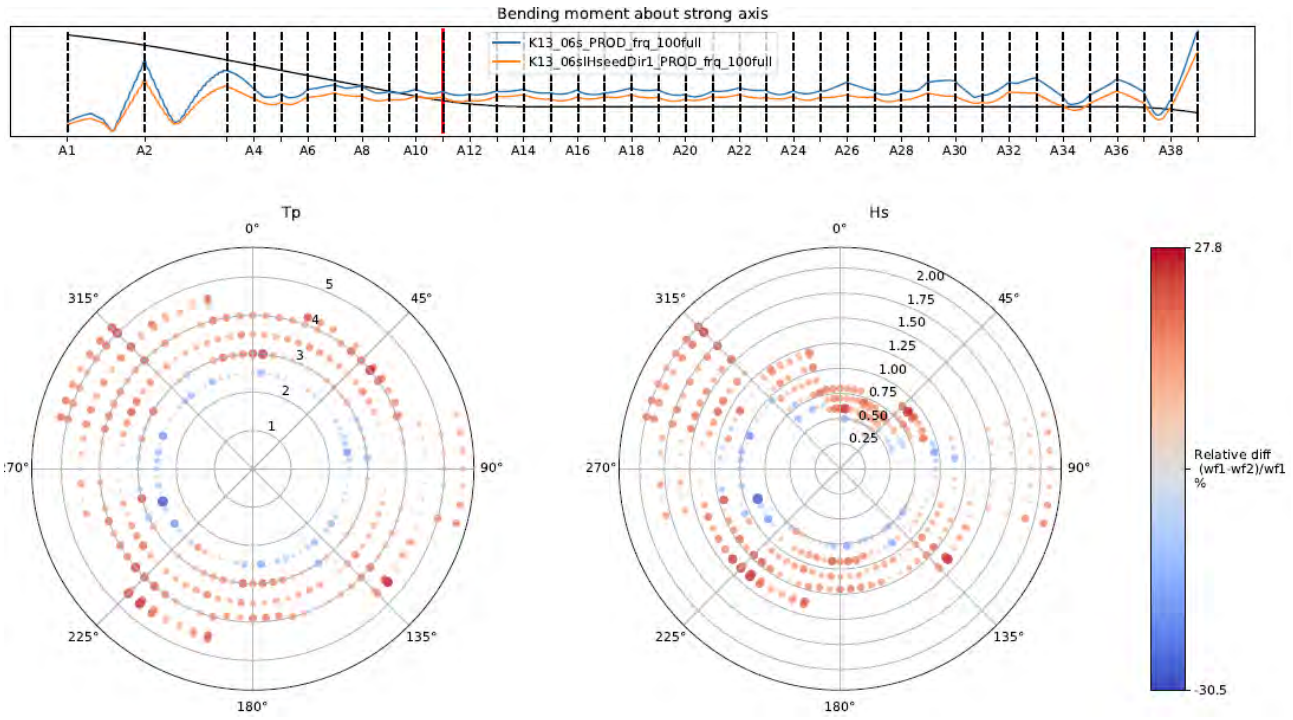


*Figure 11-6 Difference of the standard deviation for strong axis moment between fully correlated sea and a single seed with inhomogeneous sea for a range of wave directions, periods and heights. Red indicates that the inhomogeneous sea state gives lower response. The picture on top shows the maximum standard deviation from all simulations along the bridge, the difference at axis 10 is illustrated here in the rose plots.*

Variations of the wave height in the fjord was considered based on the data provided in the environmental design basis, in which waves coming from north/northwest give waves that are higher towards the south and sheltered towards the north. For waves coming from south/southwest the result is opposite. Figure 11-7 shows the variation in weak-axis moments for which some differences were found especially towards the Northern end of the bridge.

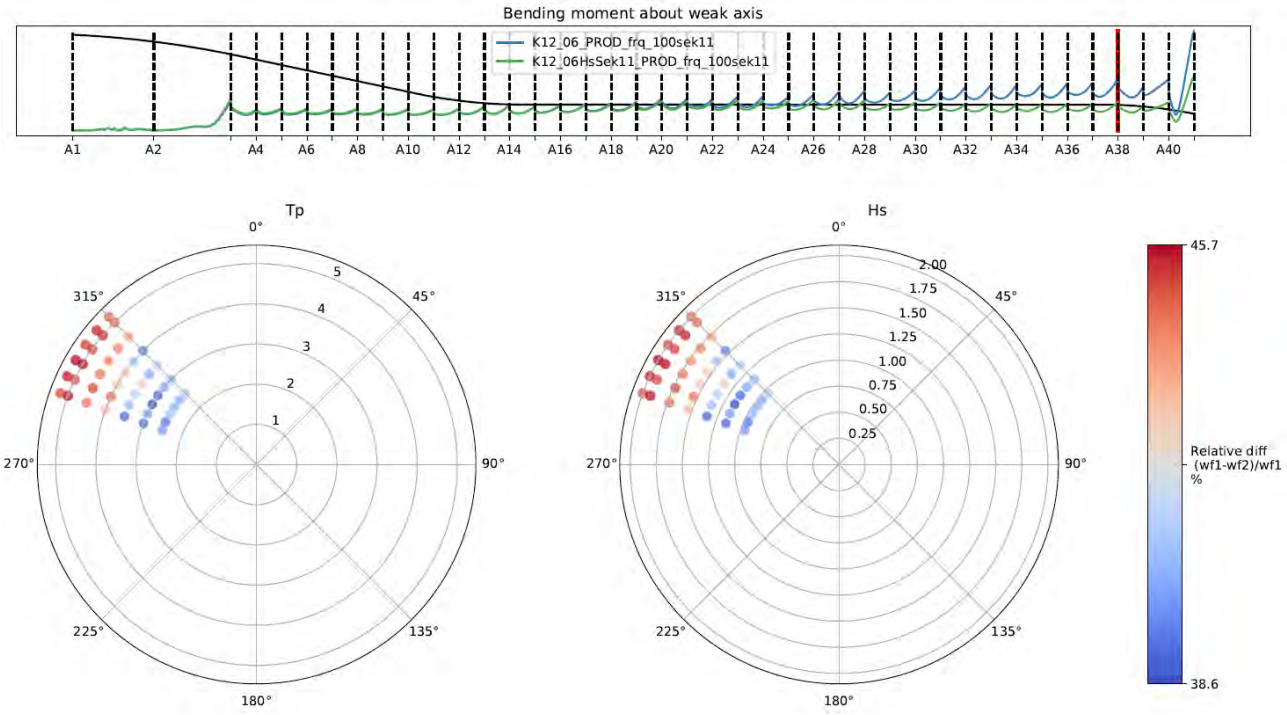


*Figure 11-7 Difference of the standard deviation for weak axis moment between inhomogeneous sea with different wave height for waves from 285 and 315 degrees. Red indicates that the inhomogeneous sea state gives lower response. The picture on top shows the maximum standard deviation from all simulations along the bridge, the difference at axis 38 is illustrated here in the rose plots.*

Even though the extreme response is reduced, the response for a certain wave direction and period may very well increase as a function of inhomogeneity. This shows that one must carefully assess the effect of inhomogeneous sea states on a consequence level. As an example, increasing the response at certain critical periods may increase the risk of parametric excitation. When the wave height was varied along the bridge, an increase in maximum bending moments was observed towards the bridge ends.

The studies performed show that spatial variations of wave properties along the bridge may have a significant influence on global responses that are hard to anticipate. Moreover, it cannot be concluded in general that neglecting these effects is conservative, and the effect of inhomogeneous sea states should be further analysed. In the present phase, the study has focused on maximum loads, while the consequences for fatigue life have not been explored. Furthermore, the focus has been on the phase of wave excitation loads and varying wave height. One should also consider, and possibly analyse, spatial changes in wave periods, wave spectra, wave spreading, wave direction and current. This is a comprehensive list of parameters, and rational ways to simplify the analysis matrix and to process results statistically are required. For such assessment to be meaningful, metocean data with detail level beyond what is presently available is required.

## 11.6 Freeboard exceedance

A methodology to assess the effect of freeboard exceedance has been developed where the effect of water on the pontoon deck is accounted for. Assumptions were made to estimate the relative wave elevation conservatively. A model was implemented in Orcaflex to apply loads due to the water column on the deck. A two-step sensitivity study was performed; one with a single pontoon and the global bridge response represented as stiffness and one in which the freeboard exceedance model was implemented in the global analysis model of the bridge.

Figure 11-8 shows an example of the loads induced by freeboard exceedance and the resulting floater motion for a 100-year sea state on a single pontoon. Even though there are several events where the freeboard is exceeded, the induced loads have only a moderate effect on the heave and roll motions. In general, the effect on heave motion is more significant than on roll motion. The heave force “impulses” are relatively short and are more likely to amplify responses with short natural periods.

In the global model the response is more complicated to assess. In order to provoke a change in the response an unrealistically severe sea state with $H_s$ 3.5 m and $T_p$ 5.2 seconds was chosen (outside of the 10 000-year limit) and compared with a 100-year condition with $H_s$ 2.1 m for the same period. The results (an example in Figure 11-9) for the case with the 100-year wind wave does not show any influence from freeboard exceedance. For the generic extreme case there is some increase in both the strong axis and the weak axis moment due to freeboard exceedance. However, one should keep in mind that this wave is significantly higher than the 10 000-year sea state given in the metocean design basis.

A more comprehensive study of the effect of freeboard exceedance should be performed in the next stage of the project. In general, it is found that imposed loads due to excess of a pontoon freeboard may reduce responses with long natural periods and amplify responses with short natural periods, but it is not possible to make a firm conclusion on the applicability of a 3.5 m freeboard. In such future works it is recommended to verify the freeboard model with model tests or CFD calculations.

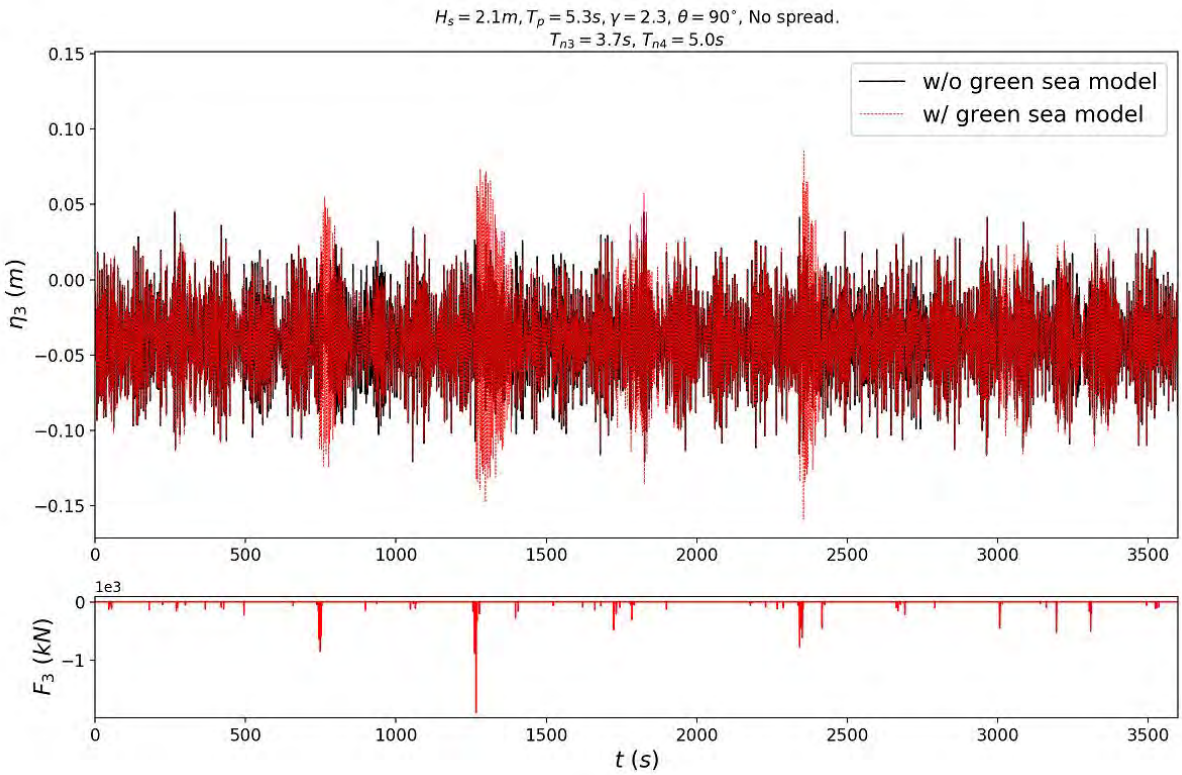


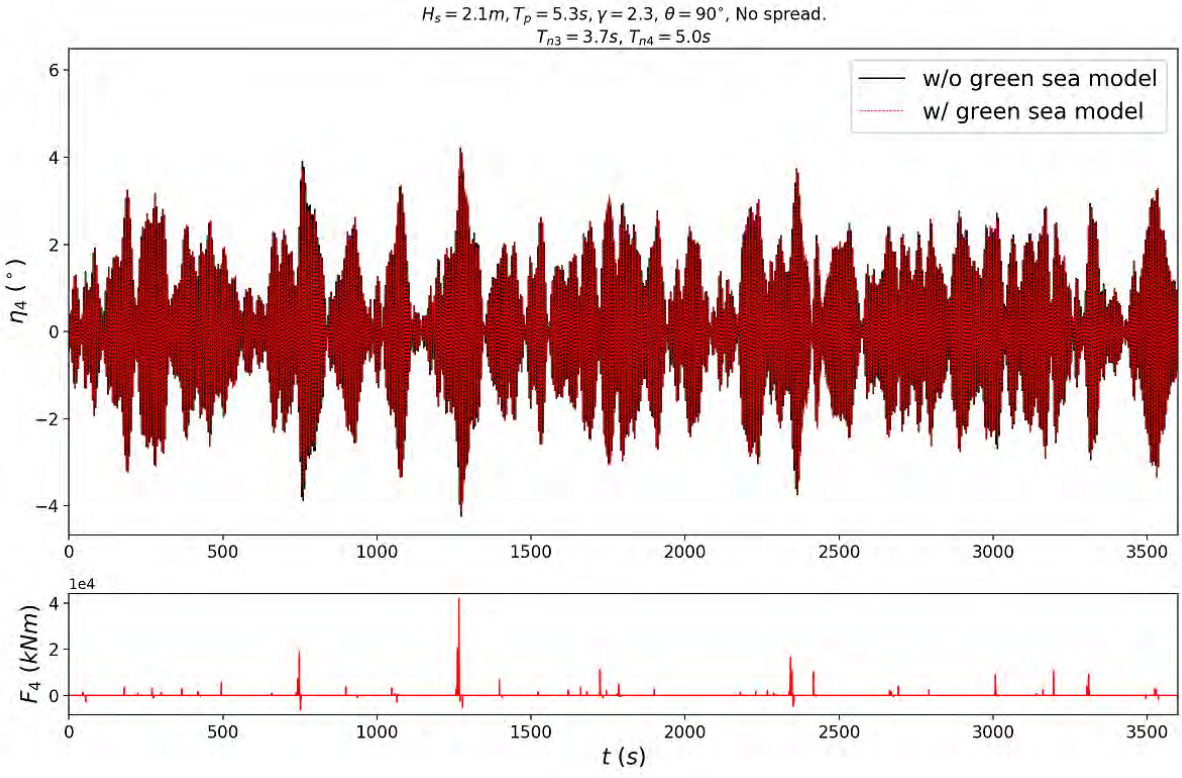


*Figure 11-8 Time series of applied loads and resulting pontoon motions in heave and roll for $H_s = 2.1\ m, T_p = 5.3\ s$ with $T_{n3} = 3.7\ s, T_{n4} = 5.0\ s$ and no wave spreading.*

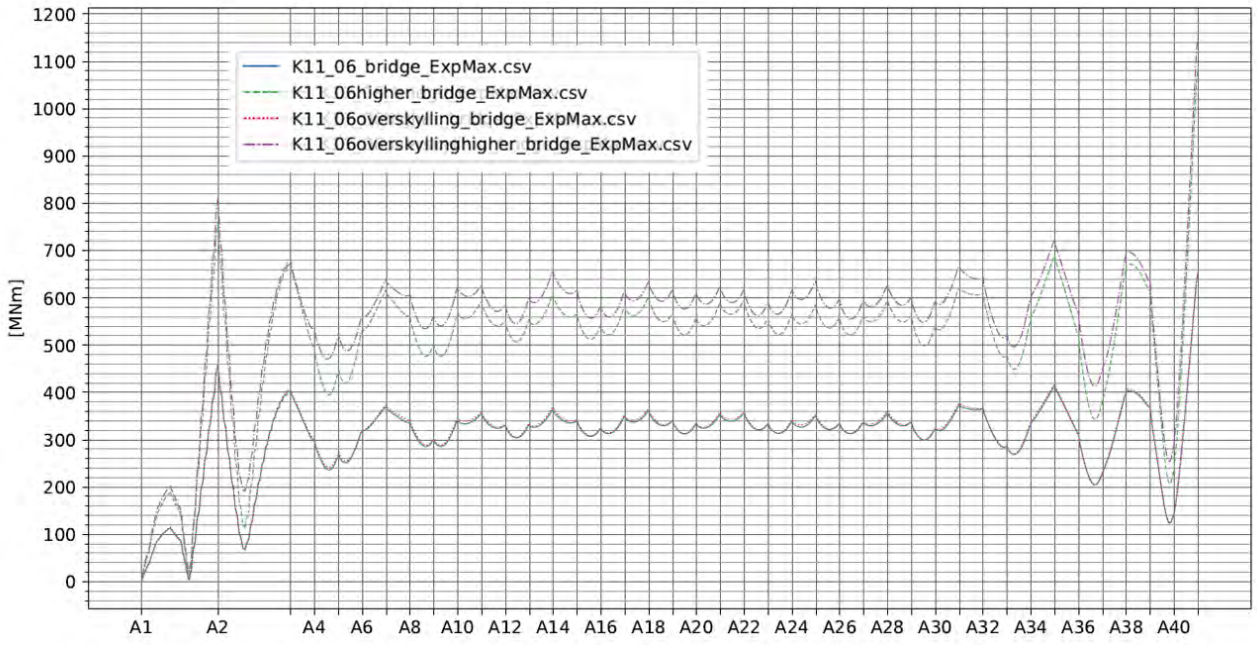


*Figure 11-9 Strong-axis bending moment from global analysis simulation for the bridge model K11_06 with and without freeboard exceedance model.*

# 12 Parametric resonance

The main purpose of phase 5 of the E39 Bjørnafjorden project is to identify and document which of the four described bridge alternatives that may be regarded as the best solution. In this context the possibility of parametric excitation and parametric resonance has been looked into.

In contrast to traditional resonance, where an external force applied at or near a natural frequency of the structure results in resonance, parametric resonance is caused by an oscillating variation of one or more of the system properties. There are several parameters that could, in principle, trigger such resonances:

- Geometric stiffness changes due to axial force variation
- Geometric stiffness changes due to *bending moments* in girder
- Added mass due to changing draft or rotations of pontoons
- Hydrostatic stiffness (from restoring forces) due to changing draft or rotations of pontoons

However, for the Bjørnafjorden Bridge the axial force variation that induces variation in the geometric stiffness of the system has been considered most critical. This parameter variation may be crucial for the evaluation of the safety of the concept. Parametric resonance may be far more aggressive than forced resonance due to the exponential growth of response over time [12] [13]. The slender girder for this bridge makes the effect of the axial force variation an important risk to consider for the concepts; the complex dynamic behaviour and the combined, stochastic excitation nature makes it challenging to assess.

An attempt to give a simple description of a complex and challenging problem may be as follows: the variation of the axial force in the slender girder of the Bjørnafjorden floating bridge give source of stiffness variation that leads to amplification of the load effects at frequencies other than the loading frequencies.

The challenge has thus been addressed by the looking into the following topics:

- Determination of the axial force variation for the different concepts and for different loadings
- Applying the defined criterion for possible onset of parametric excitation on the possible concepts
- Establishing a criterion for evaluation of a final level for the parametric excitation response taking into account the effect of present nonlinear/quadratic damping
- Establishing how the stochastic nature of the loading should be treated
- Establishing procedures for evaluating the effects of:
    - the magnitude of the external force
    - the external static forces
    - the effect of wide-bandedness

Based on these studies and the established procedures, the robustness of the four concepts regarding this topic have been documented and compared in a quantitative manner, see Table 12-1.

The main finding is that the curved concepts are prone to parametric excitation from swell waves, as these concepts all have an axial eigenmode with a high modal force and low linear damping in the swell frequency range and the triggered eigenmode at around half the frequency also has low linear damping. The mooring line damping for the side anchored concepts gives a significant contribution to the damping both for the critical axial eigenmode and the triggered eigenmode. This means that the K12 concept is considered robust with regards to parametric excitation, even though the concept does not fulfil the onset criterion.

## 12.1 Summary of procedures used

Full description of methodology and bases for the calculations is given in Appendix S and enclosures to that appendix. Here only a summary of procedures and major results are summarized.

The first step in a quantitative evaluation procedure of the parametric excitation caused by axial force variation is identification of the global axial force response of the four concepts. Three loading regimes are studied; swell waves, wind generated waves and wind loading. The loading regimes are evaluated individually to establish the correct size of axial level within each regime and to get loading levels that may be robust for the further treatment. As a part of this determination of the axial force variation, detailed screening is performed. Such screenings for the wave loading are mandatory in order to determine the correct axial force level. Especially the swell loading may easily be underestimated if this screening is not performed detailed enough.

The evaluation of the parametric resonance phenomena is here handled by procedures based on evaluation of uncoupled modes as proposed in Øiseth et al. [14]. The complex nature of parametric resonance of stochastically excited systems motivates a simplified approach to deal with the phenomenon. The traditional approach for the nonlinear analysis of systems exposed to stochastic excitations which relies on Monte Carlo simulation of multiple deterministic excitation time series from the stochastic description, is believed not to capture the effects of parametric resonance in a reasonable quantitative manner.

Thus, the next step is evaluation of each concept using the criterion suggested in Øiseth et al. [14] in order to determine whether onset of parametric excitation do occur. As this criterion only evaluate onset of parametric excitation, it must rely on linear damping only. If this procedure indicate that parametric excitation may occur, a new developed criterion is used to quantify the severity of the potential parametric excitation. Based on this criterion a terminal level of the parametric excitation is determined where also nonlinear relevant damping for the concept is included.

As a third step the robustness of the concepts are evaluated by quantifying the effect that variation in assumed damping level and axial force level will have on the response.

## 12.2 Concept evaluation

The main finding of the performed work is that concepts K11, K12 and K14 are all prone to parametric resonance from swell waves, as there is a critical axial eigenmode with high modal axial force with low linear damping in the swell frequency range (around 13 seconds). Also, the triggered eigenmode around half the frequency has low linear damping. Consequently, all curved concepts do not fulfil the defined onset criterion, proposed by client. The only concept that fulfil this criterion is the K13 concept, which does not build-up net dynamic axial forces in the girder and thus has not significant global variation of the geometric stiffness.

The moored line damping for the side anchored concepts (K12 and K14) contributes to a significant damping contribution both for the critical axial eigenmode and the triggered eigenmode. The mooring damping reduces the axial force response and ensures a high damping level at the triggered eigenmode. Because of the mooring damping contribution, the K12 and K14 concepts are found to be *robust* with regards to parametric resonance, even though the concepts fail the onset criterion

The K11 concept has a low level of quadratic damping and have a significantly higher axial force response. As such, there is a risk for an unacceptable response from parametric excitation. Thus, *the K11 concept does not show the necessary robustness* for parametric resonance that AMC requires at this stage of concept development and with the current knowledge about the phenomenon.

A summary of results is given in Table 12-1. More detailed description of assumptions, procedures, calculations and results are given in Appendix S.

*Table 12-1 Overview of results for parametric excitation. The onset criterion denotes the recommended procedure from client for evaluation of parametric resonance. The 100-year and 10 000-year terminal response value denotes the expected dynamic response for a probability of exceedance of 0.01% and 10%, respectively. The threshold response robustness check value denotes the calculated response including a 20% reduction of quadratic damping and a 20% increase of the axial force response level.*

| Concept | Condition | Return Period | Onset Criterion | Threshold Response [MPa] | Threshold Response Robustness Check [MPa] |
|---|---|---|---|---|---|
| K11 | Swell | 100 | fails | 475 | 752 |
| | | 10000 | fails | 332 | 537 |
| | Windsea | 100 | ok | *na.* | *na.* |
| | | 10000 | ok | *na.* | *na.* |
| | Wind | 100 | ok | *na.* | *na.* |
| | | 10000 | ok | *na.* | *na.* |
| K12 | Swell | 100 | fails | 26 | 43 |
| | | 10000 | fails | 16 | 27 |
| | Windsea | 100 | ok | *na.* | *na.* |
| | | 10000 | ok | *na.* | *na.* |
| | Wind | 100 | ok | *na.* | *na.* |
| | | 10000 | ok | *na.* | *na.* |
| K13 | Swell | 100/10000 | ok | *na.* | *na.* |
| | Windsea | 100/10000 | ok | *na.* | *na.* |
| | Wind | 100/10000 | ok | *na.* | *na.* |
| K14 | Swell | 100 | fails | 30 | 56 |
| | | 10000 | fails | 4 | 17 |
| | Windsea | 100 | ok | *na.* | *na.* |
| | | 10000 | ok | *na.* | *na.* |
| | Wind | 100 | ok | *na.* | *na.* |
| | | 10000 | ok | *na.* | *na.* |

## 12.3 Mitigation effects regarding parametric resonance

A target for future work could be to introduce mitigations to parametric resonance in order to adjust the concept K12 to a revised K11 by removing mooring lines.

One promising mitigation that have been looked into is to reduce the number of mooring lines and introduce a damper system at tower location. Thus, a reduction in no. of anchor positions may be achieved or the concept may be brought back to K11. Passive fluid viscous dampers may be used. Similar dampers have been used previously on long span bridges with the purpose of controlling seismic response. These dampers will consequently work in a range of much higher frequencies than required for controlling parametric excitation on Bjørnafjorden. To bring the concept back to r K11, the dampers must be effective for periods higher than 10 seconds. For the damper to be effective at the tower position, the back span of stay cable bridge must be long enough and be able to move in

transverse direction. If piers in back span are used, these must be provided with sliding bearings. Calculations for K11 show that optimal damping level is 20 MNs/m giving a damping ratio of 3 to 4 % for the most relevant horizontal modes (mode 4 and 5). For comparison, literature (Kovacs) gives a formula for optimal damping ratio for damped stay cables of 0.5 xc/L, where Xc is the free length from abutment south to damper position at tower and L is the bridge length. Taking Xc to be 400 m and L to be 5500 m the damping ratio will be 3.6%. This level of damping should be high enough to supress the effect of parametric resonance. The maximum damping force and movement are not determined at this stage, but the force is believed to be in the range of 5 to 10 MN. Using two dampers, each must have a capacity of approximately 5 MN which seems feasible. Further work comprises verification that the damper will work at the specified range of frequencies, determination of force and cyclic deformation in dampers including the static deformation due to middle wind and temperature changes. It will later be beneficial to contact potential suppliers for assistance.

Please note that this possible mitigation according to the cost estimations performed in this phase, will not reduce the overall cost of the project, since the total cost is higher than for the preferred solution.

Other possible mitigations that have been looked into, is a change in cross-sectional area or a change of horizontal radius. Critical loading condition, ref. Section 12.2 is swell waves (axial mode with an eigen period of approximately 13 seconds, mode 6. The eigen period of the axial mode is direct related to radius R, axial stiffness AE and distributed mass m, simplified giving the eigen period T= $2\pi R (m/AE)^{0.5}$ (ring analogy). In order to reduce the parametric excitation from swell sea, one may double the area of the steel girder. The eigen period is then lowered to approximately 10 seconds, but the increased steel area will give an unacceptable increased cost. A second option is to reduce the radius to 3000 m which effectively reduces the axial mode to 8 seconds. The parametric excitation from swell sea was then solved. However, such a period may be a problem for the 10.000-year wind sea storm which have a peak period of 6.1 seconds. A compromise with radius of 3500 m could then be a choice. In order to eliminate parametric excitation, the axial mode should preferable be lowered to 3-4 seconds. This will require a radius as low as 1500 m which will not be possible for Bjørnafjorden. Also, a radius of 3500 m will be challenging considering the road alignment at the bridge ends. These mitigations are therefore not followed further in this phase of the project.

# 13 Fatigue analyses

## 13.1 General

The scope for the fatigue assessment is focused on structural details that are considered important with respect to concept selection and structural details/dimensions that will be governed by fatigue, and hence may have a cost impact. Details that are believed not to bring significant increase in structural dimensions or cost has not been prioritized.

The following main structural components has been subject to fatigue checks, where selected details for each component have been assessed:

- Bridge girder
- Bridge girder / column connection
- Pontoon / Column connection
- Mooring lines
- Stay Cables

For details about analysis methodology and results reference is made to Appendix I.

## 13.2 Bridge girder

The structural configuration of the bridge girder deck with typical welding details is shown below in Figure 13-1. The following details are selected for fatigue calculation:

- Transverse plate welds outside of traffic lanes (Detail type 1)
- Transverse plate welds inside of traffic lanes (Detail type 2)
- Connection between transverse frame and trapezoidal stiffener (Detail type 3)
- Longitudinal weld in trapezoidal stiffener to deck plate joint (Detail type 4)
- Trapezoidal stiffener splice (Detail type 5)

Locations on the cross-section subject to fatigue checks are shown in Figure 13-2. For the transverse weld details (detail type 1, 2 and 5) it is assumed that the transverse welds will be located close to the transverse frames and no more than 0.5m away. Detail types 2,3,4, and 5 are calculated for the worst position in the slow traffic lanes. Outside the slow lanes these detail types are not considered to be critical. The areas of the bridge girder where local traffic loads are significant is shown in Figure 13-3.

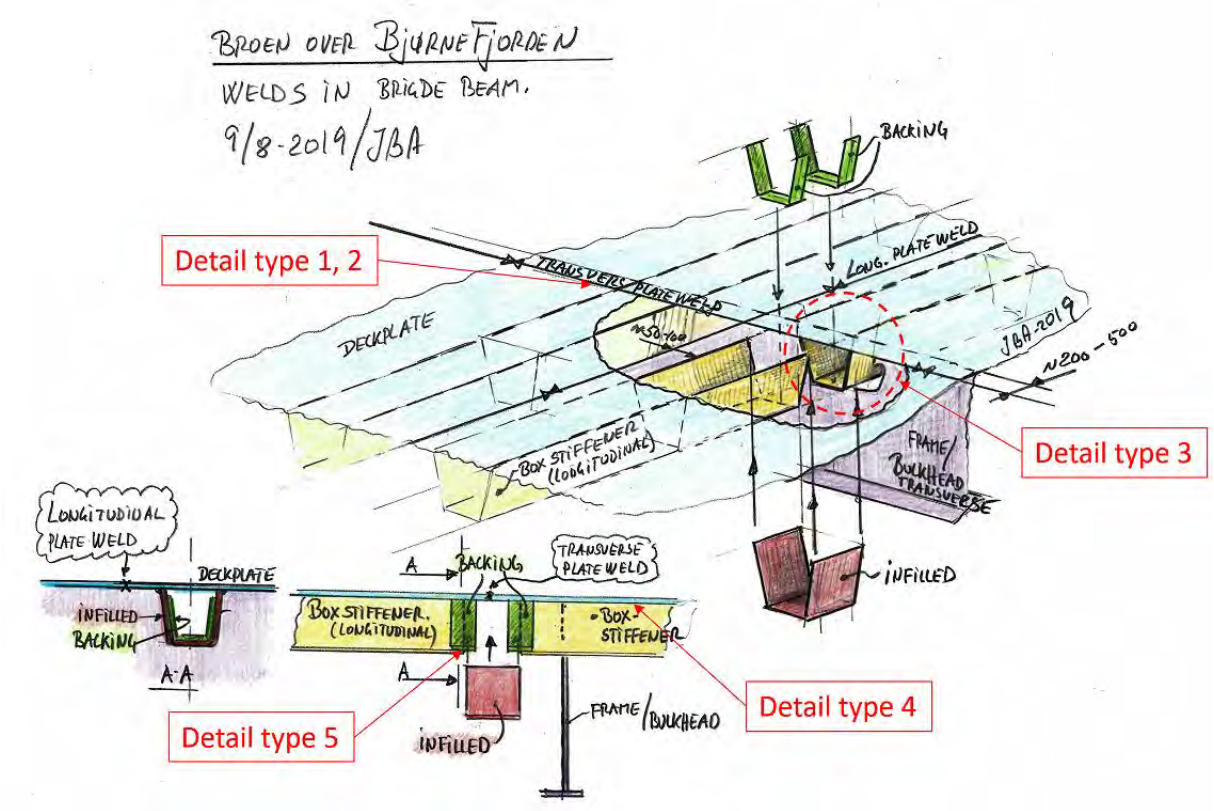


*Figure 13-1 Structural arrangement for bridge girder deck showing typical weld details*

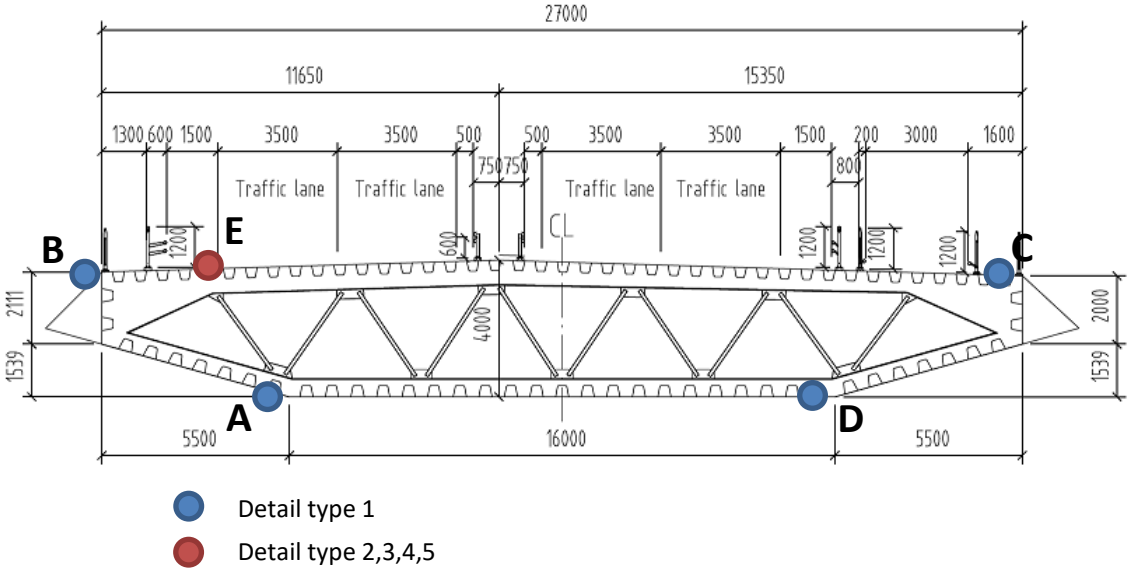


*Figure 13-2 Locations on bridge girder subject to fatigue checks*

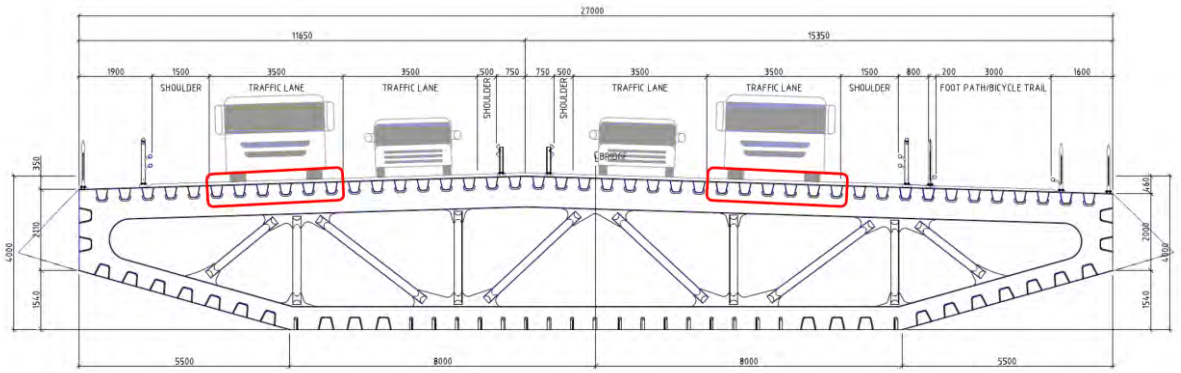


*Figure 13-3 Areas in the bridge girder where local traffic loads are significant are below the slow traffic lanes*

Calculated fatigue lives for the different detail types are given in Table 13-1. A measure that has been applied during the current project phase is to increase the plate thickness in the deck to 16mm along the entire length of the bridge to increase fatigue robustness. Still, some details which are directly subjected to local traffic loads (See Figure 13-3) have insufficient fatigue life with the applied traffic load model (FLM4). Additional measures have therefore been proposed in order to get acceptable fatigue lives.

As the applied traffic load model is considered too conservative for Norwegian roads it is proposed to develop a traffic load model based on historical/forecasted traffic data for the actual bridge location. This is expected to give a less conservative load model which will significantly improve fatigue life. A sensitivity study has been performed on the traffic load model to identify the load reduction required to achieve acceptable fatigue lives inside the slow traffic lanes. The required measures are provided in Table 13-1 for each relevant detail. Several of the typical details in the deck currently have a calculated fatigue life of around 20-30 years. The required load model reduction to achieve acceptable fatigue life for these details is to use the medium range traffic distribution and reduce axle loads to 75% of the full FLM4 axle loads.

Most of the details inside the slow traffic lanes are expected to get sufficient fatigue life with a moderate reduction in the traffic load model. However, for the cut-out detail in the transverse frames around the trapezoidal stiffeners the lowest calculated fatigue life is currently only 6 years and additional measures are required. This is a known problem-area in steel bridges and further design optimization of this detail is needed to get an acceptable fatigue life.

Another measure that has been proposed and may have significant effect on the fatigue lives is to utilize the asphalt stiffness in the local FE-analyses. In the current assessment the wheel pressure is applied uniformly on the deck plate. Research shows that by including the asphalt stiffness, the wheel load is concentrated to the webs, thereby reducing the bending in both the deck plate and trapezoidal webs compared to a uniform load distribution. For more details, see Appendix I.

*Table 13-1 Calculated fatigue lives for bridge girder with traffic load reduction measures*

| Detail type | Description | Included Load types | Fatigue life [years] | Traffic load reduction | Fatigue life with reduced load [years] |
|---|---|---|---|---|---|
| 1 | Transv. plate splice (yard) | E + Ti + $Tr_G$ | 157 | - | - |
| | Transv. plate splice (at site) | E + Ti + $Tr_G$ | 97 | - | - |
| 2 | a) Transv. plate splice (longit. stress) | E + $Tr_G$ + $Tr_L$ | 137 | - | - |
| | b) Transv. plate splice (transv. stress) | $Tr_L$ | 70 | Medium distance traffic 90% axle loads | 156 |
| 3 | a) stiffener/deck plate connection | $Tr_L$ | 21 | Medium distance traffic 75% axle loads | 122 |
| | b) stiffener/web frame connection (vertical weld at cut-out) | $Tr_L$ | 13 | Medium distance traffic 70% axle loads Reduce $N_{obs}$ to 0.25e6 | 139 |
| | c) stiffener/web frame connection (weld at edge of cut-out) | $Tr_L$ | 16 | Medium distance traffic 70% axle loads Reduce $N_{obs}$ to 0.25e6 | 180 |
| | d) Free edge on cut-out | $Tr_L$ | 6 | Medium distance traffic 70% axle loads Reduce $N_{obs}$ to 0.25e6 | 60 |
| 4 | Trapezoidal longitudinal weld | $Tr_L$ | 27 | Medium distance traffic 80% axle loads | 123 |
| 5 | Trapezoidal splice detail | E + $Tr_G$ + $Tr_L$ | 32 | Medium distance traffic 75% axle loads | 103 |

**Load types:**
E: Global environmental loads (wind, wind waves and swell)
Ti: Global tidal loads
$Tr_G$: Global traffic loads
$Tr_L$: Local traffic loads

## 13.3 Bridge girder/column and pontoon/column connections

The most highly stressed areas in the columns are in the vicinity of the column corners towards the bridge girder and towards the pontoons. Cast pieces are proposed for these locations and the fatigue checks performed in this assessment are for the butt welds between the bridge girder/column plating and the cast pieces.

All column top locations along the bridge has been checked and the worst location is at Axis 3 where the calculated fatigue life is 44 years and 47 years for the girder side and column side respectively. To achieve a fatigue life of 100 years on the girder side the stresses must be reduced to the equivalent of an SCF of 1.50 in the current calculation. The column top at Axis 4 has a calculated fatigue life of 89 years (column side). All other column top locations are found to have sufficient fatigue lives. It is expected that sufficient fatigue life can be achieved at Axes 3 and 4 by increasing structural dimensions locally.

At the column bottom towards the pontoon the dynamic stresses are significantly lower and fatigue is not expected to be a problem. The lowest fatigue life is found to be around 9000 years, which indicate that cast pieces may not be necessary at the column to pontoon connection from a fatigue point of view.

## 13.4 Mooring lines

The mooring line top chains have been assessed by both tension fatigue method and OPB/IPB method. For the tension method OPB/IPB effects are included by applying an SCF of 1.15. The two methods give similar results. With the OPB/IPB method the lowest fatigue life is found at line 2 with 110 years. In comparison, the tension fatigue calculation gives a fatigue life of 120 years at the same location. The top chains are planned to be replaced once, which means that this chain has a utilization of 0.45. For the bottom chain the highest utilization is also found at line 2 with 100 years life. The bottom chains are not planned to be replaced, and this chain hence has a fatigue utilization of 1.0. It is noted that the effect of OPB/IPB is expected to be less at the anchor side and the applied SCF of 1.15 is considered conservative for the bottom chain.

## 13.5 Stay cables

Fatigue lives in the stay cables are found to be very high. The main contributors to fatigue are traffic and tide. Traffic contributes to most of the fatigue near the tower and tide contributes to most of the fatigue in the northern end near Axis 3.

# 14 Ship collision

This section gives highlight of the global ship collision assessment. For details on global and local ship collision response see Appendix J.

## 14.1 Summary

The ship collision appendix J describes status of ship collisions analysis in the concept development work of a floating bridge over Bjørnafjorden. Both global and local effects were considered, and LS-DYNA was used as the main calculation tool. The only damping sources that gives a significant contribution to the bridge response following an impact are viscous damping on pontoons and mooring lines, causing an improved response with more mooring. Comparison of global behavior in Orcaflex and LS-DYNA reveal similar but not identical responses, showing that the main hydrodynamic properties are captured adequately in LS-DYNA. Mooring contributes significantly to energy dissipation.

The bridge is compliant in the transverse direction, and pontoon impacts will yield increasing local deformation for increasing deviation in impact direction from the transverse direction. Around 200 MJ is to be dissipated locally for the worst conditions, indicating significant damage to both pontoon and vessel. For pontoon collisions the energy dissipation through local plastic deformations are in the range of 40% of available kinetic energy for head-on, 60% for 45 degree offset and 80 % for 80 degree offset, where offset is the horizontal angle from the bridge transverse axis (longest pontoon axis).

Deckhouse collisions are not significantly different for head-on collision (0 deg.) and at an angle (10 deg.) in terms of energy dissipation. A slight decrease in peak bridge energy is seen for 10 deg., for which the collision force is significantly lower.

Pontoon collision and deckhouse collision cause a somewhat different global response, with pontoon collisions giving higher torsional response in the columns and bridge girder and deckhouse collisions a larger strong-axis bending moment response towards either end. For pontoon collisions the strong-axis bending moment is stiffness-dominated close to either end of the bridge, and there are minimal concept differences. For deckhouse collisions the southern scenarios are further out on the bridge, and the mooring stiffness contributes significantly to reduce peak loads towards the southern end of the bridge. In the north abutment high loads are observed, and the bridge responds in a stiffness-dominated manner for these collisions. The abutment load is thus proportional to the collision force; a relation that is not observed for the central sections of the bridge.

The overall bridge girder capacity is sufficient to avoid severe consequences of damage and shown to be robust in the post-damage phase for a 100-year environmental condition (see Appendix G). However, a few aspects were identified for further design development:

- The torsional resistance of the columns is currently too low when the impact direction deviates from the transverse direction of the pontoon and should be a point of focus in further design development. This will be dimensioning for the columns along the entire bridge.
- The wind nose on the bridge girder was considered as non-structural, and the bridge girder is constructed with vertical sides. Local analysis of collisions between a deck house and the bridge girder gave high contact forces due to a punching-type deformation into the striking vessel, which yields large global moments towards the Northern abutment. A mitigating measure may be to include a structural wind nose for the northernmost sections of the bridge girder.

## 14.2 Input definitions

Design scenarios are selected as pr. the design basis with clarifications as shown in the table below.

| CC 125m | Displacement | Velocity | LOA | Energy |
|---|---|---|---|---|
| Element | [tonne] | [m/s] | [m] | [MJ] |
| Bridge girder North (of A23) | 14855 | 5.8 | 138 | 275 |
| Bridge girder South (of A23) | 21123 | 6.2 | 206 | 447 |
| Pontoon, Axis 3 | 14566 | 6.2 | 142 | 308 |
| Pontoon, Axis 4-5 | 13851 | 6.2 | 140 | 293 |
| Pontoon, Axis 6-23 | 13232 | 5.1 | 136 | 189 |
| Pontoon, Axis 24-40 | 10662 | 5.1 | 122 | 153 |

The main contributor to ship collision risks in the above table were from vessels passing along the Western side of the bridge and not from vessels crossing the bridge. During the project it was reported that an agreement on a re-routing of the navigational channel was close, which in large will prevent ships from sailing directly towards the bridge. This is expected to give a significant decrease of collision energies at a $10^{-4}$ annual probability level, but as this was not yet quantified the simulations were performed with the design scenarios as pr. the design basis. A sensitivity study showed that a 50% decrease of impact energy gave around a 20% decrease in global bridge response, whereas the torsional deformation of the column was more than halved.

## 14.3 Response to ship collisions

### *14.3.1 Bridge girder response*

Only strong axis-results are shown in the following. For other result components see Appendix J.

Large moments are observed in the Northern abutment, in which the response is stiffness-dominated for impacts close to the abutment.

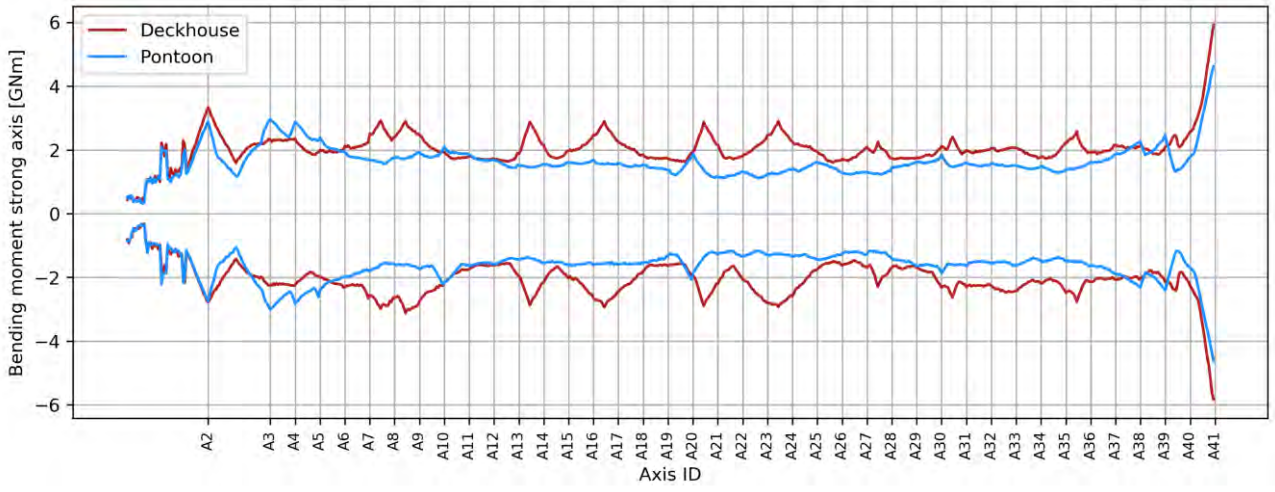


*Figure 14-1 Strong-axis moment envelopes for the bridge girder for K12_06*

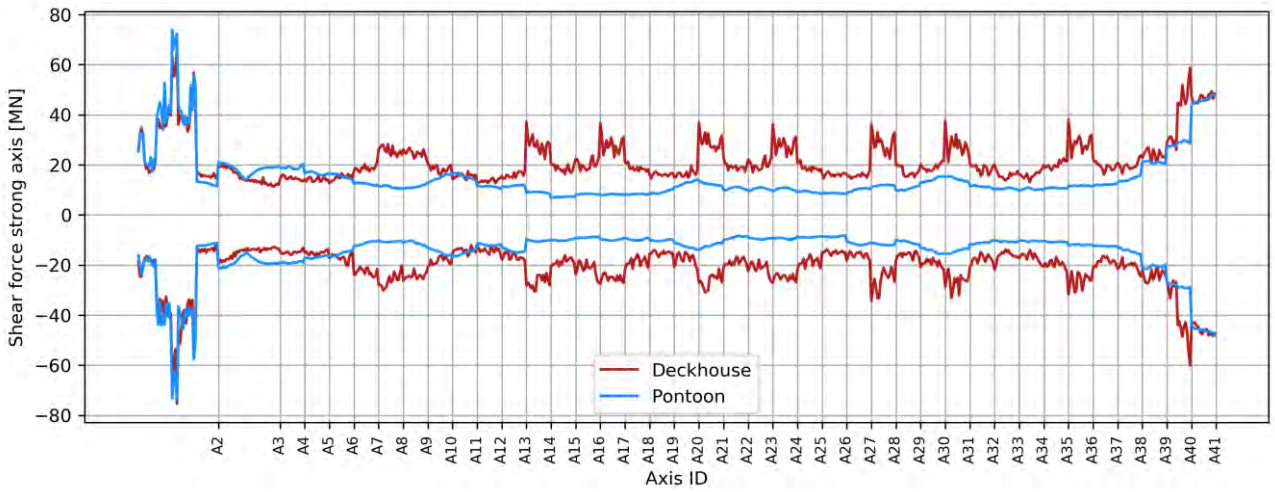


*Figure 14-2 Transverse shear force envelopes for the bridge girder for K12_06*

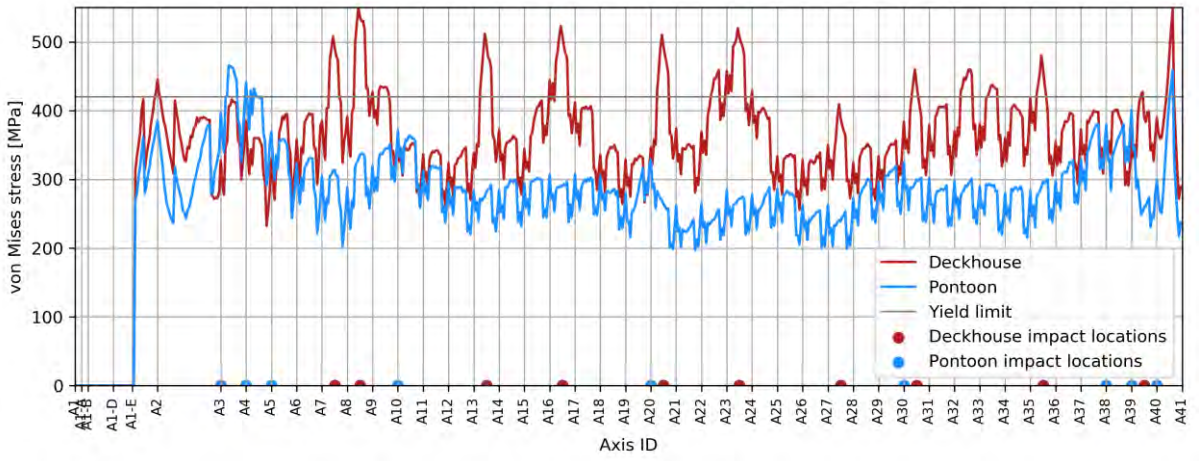


*Figure 14-3 Envelope of resulting stress level in bridge girder for K12_06.*

### *14.3.2 Column response*

Figure 14-4 and Figure 14-6 show key column responses enveloped over all simulated scenarios. Columns in the back span are termed BCEi, whereas columns in the floating bridge are termed Ai, both counting from south to north. A step in torsional response is found north of axis 23, related to the difference in collision energy north of this limit as defined in [15].

The torsional moment in columns for impact to pontoons at increases rapidly with increasing directional deviation from impact in the transverse bridge axis (the bridge is less flexible for impacts along than transverse to the bridge direction). Torsional moments in the columns increase from around 100 MNm to 1600 MNm as the impact direction changes from 0 to 80 degrees (from transverse to nearly longitudinal).

The torsional collision response is dimensioning for the columns. An optimization of the column design is required during the next phase of the project. See Appendix J and K for further discussions.

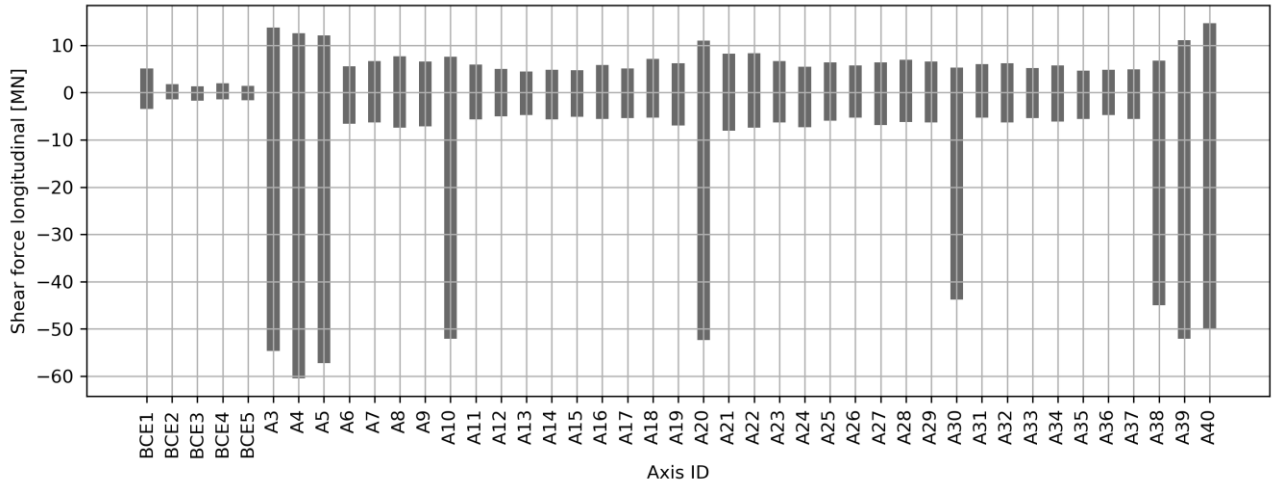


*Figure 14-4 Longitudinal shear force response from ship collision, top of column for K12_06*

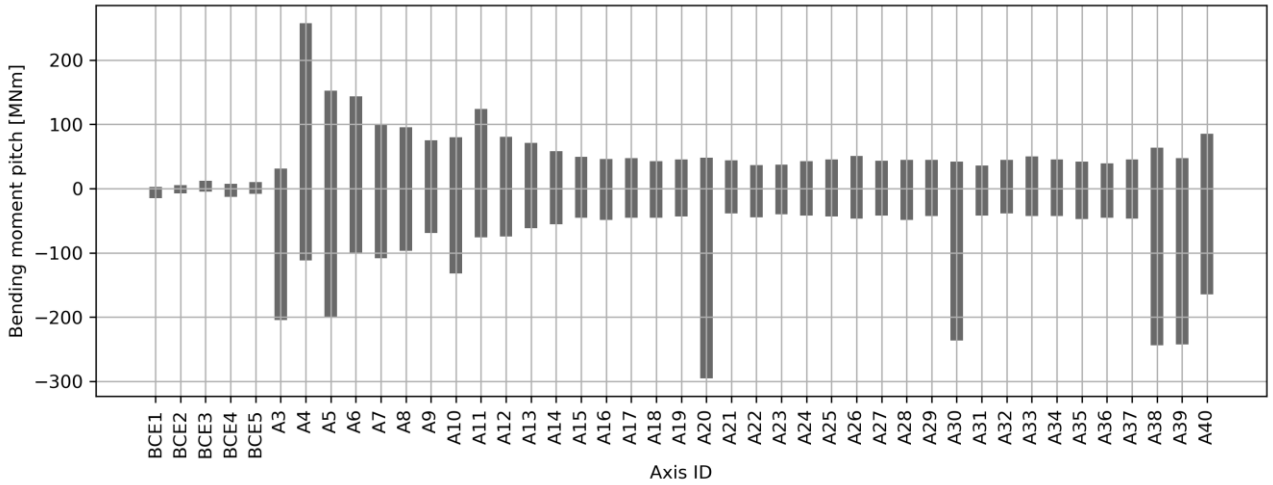


*Figure 14-5 Pitch moment response from ship collision, top of column for K12_06*

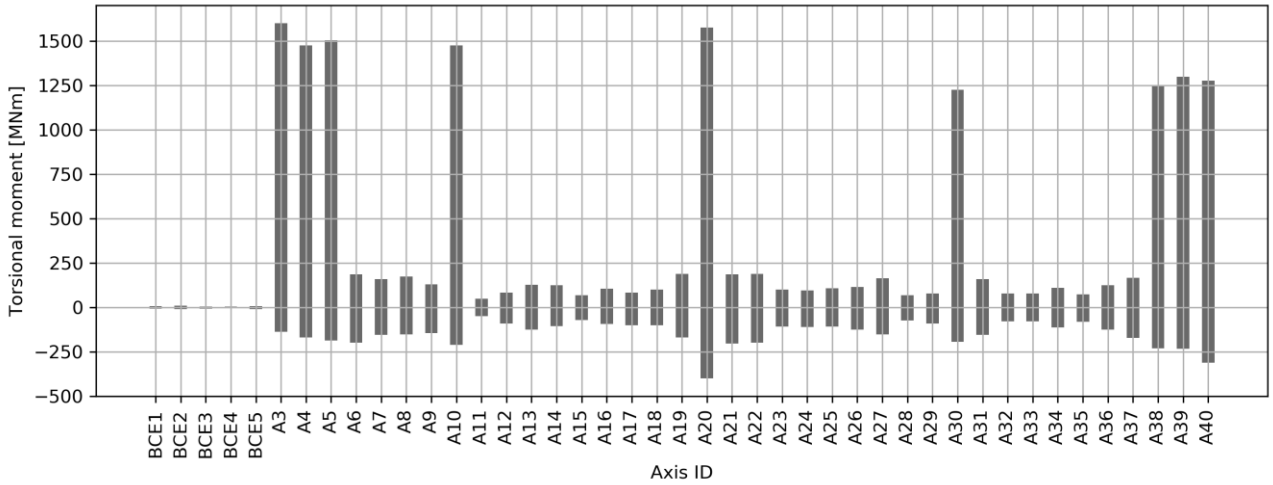


*Figure 14-6 Torsional moment response for all concepts, top of column for K12_06*

### *14.3.3 Mooring line response*

The mooring line response was evaluated in more detail based on models with nonlinear mooring stiffness calibrated to each mooring cluster's nonlinear stiffness properties. The simulations were performed for both pontoon and deckhouse collisions, but the latter causes the largest bridge deflections and thereby the greatest mooring line utilization. Impact transverse to the bridge in both directions were considered (0 and 180 deg. from the transverse axis).

The table below shows the maximum displacements of the moored pontoons and the maximum mooring line forces. The forces are well below the breaking strength of the mooring line, and ship collisions are thus not dimensioning for the anchor line strength. See appendix M for an evaluation of the force levels w.r.t anchors.

*Table 14-1 Maximum displacements of the moored pontoons*

| Ship impact (m) | | Cluster 1 | Cluster 2 | Cluster 3 |
|---|---|---|---|---|
| K12 | from West | -10.8 | -10.7 | -6.6 |
| | from East | 9.4 | 10.3 | 6.7 |

*Table 14-2 Maximum mooring line forces*

| | Top | Bottom |
|---|---|---|
| Mooringline1 | 9 | 8.5 |
| Mooringline2 | 10.3 | 9.7 |
| Mooringline3 | 8.2 | 7.6 |
| Mooringline4 | 7.3 | 6.6 |
| Mooringline5 | 7.5 | 7 |
| Mooringline6 | 7.2 | 6.7 |
| Mooringline7 | 7.6 | 7 |
| Mooringline8 | 10.5 | 9.9 |
| Mooringline9 | 8.6 | 8.1 |
| Mooringline10 | 4.5 | 4 |
| Mooringline11 | 7.4 | 6.8 |
| Mooringline12 | 8.9 | 8.4 |